π^+ PHOTOPRODUCTION AT ANGLES FROM 6° TO 90° C. M. AND ENERGIES FROM 589 TO 1269 MeV

Thesis by
Stanley Duane Ecklund

In Partial Fulfillment of the Requirements

For the Degree of
Doctor of Philosophy

California Institute of Technology
Pasadena, California
1967
(Submitted November 17, 1966)

ACKNOWLEDGMENTS

This experiment was supervised by Professor Robert L. Walker. His interest, encouragement, suggestions and active participation contributed greatly to the success of the experiment and are greatly appreciated.

The interest and encouragement of Professor Robert F. Bacher are appreciated.

The data analysis of this experiment was done in collaboration with Dr. H. A. Thiessen. Since our experiments were similar, a substantial portion of the data analysis could incorporate the same computer programs. I am indebted to Dr. Thiessen for many helpful discussions as well as his contributions to the programming.

I am indebted to Dr. Charles Peck for many helpful discussions concerning the spectrometer. For many useful and helpful discussions I am also indebted to Mike G. Hauser, Frank B. Wolverton and Carl R. Clinesmith.

The Freon Cherenkov counter was designed and constructed by Frank B. Wolverton.

The electronic instruments used in this experiment result, to a large extent, from the work of Dr. J. H. Marshall III. Their excellent reliability made the collection of a large quantity of data feasible.

The competent technical support of synchrotron personnel was essential to the success of this experiment. In particular I would like to thank Lawrence Loucks, Alfred Neubieser and Earl Emery for maintenance of the synchrotron and the liquid hydrogen target.

The financial support of the National Science Foundation and the U. S. Atomic Energy Commission is gratefully acknowledged.

ABSTRACT

The differential cross section for the reaction $\gamma p \rightarrow \pi^+ n$ was measured at 32 laboratory photon energies between 589 and 1269 MeV at the Caltech Synchrotron. At each energy, data have been obtained at typically fifteen π^+ c. m. angles between 6° and 90°. A magnetic spectrometer was used to detect the π^+ photoproduced in a liquid hydrogen target. Two Cherenkov counters were used to reject the background of positrons and protons. The data clearly show the presence of a pole in the production amplitude due to the one pion exchange. Moravcsik fits to the 32 angular distributions, including data from another experiment, are presented. The extrapolation of these fits to the pole gives a value for the pion-nucleon coupling constant of 14.5 which is consistent with the accepted value. The second and third pion-nucleon resonances are evident as peaks in the total cross section and as changes in the shape of the angular distributions. At the third resonance there is evidence for both a D5/2 and an F5/2 amplitude. The absence of large variations in the 0° and 180° cross sections implies that the second and third resonances are mostly produced from an initial state with helicity $\pm$ 3/2.

To Marian

TABLE OF CONTENTS

APPENDICES

LIST OF FIGURES

LIST OF FIGURES (cont.)

LIST OF TABLES

I. INTRODUCTION

Improvements in beam intensity and in the detection apparatus have made it possible to measure the cross section for π^+ photoproduction in considerably greater detail than was achieved in the earlier measurements.[1, 2, 3] In particular, this experiment provides 516 data points at forward angles in the region of the second and third resonances, with improved energy resolution. This quantity of data is useful in determining the angular momentum states present.

Of the various Feynman diagrams which might contribute to π^+ photoproduction, the one pion exchange (OPE, commonly called the retardation term or photoelectric term or simply the π pole) is most evident in the data. Because it contributes a pole in the photoproduction amplitude close to the physical region at $\cos\theta = 1/\beta$, it produces high powers of $\cos\theta$ in the angular distribution. As would be expected, this makes it impossible to fit the data with a polynomial in $\cos\theta$ unless terms of very high order are included. On the other hand, a Moravcsik fit[4] which takes account of the denominator of the OPE explicitly, works very well. This fit gives a measurement of the pion-nucleon coupling constant, $G^2/4\pi$, consistent with that obtained from πN scattering. The negative intrinsic parity of the pion is also revealed by the fit. If the OPE amplitude is separated from other contributions, the cross section may be written in the form

$$\sigma(\theta) = \frac{q}{k} |A_{OPE} + A|^2$$

$$\sigma(\theta) = \frac{q}{k} [|A_{OPE}|^2 + |A|^2 + 2\mathrm{Re}(A_{OPE} A)] \quad .$$

FIGURE 1

Feynman Diagrams

Meson exchanges

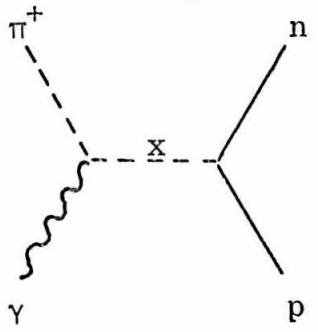

x = π^+ (139)

ρ^+ (760)

Intermediate states

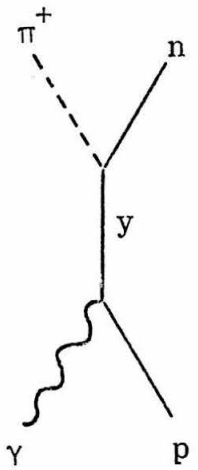

y = N (938)

Δ (1238), P 3/2

N*(1519), D 3/2, P 1/2, S 1/2

N*(1688), F 5/2, D 5/2

Δ (1950), F 7/2

Baryon exchanges

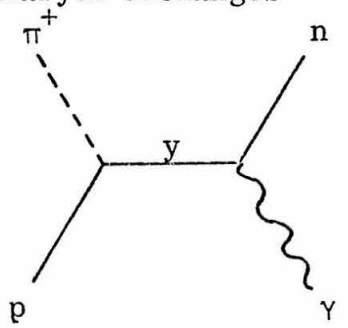

The cross section due to the π pole alone[5] is given in the c. m. system by

$$\sigma_{OPE}(\theta) = \frac{q}{k} \left| A_{OPE} \right|^2$$

$$= \frac{e^2 2G^2}{(4\pi)^2} \frac{q}{k} \frac{1}{4W^2} \frac{\beta^2 \sin^2\theta}{2k^2(1-\beta\cos\theta)^2} \left[(M_2 \pm M_1)^2 - m^2 + 2k\omega(1-\beta\cos\theta) \right]$$

where q = pion momentum

k = photon momentum

$e^2/4\pi = 1/137$

$G^2/4\pi$ = πN coupling constant (14.7)

W = total energy

β = velocity of emerging π^+

θ = π^+ angle relative to photon

ω = pion energy

m = pion mass (139.63 MeV)

M_1 = proton mass (938.213 MeV)

M_2 = neutron mass (939.506 MeV)

in $(M_2 \pm M_1)$ the + sign is taken for a scalar meson and the - for a pseudoscalar meson.

The interference term has the form

$$\frac{q}{k} 2R_e (A_{OPE}A) \sim \frac{\sin^2\theta}{(1 - \beta\cos\theta)} \times \text{Polynomial in } \cos\theta$$

provided that A does not contain pole terms. The other exchange diagrams (ρ^+, baryons) do cause poles in A, but since these poles are farther from the physical region, they may be approximated by a polynomial. The usual Moravcsik fit is obtained by fitting the product $(1 - \beta \cos\theta)^2 \sigma(\theta)$ to a polynomial in $\cos\theta$. Fits equivalent to this which illustrate more clearly the states occurring in A are presented in Section V of this thesis.

In photoproduction a resonant state of definite spin and parity may be produced from two different initial states corresponding to different relative spins of the incident photon and nucleon. The determination of a resonant amplitude thus requires two complex parameters instead of one as in pion-nucleon scattering. The two parameters are usually specified according to electric and magnetic transitions or by the initial helicity. Recent theoretical work with SU(3) sum rules[6] predicts ratios of electric to magnetic production of the second and third resonances consistent with the data.

In the absence of a dynamical theory of photoproduction at high energies, a general phenomenological analysis of the angular distributions is considered. Ideally, the result of such an analysis is a set of multipole coefficients specifying the strength of each angular momentum and parity state produced by a given initial state (electric or magnetic). Determination of the multipole coefficients

requires detailed polarization measurements in addition to cross section measurements. The existing polarization data, which lie below the third resonance, are quite useful but are still far from sufficient to specify a unique set of coefficients. Consequently, a phenomenological analysis must incorporate a specific model to reduce the number of parameters to be determined. It is possible, however, to come to some conclusions without a model by considering the Moravcsik-equivalent fits. The conclusions thus obtained are a convenient starting point in designing a reasonable model.

The recent phase shift analyses[7, 8, 9, 10, 11] of πN scattering show that the second and third resonance region is more complicated than once thought. Instead of a single resonant state for each peak in the total cross section, several resonant states are present. While unique solutions and general agreement between the work of different authors have apparently not been realized, the general features are that there are resonant D 5/2 and F 5/2, and possibly S 1/2 and P 3/2 amplitudes near 1700 MeV (total c. m. energy) and resonant S 1/2, P 1/2 and D 3/2 amplitudes near 1500 MeV. The situation is complicated because some of these resonant states are highly absorptive and are not always well approximated by a simple Breit-Wigner form in energy, making a parameterization difficult. The complications seen in πN scattering are expected to show up in π photoproduction as well, and indeed, some are evident and will be discussed in the section on data fitting.

II. METHOD AND APPARATUS

The basic method used in this experiment to measure the two body reaction $\gamma p \rightarrow \pi^+ n$ has been described many times[1, 2, 3]. The description given here will accordingly be short and most of the details are left to the appendices.

The bremsstrahlung beam from the 1.5 GeV California Institute of Technology Synchrotron illuminated a three inch liquid hydrogen target. A magnetic spectrometer which was pivoted at the target was used to measure the yield of positively charged particles at a given angle and momentum. The spectrometer momentum aperture was divided into four parts so that measurements at four different momenta could be obtained simultaneously. Positrons, protons and π^+ mesons were separated by two Cherenkov counters and time of flight restrictions. The c.m. angle and energy are uniquely determined from the spectrometer angle and momentum by two-body kinematics.

For a given π^+ angle and momentum there is a minimum photon energy needed to produce an additional pion. The synchrotron energy was kept below this threshold for three of the four momentum channels. Approximately one third of the other channel overlapped the 2π threshold, but no significant yield due to this was encountered for two reasons. First, the 2π production, being a three-body final state, contributes a π yield which increases slowly at threshold. Secondly, the 2π cross section is small at threshold[12, 13, 14], not becoming large until a resonance $\Delta(1238)$ is produced with a pion. The yields shown in Figure 4 demonstrate that the 2π contamination was negligible as does the smoothness, as a function of energy, of the cross section data obtained.

Contaminations from other photoproduced mesons (ρ, K, η) were similarly eliminated by kinematic constraints and the maximum energy of the bremsstrahlung beam. Muons are presumed to come only from π^+ decay and no attempt was made to distinguish them from π^+. The measured yields were corrected for the π^+ which decayed and the μ^+ from π^+ decay which were counted in the spectrometer.

The layout of the apparatus is shown in Figure 2. The beam was collimated and "scraped" twice, before and after an upstream hydrogen target, and cleared of charged particles with a magnetic field before entering the downstream target used in this experiment. The beam was stopped and its total energy was measured in a thick plate ionization chamber surrounded, except for the beam entrance, with lead and concrete. Two auxiliary monitors, a thin ionization chamber upstream from the hydrogen target and a two-counter telescope under the hydrogen target, were also used to monitor the beam. A quantameter[15] was used to calibrate the three monitors.

The spectrometer deflected charged particles in a vertical plane by 27.3° with a radius of curvature of 105 inches (Figure 2). Counters A1 and S2 a, b, c, d determined the solid angle and momentum acceptances. "Fan" counters, mounted on each pole face, were used to veto particles scattering from the magnet pole face. The Plexiglas Cherenkov counter (LC) had a velocity threshold of 0.9 c and counted only π^+, e^+ and μ^+ for the momentum range (500 to 1200 MeV/c) used in this experiment. The freon gas Cherenkov counter (FC) had a threshold of 0.999 c, and counted only e^+. The 0.5 inch of lead and the last counter, S3, eliminated electrons below the FC threshold which could result from conversion of gamma rays in A1 or elsewhere when the spectrometer was at small angles to the photon beam. The

other counters were scintillators used to measure time of flight and to reduce accidental coincidences.

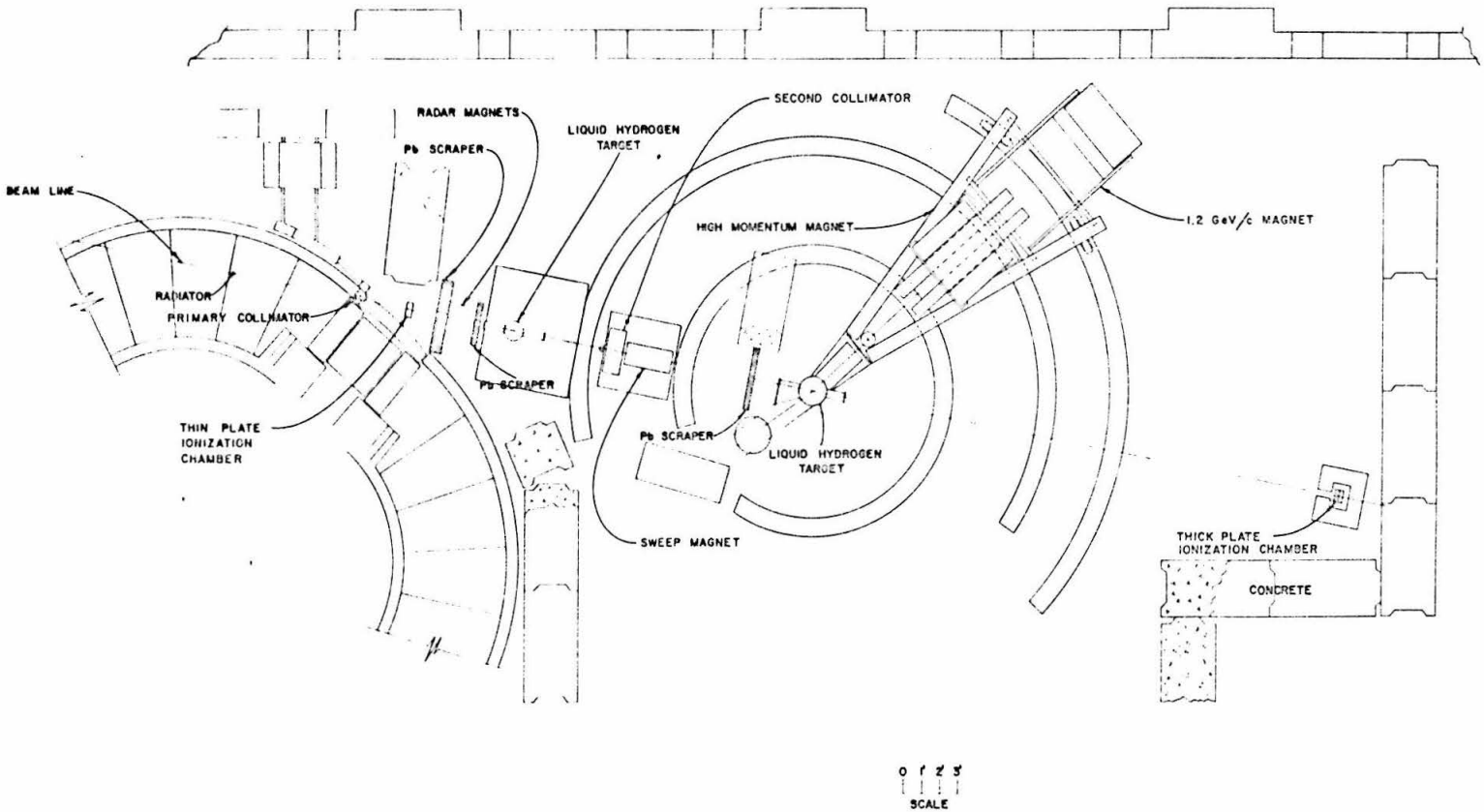

FIGURE 2. Experimental Setup

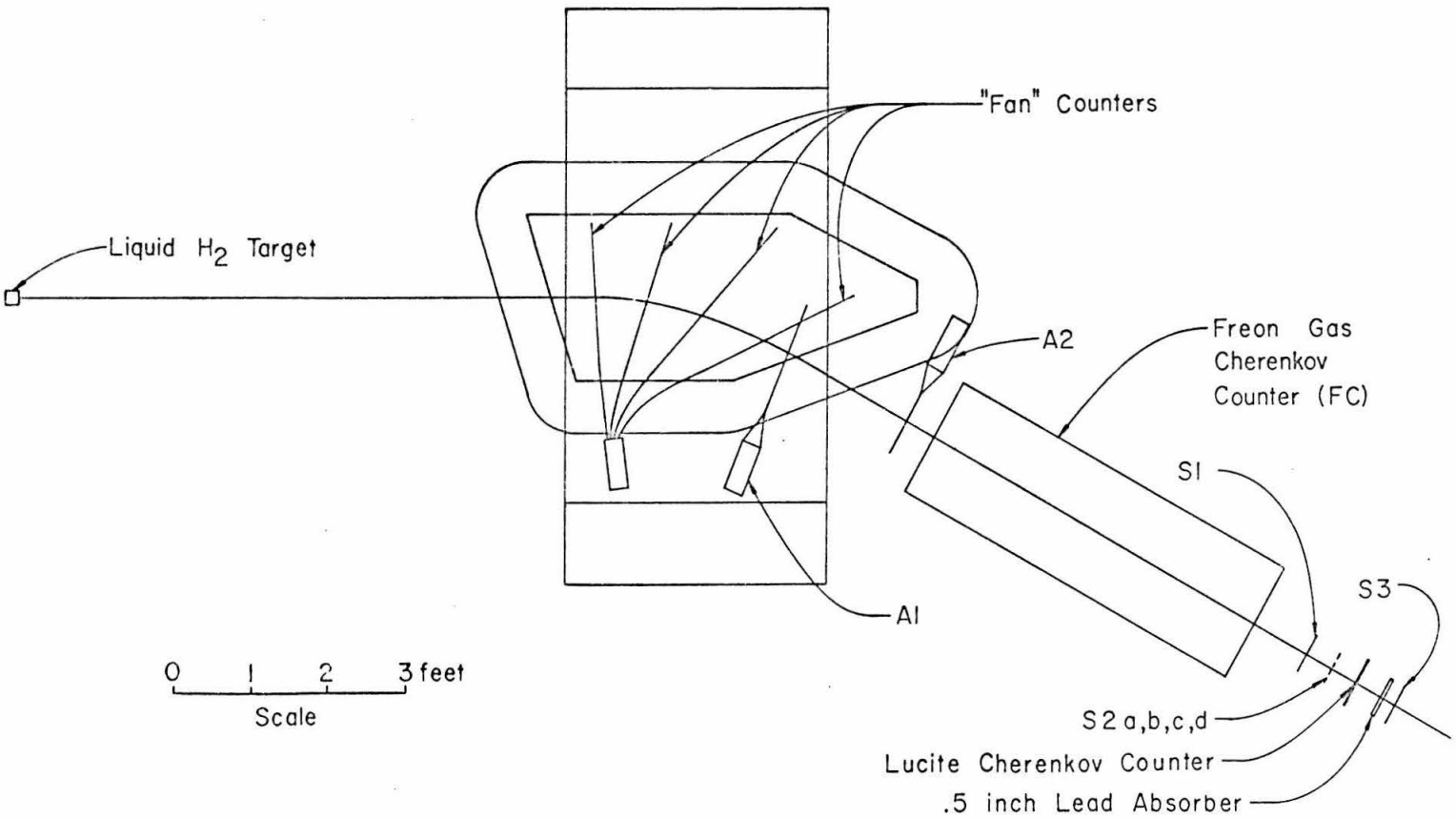

FIGURE 3. Spectrometer

III. PROCEDURE

The π^+ yield was obtained at four momenta and one angle for each setting of the spectrometer and bremsstrahlung endpoint. Three hundred runs at 129 different settings were taken, resulting in 516 cross section measurements. The length of a typical run varied from one half to two hours, depending on the setting and the available beam intensity.

To be recorded, particles passing through the spectrometer had to satisfy fast (4 ns) coincidence requirements between A1 and S1, A2 and S1, and a slower (50 ns) coincidence with S3 and one of the S2 counters. A fast (12 ns) coincidence, Fan · S1, was used to veto events scattering from the pole tips. A π^+ event was defined as an event with an LC count and no count from the freon Cherenkov counter. In addition to the π yield, one of the following was also monitored: the proton yield, the positron yield, the miss rate in S3, or the A2 efficiency. The worst background rates were encountered at a laboratory angle of 3.5° where the π^+: p: e^+ yields were in the ratio 1:3:3. The positron rate decreased rapidly with increasing angle to as low as 1% of the π^+ yield at 15°. The freon counter electron efficiency was better than 99.8%, which was more than adequate. The LC efficiency was measured as $(0.3 \pm 0.3)\%$ for protons and $(98.4 \pm 0.5)\%$ for pions.

As proof of the π^+ selection at the momentum and angle specified, excitation curves were measured by changing only the synchrotron energy. Figure 4 shows the results for π^+ and π^- yields. All four momentum channels are included in Figure 4, but are plotted so as to account for the relative photon energy of each channel. The ordinate is given by

$$\text{Effective } E_o = E_o - \frac{\partial K}{\partial P}(P_J - P_o)$$

where

E_o = synchrotron energy

P_J = mean momentum of J^{th} channel

P_o = central momentum of magnet

K = photon energy corresponding to single π^+ production of momentum P, and angle θ

$\frac{\partial K}{\partial P} \approx 1.18$.

The cross section data were taken with E_o nominally set 130 MeV above the photon energy defined by the central momentum of the magnet. This corresponds to $E_o = 1148$ MeV for the momentum and angle in Figure 4. Notice that the yield below threshold was $\leq 1\%$ of the normal yield at this setting. The data shown have not been corrected for empty target background so that some of the π^- yield was single π^- production from neutrons in the Mylar cup of the hydrogen target.

Cross section measurements were made with eight values of E_o. At each E_o settings of angle and momentum were chosen to give c. m. angles between 6^o and 90^o at a constant mean photon energy. At each setting, measurements at four energies were obtained corresponding to the four spectrometer channels. In this way 32 angular distributions were obtained. The fixed momentum apertures cause the separation of the four photon energies to

increase slightly with angle so the angular distributions obtained are at only approximately constant energies (see Appendix VI and Figure 29). A typical set of measured yields is shown in Figure 5. The cross section was calculated from the difference between full and empty target runs. Corrections were made for counter efficiencies, nuclear absorption, multiple scattering, and π^+ decay in flight. Details of the calculations are given in the appendices.

The data reduction method of this experiment was essentially the same as that of H. A. Thiessen's experiment[16]. Consequently, much of the task of writing computer programs was shared between us.

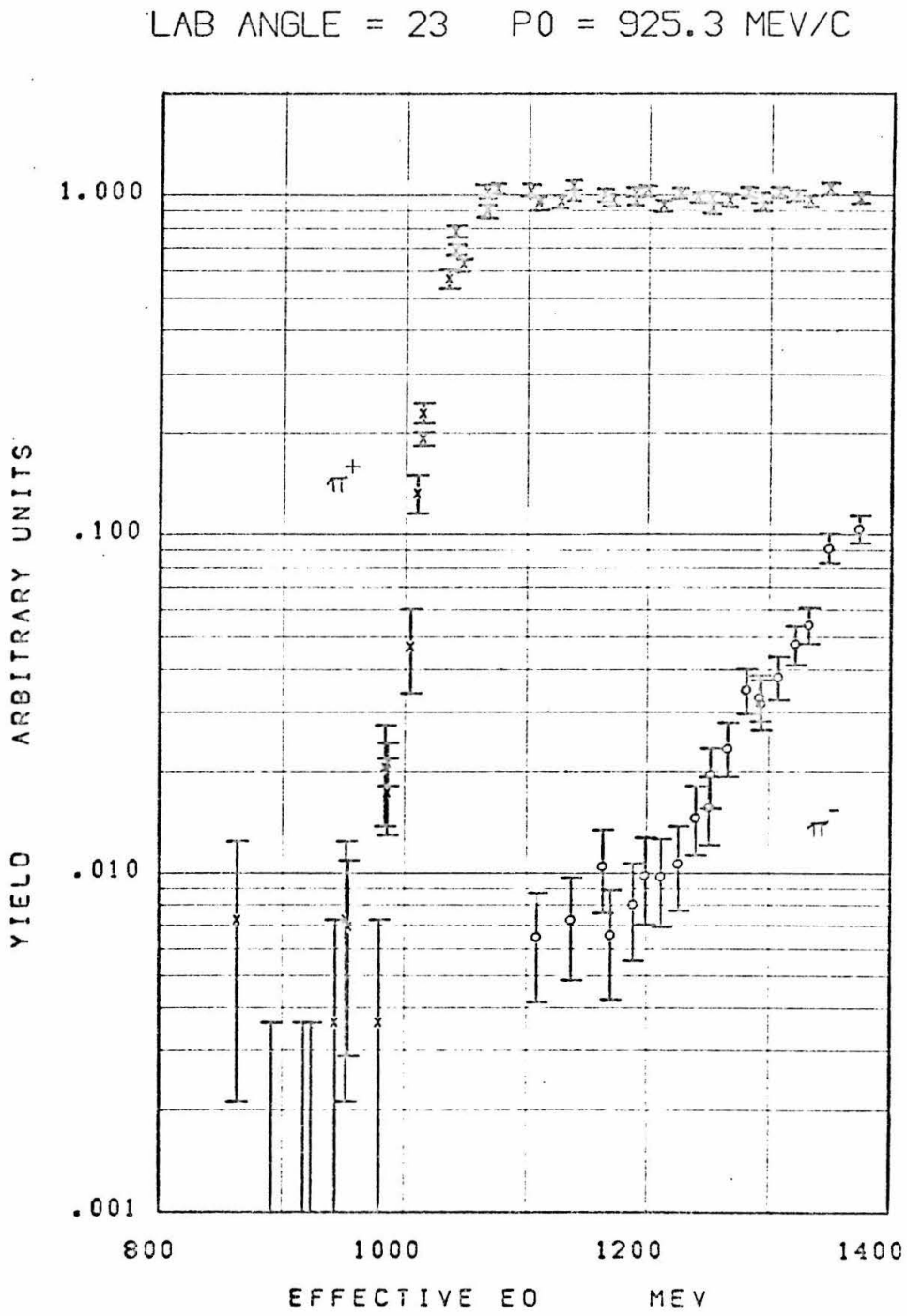

FIGURE 4. Yield vs. E_o

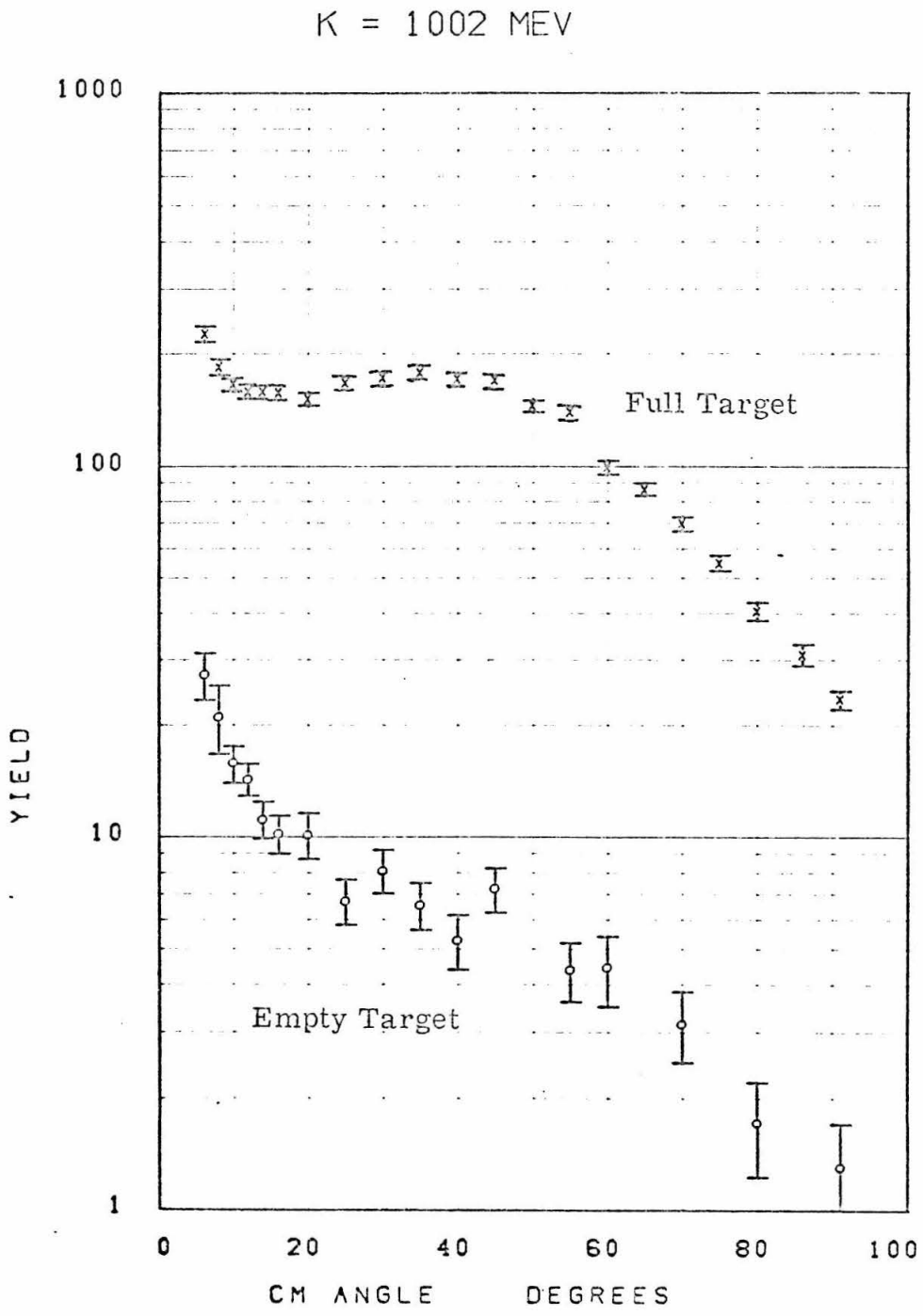

FIGURE 5. π^+ Yield vs. Angle

IV. RESULTS

The measured cross sections were interpolated to constant energy in order to display angular distributions. Table 1 and Figures 6.1 - 6.32 show the results. Also shown are some of the data of the experiment of H. A. Thiessen[16], interpolated to the appropriate energy. The curves are Moravcsik - equivalent fits with eight parameters and a fixed coupling constant of 14.7. To illustrate the overall shape of the cross section as a function of energy and angle, the fitted curves are displayed in an isometric view in Figure 7.

A check for systematic changes in the measurements over the period of the experiment was made in the following manner. The cross sections measured in each run were compared with those given by the Moravcsik - equivalent fits, linearly interpolated to the energy at which the measurements were made. Most of the settings were measured several times so this comparison checked consistency among runs at the same setting as well as the shape of the fit and the interpolation scheme used to obtain angular distributions. The following quantity was calculated and its frequency distribution is shown in Figure 9:

$$\chi = \frac{\sigma_i - \sigma_{fit}}{\Delta\sigma_i}$$

where σ_i = cross section from i^{th} run

σ_{fit} = cross section from fit evaluated at energy and angle of i^{th} run

$\Delta\sigma_i$ = standard deviation in σ_i.

This distribution compares favorably with the expected distribution which is a Gaussian of unit standard deviation.

The results of this experiment are compared with earlier experiments in Figures 8.1 - 8.7. The smooth curves are the Moravcsik-equivalent fits obtained in this experiment. For most energies, the agreement is as good as can be expected. The agreement between this experiment and H. A. Thiessen's was checked at places where the data overlap (Figures 6.1 - 6.13). The Moravcsik-equivalent fits were repeated with a variable scale factor for the data of one experiment relative to the other. The average scale factor differed from unity by $3 \pm 3\%$, the cross sections obtained from this experiment being the larger. This difference was not taken as significant and no scale factor was included in any of the fits presented in this thesis.

The errors quoted with the cross sections are standard deviations resulting from counting statistics and the 1.5% beam monitoring error added in quadrature for each run. The constant or slowly varying errors are listed in Table 2. The error in c.m. angle is less than 0.05 degree for any point. The calibration of the laboratory photon energy is considered consistent between points to better than 0.2%, and accurate overall to 0.5%.

The root-mean-square energy resolution in laboratory photon energy varies from 1.4% to 2.5% depending upon angle and energy (Appendix VI, Table 16). The angular resolution is typically 0.8° (rms) in c.m. angle. The error in the measured cross section due to the finite resolution in angle and energy was estimated for extreme cases to be less than 0.3% and 2% respectively.

TABLE 1

Interpolated Cross Sections

K lab is the laboratory photon energy in MeV.
Cross section is in microbarns/steradian in the c. m. system.
c. m. angle is in degrees.

CM ANGLE	K LAB	CROSS SECTION	CM ANGLE	K LAB	CROSS SECTION
6.04	589	17.88 +- 0.76	6.08	603	16.69 +- 0.71
8.02	589	16.37 +- 0.71	8.07	603	18.22 +- 0.72
10.14	589	15.62 +- 0.51	10.21	603	15.71 +- 0.48
12.11	589	14.88 +- 0.64	12.18	603	14.36 +- 0.61
14.07	589	13.37 +- 0.45	14.16	603	13.59 +- 0.45
16.04	589	13.21 +- 0.55	16.14	603	12.58 +- 0.52
20.00	589	11.93 +- 0.49	20.12	603	11.42 +- 0.48
24.96	589	11.38 +- 0.58	25.11	603	11.11 +- 0.56
29.93	589	11.12 +- 0.48	30.11	603	11.09 +- 0.46
34.90	589	10.07 +- 0.56	35.11	603	11.74 +- 0.58
39.86	589	10.60 +- 0.31	40.09	603	10.58 +- 0.31
49.83	589	10.30 +- 0.57	50.09	603	9.49 +- 0.55
59.79	589	10.01 +- 0.42	60.09	603	10.15 +- 0.42
6.12	618	18.84 +- 0.74	6.16	635	17.34 +- 0.70
8.12	618	17.46 +- 0.69	8.18	635	16.27 +- 0.66
10.27	618	15.38 +- 0.48	10.35	635	15.70 +- 0.48
12.26	618	14.31 +- 0.60	12.35	635	14.50 +- 0.59
14.25	618	13.13 +- 0.43	14.35	635	13.82 +- 0.44
16.25	618	13.49 +- 0.53	16.36	635	12.49 +- 0.50
20.25	618	11.34 +- 0.47	20.39	635	10.83 +- 0.44
25.26	618	11.08 +- 0.55	25.44	635	11.50 +- 0.55
30.29	618	10.43 +- 0.45	30.50	635	10.96 +- 0.45
35.31	618	10.85 +- 0.55	35.55	635	10.83 +- 0.54
40.33	618	10.97 +- 0.30	40.59	635	10.76 +- 0.30
50.38	618	11.20 +- 0.57	50.70	635	10.61 +- 0.56
60.42	618	10.27 +- 0.42	60.78	635	10.53 +- 0.42
6.06	647	18.87 +- 0.57	6.10	663	18.18 +- 0.54
8.02	647	16.16 +- 0.51	8.08	663	17.86 +- 0.52
10.16	647	15.85 +- 0.41	10.22	663	15.55 +- 0.40
12.10	647	14.82 +- 0.39	12.18	663	14.51 +- 0.38
14.07	647	14.40 +- 0.40	14.16	663	13.72 +- 0.39
16.04	647	13.51 +- 0.41	16.15	663	12.96 +- 0.39
19.99	647	11.95 +- 0.35	20.12	663	11.69 +- 0.34
24.94	647	10.76 +- 0.33	25.11	663	11.03 +- 0.33
29.91	647	11.17 +- 0.33	30.11	663	10.92 +- 0.32
39.85	647	11.19 +- 0.23	40.09	663	11.49 +- 0.23
49.79	647	11.73 +- 0.36	50.09	663	11.60 +- 0.35
59.77	647	10.96 +- 0.36	60.09	663	11.33 +- 0.35
69.73	647	9.97 +- 0.32	70.09	663	10.10 +- 0.31
79.71	647	8.50 +- 0.27	80.08	663	8.45 +- 0.27

CM ANGLE	K LAB	CROSS SECTION	CM ANGLE	K LAB	CROSS SECTION
6.14	680	18.44 +- 0.53	6.18	698	16.55 +- 0.49
8.13	680	15.82 +- 0.49	8.19	698	16.28 +- 0.48
10.29	680	16.46 +- 0.40	10.37	698	15.05 +- 0.38
12.27	680	13.97 +- 0.36	12.36	698	14.08 +- 0.36
14.26	680	13.59 +- 0.38	14.37	698	13.29 +- 0.37
16.26	680	12.31 +- 0.38	16.38	698	12.68 +- 0.38
20.26	680	12.30 +- 0.34	20.40	698	11.31 +- 0.32
25.27	680	11.26 +- 0.32	25.46	698	11.06 +- 0.31
30.30	680	11.23 +- 0.33	30.52	698	11.21 +- 0.32
40.36	680	11.76 +- 0.23	40.63	698	11.70 +- 0.23
50.39	680	12.17 +- 0.35	50.72	698	11.85 +- 0.34
60.45	680	10.95 +- 0.34	60.81	698	11.35 +- 0.35
70.47	680	10.70 +- 0.32	70.87	698	10.38 +- 0.31
80.48	680	8.91 +- 0.27	80.89	698	8.93 +- 0.27
6.05	715	17.28 +- 0.67	6.09	733	14.92 +- 0.61
8.01	715	14.56 +- 0.61	8.07	733	14.14 +- 0.59
10.16	715	14.85 +- 0.47	10.23	733	13.45 +- 0.45
12.11	715	13.95 +- 0.45	12.20	733	12.13 +- 0.42
14.07	715	12.72 +- 0.43	14.17	733	11.80 +- 0.41
16.05	715	12.85 +- 0.37	16.16	733	11.17 +- 0.34
19.99	715	11.19 +- 0.41	20.13	733	10.34 +- 0.38
24.94	715	10.20 +- 0.53	25.11	733	9.54 +- 0.50
29.90	715	11.27 +- 0.48	30.10	733	10.16 +- 0.45
34.86	715	10.50 +- 0.55	35.09	733	9.64 +- 0.51
39.83	715	11.70 +- 0.34	40.10	733	10.53 +- 0.31
49.77	715	11.79 +- 0.61	50.08	733	10.63 +- 0.55
59.74	715	11.67 +- 0.61	60.09	733	9.99 +- 0.55
69.70	715	10.83 +- 0.60	70.09	733	10.74 +- 0.58
79.68	715	9.66 +- 0.31	80.08	733	9.20 +- 0.29
6.14	752	13.53 +- 0.58	6.19	772	14.33 +- 0.56
8.13	752	14.53 +- 0.57	8.19	772	13.44 +- 0.54
10.31	752	12.50 +- 0.41	10.39	772	11.68 +- 0.40
12.29	752	11.69 +- 0.40	12.38	772	11.49 +- 0.39
14.27	752	11.32 +- 0.39	14.39	772	9.97 +- 0.36
16.28	752	10.09 +- 0.32	16.40	772	9.59 +- 0.31
20.28	752	9.61 +- 0.36	20.43	772	9.03 +- 0.34
25.29	752	9.71 +- 0.49	25.48	772	8.58 +- 0.46
30.32	752	9.11 +- 0.41	30.54	772	8.43 +- 0.39
35.34	752	8.87 +- 0.48	35.60	772	8.78 +- 0.47
40.37	752	9.54 +- 0.29	40.66	772	8.71 +- 0.27
50.42	752	10.08 +- 0.52	50.76	772	8.63 +- 0.47
60.46	752	9.60 +- 0.52	60.85	772	7.98 +- 0.45
70.49	752	9.38 +- 0.52	70.91	772	7.90 +- 0.45
80.50	752	7.99 +- 0.26	80.94	772	6.85 +- 0.23

CM ANGLE	K LAB	CROSS SECTION	CM ANGLE	K LAB	CROSS SECTION
6.06	793	14.51 +- 0.54	6.10	813	14.41 +- 0.51
8.02	793	12.67 +- 0.49	8.08	813	13.06 +- 0.49
10.18	793	12.25 +- 0.30	10.25	813	12.01 +- 0.29
12.12	793	10.98 +- 0.40	12.21	813	11.36 +- 0.39
14.07	793	10.17 +- 0.27	14.18	813	10.67 +- 0.26
16.04	793	9.66 +- 0.37	16.16	813	9.45 +- 0.35
18.01	793	9.60 +- 0.36	18.15	813	9.39 +- 0.35
19.99	793	8.86 +- 0.26	20.14	813	8.37 +- 0.25
24.94	793	8.71 +- 0.42	25.12	813	8.69 +- 0.41
29.88	793	8.28 +- 0.25	30.10	813	8.16 +- 0.24
34.86	793	7.64 +- 0.33	35.10	813	7.94 +- 0.33
39.83	793	7.88 +- 0.13	40.10	813	7.45 +- 0.12
49.75	793	7.09 +- 0.21	50.08	813	6.35 +- 0.19
59.71	793	6.30 +- 0.32	60.08	813	5.50 +- 0.28
69.68	793	5.72 +- 0.22	70.08	813	4.80 +- 0.20
79.67	793	5.64 +- 0.32	80.09	813	4.36 +- 0.27
6.15	834	14.14 +- 0.50	6.20	857	13.28 +- 0.47
8.15	834	13.34 +- 0.48	8.21	857	12.22 +- 0.45
10.33	834	11.24 +- 0.27	10.42	857	11.16 +- 0.26
12.31	834	10.81 +- 0.37	12.41	857	10.28 +- 0.36
14.29	834	9.88 +- 0.25	14.41	857	9.64 +- 0.24
16.29	834	8.87 +- 0.33	16.42	857	8.70 +- 0.32
18.29	834	8.20 +- 0.32	18.44	857	8.33 +- 0.32
20.29	834	7.88 +- 0.24	20.47	857	8.38 +- 0.24
25.31	834	7.66 +- 0.38	25.52	857	8.05 +- 0.38
30.32	834	7.73 +- 0.22	30.57	857	7.43 +- 0.22
35.37	834	7.36 +- 0.31	35.65	857	7.63 +- 0.31
40.39	834	7.05 +- 0.12	40.70	857	6.88 +- 0.11
50.43	834	5.90 +- 0.18	50.80	857	5.80 +- 0.18
60.47	834	4.98 +- 0.27	60.89	857	4.90 +- 0.26
70.50	834	4.04 +- 0.17	70.96	857	3.58 +- 0.16
80.52	834	3.99 +- 0.25	80.99	857	3.09 +- 0.21
6.05	880	13.88 +- 0.42	6.10	902	12.30 +- 0.38
8.00	880	11.70 +- 0.48	8.06	902	11.53 +- 0.45
10.16	880	10.64 +- 0.39	10.24	902	10.38 +- 0.38
12.11	880	10.55 +- 0.28	12.21	902	9.60 +- 0.26
14.07	880	9.55 +- 0.37	14.18	902	9.34 +- 0.36
16.06	880	9.32 +- 0.25	16.18	902	8.47 +- 0.24
19.98	880	8.42 +- 0.34	20.12	902	8.17 +- 0.33
29.87	880	7.92 +- 0.24	30.10	902	8.43 +- 0.24
39.80	880	7.25 +- 0.14	40.09	902	7.81 +- 0.14
49.74	880	6.51 +- 0.22	50.08	902	6.81 +- 0.22
59.68	880	4.89 +- 0.23	60.06	902	5.12 +- 0.23
69.64	880	3.31 +- 0.24	70.07	902	3.39 +- 0.24
79.62	880	2.69 +- 0.23	80.06	902	2.70 +- 0.23

CM ANGLE	K LAB	CROSS SECTION	CM ANGLE	K LAB	CROSS SECTION
6.15	926	12.37 +- 0.37	6.20	951	10.76 +- 0.35
8.13	926	10.80 +- 0.43	8.20	951	8.84 +- 0.38
10.32	926	9.69 +- 0.35	10.41	951	8.22 +- 0.32
12.31	926	9.62 +- 0.25	12.41	951	8.69 +- 0.23
14.30	926	8.48 +- 0.32	14.42	951	7.74 +- 0.31
16.31	926	8.31 +- 0.23	16.44	951	7.90 +- 0.22
20.29	926	8.10 +- 0.33	20.46	951	8.08 +- 0.32
30.33	926	7.92 +- 0.23	30.59	951	8.10 +- 0.23
40.40	926	7.92 +- 0.14	40.72	951	8.41 +- 0.15
50.45	926	6.93 +- 0.23	50.83	951	7.57 +- 0.24
60.48	926	5.28 +- 0.23	60.90	951	5.34 +- 0.23
70.52	926	3.59 +- 0.24	70.98	951	3.74 +- 0.25
80.53	926	2.89 +- 0.22	81.01	951	2.54 +- 0.20
6.06	977	9.95 +- 0.26	6.11	1002	9.37 +- 0.24
8.02	977	9.22 +- 0.34	8.09	1002	7.99 +- 0.31
10.19	977	8.23 +- 0.25	10.27	1002	7.17 +- 0.22
12.12	977	8.20 +- 0.19	12.22	1002	6.98 +- 0.17
14.09	977	7.95 +- 0.22	14.21	1002	7.33 +- 0.20
16.04	977	8.00 +- 0.22	16.17	1002	7.40 +- 0.20
19.98	977	7.55 +- 0.23	20.15	1002	7.56 +- 0.23
24.92	977	8.64 +- 0.14	25.13	1002	8.62 +- 0.13
29.86	977	8.94 +- 0.20	30.10	1002	8.80 +- 0.20
34.82	977	9.42 +- 0.18	35.09	1002	9.47 +- 0.18
39.77	977	9.51 +- 0.12	40.08	1002	9.44 +- 0.12
44.75	977	9.38 +- 0.20	45.09	1002	9.51 +- 0.20
49.71	977	8.39 +- 0.26	50.07	1002	8.25 +- 0.25
54.69	977	7.38 +- 0.20	55.07	1002	8.08 +- 0.21
59.66	977	6.81 +- 0.23	60.07	1002	6.42 +- 0.22
64.64	977	5.64 +- 0.18	65.07	1002	5.75 +- 0.18
69.61	977	4.75 +- 0.10	70.06	1002	4.61 +- 0.09
74.60	977	3.58 +- 0.15	75.06	1002	4.01 +- 0.15
79.59	977	2.89 +- 0.15	80.05	1002	3.04 +- 0.15
84.59	977	2.38 +- 0.13	85.06	1002	2.42 +- 0.13
89.58	977	2.15 +- 0.08	90.05	1002	2.04 +- 0.07

CM ANGLE	K LAB	CROSS SECTION
6.17	1028	7.76 +- 0.21
8.16	1028	7.52 +- 0.29
10.36	1028	6.92 +- 0.21
12.32	1028	6.59 +- 0.16
14.33	1028	6.95 +- 0.19
16.31	1028	6.90 +- 0.19
20.32	1028	6.98 +- 0.21
25.33	1028	8.43 +- 0.13
30.34	1028	8.81 +- 0.19
35.37	1028	9.49 +- 0.17
40.39	1028	9.37 +- 0.12
45.43	1028	9.50 +- 0.20
50.44	1028	8.15 +- 0.24
55.47	1028	7.70 +- 0.20
60.49	1028	6.12 +- 0.21
65.51	1028	5.68 +- 0.17
70.52	1028	4.52 +- 0.09
75.53	1028	3.64 +- 0.14
80.53	1028	2.78 +- 0.13
85.54	1028	2.24 +- 0.12
90.54	1028	2.02 +- 0.07
6.06	1074	7.03 +- 0.21
8.03	1074	6.38 +- 0.20
10.20	1074	5.83 +- 0.16
12.13	1074	5.75 +- 0.15
14.08	1074	5.92 +- 0.20
16.04	1074	5.99 +- 0.15
19.99	1074	6.58 +- 0.16
24.92	1074	7.54 +- 0.18
29.85	1074	7.38 +- 0.13
34.81	1074	8.19 +- 0.15
39.77	1074	8.28 +- 0.08
44.73	1074	8.08 +- 0.17
49.70	1074	7.29 +- 0.18
54.67	1074	6.77 +- 0.17
59.64	1074	5.44 +- 0.10
64.61	1074	4.63 +- 0.14
69.59	1074	3.83 +- 0.08
74.57	1074	2.80 +- 0.15
79.56	1074	2.51 +- 0.13
84.56	1074	1.86 +- 0.13
89.55	1074	1.69 +- 0.11

CM ANGLE	K LAB	CROSS SECTION
6.22	1056	7.45 +- 0.20
8.23	1056	6.81 +- 0.27
10.45	1056	6.00 +- 0.19
12.44	1056	5.69 +- 0.15
14.46	1056	5.92 +- 0.17
16.45	1056	6.14 +- 0.18
20.49	1056	6.72 +- 0.21
25.55	1056	7.78 +- 0.12
30.60	1056	8.00 +- 0.18
35.67	1056	8.24 +- 0.16
40.72	1056	8.67 +- 0.11
45.79	1056	8.49 +- 0.18
50.84	1056	7.56 +- 0.23
55.90	1056	6.72 +- 0.17
60.94	1056	5.68 +- 0.20
65.98	1056	4.96 +- 0.15
71.01	1056	4.01 +- 0.08
76.03	1056	3.41 +- 0.13
81.04	1056	2.56 +- 0.12
86.05	1056	2.09 +- 0.11
91.06	1056	1.74 +- 0.06
6.11	1102	6.48 +- 0.20
8.09	1102	5.34 +- 0.17
10.28	1102	5.31 +- 0.14
12.24	1102	5.16 +- 0.14
14.20	1102	5.28 +- 0.18
16.18	1102	5.48 +- 0.14
20.16	1102	5.84 +- 0.15
25.13	1102	6.41 +- 0.16
30.10	1102	6.52 +- 0.12
35.10	1102	6.43 +- 0.13
40.08	1102	6.81 +- 0.07
45.09	1102	6.39 +- 0.15
50.08	1102	6.03 +- 0.16
55.08	1102	5.28 +- 0.14
60.08	1102	4.24 +- 0.09
65.06	1102	3.95 +- 0.12
70.05	1102	3.03 +- 0.07
75.06	1102	2.47 +- 0.13
80.05	1102	1.91 +- 0.11
85.06	1102	1.55 +- 0.11
90.05	1102	1.32 +- 0.09

CM ANGLE	K LAB	CROSS SECTION	CM ANGLE	K LAB	CROSS SECTION
6.17	1131	5.51 +- 0.17	6.22	1162	5.34 +- 0.17
8.17	1131	4.95 +- 0.16	8.24	1162	4.49 +- 0.15
10.38	1131	4.48 +- 0.13	10.47	1162	4.03 +- 0.12
12.35	1131	4.64 +- 0.13	12.46	1162	4.13 +- 0.12
14.32	1131	5.13 +- 0.18	14.46	1162	4.45 +- 0.16
16.32	1131	4.77 +- 0.13	16.48	1162	4.17 +- 0.12
20.34	1131	4.92 +- 0.13	20.52	1162	4.52 +- 0.13
25.34	1131	5.37 +- 0.14	25.58	1162	5.05 +- 0.13
30.36	1131	5.67 +- 0.11	30.63	1162	5.02 +- 0.10
35.39	1131	5.52 +- 0.11	35.70	1162	4.72 +- 0.10
40.41	1131	5.62 +- 0.06	40.76	1162	4.73 +- 0.06
45.45	1131	5.20 +- 0.13	45.83	1162	4.42 +- 0.12
50.47	1131	4.75 +- 0.13	50.89	1162	3.82 +- 0.12
55.49	1131	4.42 +- 0.12	55.94	1162	3.33 +- 0.10
60.51	1131	3.39 +- 0.07	60.98	1162	2.60 +- 0.06
65.52	1131	2.91 +- 0.10	66.01	1162	2.20 +- 0.08
70.53	1131	2.43 +- 0.06	71.04	1162	1.82 +- 0.05
75.55	1131	1.68 +- 0.10	76.07	1162	1.38 +- 0.09
80.55	1131	1.68 +- 0.09	81.08	1162	1.19 +- 0.08
85.57	1131	1.26 +- 0.10	86.10	1162	1.03 +- 0.09
90.56	1131	1.21 +- 0.08	91.09	1162	0.89 +- 0.07
6.08	1174	5.80 +- 0.30	6.13	1204	5.01 +- 0.26
8.03	1174	4.70 +- 0.20	8.10	1204	4.15 +- 0.19
10.22	1174	4.64 +- 0.17	10.31	1204	4.16 +- 0.16
12.15	1174	4.39 +- 0.27	12.26	1204	4.09 +- 0.25
14.10	1174	3.91 +- 0.25	14.22	1204	4.10 +- 0.24
16.07	1174	4.44 +- 0.19	16.21	1204	3.92 +- 0.17
20.01	1174	4.18 +- 0.25	20.18	1204	4.13 +- 0.24
24.94	1174	5.30 +- 0.30	25.15	1204	4.52 +- 0.27
29.87	1174	5.13 +- 0.40	30.12	1204	5.21 +- 0.38
34.82	1174	4.38 +- 0.37	35.11	1204	4.77 +- 0.37
39.79	1174	4.69 +- 0.14	40.12	1204	3.96 +- 0.12
49.71	1174	3.85 +- 0.21	50.09	1204	3.24 +- 0.20
59.66	1174	2.63 +- 0.22	60.09	1204	1.98 +- 0.19
69.62	1174	1.48 +- 0.17	70.09	1204	1.62 +- 0.17
79.59	1174	1.06 +- 0.16	80.08	1204	0.95 +- 0.14
89.58	1174	0.68 +- 0.07	90.09	1204	0.71 +- 0.07

CM ANGLE	K LAB	CROSS SECTION	CM ANGLE	K LAB	CROSS SECTION
6.19	1235	4.76 +- 0.25	6.25	1269	4.38 +- 0.24
8.17	1235	3.76 +- 0.17	8.25	1269	3.29 +- 0.16
10.40	1235	3.73 +- 0.14	10.50	1269	3.29 +- 0.14
12.37	1235	3.48 +- 0.24	12.49	1269	3.31 +- 0.22
14.36	1235	3.84 +- 0.23	14.49	1269	3.46 +- 0.22
16.36	1235	3.81 +- 0.17	16.52	1269	3.37 +- 0.16
20.36	1235	3.99 +- 0.23	20.55	1269	4.15 +- 0.24
25.37	1235	4.58 +- 0.27	25.61	1269	4.63 +- 0.26
30.38	1235	4.01 +- 0.33	30.66	1269	3.90 +- 0.33
35.41	1235	4.00 +- 0.34	35.73	1269	4.46 +- 0.36
40.45	1235	3.78 +- 0.12	40.81	1269	3.67 +- 0.11
50.50	1235	2.74 +- 0.17	50.92	1269	2.52 +- 0.17
60.53	1235	1.98 +- 0.18	61.02	1269	1.57 +- 0.16
70.57	1235	1.07 +- 0.13	71.09	1269	1.09 +- 0.14
80.59	1235	0.65 +- 0.11	81.14	1269	0.62 +- 0.12
90.60	1235	0.56 +- 0.06	91.15	1269	0.57 +- 0.06

FIGURE 6

The data are shown as angular distributions together with Moravcsik - equivalent fits.

This experiment

H. A. Thiessen[16]

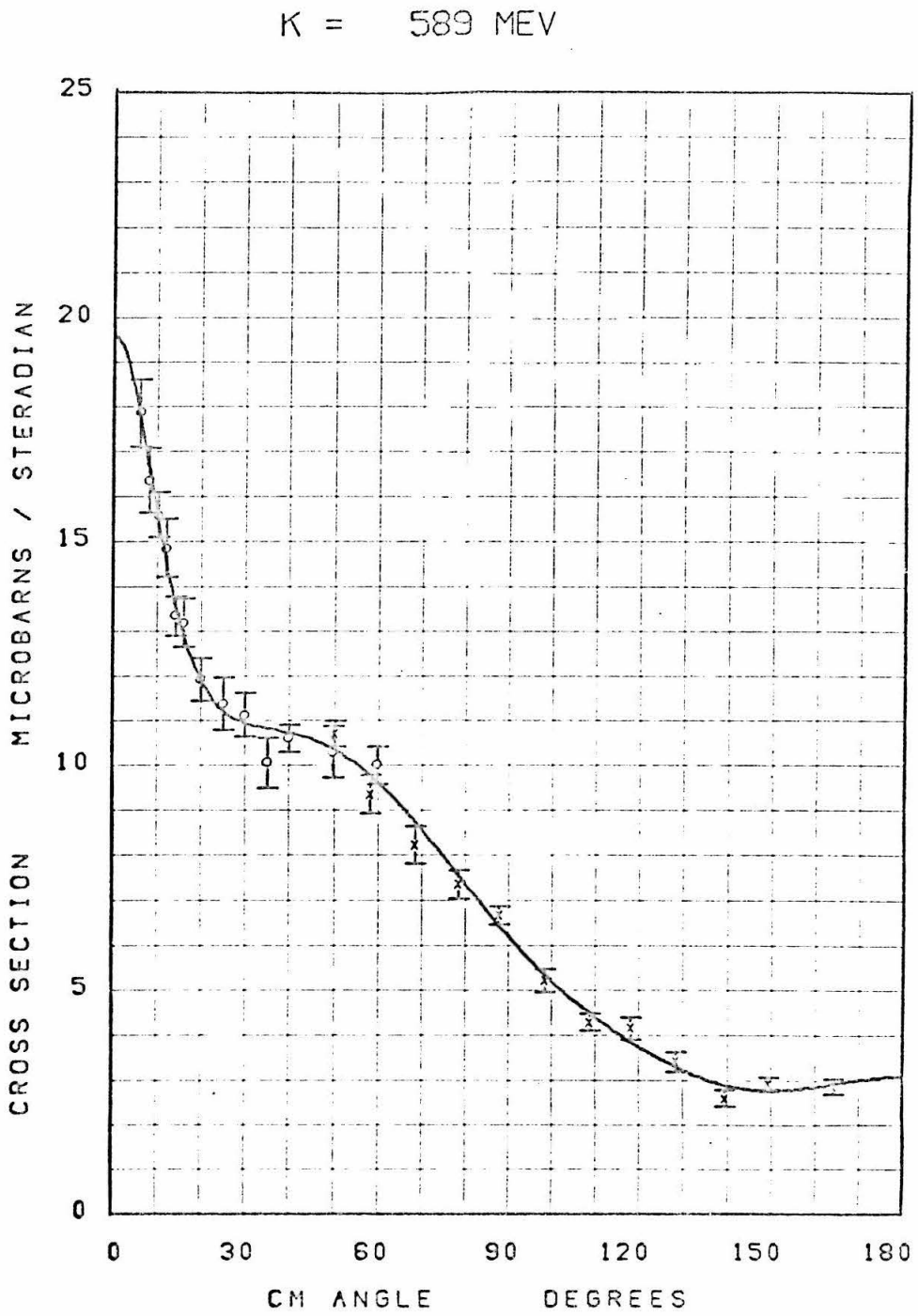
K = 589 MEV
CROSS SECTION MICROBARNS / STERADIAN
25
20
15
10
5
0
0
30
60
90
120
150
180
CM ANGLE DEGREES

FIGURE 6.1

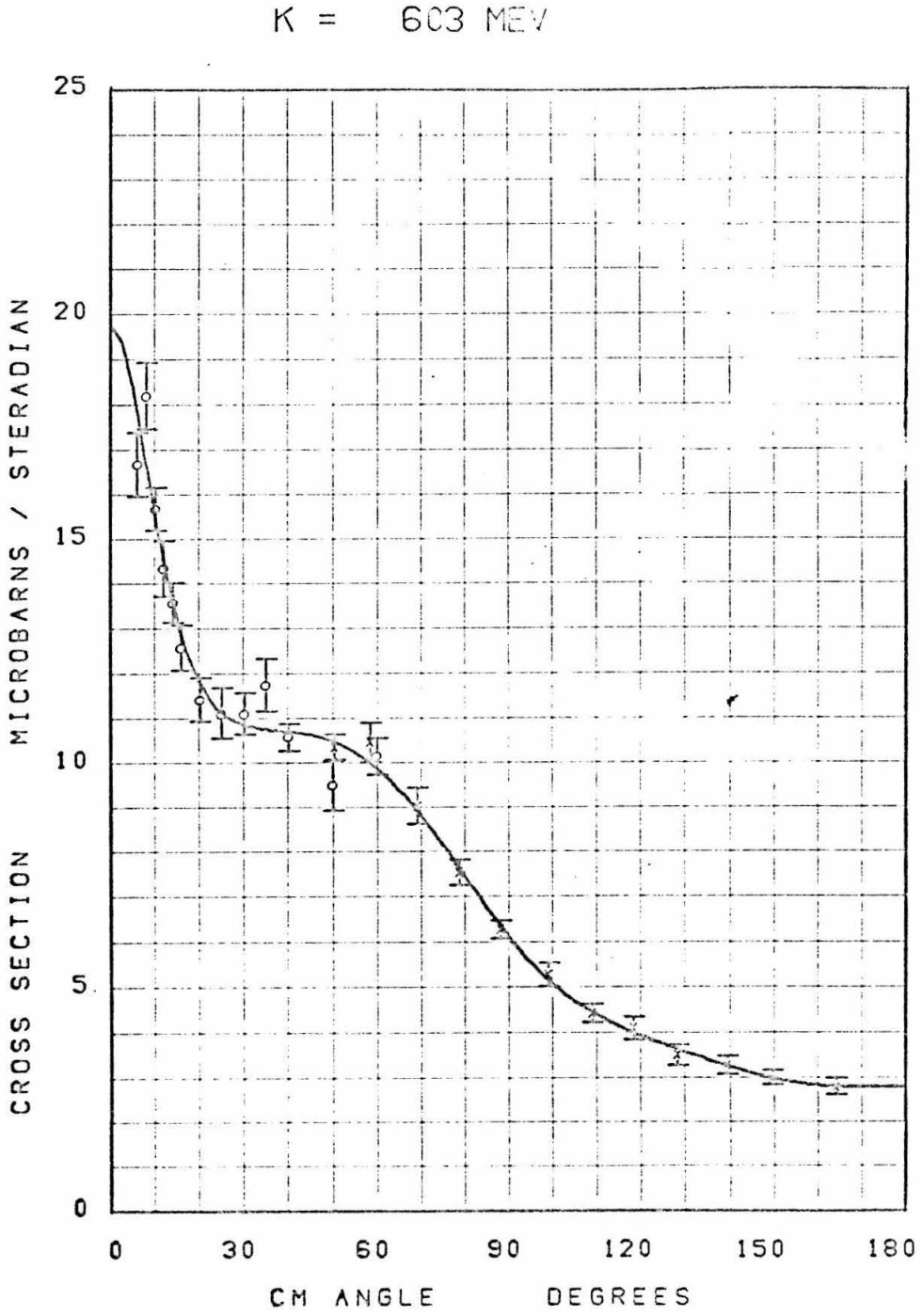
K = 603 MEV
CROSS SECTION MICROBARNS / STERADIAN
25
20
15
10
5
0
0
30
60
90
120
150
180
CM ANGLE DEGREES

FIGURE 6.2

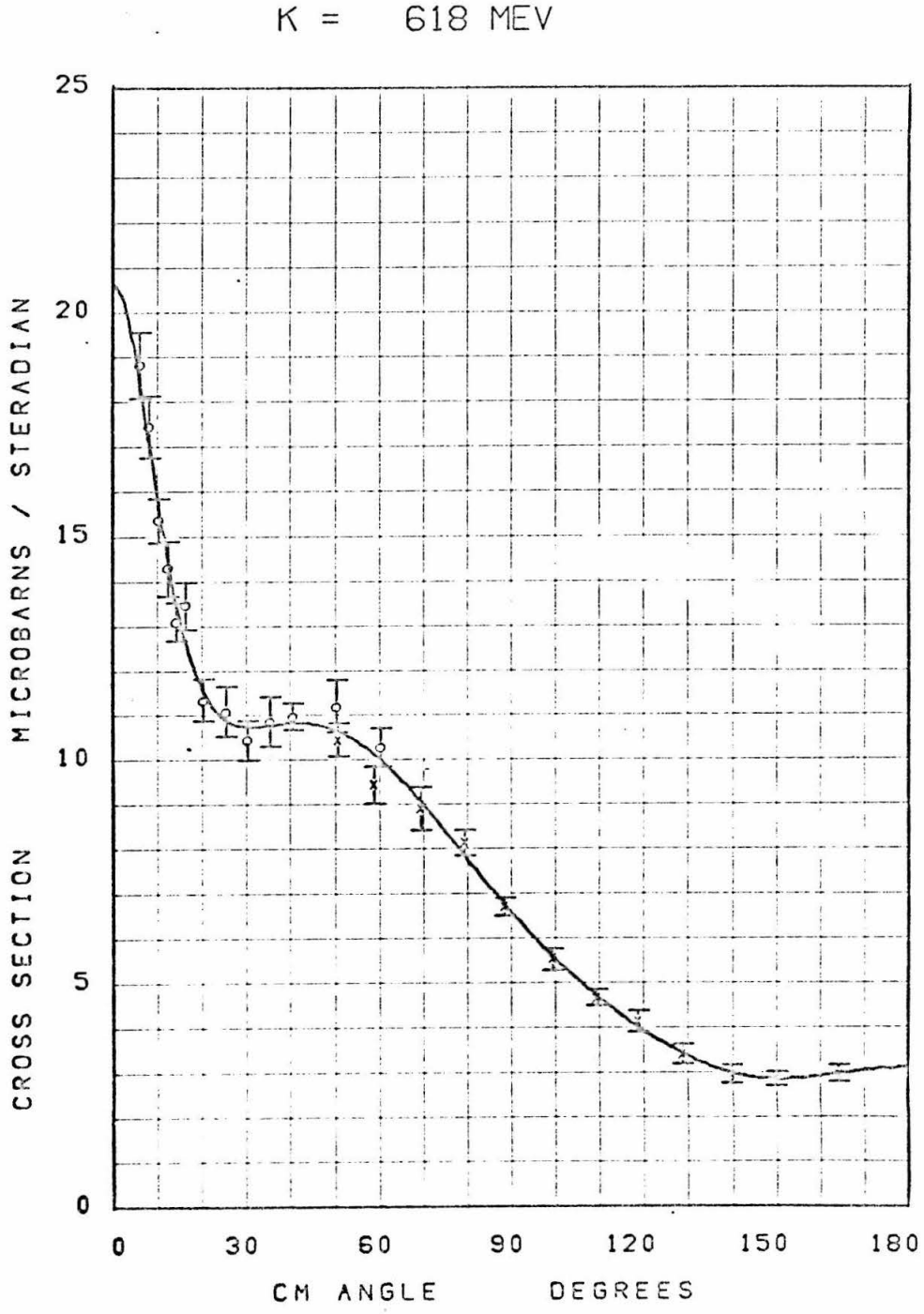
K = 618 MEV
CROSS SECTION MICROBARNS / STERADIAN
25
20
15
10
5
0
0
30
60
90
120
150
180
CM ANGLE DEGREES

FIGURE 6.3

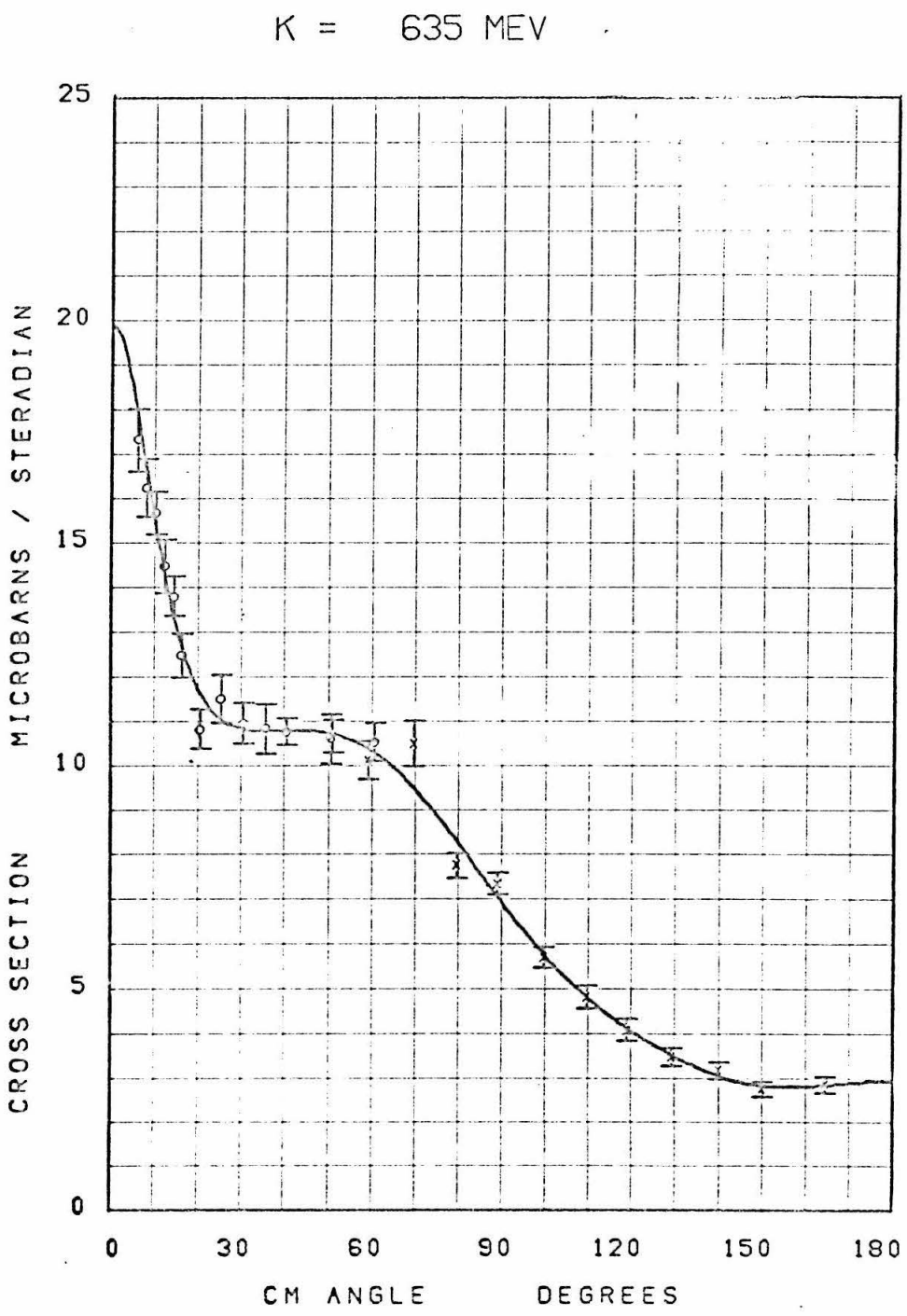
K = 635 MEV
CROSS SECTION MICROBARNS / STERADIAN
25
20
15
10
5
0
0
30
60
90
120
150
180
CM ANGLE DEGREES

FIGURE 6.4

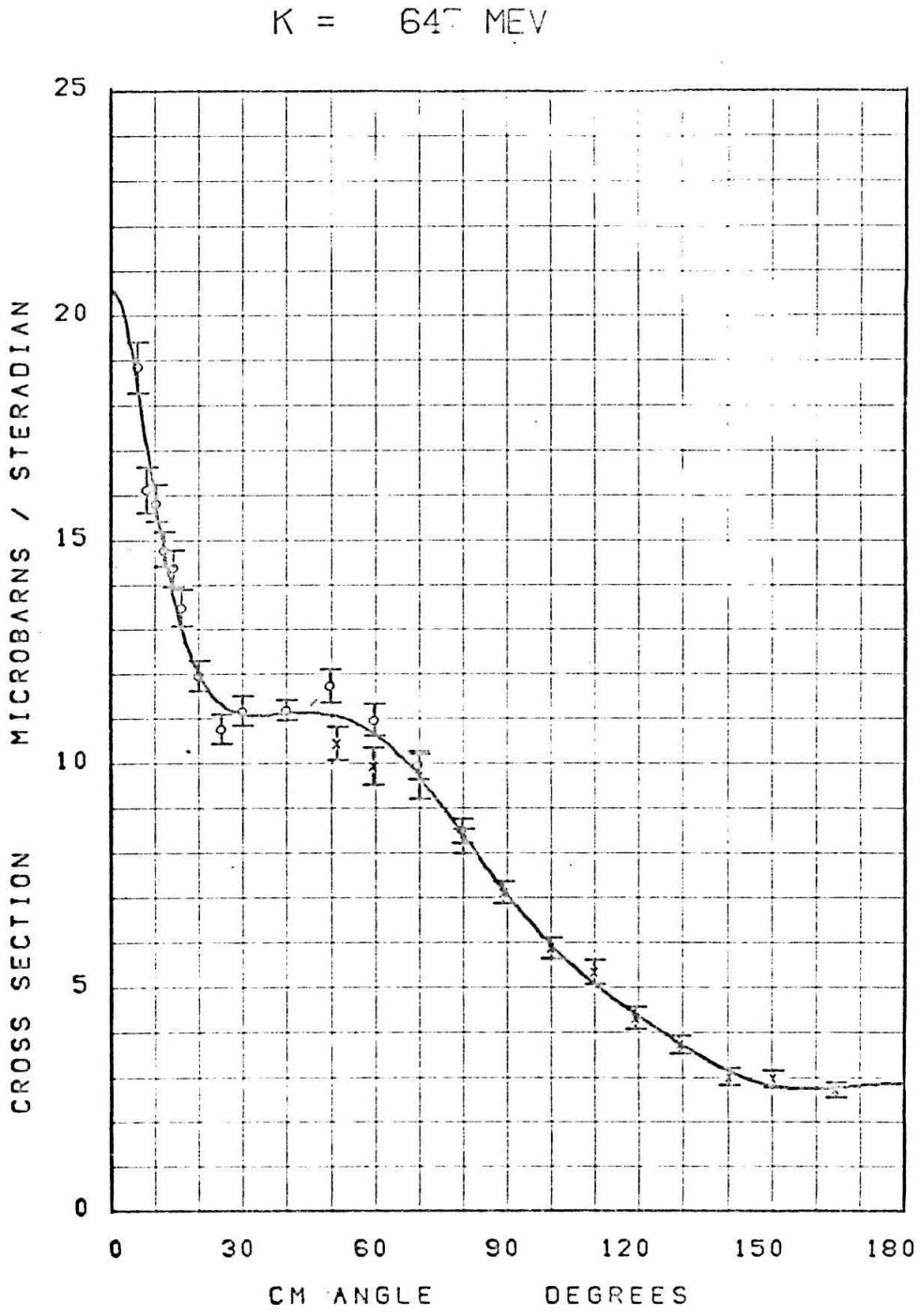
K = 647 MEV
25
20
15
10
5
0
CROSS SECTION MICROBARNS / STERADIAN
0
30
60
90
120
150
180
CM ANGLE DEGREES

FIGURE 6.5

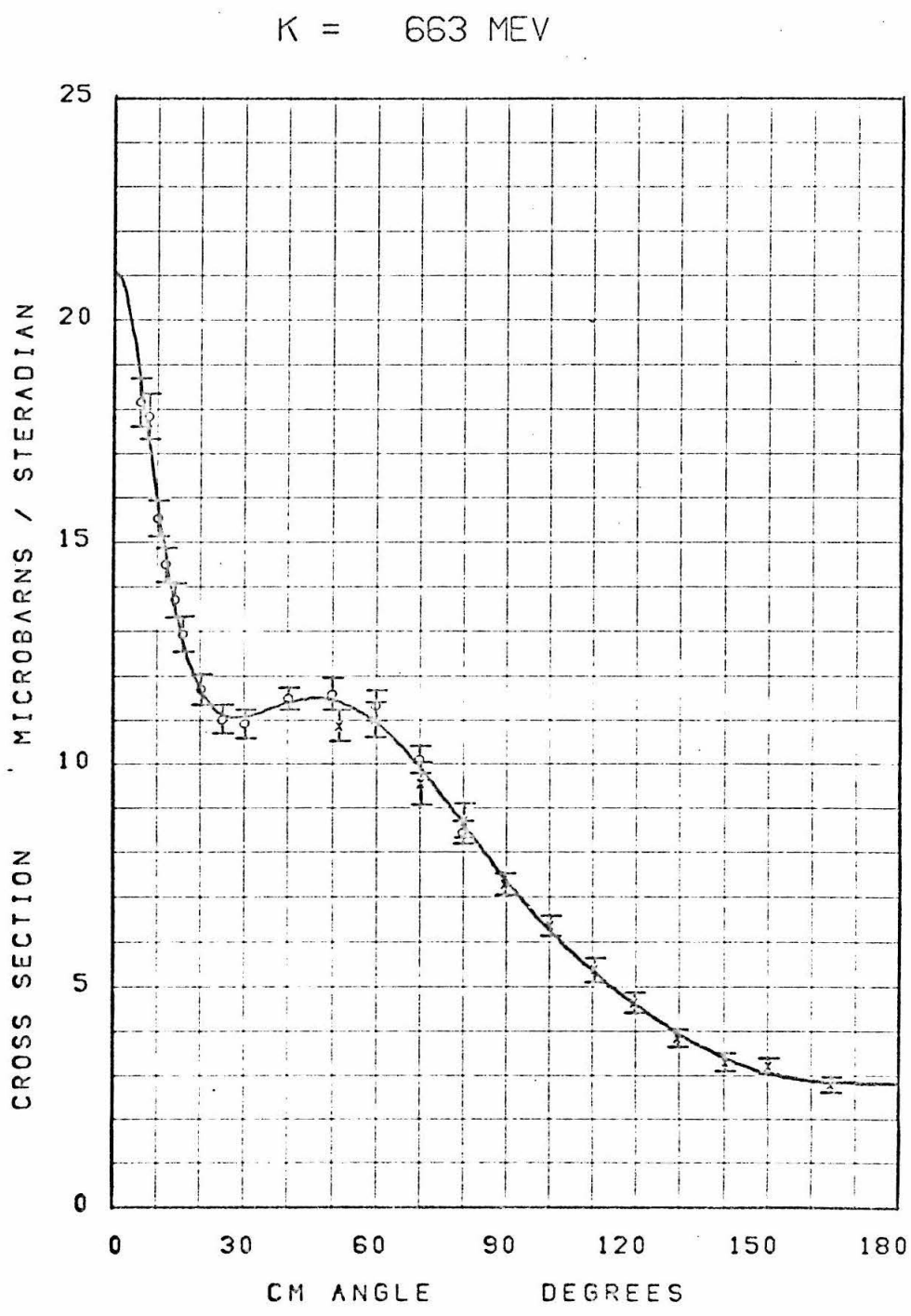
K = 663 MEV
CROSS SECTION MICROBARNS / STERADIAN
25
20
15
10
5
0
0
30
60
90
120
150
180
CM ANGLE DEGREES

FIGURE 6.6

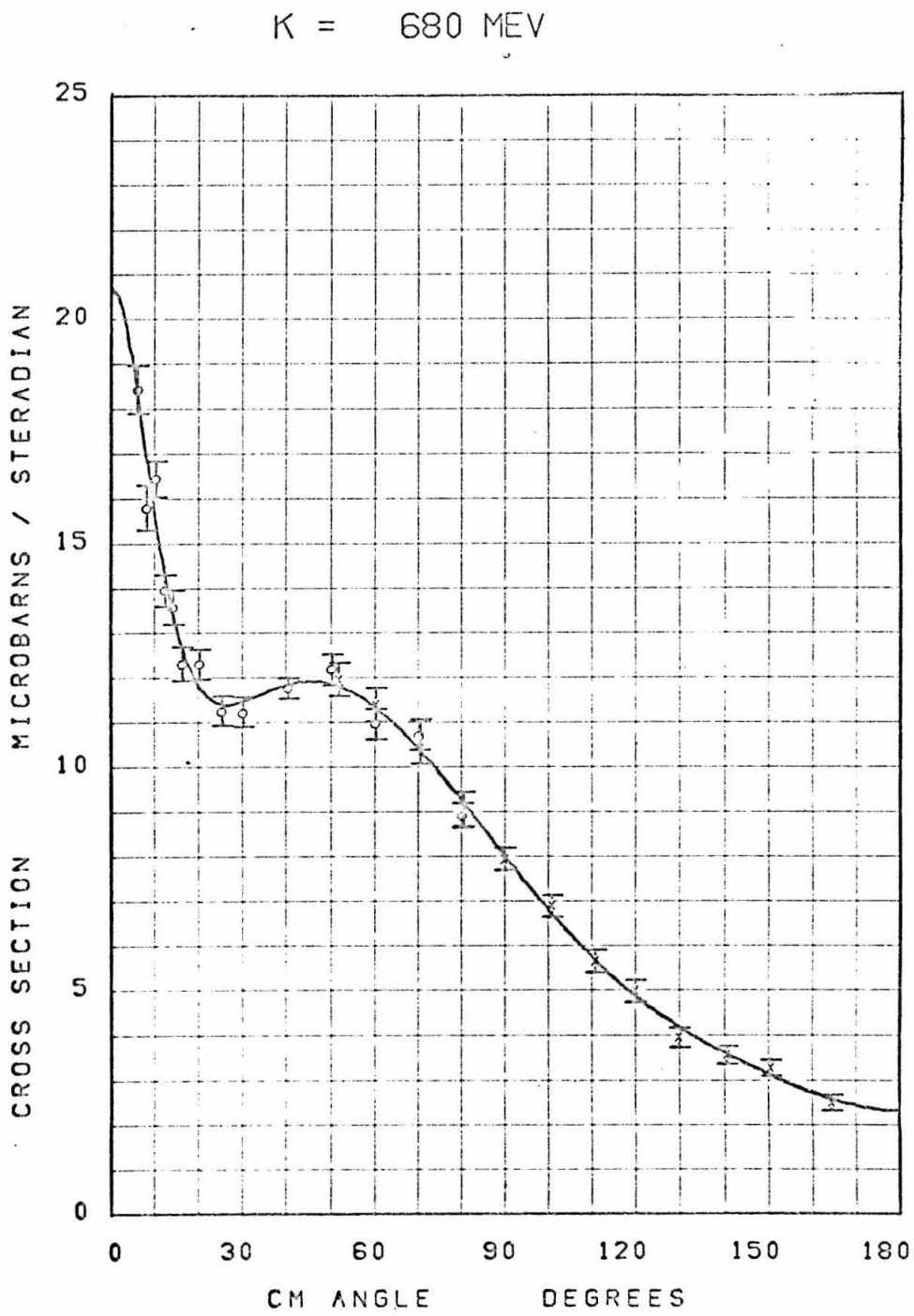
K = 680 MEV
CROSS SECTION MICROBARNS / STERADIAN
25
20
15
10
5
0
0
30
60
90
120
150
180
CM ANGLE DEGREES

FIGURE 6.7

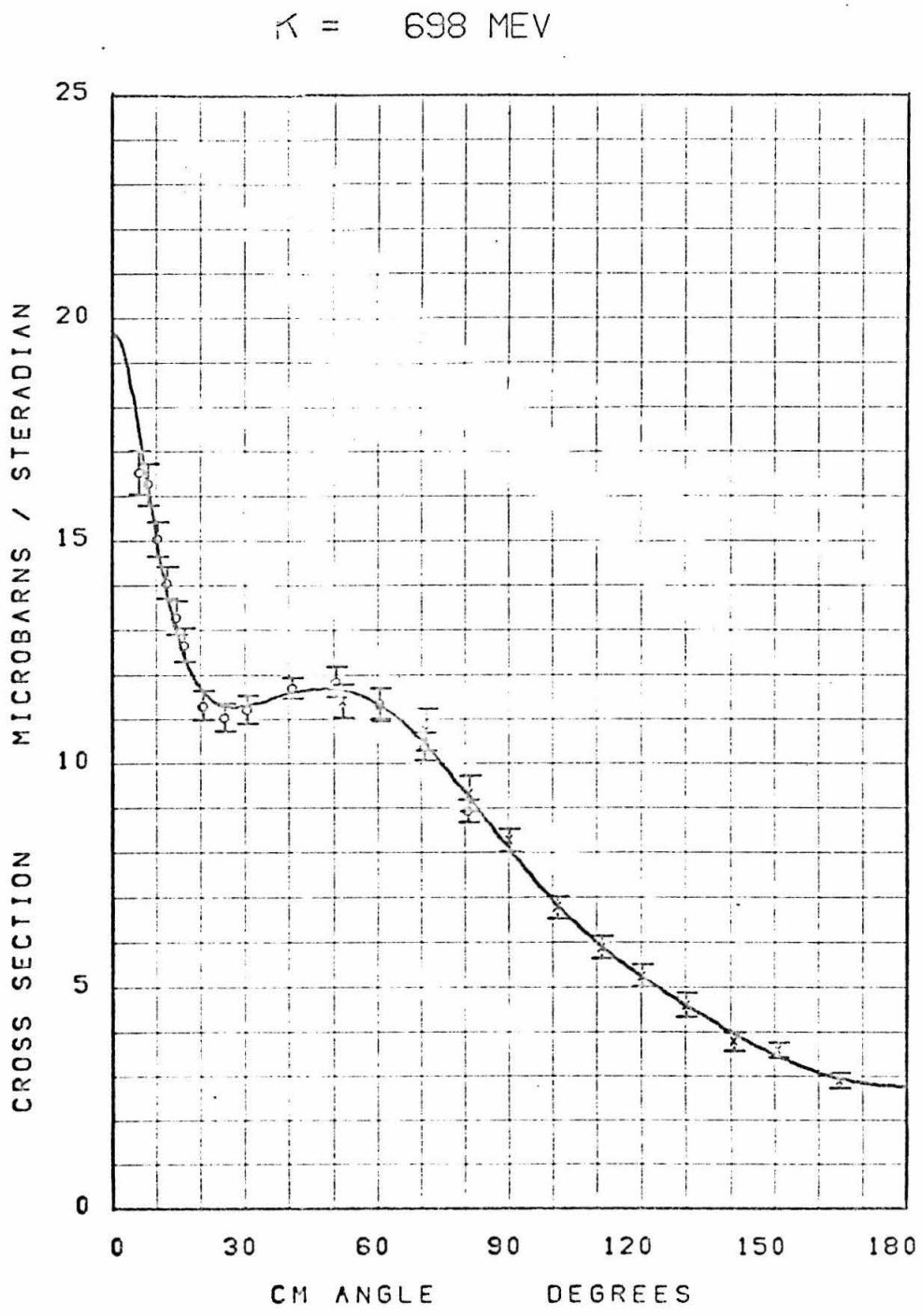
K = 698 MEV
CROSS SECTION MICROBARNS / STERADIAN
25
20
15
10
5
0
0
30
60
90
120
150
180
CM ANGLE DEGREES

FIGURE 6.8

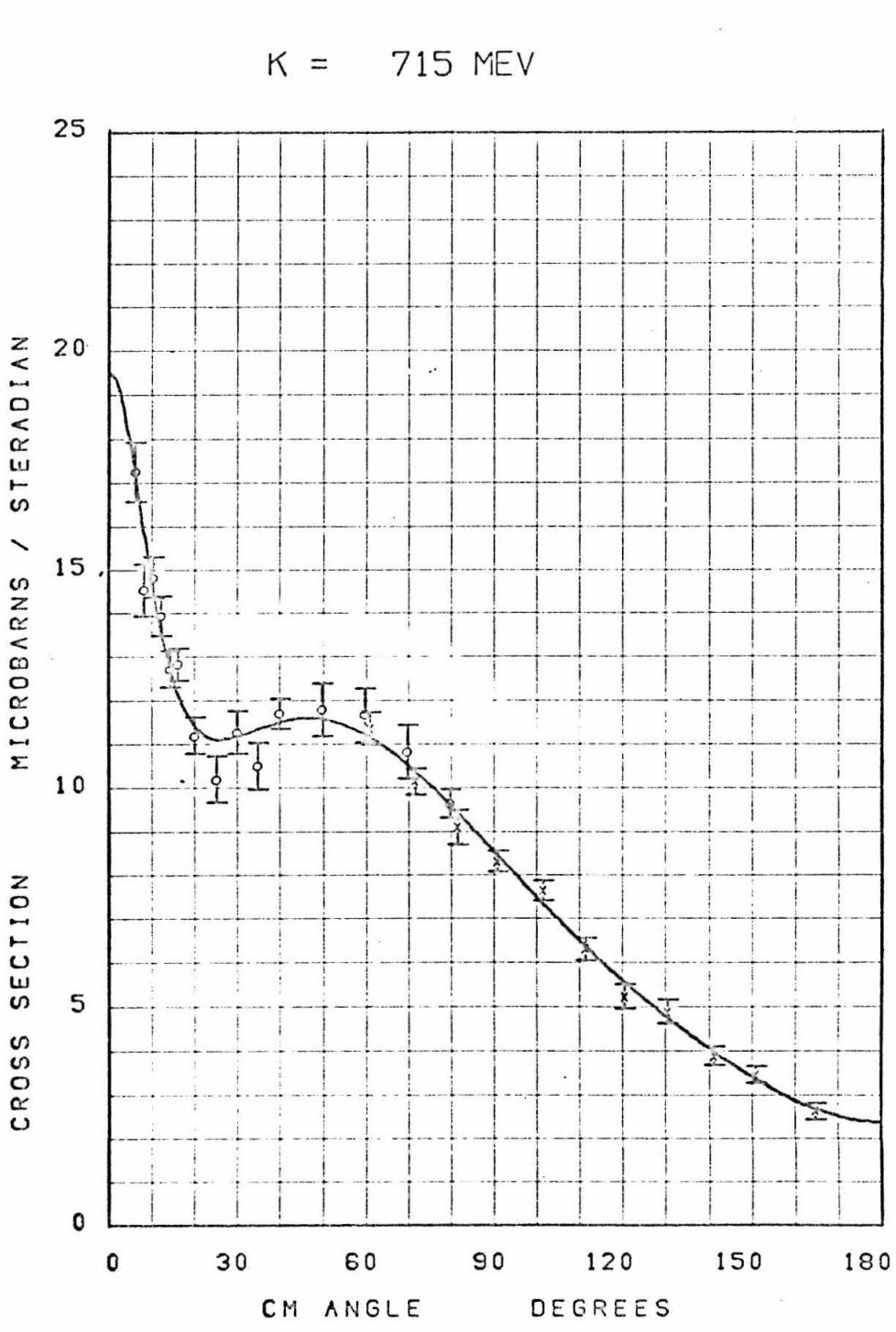
K = 715 MEV
CROSS SECTION MICROBARNS / STERADIAN
25
20
15
10
5
0
0
30
60
90
120
150
180
CM ANGLE DEGREES

FIGURE 6.9

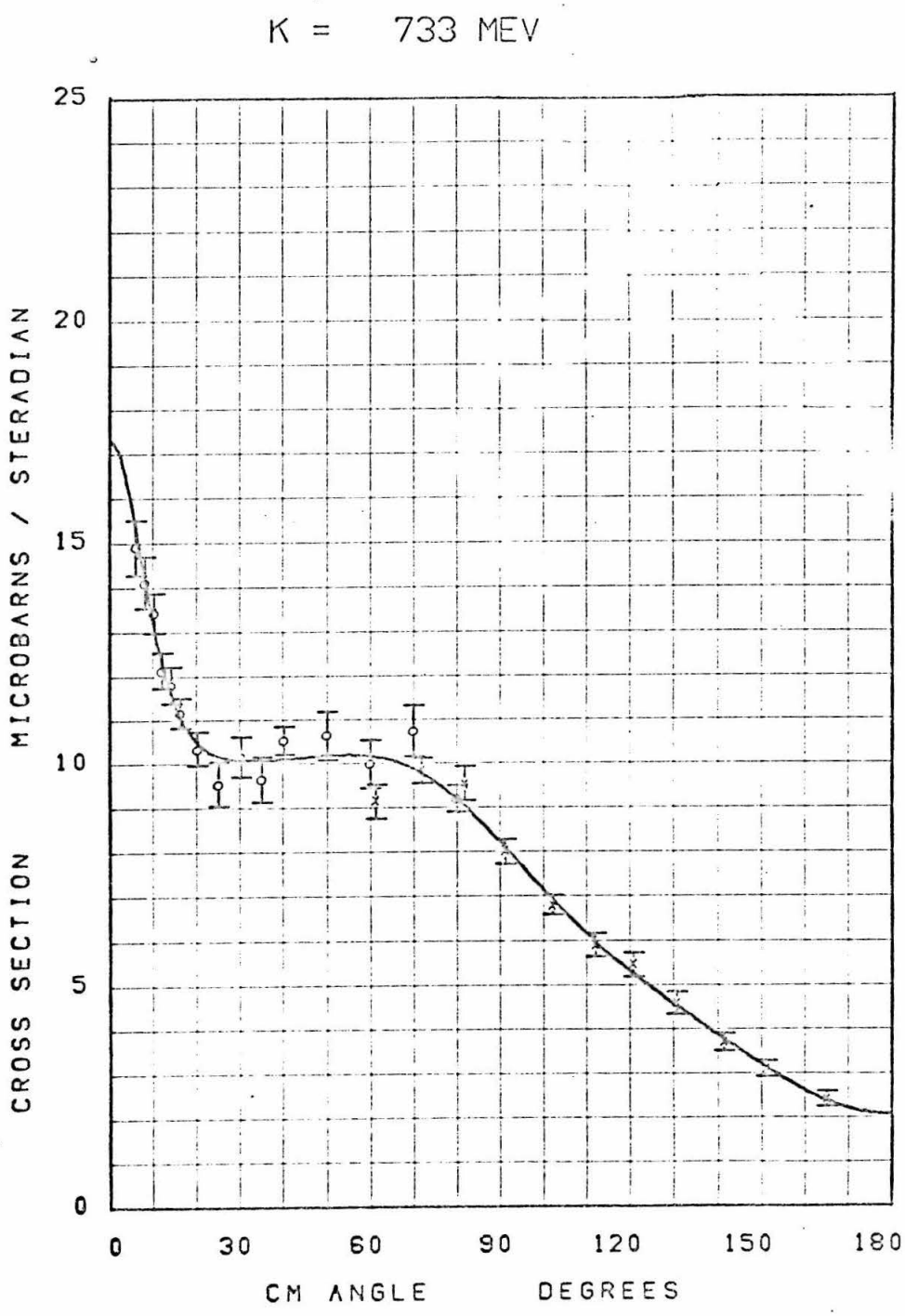
K = 733 MEV
CROSS SECTION MICROBARNS / STERADIAN
25
20
15
10
5
0
0
30
60
90
120
150
180
CM ANGLE DEGREES

FIGURE 6.10

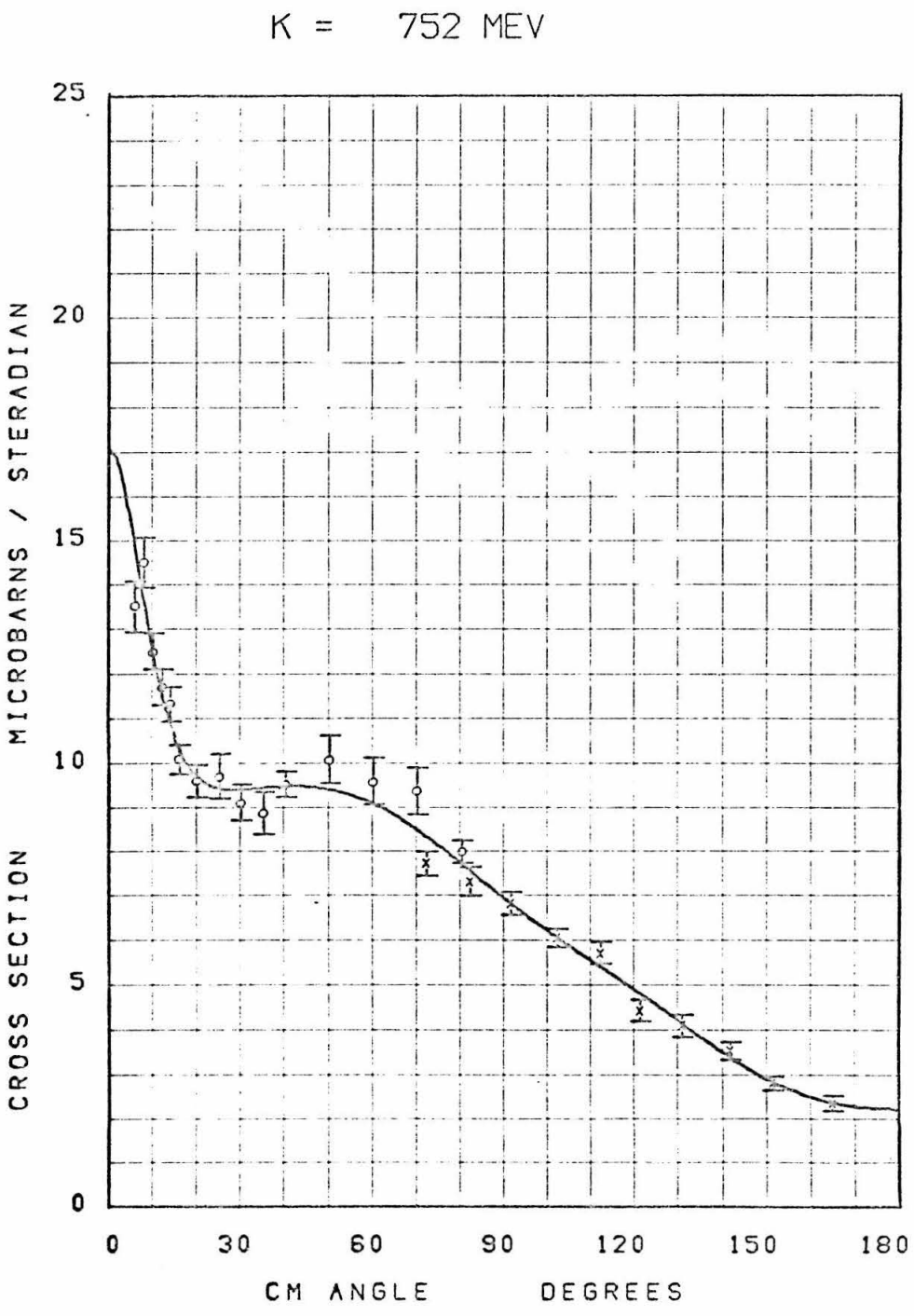
K = 752 MEV
CROSS SECTION MICROBARNS / STERADIAN
25
20
15
10
5
0
0
30
60
90
120
150
180
CM ANGLE DEGREES

FIGURE 6.11

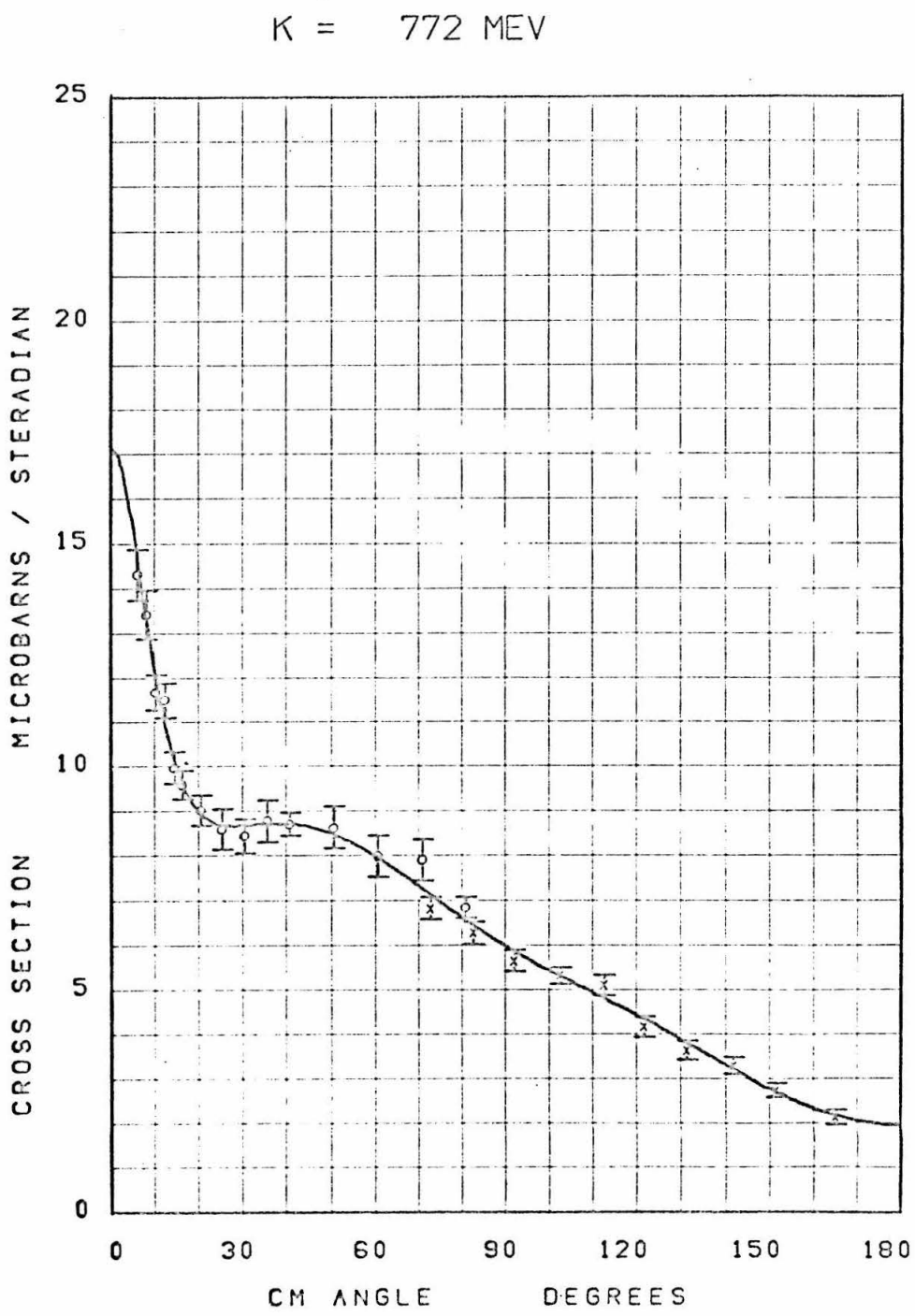
K = 772 MEV
CROSS SECTION MICROBARNS / STERADIAN
25
20
15
10
5
0
0
30
60
90
120
150
180
CM ANGLE DEGREES

FIGURE 6.12

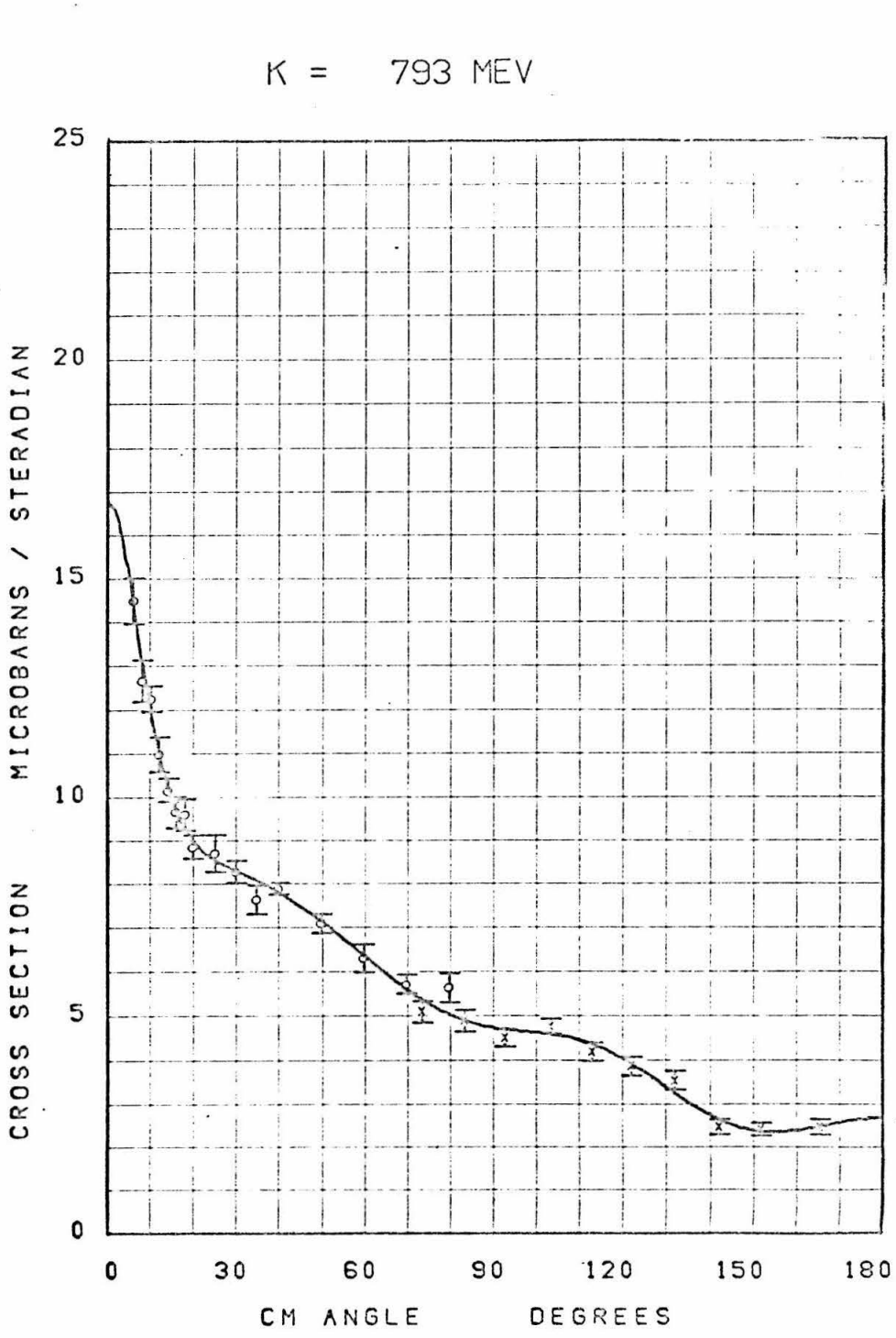
K = 793 MEV
CROSS SECTION MICROBARNS / STERADIAN
25
20
15
10
5
0
0
30
60
90
120
150
180
CM ANGLE DEGREES

FIGURE 6.13

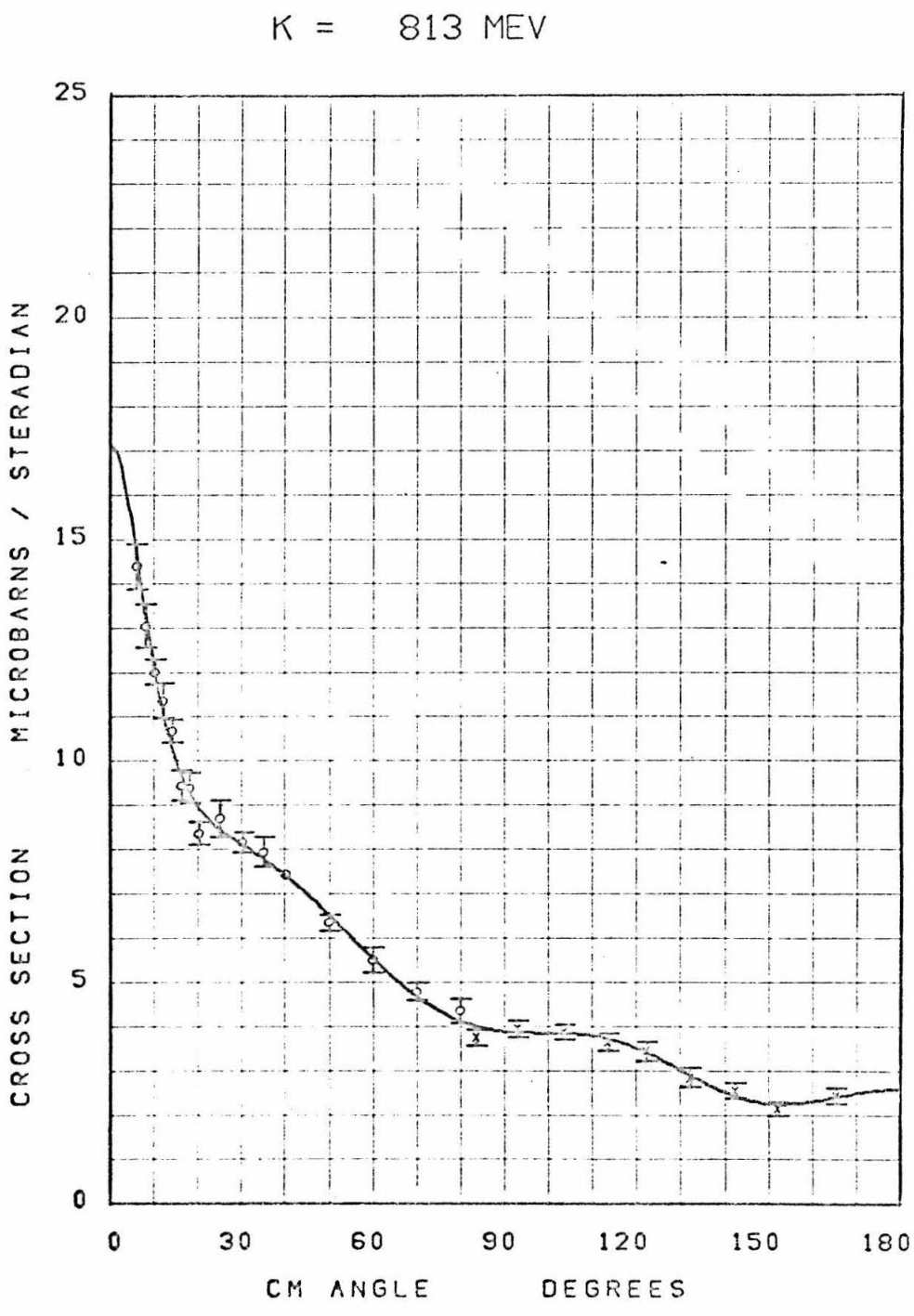
K = 813 MEV
CROSS SECTION MICROBARNS / STERADIAN
25
20
15
10
5
0
0
30
60
90
120
150
180
CM ANGLE DEGREES

FIGURE 6.14

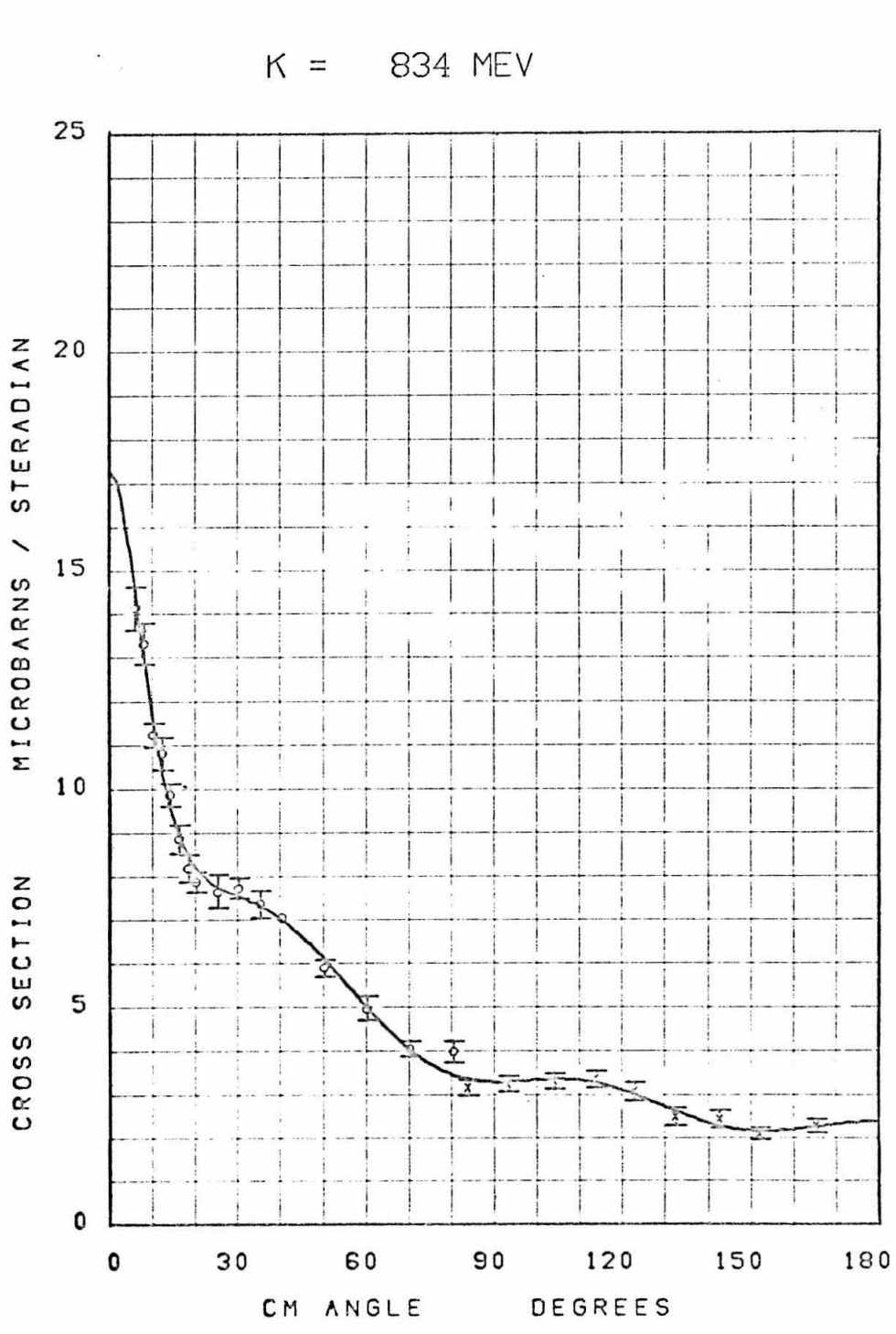
K = 834 MEV
CROSS SECTION MICROBARNS / STERADIAN
25
20
15
10
5
0
0
30
60
90
120
150
180
CM ANGLE DEGREES

FIGURE 6.15

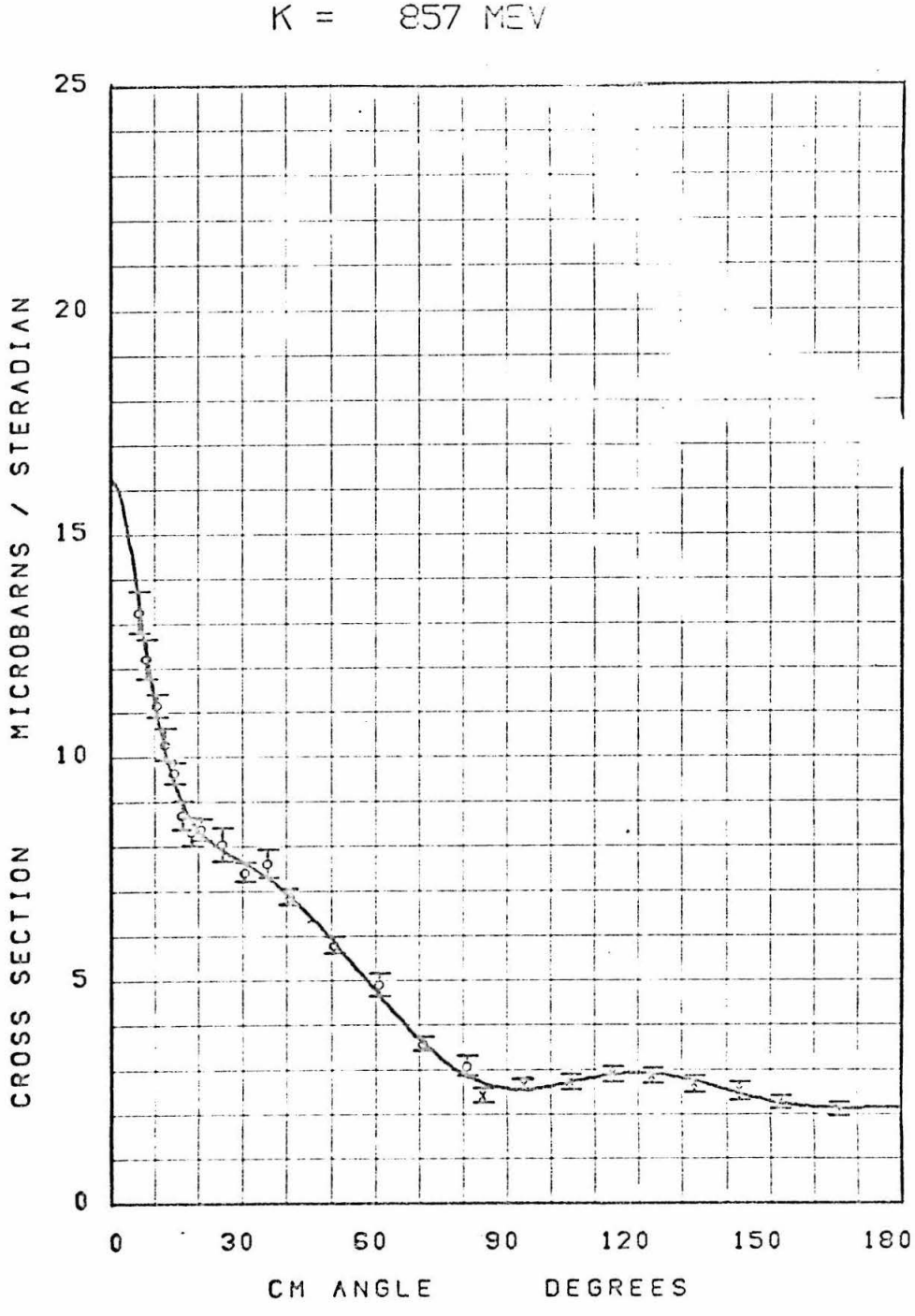
K = 857 MEV
CROSS SECTION MICROBARNS / STERADIAN
25
20
15
10
5
0
0
30
60
90
120
150
180
CM ANGLE DEGREES

FIGURE 6.16

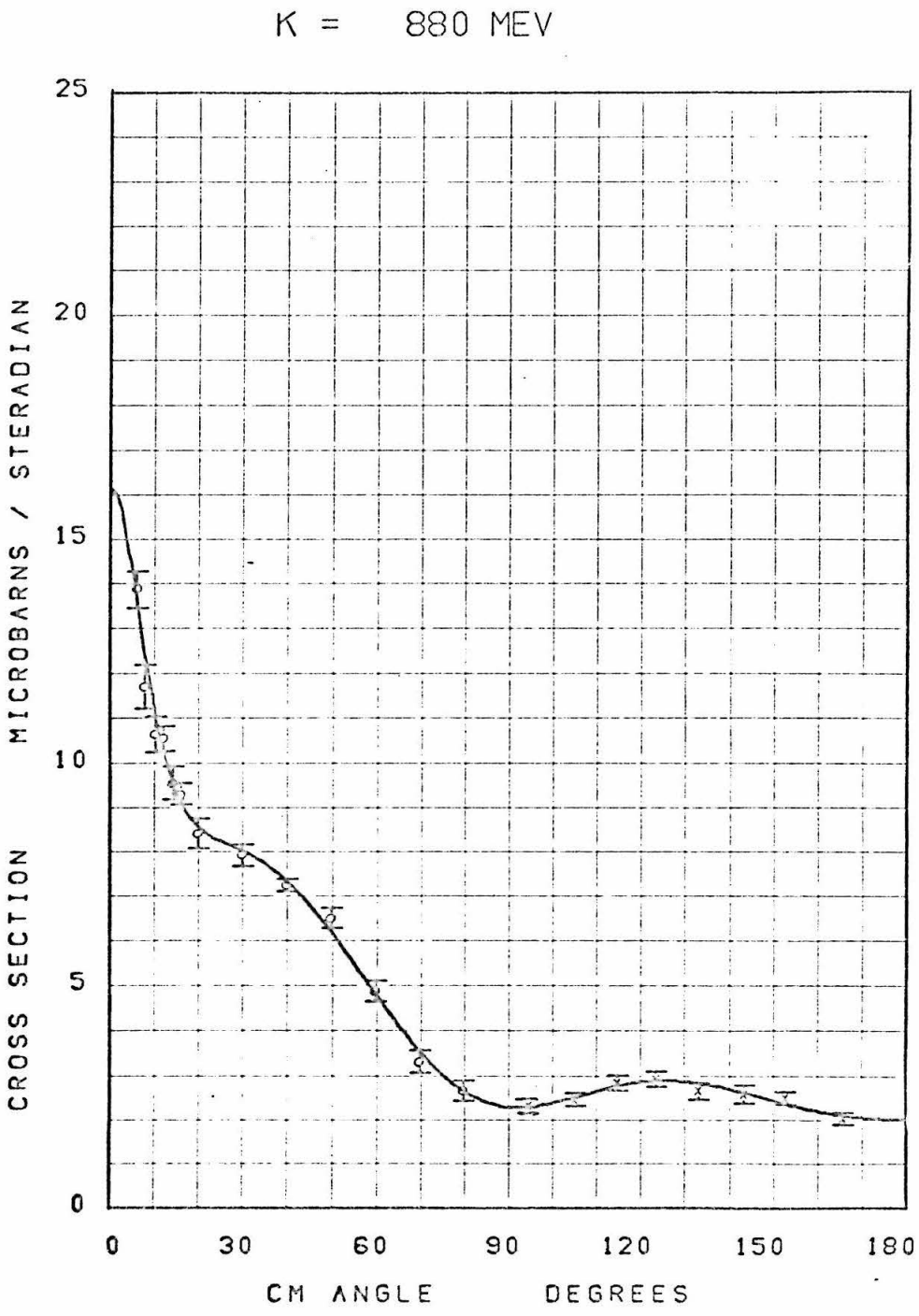
K = 880 MEV
CROSS SECTION MICROBARNS / STERADIAN
25
20
15
10
5
0
0
30
60
90
120
150
180
CM ANGLE DEGREES

FIGURE 6.17

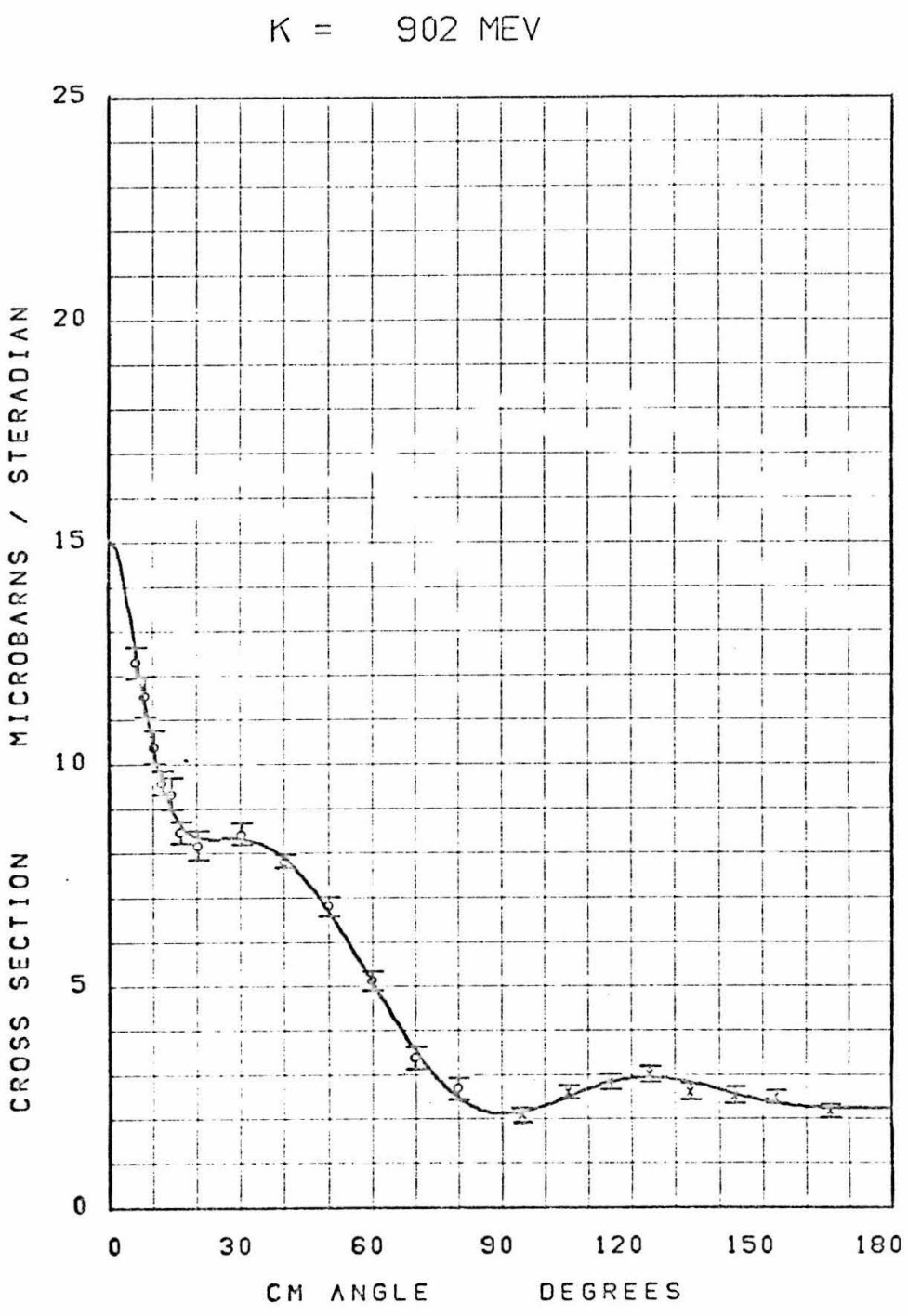
K = 902 MEV
CROSS SECTION MICROBARNS / STERADIAN
25
20
15
10
5
0
0
30
60
90
120
150
180
CM ANGLE DEGREES

FIGURE 6.18

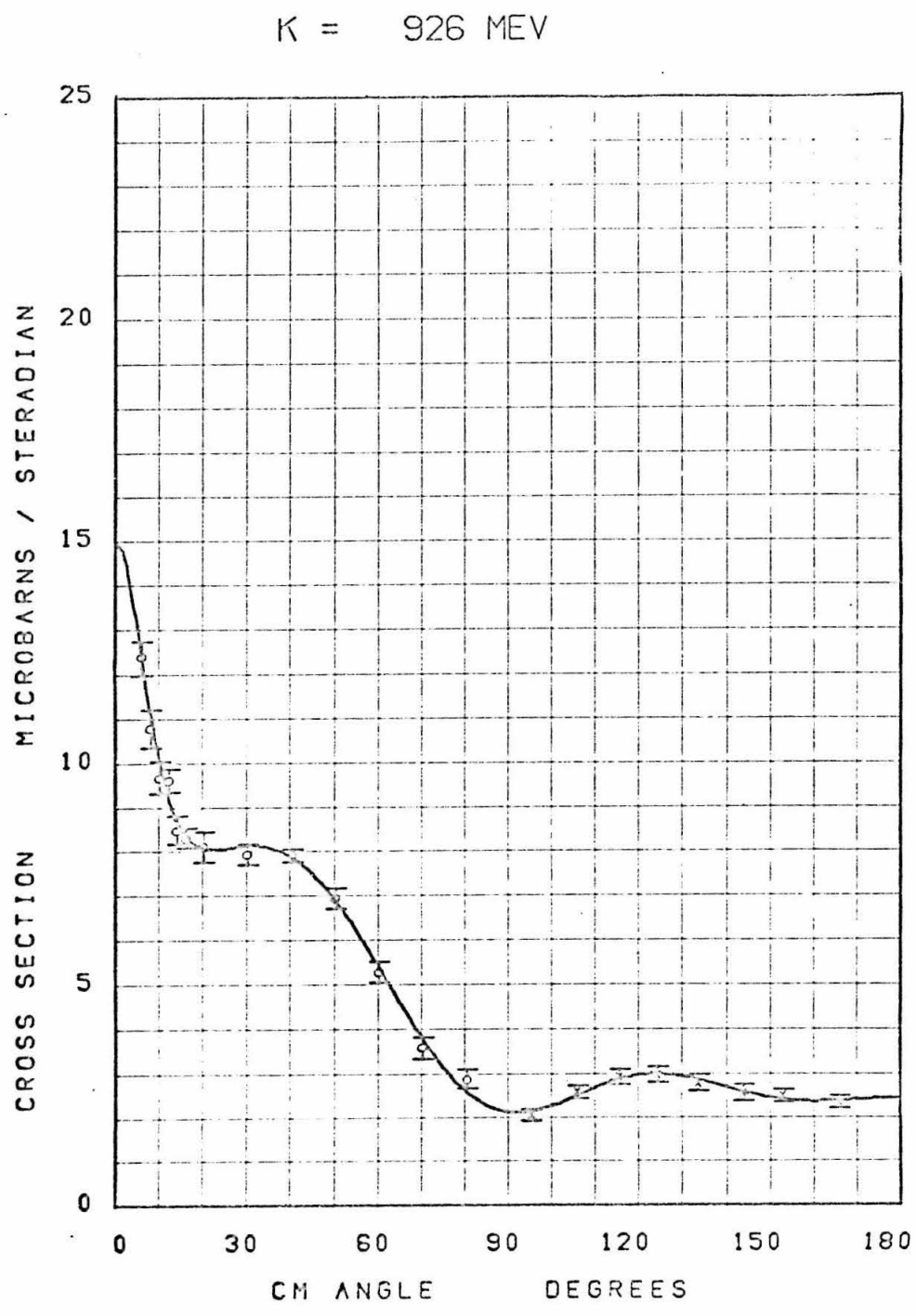
K = 926 MEV
CROSS SECTION MICROBARNS / STERADIAN
25
20
15
10
5
0
0
30
60
90
120
150
180
CM ANGLE DEGREES

FIGURE 6.19

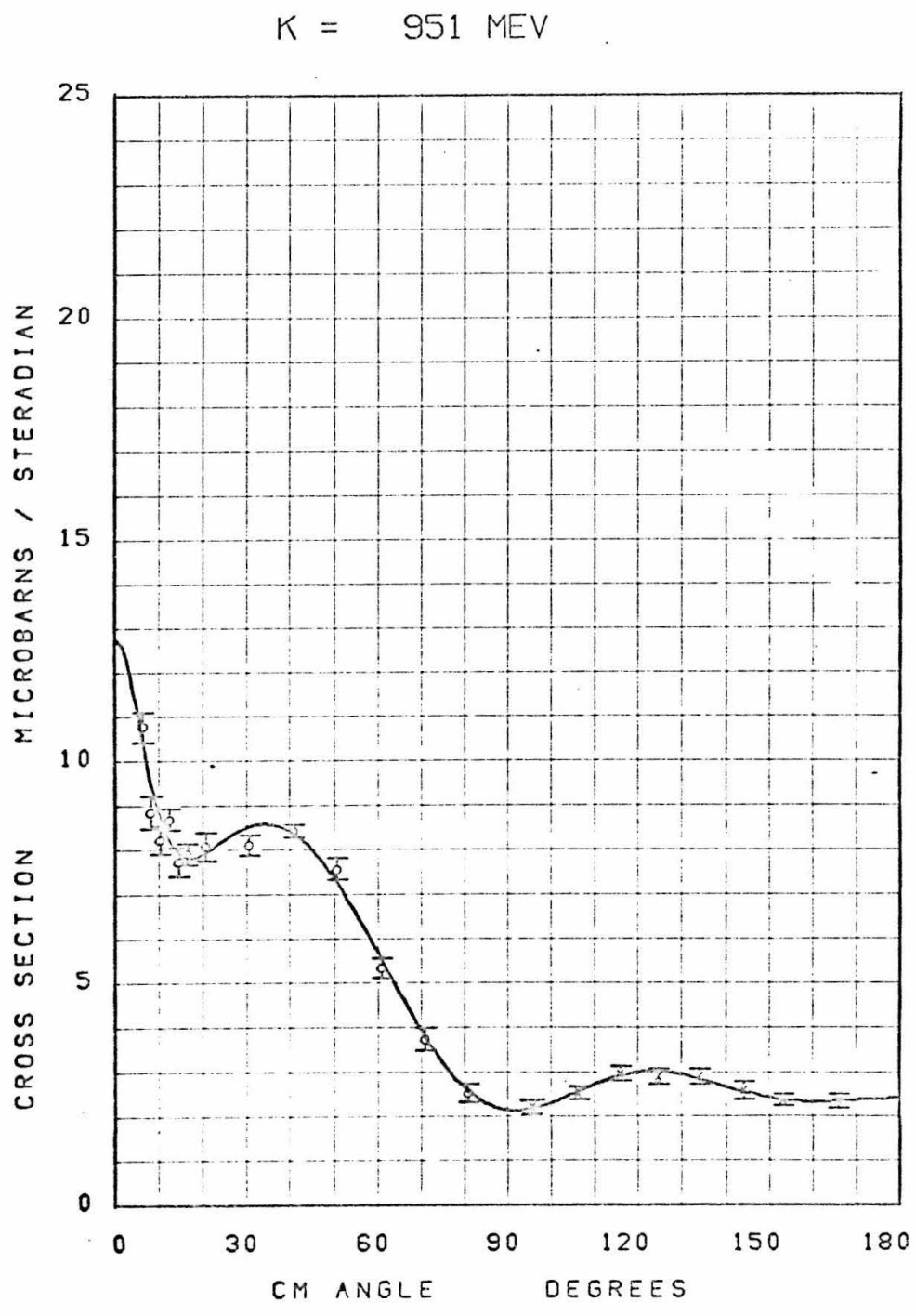
K = 951 MEV
CROSS SECTION MICROBARNS / STERADIAN
25
20
15
10
5
0
0
30
60
90
120
150
180
CM ANGLE DEGREES

FIGURE 6.20

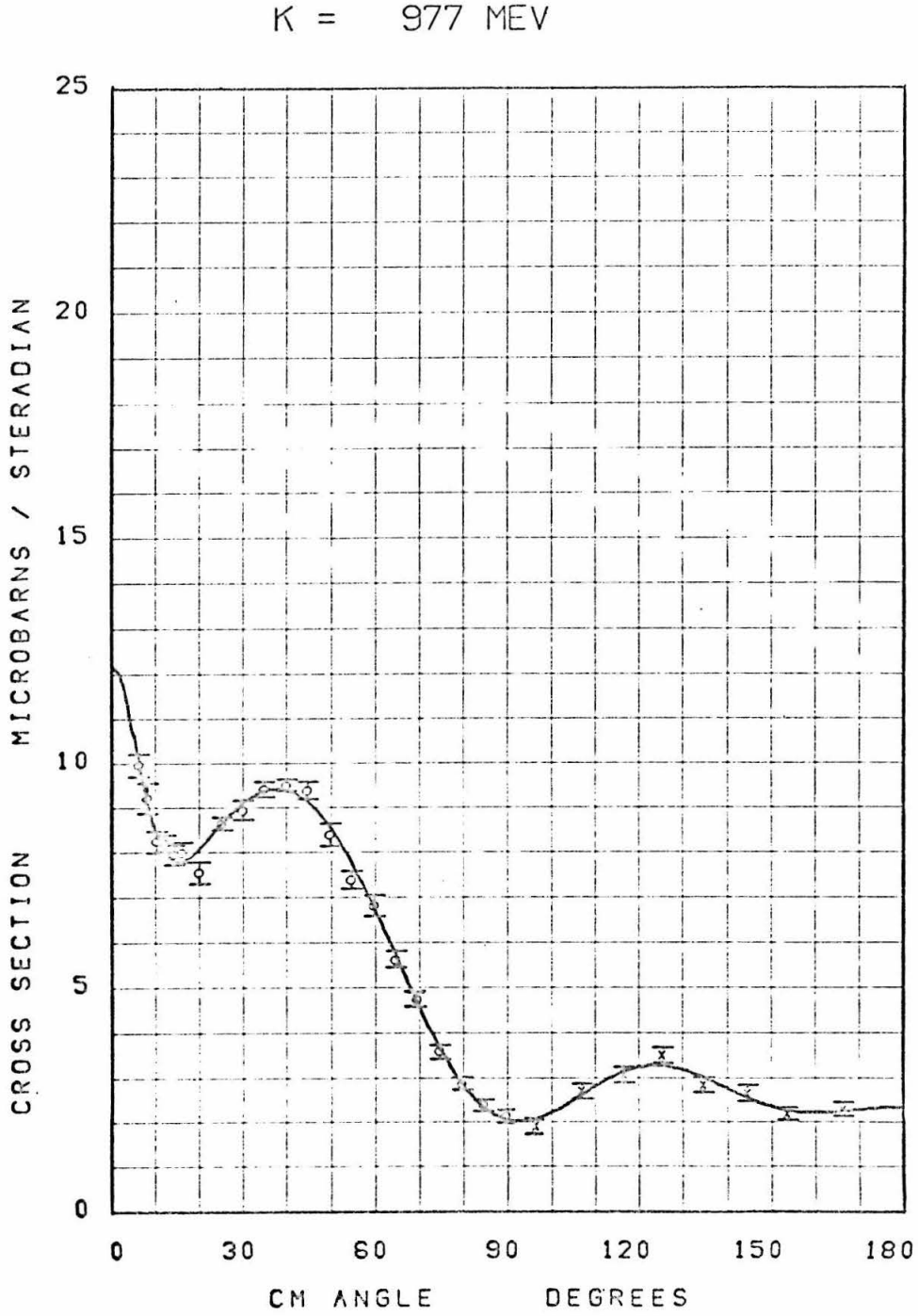
K = 977 MEV
CROSS SECTION MICROBARNS / STERADIAN
25
20
15
10
5
0
0
30
60
90
120
150
180
CM ANGLE DEGREES

FIGURE 6.21

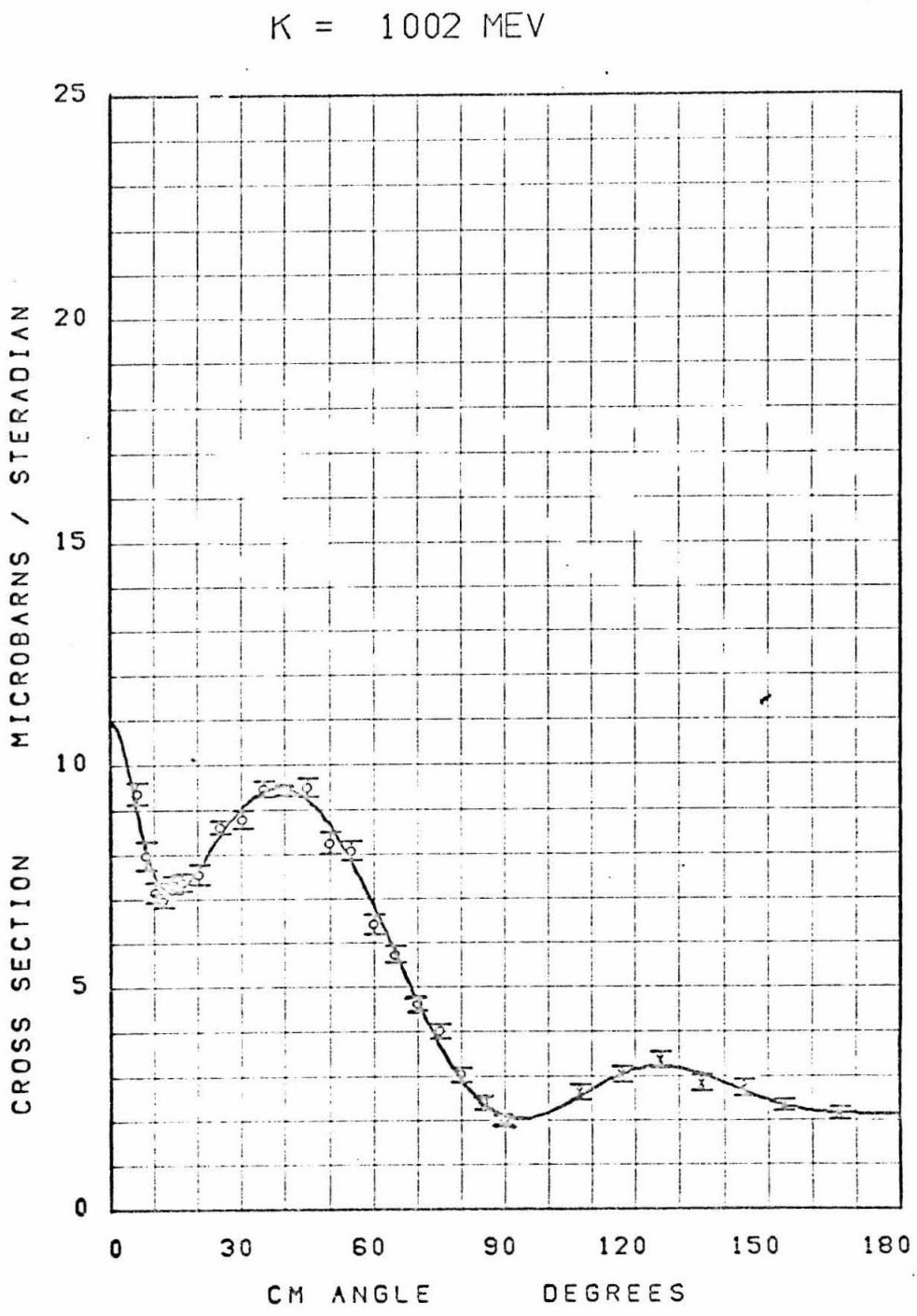
K = 1002 MEV
CROSS SECTION MICROBARNS / STERADIAN
25
20
15
10
5
0
0
30
60
90
120
150
180
CM ANGLE DEGREES

FIGURE 6.22

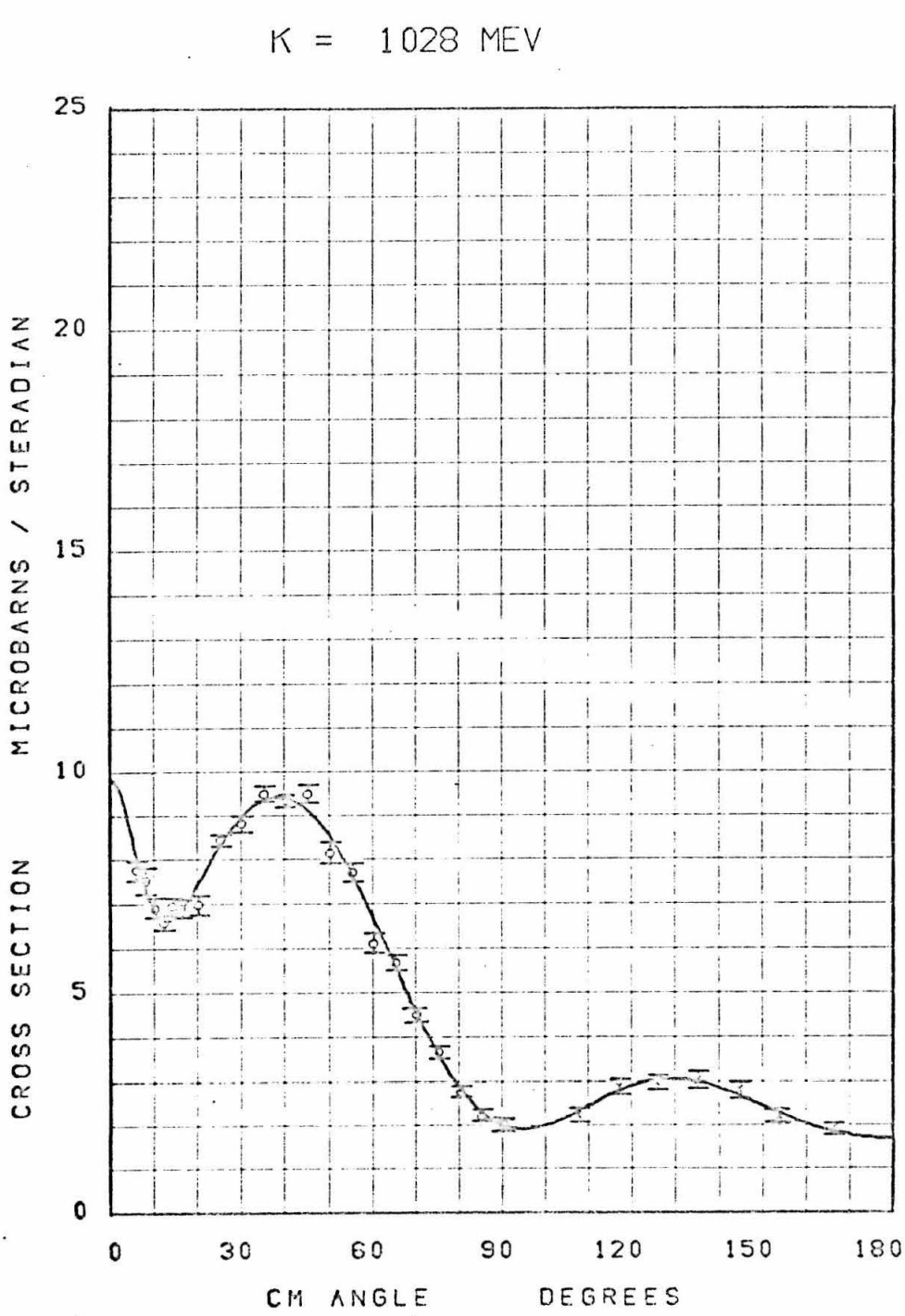
K = 1028 MEV
CROSS SECTION MICROBARNS / STERADIAN
25
20
15
10
5
0
0
30
60
90
120
150
180
CM ANGLE DEGREES

FIGURE 6.23

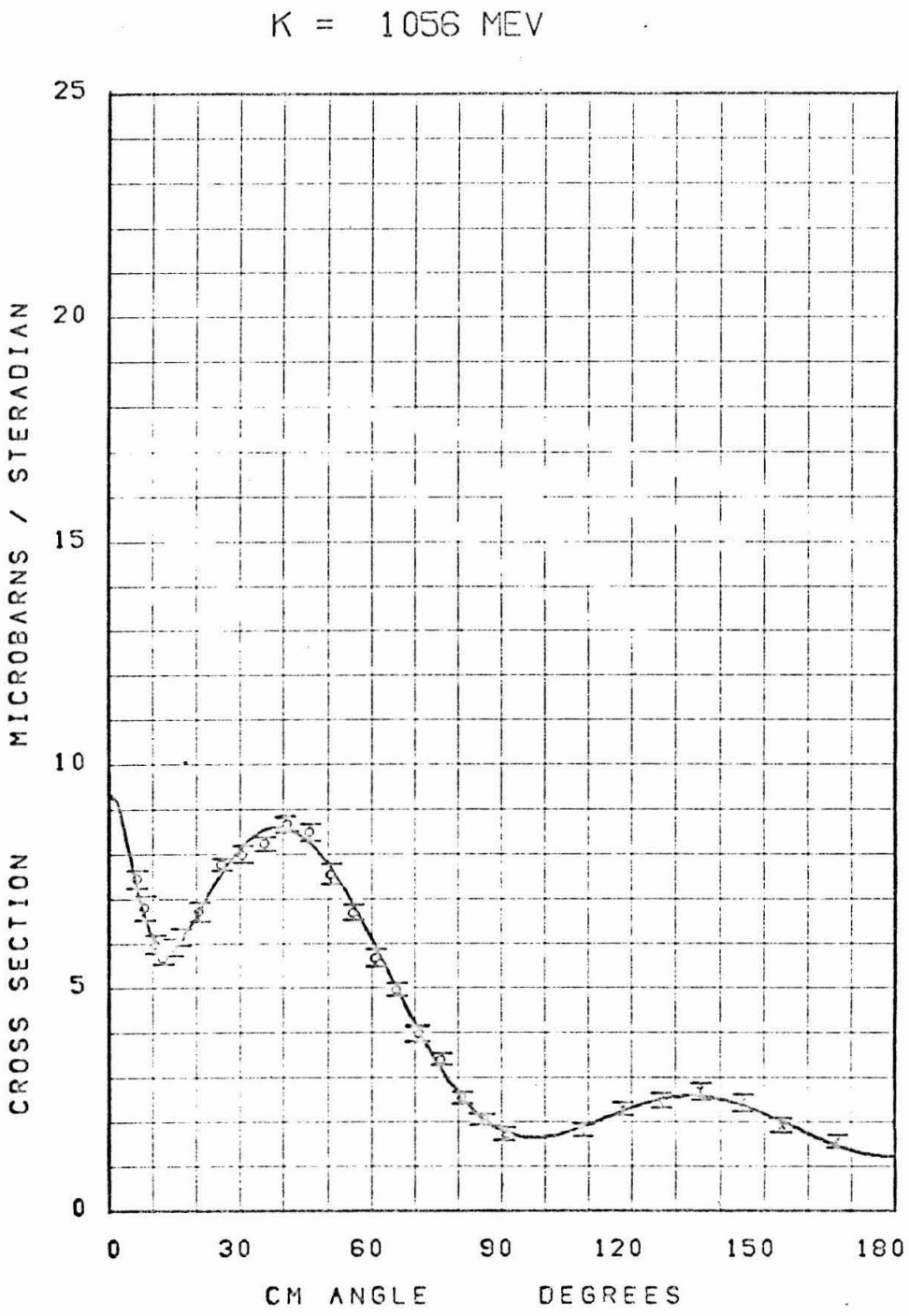
K = 1056 MEV
CROSS SECTION MICROBARNS / STERADIAN
25
20
15
10
5
0
0
30
60
90
120
150
180
CM ANGLE DEGREES

FIGURE 6.24

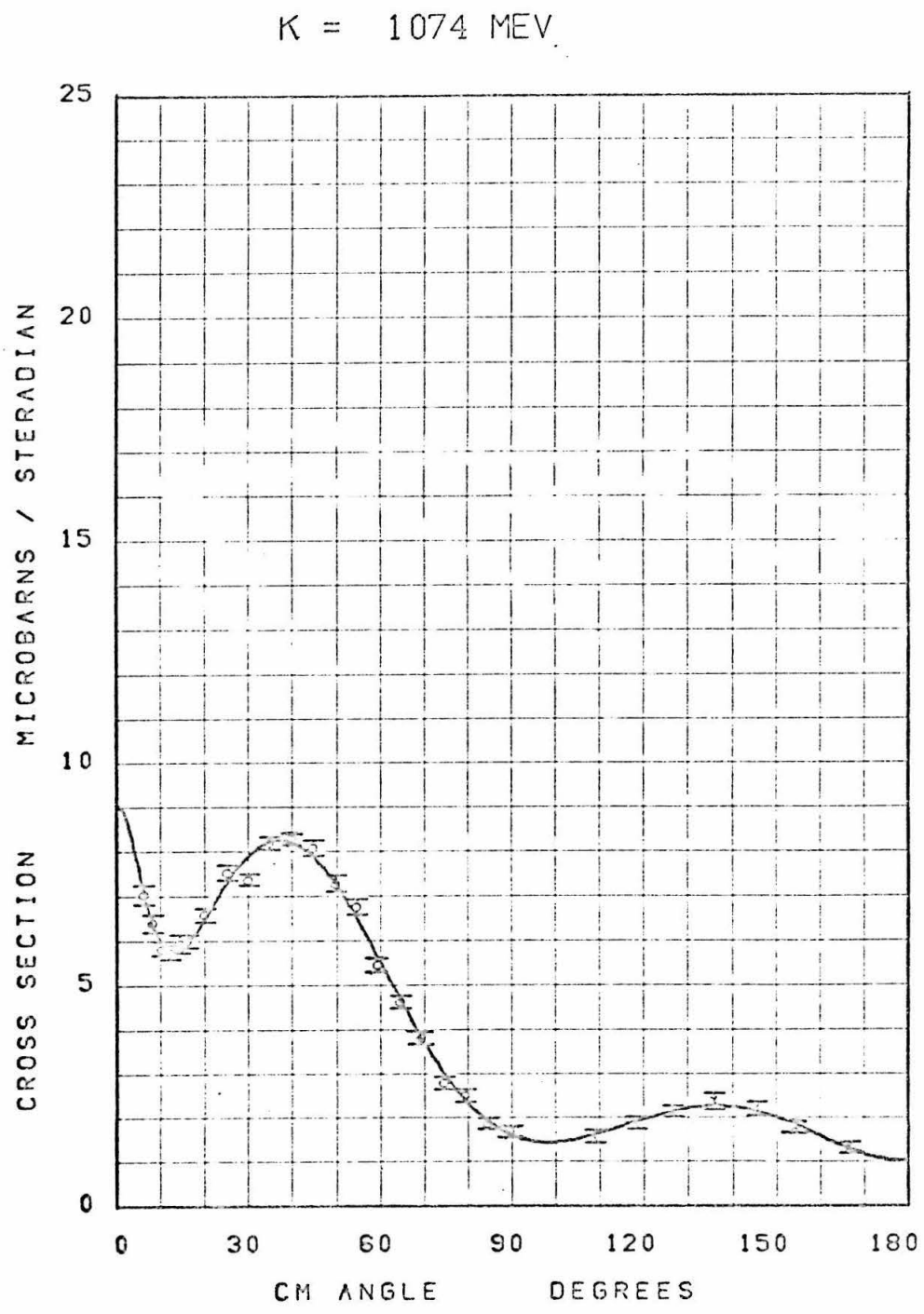
K = 1074 MEV
CROSS SECTION MICROBARNS / STERADIAN
25
20
15
10
5
0
0
30
60
90
120
150
180
CM ANGLE DEGREES

FIGURE 6.25

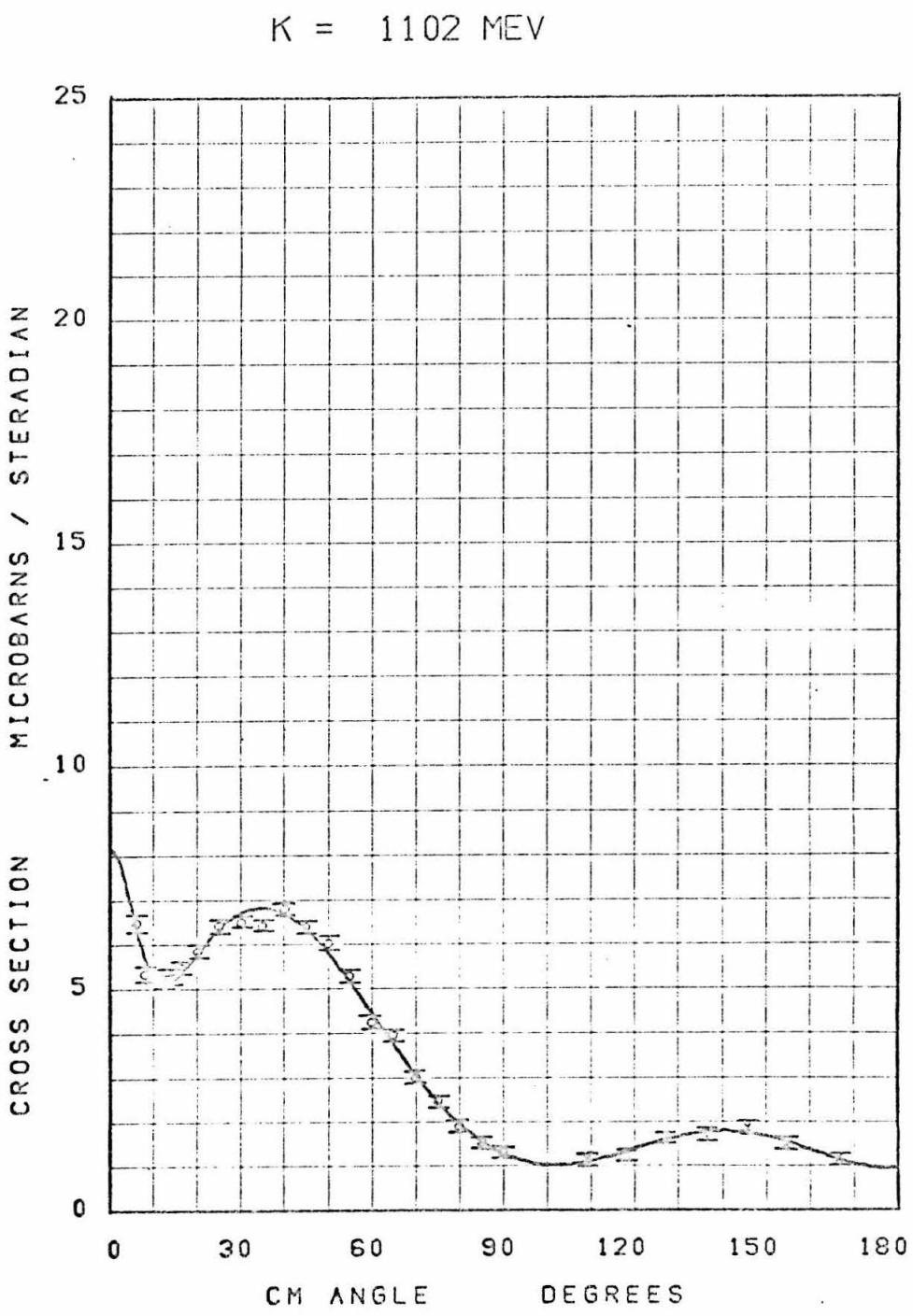
K = 1102 MEV
CROSS SECTION MICROBARNS / STERADIAN
25
20
15
10
5
0
0
30
60
90
120
150
180
CM ANGLE DEGREES

FIGURE 6.26

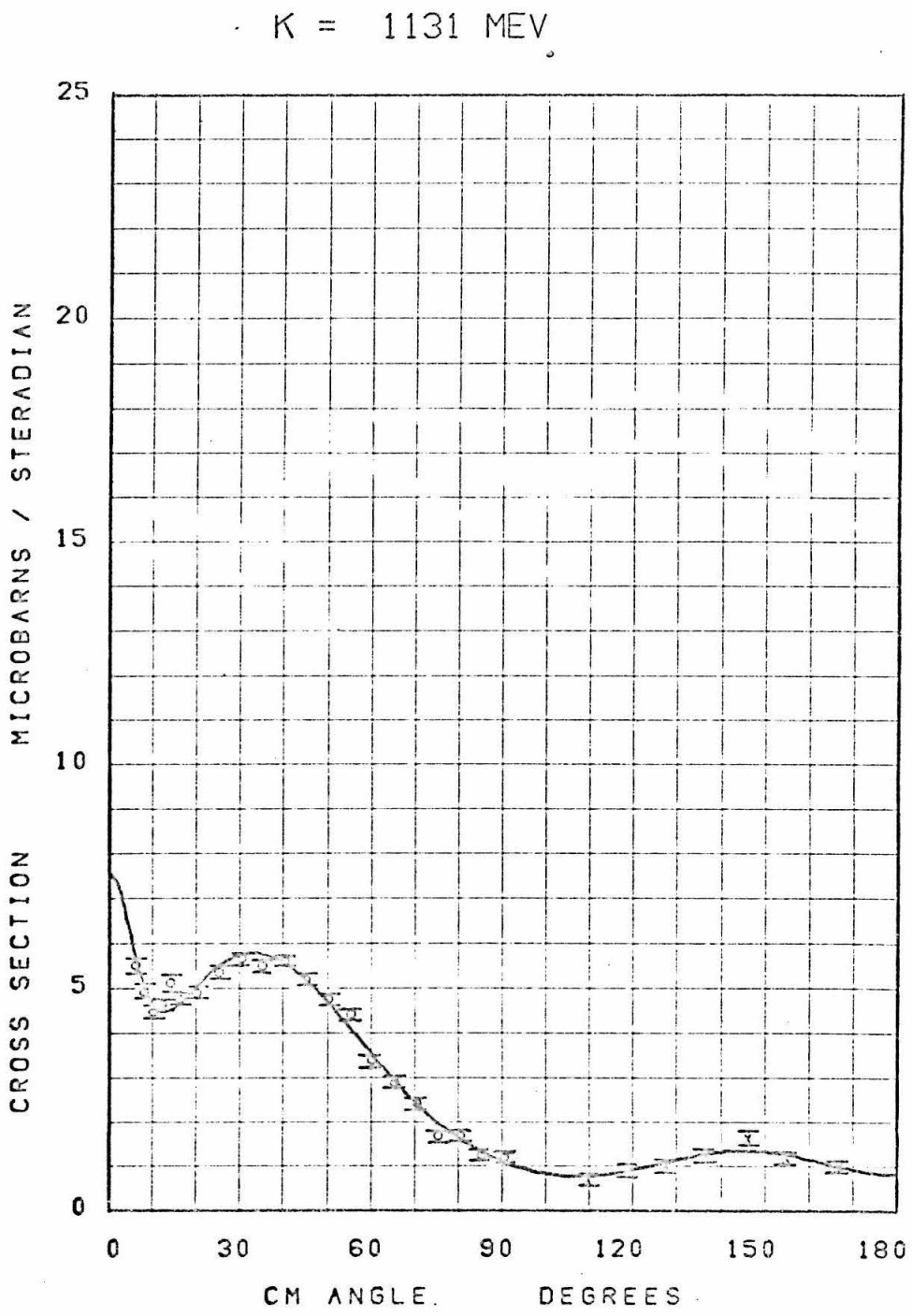
K = 1131 MEV
CROSS SECTION MICROBARNS / STERADIAN
25
20
15
10
5
0
0
30
60
90
120
150
180
CM ANGLE. DEGREES

FIGURE 6.27

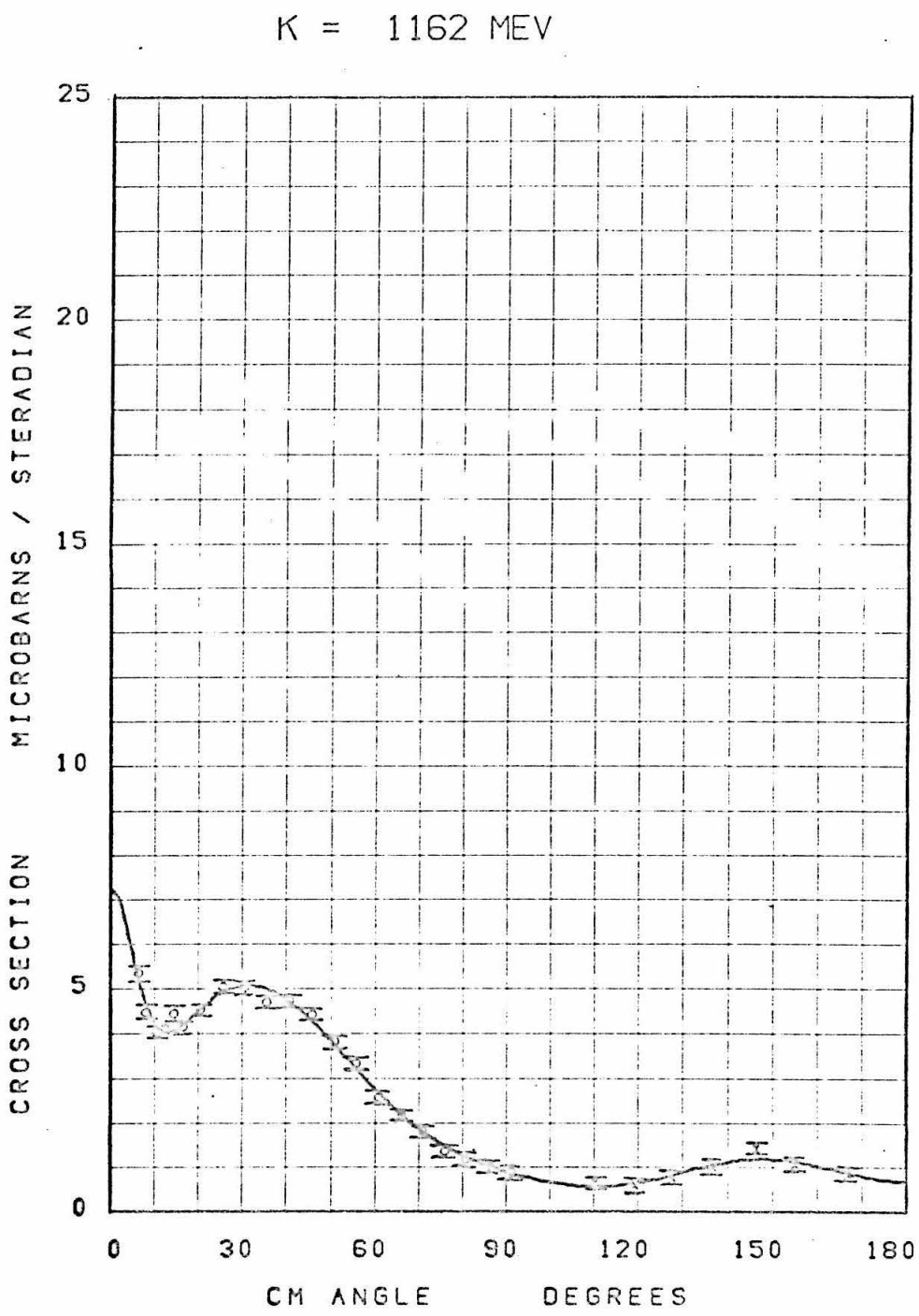
K = 1162 MEV
CROSS SECTION MICROBARNS / STERADIAN
25
20
15
10
5
0
0
30
60
90
120
150
180
CM ANGLE DEGREES

FIGURE 6.28

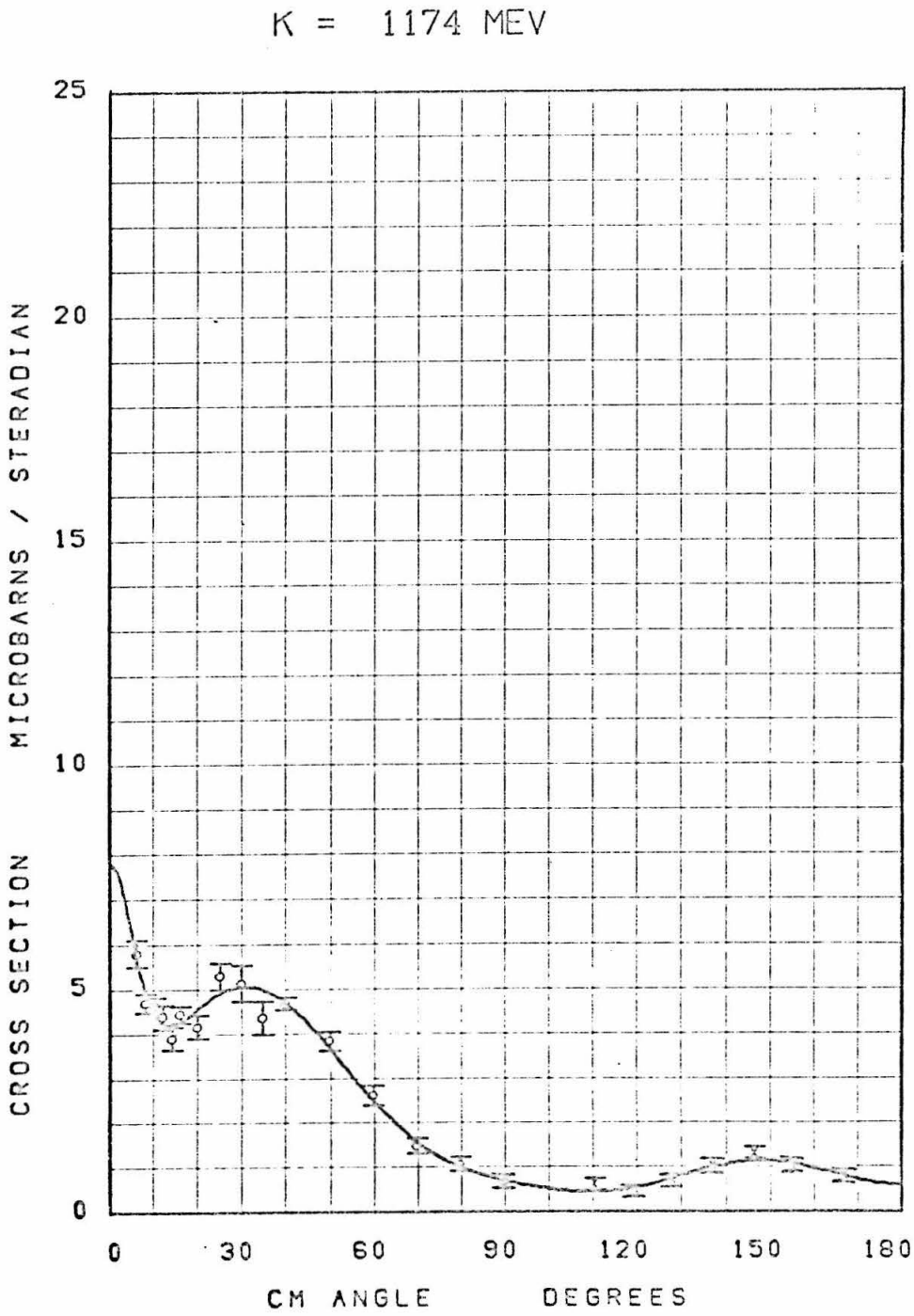
K = 1174 MEV
25
20
15
10
5
0
CROSS SECTION MICROBARNS / STERADIAN
0
30
60
90
120
150
180
CM ANGLE DEGREES

FIGURE 6.29

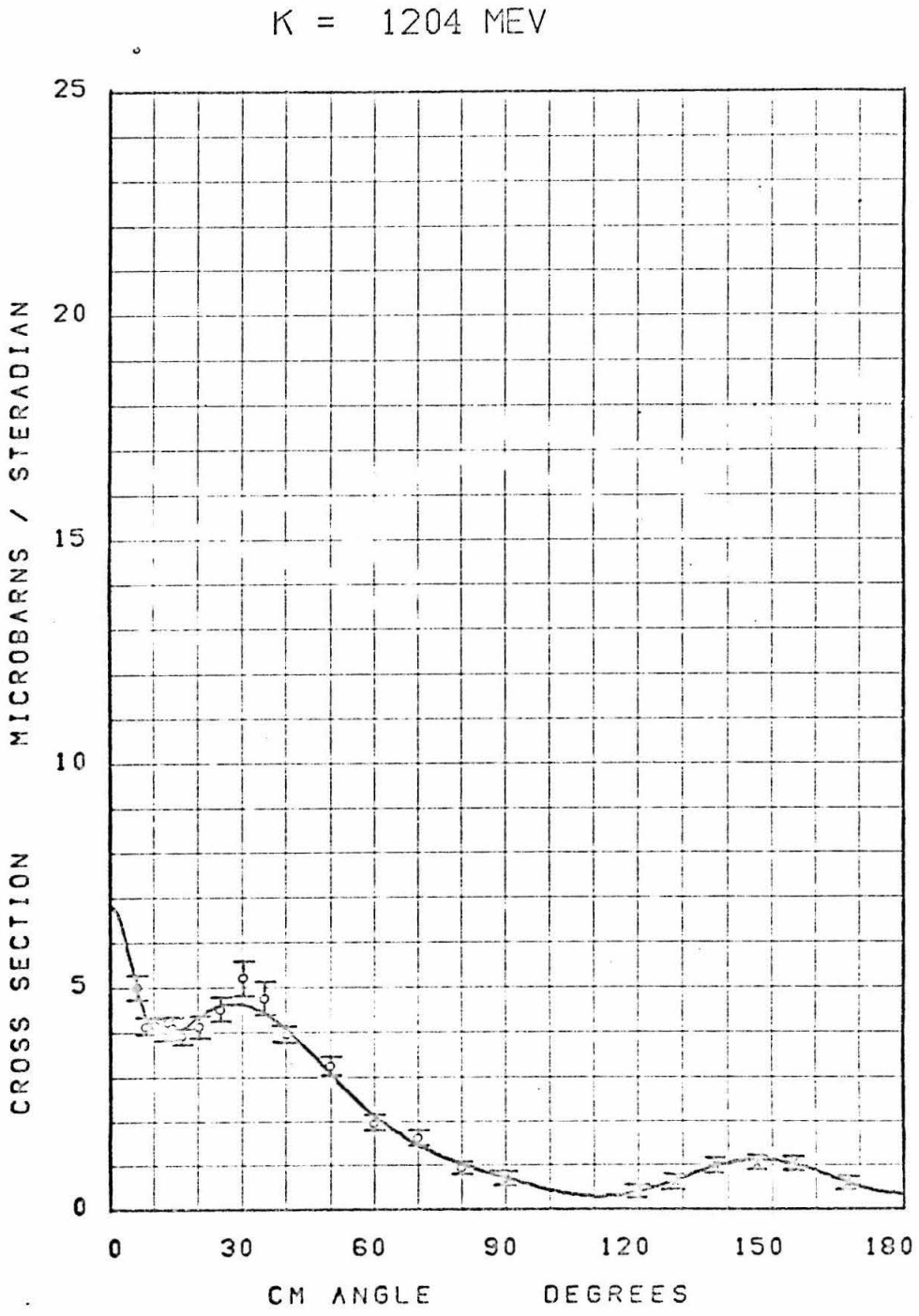
K = 1204 MEV
CROSS SECTION MICROBARNS / STERADIAN
25
20
15
10
5
0
0
30
60
90
120
150
180
CM ANGLE DEGREES

FIGURE 6.30

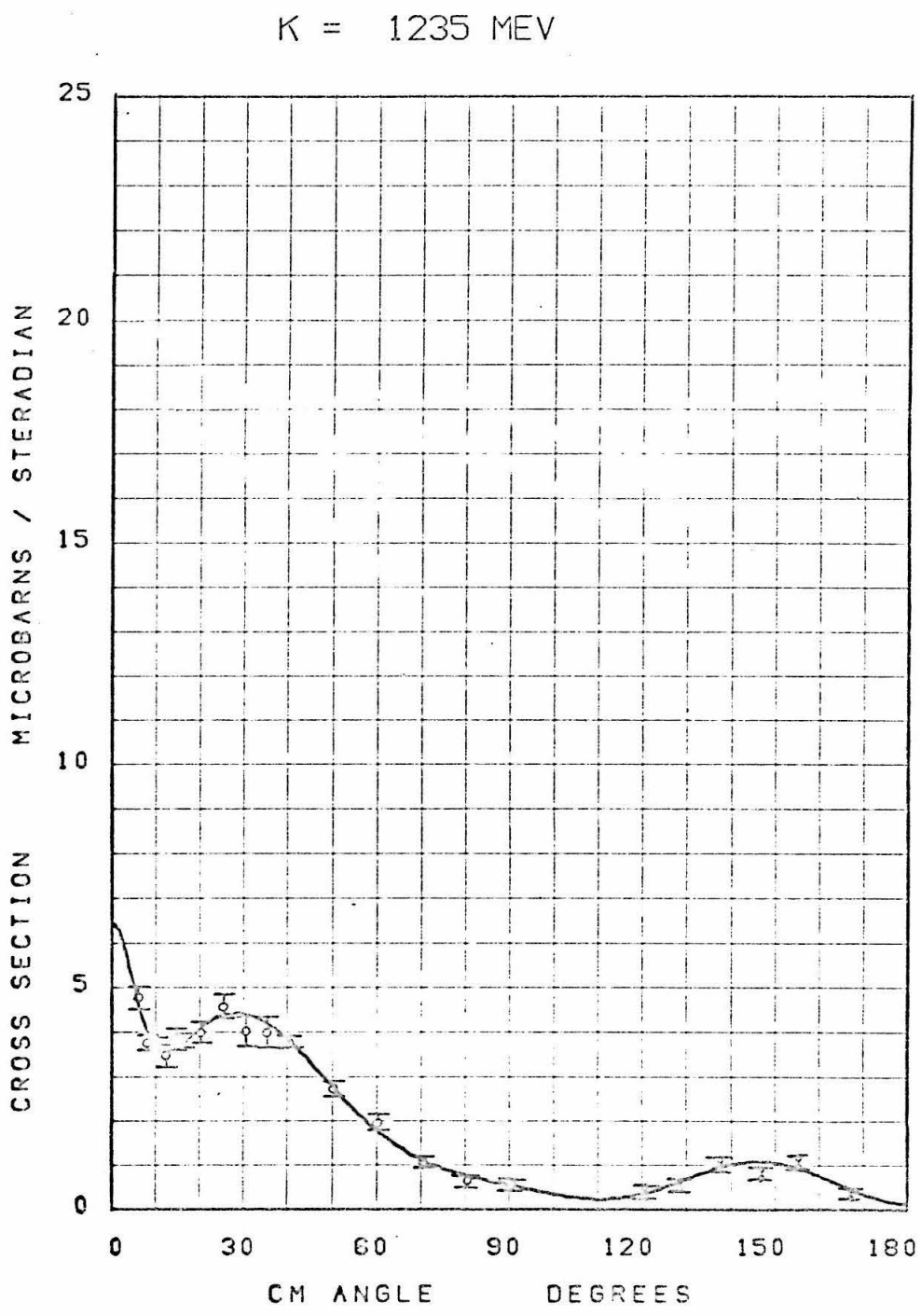
K = 1235 MEV
CROSS SECTION MICROBARNS / STERADIAN
25
20
15
10
5
0
0
30
60
90
120
150
180
CM ANGLE DEGREES

FIGURE 6.31

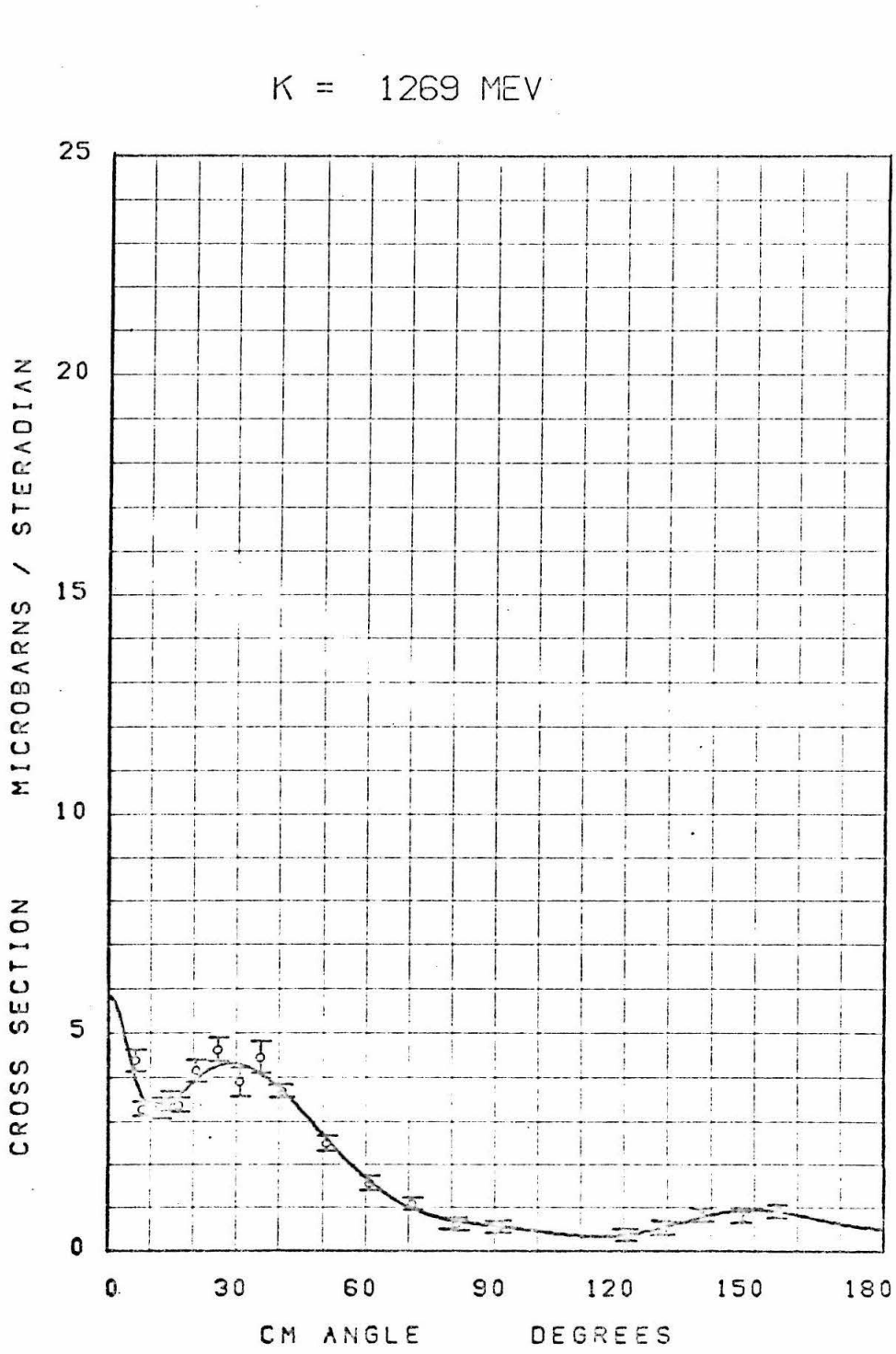
K = 1269 MEV
25
20
15
10
5
0
CROSS SECTION MICROBARNS / STERADIAN
0
30
60
90
120
150
180
CM ANGLE DEGREES

FIGURE 6.32

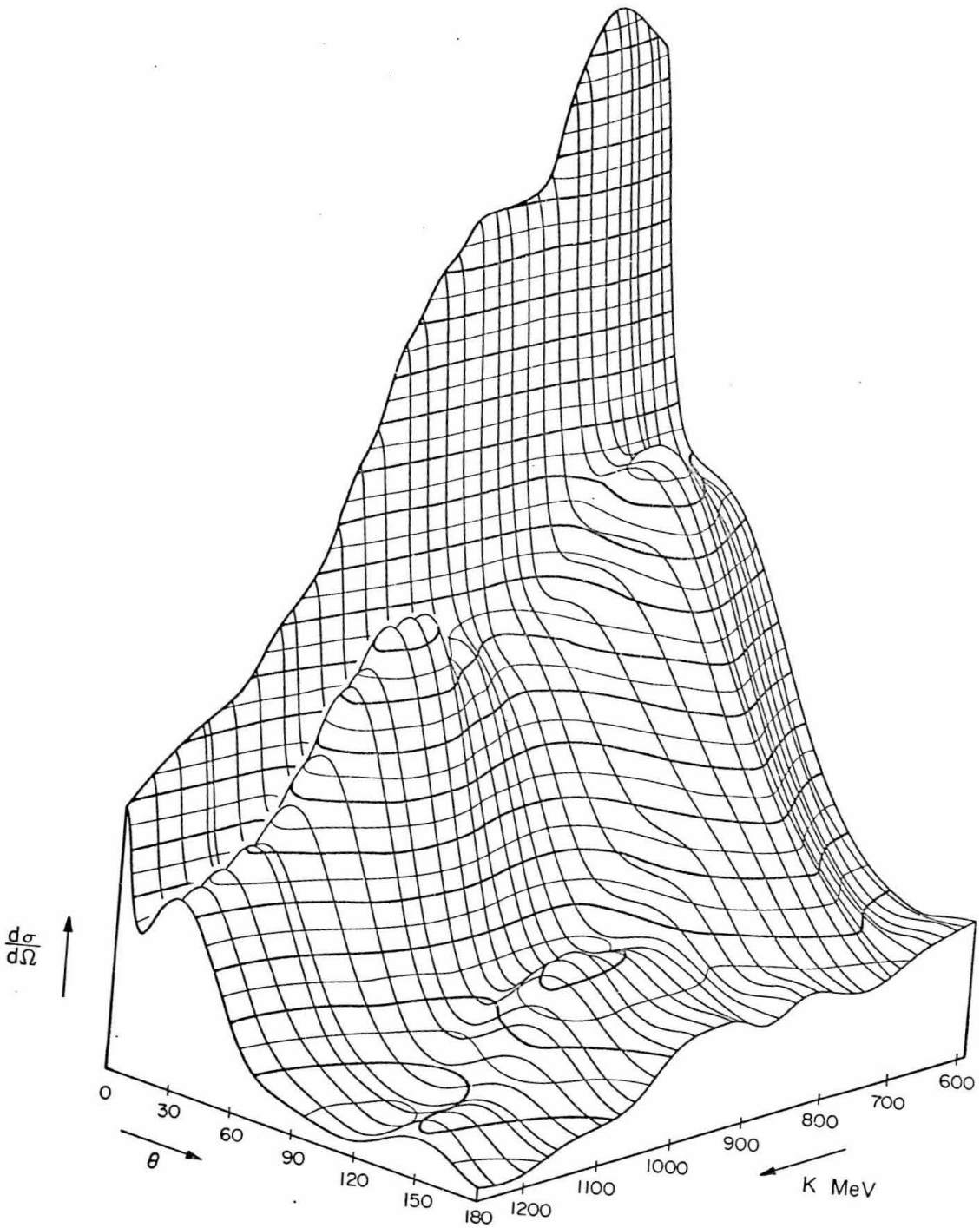
$\frac{d\sigma}{d\Omega}$
0
30
60
90
120
150
180
θ
600
700
800
900
1000
1100
1200
K MeV

FIGURE 7

FIGURES 8.1 - 8.7

Comparisons With Other Experiments

The smooth curve is from this experiment.
The symbols plotted designate the source of data.

J	Beneventano[17]
D	Boyden[2]
F	Dixon[1]
E	Dixon, Boyden[2]
B	Kilner[3]

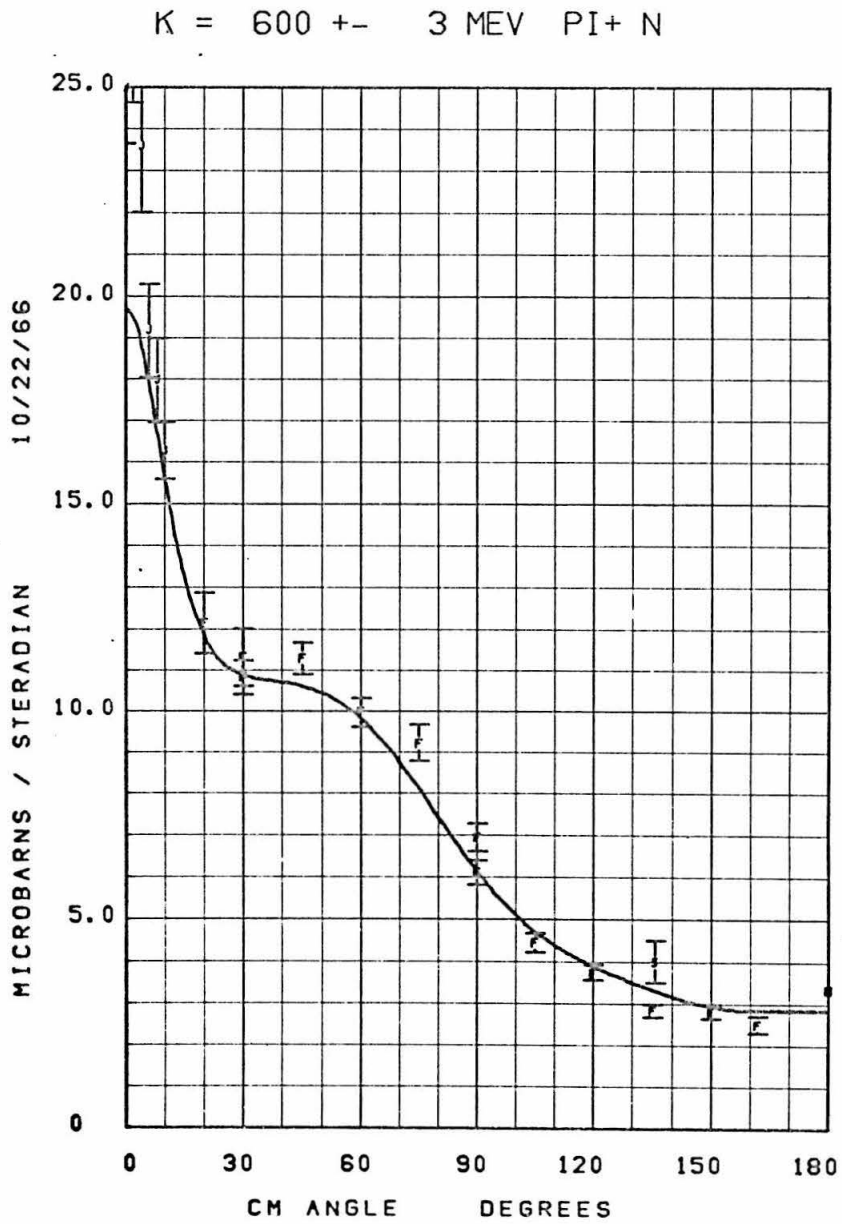
K = 600 +- 3 MEV PI+ N
25.0
20.0
15.0
10.0
5.0
0
10/22/66
MICROBARNS / STERADIAN
0
30
60
90
120
150
180
CM ANGLE DEGREES

FIGURE 8.1

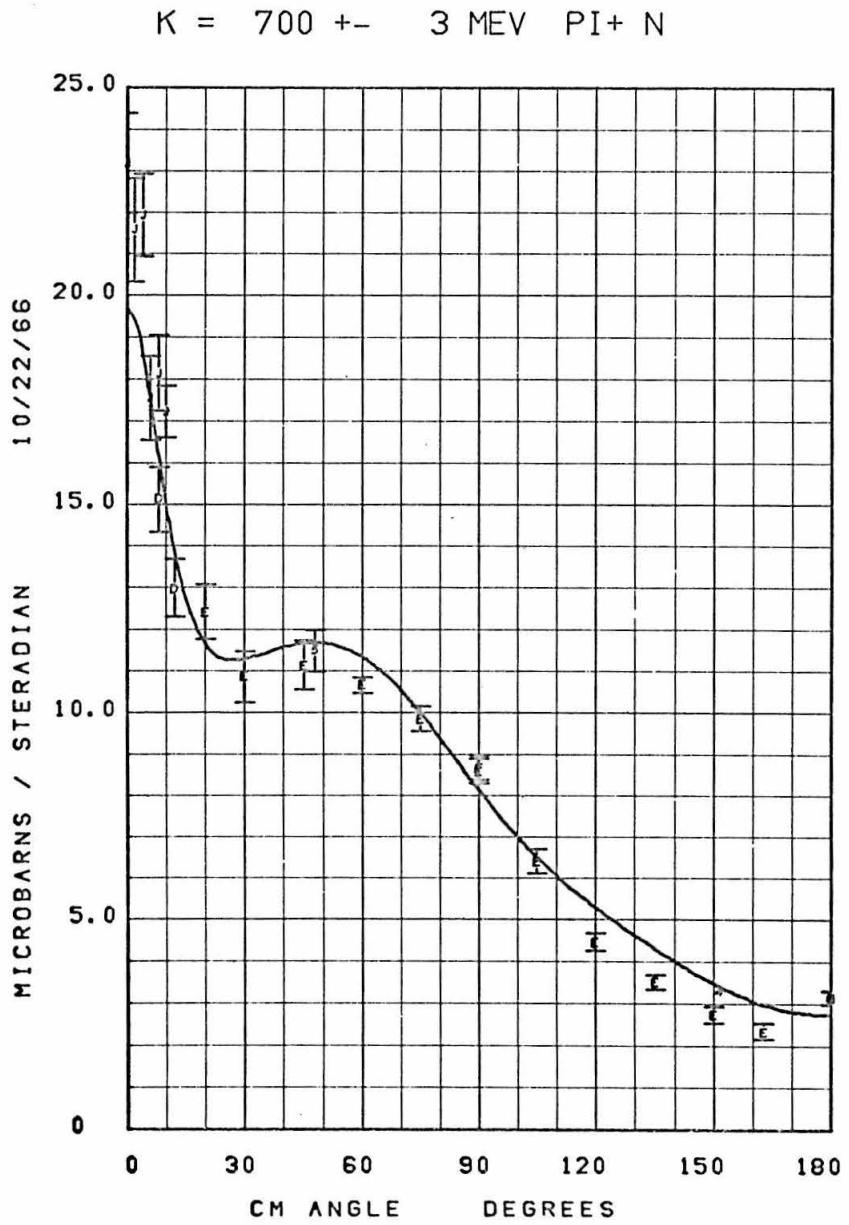
K = 700 +- 3 MEV PI+ N
25.0
20.0
15.0
10.0
5.0
0
MICROBARNS / STERADIAN
10/22/66
0
30
60
90
120
150
180
CM ANGLE DEGREES

FIGURE 8.2

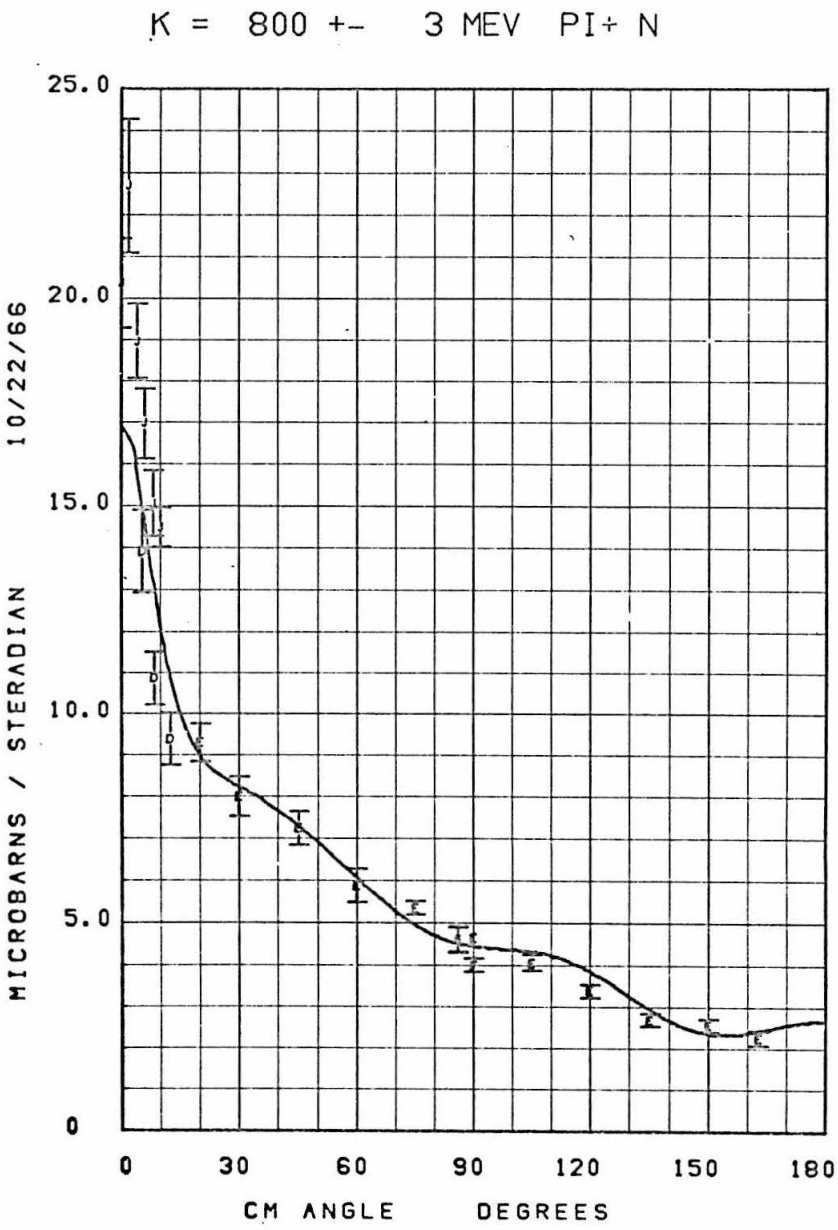
K = 800 +- 3 MEV PI+ N
25.0
20.0
15.0
10.0
5.0
0
MICROBARNS / STERADIAN
10/22/66
0
30
60
90
120
150
180
CM ANGLE DEGREES

FIGURE 8.3

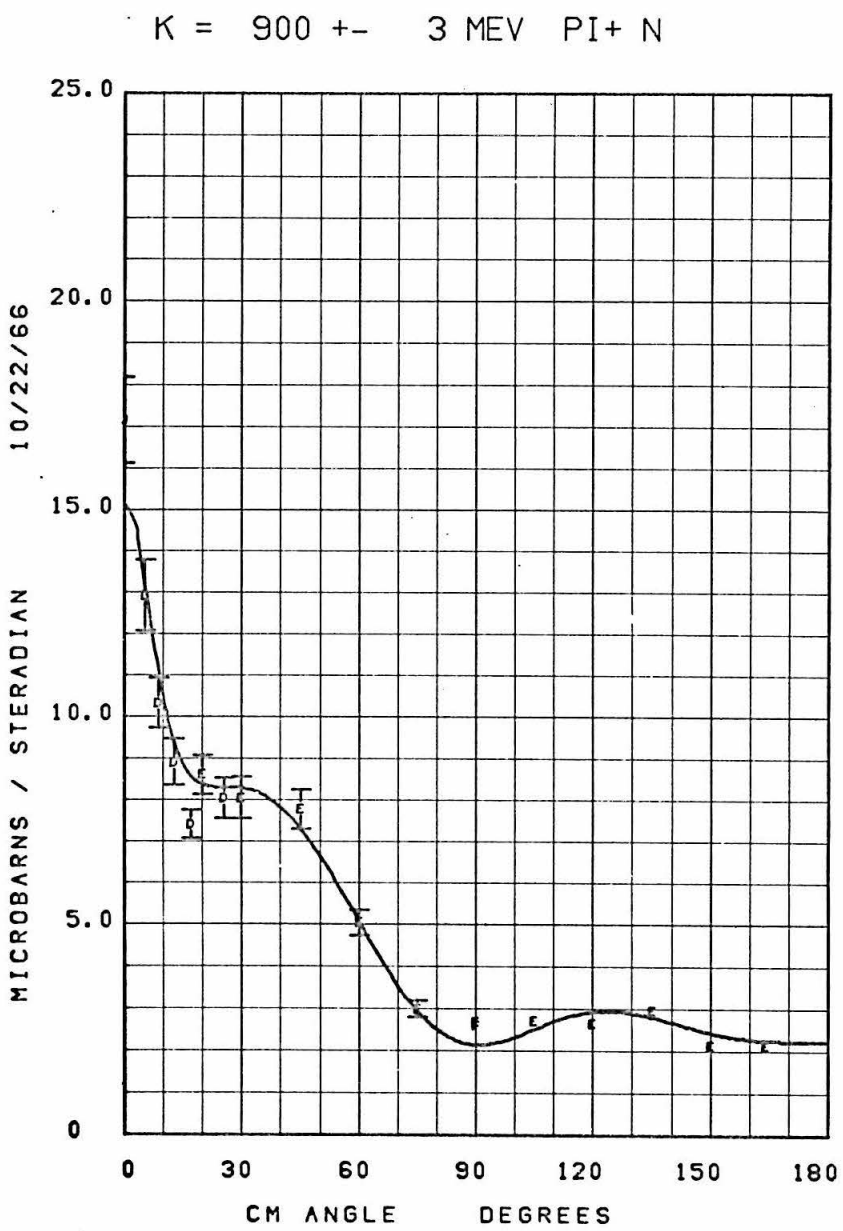
K = 900 +- 3 MEV PI+ N
10/22/66
MICROBARNS / STERADIAN
25.0
20.0
15.0
10.0
5.0
0
0
30
60
90
120
150
180
CM ANGLE DEGREES

FIGURE 8.4

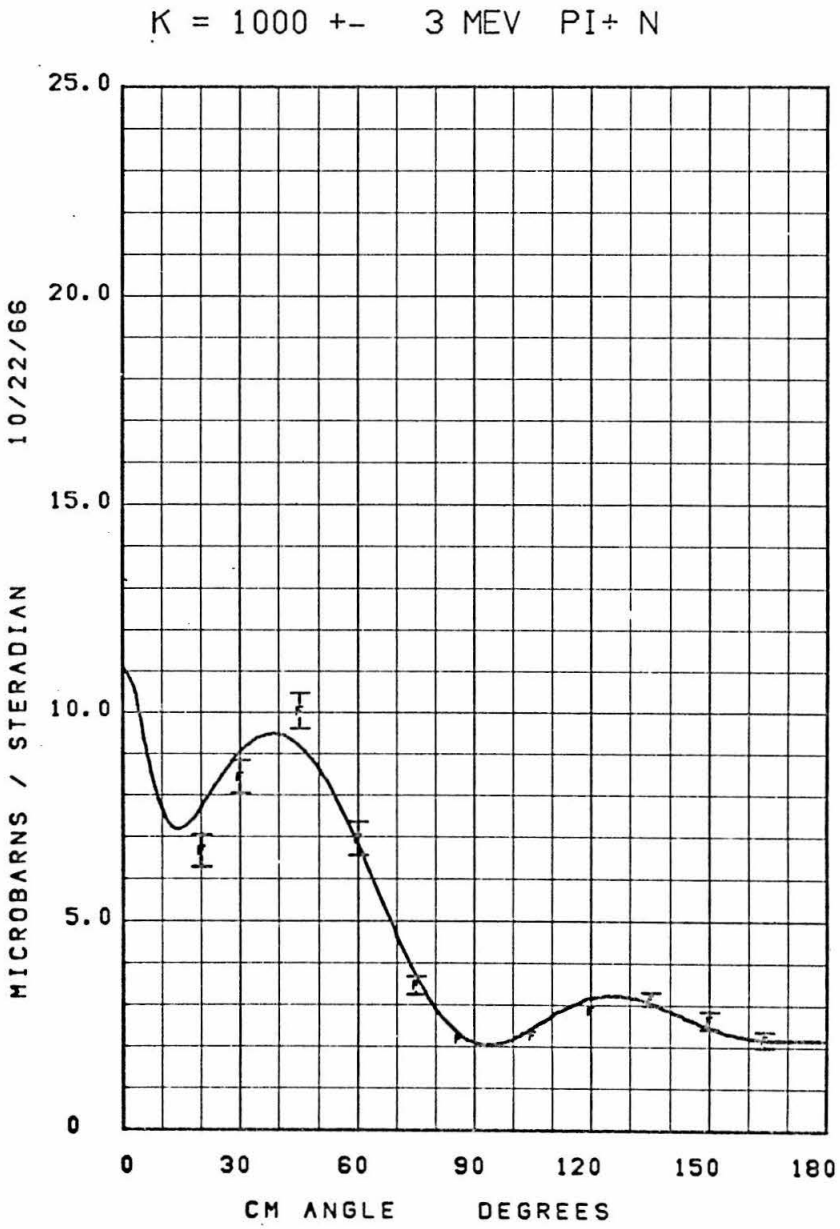
K = 1000 +- 3 MEV PI+ N
25.0
20.0
15.0
10.0
5.0
0
10/22/66
MICROBARNS / STERADIAN
0
30
60
90
120
150
180
CM ANGLE DEGREES

FIGURE 8.5

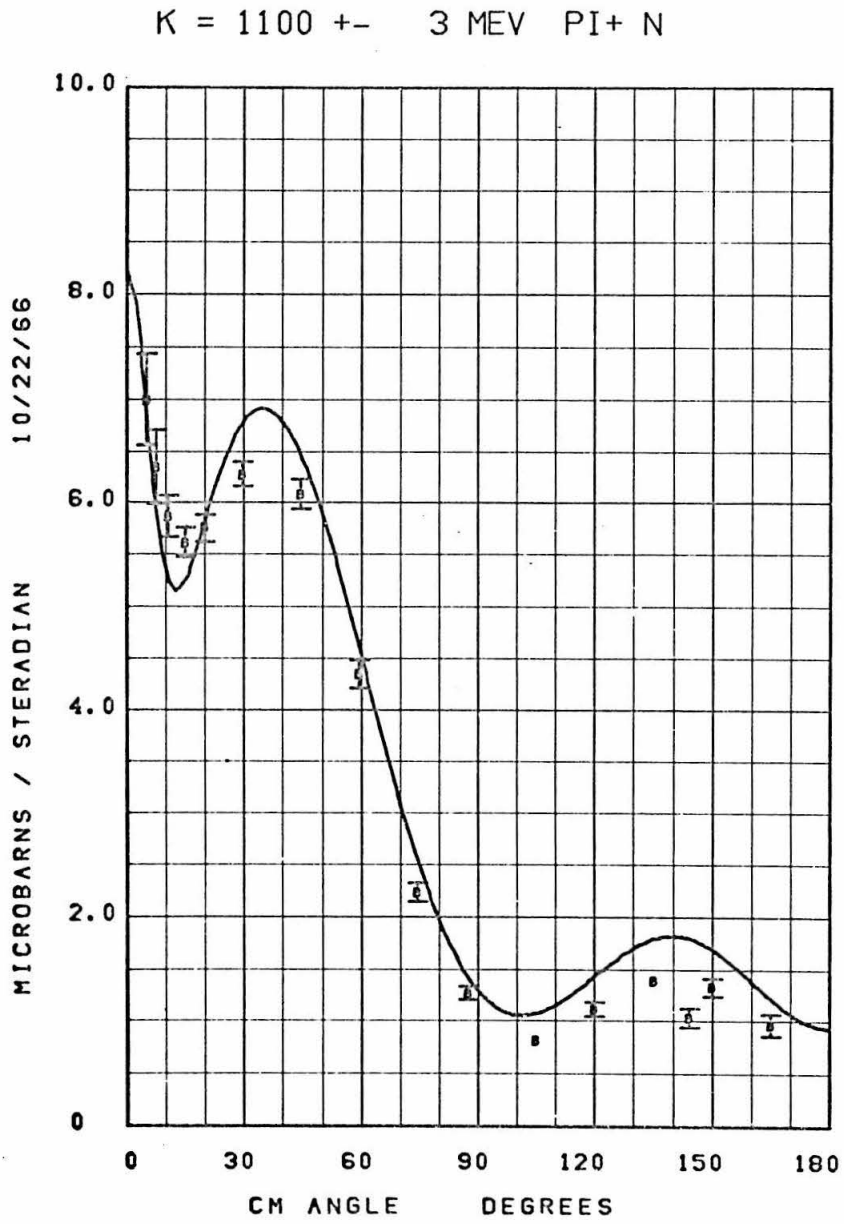
K = 1100 +- 3 MEV PI+ N
10.0
8.0
6.0
4.0
2.0
0
MICROBARNS / STERADIAN
10/22/66
0
30
60
90
120
150
180
CM ANGLE DEGREES

FIGURE 8.6

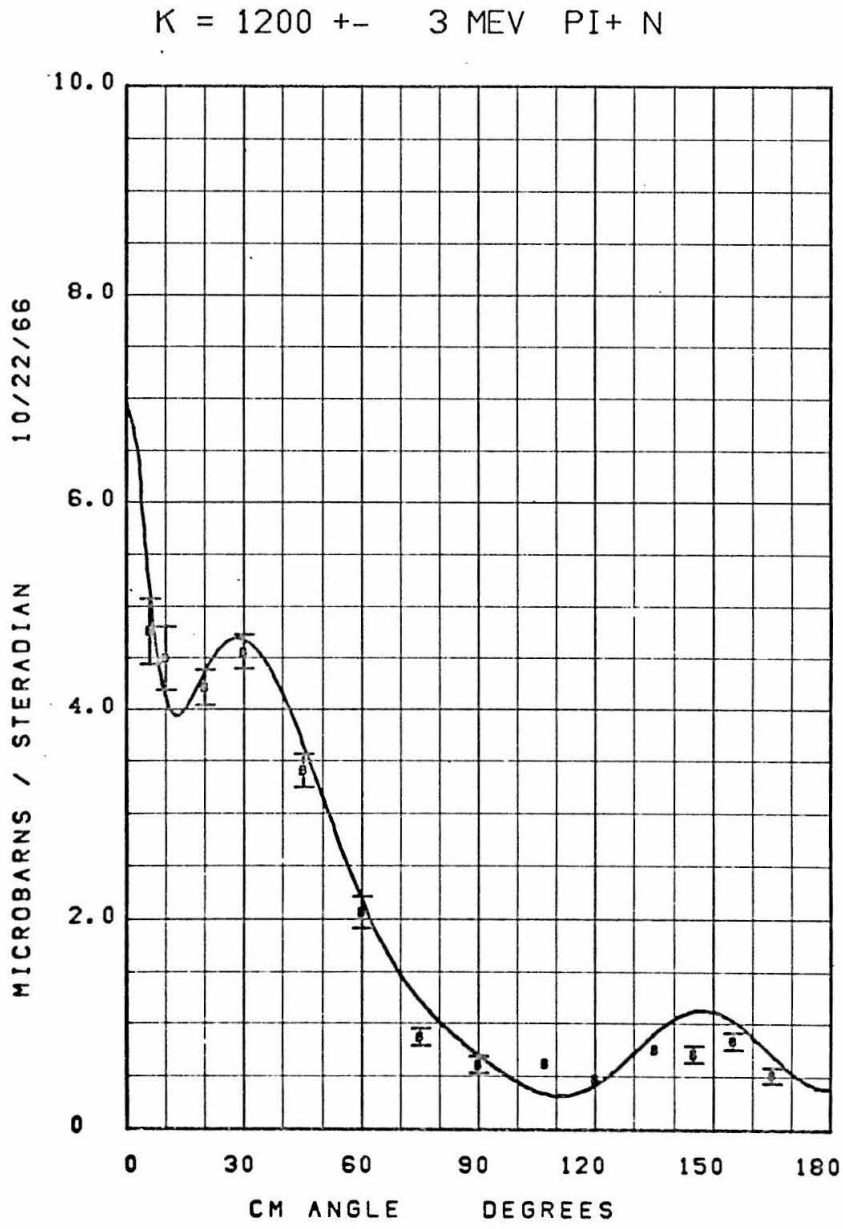
K = 1200 +- 3 MEV PI+ N
10.0
8.0
6.0
4.0
2.0
0
10/22/66
MICROBARNS / STERADIAN
0
30
60
90
120
150
180
CM ANGLE DEGREES

FIGURE 8.7

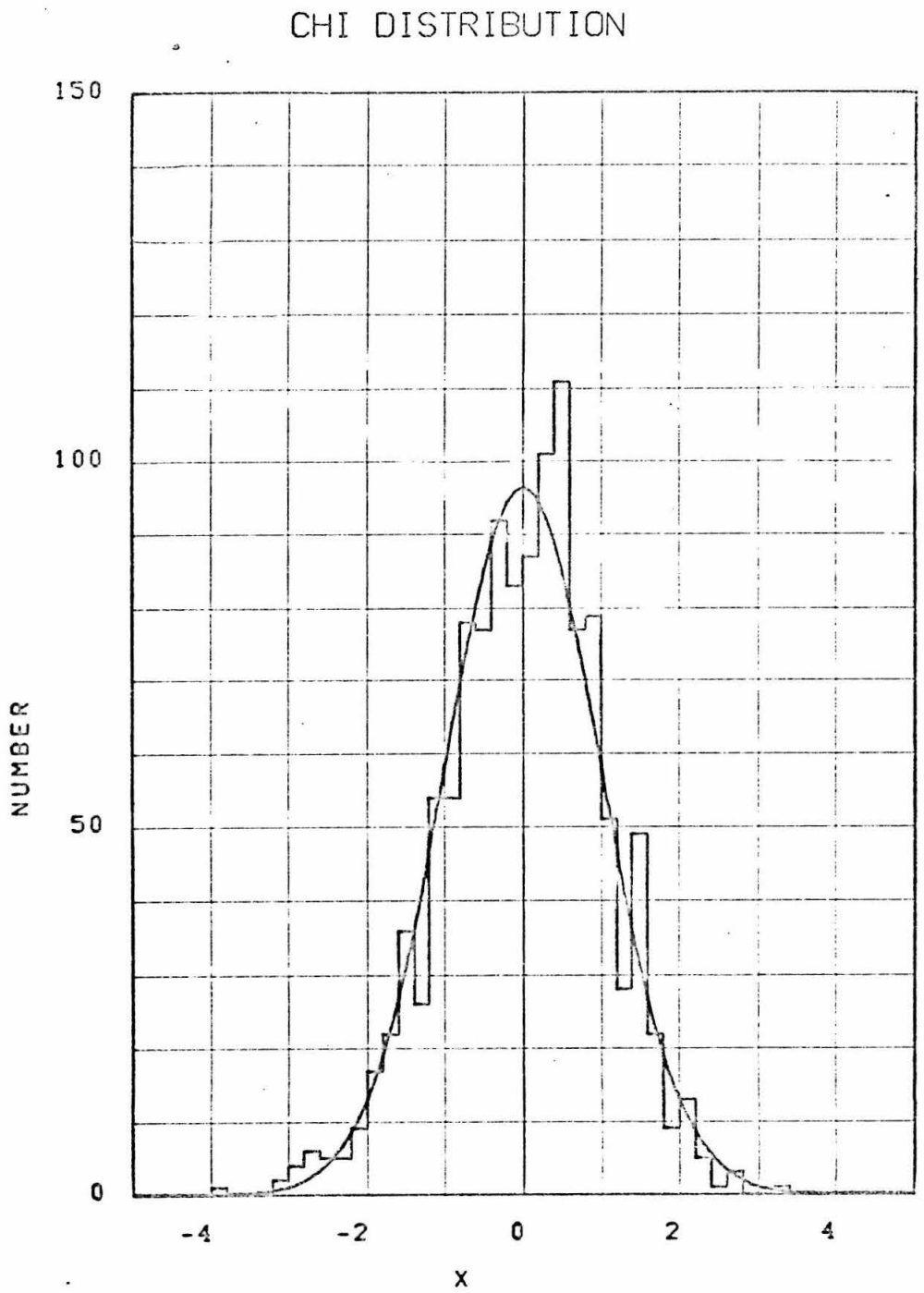

FIGURE 9. The observed χ distribution, plotted as a histogram, is compared with the expected Gaussian distribution.

TABLE 2

Systematic Errors

Source	Error
Decay Correction	1.0%
Magnet Acceptance	1.0%
Absorption Correction	2.0%
Absolute Beam Calibration	3.0%
Counter Efficiencies	0.5%
Target Density and Thickness	1.0%
Bremsstrahlung Shape	1.5%
Quadrature Sum	4.3%
Absolute Sum	10.0%

V. DATA FITTING

As noted in the introduction, a Moravcsik fit[4] to the angular distributions describes the data very well. It has the disadvantage, however, of scrambling the effects of a definite angular momentum state among many of the coefficients. Suppose for example, the cross section is entirely due to a F 5/2 amplitude produced from an initial helicity 3/2. Then

$$\sigma(X) = d\,(1 - X^2)\,(1 + 15\,X^2)$$

where

$X = \cos\theta$

$\theta = \pi^+$ c. m. angle relative to photon

d = a positive constant.

The Moravcsik coefficients, B(J), are defined by

$$\sigma(X)\,(1 - \beta X)^2 = \sum_{J=0}^{M} B(J)\,X^J \qquad (1)$$

where β = velocity of π^+ in the c. m. system. For the cross section given above, we have

$$d[1 - 2\beta X + (\beta^2 + 14)X^2 - 28\beta X^3 + (14\beta^2 - 15)X^4 + 30\beta X^5 - 15\beta^2 X^6]$$

$$= \sum_{J=0}^{M} B(J)\, X^J .$$

Thus, six Moravcsik coefficients are needed to describe this cross section. A more useful but equivalent fit is the following:

$$\sigma(X) = C(0)\, \sigma_{OPE}(X) + C(1)\, \sigma_I(X) + \sum_{J=2}^{M} C(J)\, P_{J-2}(X) \qquad (2)$$

$\sigma_{OPE}(X)$ = cross section due to the one π exchange

$$\sigma_I(X) = \frac{1 - X^2}{1 - \beta X} - (1 + X)$$

$P_L(X) = L^{th}$ Legendre polynomial.

The function σ_{OPE} introduces the one π exchange denominator, and its coefficient $C(0)$ is proportional to the π - N coupling constant. The second function, $\sigma_I(X)$, allows for interference with the one π exchange. The cross section due to interference of the one π exchange with states of total angular momentum less than or equal to j has the form

$$\frac{1 - X^2}{1 - \beta X}(a_0 + a_1 + \cdots + a_N X^N)$$

where $N = j - 1/2$. Equation (2) can be written in this form by proper choice of C(1) through C(N + 3). The particular form of $\sigma_I(X)$ used is, of course, not unique. For states with total angular momentum less than or equal to j, the cross section is in general a polynomial of order 2j. Therefore, Equation (2) with $M \geq 4$ is sufficiently general to account for one π exchange and all angular momentum states with $j \leq (M - 2)/2$. The coefficients C(J) are, in fact, related to the B(J) by a non-singular linear transformation which depends only on β. The usefulness of the form of Equation (2) can be seen in the example of the F 5/2 state: only three of the C(J) coefficients, C(2), C(4), and C(6) are needed.

To obtain information from the coefficients, C(J), it is necessary to relate them to phenomenological partial wave amplitudes which specify the states of interest. A convenient set of parameters, which we shall call "helicity coefficients", is chosen by specifying the initial helicity[18], the total angular momentum, and the final orbital angular momentum (or parity). We will implicitly assume conservation of angular momentum and parity. For convenience we will take the photon helicity to be +1, since the cross section, when summed over the nucleon spins, is the same for both helicities.

Helicity Coefficient	Orbital Angular Momentum	Total Angular Momentum	Initial Helicity
$A_{\ell-}$	ℓ	$\ell - 1/2$	1/2
$A_{\ell+}$	ℓ	$\ell + 1/2$	1/2
$B_{\ell-}$	ℓ	$\ell - 1/2$	3/2
$B_{\ell+}$	ℓ	$\ell + 1/2$	3/2

These parameters mix electric (E) and magnetic (M) states according to

$$A_{\ell-} = \frac{1}{2}(-\ell + 1)\, E_{\ell-} + \frac{1}{2}(\ell + 1)\, M_{\ell-}$$

$$A_{\ell+} = \frac{1}{2}(\ell + 2)\, E_{\ell+} + \frac{1}{2}\,\ell\, M_{\ell+}$$

$$B_{\ell-} = E_{\ell-} + M_{\ell-}$$

$$B_{\ell+} = E_{\ell+} - M_{\ell+}$$

where $E_{\ell\pm}$, $M_{\ell\pm}$ are the parameters defined by CGLN[19]. The cross section is given by

$$\sigma(X) = \frac{1}{2}\frac{q}{k}\left\{(1 - X)\,|G_1|^2 + \frac{1 - X^2}{4}\left[(1 + X)\,|G_2|^2 + (1 - X)\,|G_3|^2\right] + (1 + X)\,|G_4|^2\right\}$$

where the G_i are amplitudes of definite initial and final helicity.

Initial Helicity	Final Helicity	
1/2	- 1/2	$G_1 = \sum_{\ell=0} (A_{\ell+} + A_{\ell+1\,-})\,(P'_{\ell+1}(X) + P'_{\ell}(X))$
3/2	1/2	$G_2 = \sum_{\ell=1} (B_{\ell+} - B_{\ell+1\,-})\,(P''_{\ell+1}(X) - P''_{\ell}(X))$

Initial Helicity	Final Helicity	
3/2	- 1/2	$G_3 = \sum_{\ell=1} (B_{\ell+} + B_{\ell+1\,-}) (P''_{\ell+1}(X) + P''_{\ell}(X))$
1/2	1/2	$G_4 = \sum_{\ell=0} (A_{\ell+} - A_{\ell+1\,-}) (P'_{\ell+1}(X) - P'_{\ell}(X))$

An advantage of this choice of states is that the $A_{\ell\pm}$ coefficients do not interfere with the $B_{\ell\pm}$ coefficients in the cross section. The CGLN[19] invariant amplitudes, F_i, are related to the helicity amplitudes G_i by the relations

$$G_1 = F_1 + F_2 + 1/2\,(1 + X)\,(F_3 + F_4)$$

$$G_2 = F_3 + F_4$$

$$G_3 = F_3 - F_4$$

$$G_4 = F_1 - F_2 - 1/2\,(1 - X)\,(F_3 - F_4)\,.$$

The cross section, which is bilinear in the helicity coefficients is given as a linear combination of Legendre polynomials in Table 3 for $\ell \leq 3$. The integrated cross section may be obtained from the coefficient of $P_o(X)$ in the table or from

$$\sigma_T = 4\pi \frac{q}{k} \sum_j \Big[\frac{(2j-1)(2j+1)(2j+3)}{32} \left(|B_{\ell+}|^2 + |B_{\ell+1\,-}|^2 \right) + \frac{2j+1}{2} \left(|A_{\ell+}|^2 + |A_{\ell+1\,-}|^2 \right) \Big]$$

TABLE 3

Cross Section Helicity Coefficient Expansion

The cross section is expanded in terms of helicity coefficients and Legendre polynomials, $P_n(X)$. By labeling the coefficients according to total angular momentum and parity, the symmetry of the expansion shortens the table. Let

$$A_{\ell\pm} = a_{1/2\ j\ p}$$

$$B_{\ell\pm} = a_{3/2\ j\ p}$$

where

$$j = \ell \pm 1/2$$

$$p = -(-1)^{\ell} \ .$$

Notice the first index λ of $a_{\lambda jp}$ is the initial helicity. The general form of the cross section is

$$\sigma(X) = \frac{q}{k} \sum_{n=0} P_n(X) \sum_{\substack{\lambda jj'pp' \\ j' \le j \\ \ell' \le \ell}} \gamma^n_{\lambda jj'pp'} \ \mathrm{Re}(a^*_{\lambda jp}\, a_{\lambda j'p'}) \ .$$

The factors $\gamma^n_{\lambda jj'pp'}$ are given in the table. They depend on the relative parity $p \cdot p'$ rather than each parity independently. The restrictions $j' \le j$, $\ell' \le \ell$ in the sum mean each term occurs only once in the sum; i. e., one does not include both $\mathrm{Re}(A^*_{3-}\ A_{2+})$

and $\mathrm{Re}(A^{*}_{2+}\, A_{3-})$ since they are equal. As an example, if only $j = 3/2$ terms are present, the cross section is given by

$$\sigma(X) = \frac{q}{k} \Big\{ \left(|A_{1+}|^2 + |A_{2-}|^2 \right) \left(2P_0(X) + 2P_2(X)\right.$$

$$+ \mathrm{Re}(A^{*}_{2-}\, A_{1+}) \left(-\frac{4}{5} P_1(X) - \frac{36}{5} P_3(X)\right)$$

$$+ \left(|B_{1+}|^2 + |B_{2-}|^2 \right) \left(\frac{3}{2} P_0(X) - \frac{3}{2} P_2(X)\right)$$

$$+ \mathrm{Re}(B^{*}_{2-}\, B_{1+}) \left(-\frac{9}{2} P_1(X) + \frac{9}{2} P_3(X)\right) \Big\} \ .$$

TABLE 3

				P_o	P_1	P_2	P_3	P_4	P_5	P_6
λ	j	j'	p· p'	n=0	n=1	n=2	n=3	n=4	n=5	n=6
$\frac{1}{2}$	$\frac{7}{2}$	$\frac{7}{2}$	+	4		$\frac{1100}{231}$		$\frac{324}{77}$		$\frac{100}{33}$
	$\frac{5}{2}$	$\frac{5}{2}$	+	3		$\frac{24}{7}$		$\frac{18}{7}$		
			-		$-\frac{18}{35}$		$-\frac{16}{5}$		$-\frac{100}{7}$	
	$\frac{3}{2}$	$\frac{3}{2}$	+	2		2				
			-		$-\frac{4}{5}$		$-\frac{36}{5}$			
	$\frac{1}{2}$	$\frac{1}{2}$	+	1						
			-		- 2					
	$\frac{7}{2}$	$\frac{5}{2}$	+			$-\frac{8}{7}$		$-\frac{360}{77}$		$-\frac{200}{11}$
			-		$\frac{72}{7}$		8		$\frac{40}{7}$	
	$\frac{7}{2}$	$\frac{3}{2}$	+			$\frac{72}{7}$		$\frac{40}{7}$		
			-				$-\frac{8}{3}$		$-\frac{40}{3}$	

TABLE 3 (cont.)

				P_0	P_1	P_2	P_3	P_4	P_5	P_6
λ	j	j'	p · p'	n=0	n=1	n=2	n=3	n=4	n=5	n=6
$\frac{1}{2}$	$\frac{7}{2}$	$\frac{1}{2}$	+					- 8		
			-				8			
	$\frac{5}{2}$	$\frac{3}{2}$	+			$-\frac{12}{7}$		$-\frac{72}{7}$		
			-		$\frac{36}{5}$		$\frac{24}{5}$			
	$\frac{5}{2}$	$\frac{1}{2}$	+			6				
			-				-6			
	$\frac{3}{2}$	$\frac{1}{2}$	+			-4				
			-		4					

TABLE 3 (cont.)

				P_0	P_1	P_2	P_3	P_4	P_5	P_6
λ	j	j'	p · p'	n=0	n=1	n=2	n=3	n=4	n=5	n=6
$\frac{3}{2}$	$\frac{7}{2}$	$\frac{7}{2}$	+	15		$\frac{75}{7}$		$-\frac{405}{77}$		$-\frac{225}{11}$
	$\frac{5}{2}$	$\frac{5}{2}$	+	6		$\frac{12}{7}$		$-\frac{54}{7}$		
			-		$-\frac{108}{35}$		$-\frac{56}{5}$		$\frac{100}{7}$	
	$\frac{3}{2}$	$\frac{3}{2}$	+	$\frac{3}{2}$		$-\frac{3}{2}$				
			-		$-\frac{9}{5}$		$\frac{9}{5}$			
	$\frac{7}{2}$	$\frac{5}{2}$	+			$-\frac{60}{7}$		$-\frac{1440}{77}$		$\frac{300}{11}$
			-		$\frac{180}{7}$				$-\frac{180}{7}$	
	$\frac{7}{2}$	$\frac{3}{2}$	+			$\frac{90}{7}$		$-\frac{90}{7}$		
			-				-10		10	
	$\frac{5}{2}$	$\frac{3}{2}$	+			$-\frac{36}{7}$		$\frac{36}{7}$		
			-		$\frac{36}{5}$		$-\frac{36}{5}$			

where $j = \ell + 1/2$ in the sum. With the relations in Table 3, we may now examine the coefficients, C(J), of the fits given in Table 4 for M = 5, 6, 7, 8, 9.

The first question to resolve is what order fit (M) to use. We may attempt to do this by looking at the decrease in χ^2 as M is increased. Another useful technique, made possible by the large number of fits at closely spaced energies, is to look at the last coefficient C(M) as a function of energy. If C(M) varies in a continuous manner and is significantly nonzero, that is, if its value is greater in magnitude than its standard error, then it is very likely that that coefficient is needed. Using this technique, we see that one needs $M \geq 5$ (including $P_3(X)$) around the second resonance (D 3/2 (1519) at $k \approx 700$ MeV), and M = 8 ($P_6(X)$) at energies above the third resonance.

Choosing the best M for a given energy turns out to be quite difficult and often results in an approximation. This is not surprising when one considers the physical states involved. As an example, consider the region of the second resonance, D 3/2 (1519). The cross section due to a D 3/2 state (A2- and B2-) has terms only up to X^2, so one might consider M = 4 to be sufficient. However, the third resonance, F 5/2 (1688), is only 1.7 widths away. A D 3/2 - F 5/2 interference is expected, which gives an X^3 contribution. In addition, the fourth resonance, F 7/2 (1950), is about 2.4 widths from the second and F 7/2 - D 3/2 interference gives an X^5 dependence to the cross section. There are also exchange diagrams other than the π pole which contribute a small amount to each partial wave. Therefore, choosing M = 4 or even M = 5 is an approximation which neglects the presence of the higher angular momentum states. The fact that these terms are not small

TABLE 4

Coefficients From Fits With Variable Coupling Constant

Results of Moravcsik-equivalent fits are given for M = 5, 6, 7, 8, 9. (The statistical standard deviation of each coefficient is printed directly below its value.) Correlated errors are not indicated. K is the lab photon energy in MeV. D is the number of degrees of freedom. The coefficients C(I) are in units of microbarns/steradian.

K	CHISQ	D	COUPLING CONSTANT	C(I) DC(I) I = 1	2	3	4	5
589.	17.6	19	15.939	-12.028	-2.118	-3.111	1.387	-0.518
			3.471	1.733	1.816	1.569	0.491	0.312
603.	22.8	19	20.686	-14.034	-4.452	-5.209	2.087	-0.049
			3.381	1.693	1.762	1.529	0.470	0.309
618.	11.9	19	20.921	-15.197	-4.492	-5.509	1.365	-0.544
			3.446	1.733	1.788	1.555	0.467	0.307
635.	19.6	19	15.596	-12.534	-1.486	-3.006	0.445	-0.934
			3.375	1.696	1.746	1.520	0.463	0.306
647.	30.3	20	16.760	-13.172	-1.837	-3.393	0.469	-0.762
			2.771	1.359	1.422	1.235	0.386	0.267
663.	17.2	20	21.498	-15.435	-3.970	-5.509	0.783	-0.541
			2.734	1.345	1.398	1.219	0.378	0.266
680.	29.6	20	20.634	-14.517	-3.038	-4.803	0.391	-0.466
			2.718	1.336	1.381	1.210	0.371	0.266
698.	20.0	20	16.558	-12.232	-0.748	-3.205	-0.068	-0.649
			2.677	1.311	1.351	1.190	0.360	0.267
715.	26.0	20	15.694	-11.620	-0.118	-2.947	-0.543	-0.334
			3.358	1.669	1.678	1.478	0.429	0.293
733.	23.1	20	11.326	-9.432	1.567	-1.550	-1.240	-0.489
			3.147	1.570	1.563	1.383	0.394	0.277
752.	30.3	19	13.241	-9.915	-0.119	-2.661	-0.306	0.009
			3.017	1.517	1.486	1.321	0.360	0.259
772.	15.0	19	17.867	-12.191	-3.056	-5.071	0.545	0.535
			2.887	1.466	1.412	1.262	0.326	0.239
793.	31.7	20	14.752	-10.480	-2.299	-4.042	1.165	0.977
			2.279	1.204	1.119	1.021	0.235	0.201
813.	30.2	19	15.380	-10.786	-3.088	-4.368	1.813	1.192
			2.216	1.174	1.080	0.989	0.222	0.195
834.	31.4	19	20.916	-13.513	-6.119	-6.927	2.455	1.426
			2.160	1.152	1.042	0.960	0.206	0.181
857.	19.5	19	19.562	-11.842	-5.584	-6.114	3.089	1.678
			2.115	1.128	1.009	0.934	0.190	0.172
880.	20.5	15	21.655	-12.019	-6.415	-6.653	3.749	2.000
			2.326	1.204	1.097	1.012	0.222	0.192
902.	26.3	15	26.680	-12.989	-8.469	-8.264	4.551	2.312
			2.246	1.146	1.046	0.966	0.214	0.191
926.	42.0	15	28.588	-13.943	-9.163	-8.997	4.488	2.102
			2.215	1.127	1.020	0.944	0.207	0.184
951.	55.6	15	30.126	-12.713	-9.470	-9.013	4.917	2.320
			2.173	1.085	0.987	0.913	0.204	0.182
977.	256.0	23	38.919	-15.891	-13.016	-11.825	5.772	2.259
			1.643	0.819	0.733	0.686	0.126	0.128
1002.	230.1	22	41.886	-16.514	-14.053	-12.810	5.839	2.268
			1.585	0.784	0.698	0.655	0.121	0.127
1028.	272.6	22	39.570	-14.654	-12.915	-11.565	5.670	2.115
			1.511	0.737	0.657	0.618	0.114	0.122
1056.	201.2	22	39.850	-15.230	-13.299	-11.826	5.212	1.819
			1.446	0.707	0.620	0.586	0.103	0.111
1074.	194.9	22	35.589	-13.230	-11.536	-10.155	4.819	1.742
			1.380	0.674	0.591	0.557	0.102	0.102
1102.	126.2	22	26.935	-10.065	-8.404	-7.268	3.866	1.230
			1.280	0.628	0.542	0.511	0.088	0.085
1131.	93.7	22	20.727	-7.728	-6.248	-5.227	3.157	0.889
			1.185	0.580	0.495	0.469	0.077	0.076
1162.	48.3	22	19.295	-7.423	-5.970	-5.034	2.897	0.904
			1.127	0.553	0.464	0.441	0.068	0.069
1174.	35.4	17	20.022	-7.968	-6.371	-5.331	3.030	0.987
			2.048	0.967	0.834	0.777	0.139	0.106
1204.	48.6	16	14.041	-5.326	-4.023	-3.236	2.455	0.755
			1.911	0.894	0.768	0.717	0.128	0.099
1235.	65.9	16	14.920	-5.490	-4.448	-3.629	2.491	0.916
			1.880	0.879	0.744	0.693	0.116	0.092
1269.	35.3	15	14.862	-5.294	-4.373	-3.586	2.453	0.714
			1.891	0.855	0.737	0.689	0.117	0.106

K	CHISQ	D	COUPLING CONSTANT	C(I) DC(I) I = 1	2	3	4	5	6
589.	17.6	18	15.522	-11.920	-1.910	-2.952	1.303	-0.581	-0.041
			5.065	1.980	2.584	2.110	0.890	0.635	0.364
603.	18.2	18	12.952	-12.007	-0.603	-2.237	0.563	-1.193	-0.786
			4.925	1.936	2.506	2.057	0.848	0.613	0.364
618.	11.9	18	20.951	-15.205	-4.507	-5.521	1.370	-0.540	0.003
			4.935	1.978	2.508	2.075	0.822	0.602	0.360
635.	17.9	18	11.073	-11.307	0.754	-1.236	-0.393	-1.606	-0.467
			4.824	1.937	2.442	2.032	0.788	0.596	0.356
647.	26.0	19	10.882	-11.561	1.057	-1.092	-0.559	-1.604	-0.655
			3.967	1.566	1.994	1.662	0.629	0.487	0.316
663.	12.7	19	15.643	-13.803	-1.097	-3.207	-0.207	-1.366	-0.658
			3.882	1.549	1.945	1.631	0.600	0.471	0.310
680.	24.4	19	14.477	-12.779	-0.028	-2.381	-0.614	-1.318	-0.701
			3.836	1.539	1.913	1.612	0.577	0.459	0.308
698.	9.5	19	8.068	-9.820	3.386	0.125	-1.401	-1.788	-1.001
			3.744	1.507	1.857	1.571	0.546	0.441	0.308
715.	21.7	19	9.612	-9.916	2.834	-0.557	-1.510	-1.189	-0.710
			4.446	1.858	2.195	1.870	0.631	0.504	0.340
733.	20.2	19	6.691	-8.126	3.804	0.276	-1.952	-1.135	-0.554
			4.159	1.747	2.041	1.749	0.574	0.470	0.325
752.	28.1	18	9.325	-8.822	1.768	-1.107	-0.901	-0.554	-0.483
			3.999	1.685	1.952	1.682	0.537	0.458	0.324
772.	13.6	18	14.903	-11.335	-1.639	-3.892	0.116	0.128	-0.356
			3.831	1.636	1.855	1.611	0.489	0.419	0.302
793.	26.3	19	19.543	-11.969	-4.576	-5.951	1.787	1.545	0.576
			3.074	1.364	1.488	1.311	0.356	0.317	0.248
813.	25.4	18	19.924	-12.229	-5.236	-6.181	2.386	1.715	0.521
			3.034	1.346	1.457	1.289	0.343	0.308	0.238
834.	28.0	18	24.682	-14.740	-7.885	-8.425	2.903	1.841	0.418
			2.966	1.329	1.413	1.255	0.318	0.288	0.226
857.	17.3	18	16.629	-10.874	-4.216	-4.952	2.746	1.368	-0.312
			2.895	1.303	1.367	1.219	0.299	0.271	0.210
880.	16.1	14	17.485	-10.749	-4.494	-5.034	3.232	1.522	-0.459
			3.059	1.347	1.429	1.273	0.332	0.298	0.219
902.	21.5	14	22.381	-11.688	-6.504	-6.606	4.020	1.825	-0.465
			2.987	1.292	1.380	1.229	0.324	0.294	0.213
926.	29.6	14	21.719	-11.846	-6.055	-6.359	3.674	1.336	-0.728
			2.951	1.275	1.349	1.205	0.310	0.285	0.207
951.	44.2	14	23.536	-10.709	-6.522	-6.501	4.160	1.597	-0.693
			2.923	1.237	1.319	1.178	0.304	0.281	0.206
977.	98.6	22	22.802	-10.595	-5.832	-5.737	4.194	1.007	-1.822
			2.086	0.921	0.930	0.841	0.178	0.163	0.145
1002.	71.7	21	25.852	-11.310	-7.017	-6.783	4.354	0.972	-1.846
			2.033	0.886	0.895	0.812	0.169	0.164	0.147
1028.	63.3	21	21.962	-9.004	-5.271	-5.018	4.073	0.745	-2.037
			1.940	0.834	0.843	0.766	0.159	0.155	0.141
1056.	29.6	21	24.859	-10.366	-6.855	-6.314	3.905	0.719	-1.675
			1.844	0.798	0.792	0.721	0.143	0.139	0.129
1074.	57.2	21	22.383	-8.951	-6.027	-5.296	3.883	0.745	-1.536
			1.781	0.767	0.755	0.694	0.129	0.133	0.131
1102.	42.7	21	17.440	-6.926	-4.493	-3.788	3.227	0.534	-1.018
			1.649	0.716	0.691	0.637	0.113	0.114	0.111
1131.	64.2	21	15.503	-5.985	-4.122	-3.331	2.822	0.524	-0.531
			1.526	0.663	0.631	0.584	0.098	0.101	0.098
1162.	47.4	21	18.476	-7.146	-5.642	-4.739	2.845	0.851	-0.078
			1.445	0.632	0.589	0.548	0.098	0.090	0.086
1174.	33.3	16	17.215	-7.062	-5.240	-4.307	2.809	0.725	-0.221
			2.823	1.152	1.144	1.052	0.207	0.210	0.153
1204.	46.4	15	11.232	-4.421	-2.909	-2.220	2.246	0.496	-0.215
			2.691	1.082	1.074	0.992	0.190	0.201	0.145
1235.	65.2	15	13.452	-5.011	-3.874	-3.104	2.387	0.790	-0.106
			2.618	1.062	1.030	0.954	0.174	0.182	0.132
1269.	20.1	14	22.220	-7.682	-7.196	-6.193	2.978	1.279	0.561
			2.669	1.059	1.032	0.980	0.173	0.179	0.144

K	CHISQ	D	COUPLING CONSTANT	C(I) DC(I) I = 1	2	3	4	5	6	7
589.	16.2	17	9.363	-10.961	1.075	-0.806	-0.138	-1.594	-0.747	-0.457
			7.216	2.136	3.590	2.767	1.496	1.057	0.692	0.382
603.	18.0	17	10.821	-11.660	0.431	-1.486	0.077	-1.539	-1.026	-0.162
			6.966	2.096	3.463	2.691	1.408	1.006	0.663	0.376
618.	11.2	17	16.903	-14.517	-2.543	-4.075	0.476	-1.186	-0.457	-0.316
			6.892	2.140	3.427	2.694	1.344	0.976	0.655	0.375
635.	17.1	17	6.923	-10.592	2.759	0.253	-1.284	-2.247	-0.949	-0.340
			6.787	2.104	3.360	2.658	1.294	0.949	0.659	0.391
647.	22.7	18	3.566	-10.230	4.601	1.567	-2.096	-2.695	-1.473	-0.625
			5.645	1.728	2.786	2.212	1.053	0.771	0.549	0.343
663.	9.9	18	9.222	-12.602	2.001	-0.861	-1.512	-2.294	-1.376	-0.567
			5.468	1.708	2.690	2.154	0.986	0.729	0.530	0.340
680.	24.0	18	12.104	-12.323	1.112	-1.508	-1.082	-1.651	-0.964	-0.216
			5.358	1.699	2.625	2.120	0.937	0.698	0.516	0.340
698.	8.3	18	4.122	-9.036	5.275	1.587	-2.154	-2.326	-1.431	-0.364
			5.201	1.669	2.537	2.064	0.879	0.662	0.500	0.333
715.	20.0	18	3.693	-8.779	5.660	1.647	-2.624	-2.052	-1.420	-0.512
			6.392	2.057	3.102	2.534	1.070	0.838	0.648	0.398
733.	19.3	18	10.792	-8.944	1.855	-1.259	-1.209	-0.554	-0.068	0.354
			6.036	1.952	2.914	2.396	0.978	0.777	0.612	0.377
752.	25.0	17	1.438	-7.179	5.511	1.879	-2.283	-1.678	-1.406	-0.640
			6.031	1.929	2.898	2.398	0.956	0.789	0.619	0.367
772.	12.7	17	10.931	-10.458	0.237	-2.381	-0.551	-0.413	-0.796	-0.316
			5.716	1.886	2.731	2.281	0.864	0.714	0.559	0.337
793.	16.9	18	9.446	-9.470	0.145	-2.096	0.230	0.354	-0.391	-0.824
			4.505	1.589	2.141	1.816	0.620	0.501	0.401	0.269
813.	15.1	17	10.065	-9.709	-0.661	-2.415	0.926	0.610	-0.370	-0.815
			4.320	1.559	2.040	1.744	0.570	0.462	0.366	0.254
834.	17.0	17	14.825	-12.115	-3.343	-4.642	1.499	0.784	-0.419	-0.801
			4.195	1.546	1.966	1.695	0.529	0.429	0.338	0.241
857.	9.7	17	8.702	-8.723	-0.593	-1.910	1.653	0.546	-0.957	-0.637
			4.083	1.519	1.897	1.645	0.497	0.403	0.315	0.231
880.	10.7	13	10.503	-9.075	-1.370	-2.426	2.272	0.765	-1.123	-0.610
			4.280	1.527	1.959	1.694	0.528	0.441	0.359	0.262
902.	7.2	13	11.253	-9.004	-1.569	-2.470	2.539	0.659	-1.507	-0.976
			4.189	1.473	1.898	1.644	0.508	0.426	0.348	0.258
926.	8.8	13	8.419	-8.554	-0.210	-1.421	1.982	-0.005	-1.948	-1.136
			4.149	1.465	1.861	1.620	0.484	0.410	0.338	0.249
951.	16.1	13	8.130	-6.840	0.178	-0.799	2.280	0.086	-2.075	-1.295
			4.120	1.436	1.826	1.595	0.467	0.400	0.332	0.244
977.	29.2	21	7.251	-6.442	0.943	0.105	2.311	-0.401	-2.929	-1.456
			2.799	1.047	1.236	1.095	0.288	0.235	0.197	0.175
1002.	34.7	20	15.096	-8.457	-2.370	-2.753	3.060	0.058	-2.569	-1.072
			2.695	1.003	1.177	1.045	0.273	0.222	0.189	0.176
1028.	26.6	20	11.737	-6.292	-0.901	-1.252	2.888	-0.113	-2.705	-1.013
			2.572	0.946	1.109	0.986	0.252	0.210	0.179	0.167
1056.	19.0	20	19.632	-8.951	-4.652	-4.393	3.328	0.293	-2.001	-0.499
			2.447	0.909	1.042	0.932	0.228	0.191	0.162	0.154
1074.	39.1	20	15.854	-7.156	-3.295	-2.925	3.172	0.255	-1.905	-0.532
			2.350	0.875	0.991	0.890	0.211	0.176	0.157	0.149
1102.	40.0	20	15.111	-6.267	-3.531	-2.944	2.986	0.365	-1.143	-0.212
			2.167	0.819	0.902	0.816	0.184	0.153	0.134	0.128
1131.	62.0	20	13.586	-5.434	-3.339	-2.642	2.629	0.395	-0.628	-0.168
			2.005	0.761	0.825	0.748	0.164	0.134	0.118	0.114
1162.	47.2	20	19.117	-7.334	-5.900	-4.967	2.907	0.892	-0.048	0.054
			1.909	0.731	0.775	0.705	0.148	0.121	0.104	0.104
1174.	30.1	15	21.485	-8.294	-6.945	-5.825	3.182	1.043	0.061	0.275
			3.704	1.344	1.491	1.354	0.294	0.276	0.220	0.154
1204.	23.8	14	21.634	-7.421	-7.012	-5.865	3.137	1.194	0.437	0.705
			3.466	1.252	1.377	1.253	0.267	0.249	0.200	0.148
1235.	38.3	14	24.489	-8.240	-8.173	-6.936	3.297	1.487	0.645	0.735
			3.374	1.231	1.322	1.207	0.247	0.226	0.182	0.142
1269.	17.2	13	26.070	-8.795	-8.676	-7.498	3.261	1.524	0.741	0.307
			3.502	1.245	1.351	1.228	0.244	0.230	0.179	0.161

K	CHISQ	D	COUPLING CONSTANT	C(I) DC(I) I = 1	2	3	4	5	6	7	8
584.	16.2	16	8.970	-10.946	1.259	-0.683	-0.246	-1.671	-0.798	-0.494	-0.023
			10.661	2.156	5.144	3.701	2.622	1.865	1.243	0.822	0.470
603.	17.2	16	17.472	-11.977	-2.696	-3.610	1.851	-0.266	-0.163	0.455	0.409
			10.198	2.126	4.924	3.591	2.434	1.744	1.172	0.786	0.458
618.	10.8	16	21.527	-14.798	-4.719	-5.583	1.663	-0.326	0.138	0.116	0.282
			10.261	2.190	4.954	3.661	2.370	1.719	1.177	0.803	0.463
635.	17.1	16	8.355	-10.696	2.085	-0.221	-0.930	-1.989	-0.768	-0.208	0.089
			10.009	2.171	4.826	3.605	2.233	1.634	1.138	0.784	0.459
647.	22.7	17	3.592	-10.232	4.589	1.558	-2.090	-2.690	-1.470	-0.622	0.002
			7.941	1.787	3.836	2.903	1.716	1.263	0.868	0.606	0.388
663.	9.7	17	6.792	-12.383	3.146	-0.034	-2.082	-2.718	-1.663	-0.785	-0.173
			7.662	1.775	3.692	2.825	1.599	1.187	0.828	0.589	0.382
680.	22.6	17	5.958	-11.719	4.000	0.606	-2.474	-2.698	-1.678	-0.764	-0.448
			7.481	1.775	3.593	2.778	1.509	1.130	0.797	0.576	0.381
698.	7.2	17	-1.199	-8.468	7.766	3.439	-3.320	-3.213	-2.027	-0.838	-0.399
			7.236	1.754	3.462	2.706	1.410	1.068	0.753	0.559	0.378
715.	15.6	17	-10.691	-7.080	12.392	6.736	-5.655	-4.433	-3.100	-1.793	-0.914
			9.362	2.210	4.458	3.504	1.795	1.409	1.028	0.727	0.435
733.	19.3	17	11.450	-9.028	1.548	-1.493	-1.075	-0.449	0.006	0.411	0.043
			8.695	2.109	4.123	3.274	1.606	1.270	0.932	0.666	0.410
752.	23.8	16	-4.874	-6.299	8.438	4.145	-3.514	-2.648	-2.037	-1.183	-0.419
			8.343	2.090	3.943	3.168	1.476	1.187	0.878	0.616	0.383
772.	12.3	16	7.717	-9.966	1.721	-1.218	-1.150	-0.887	-1.130	-0.581	-0.213
			7.835	2.056	3.685	2.994	1.321	1.065	0.789	0.556	0.355
793.	16.0	17	13.430	-10.187	-1.684	-3.553	0.926	0.896	-0.030	-0.534	0.274
			6.162	1.760	2.883	2.380	0.961	0.761	0.553	0.407	0.269
813.	14.9	16	11.758	-10.030	-1.433	-3.034	1.207	0.828	-0.220	-0.692	0.115
			5.978	1.744	2.776	2.308	0.892	0.705	0.518	0.392	0.280
834.	17.0	16	15.061	-12.163	-3.450	-4.728	1.537	0.813	-0.399	-0.785	0.016
			5.755	1.740	2.657	2.229	0.816	0.647	0.478	0.363	0.261
857.	9.7	16	8.971	-8.780	-0.714	-2.009	1.693	0.578	-0.934	-0.619	0.017
			5.536	1.714	2.534	2.145	0.745	0.600	0.448	0.336	0.240
880.	10.2	12	7.577	-8.524	-0.074	-1.370	1.835	0.408	-1.395	-0.824	-0.183
			6.028	1.724	2.714	2.284	0.826	0.680	0.533	0.406	0.285
902.	7.1	12	10.108	-8.783	-1.067	-2.057	2.375	0.523	-1.612	-1.059	-0.071
			5.886	1.675	2.624	2.219	0.779	0.648	0.514	0.395	0.298
926.	8.7	12	9.685	-8.808	-0.760	-1.876	2.154	0.139	-1.837	-1.047	0.079
			5.756	1.669	2.543	2.165	0.728	0.611	0.487	0.376	0.249
951.	16.0	12	6.946	-6.597	0.687	-0.374	2.125	-0.043	-2.176	-1.377	-0.075
			5.657	1.642	2.473	2.117	0.688	0.583	0.468	0.364	0.245
977.	24.2	20	12.203	-7.504	-1.173	-1.694	2.909	0.157	-2.520	-1.195	0.378
			3.575	1.151	1.558	1.361	0.394	0.343	0.269	0.210	0.169
1002.	27.1	19	21.022	-9.736	-4.876	-4.919	3.756	0.700	-2.098	-0.755	0.461
			3.443	1.104	1.485	1.300	0.371	0.321	0.254	0.210	0.167
1028.	26.6	19	11.401	-6.219	-0.761	-1.131	2.850	-0.148	-2.731	-1.031	-0.026
			3.272	1.044	1.394	1.226	0.341	0.297	0.238	0.198	0.157
1056.	19.0	19	19.515	-8.925	-4.603	-4.351	3.315	0.281	-2.010	-0.505	-0.009
			3.095	1.005	1.304	1.153	0.306	0.269	0.218	0.179	0.143
1074.	28.3	19	9.191	-5.602	-0.541	-0.556	2.427	-0.364	-2.348	-0.974	-0.479
			3.106	0.995	1.299	1.146	0.310	0.258	0.207	0.181	0.146
1102.	33.2	19	10.240	-5.083	-1.537	-1.225	2.475	-0.060	-1.459	-0.450	-0.325
			2.862	0.937	1.183	1.049	0.269	0.224	0.181	0.157	0.125
1131.	38.6	19	5.388	-3.386	-0.024	0.237	1.817	-0.296	-1.136	-0.544	-0.527
			2.626	0.871	1.073	0.956	0.234	0.196	0.158	0.138	0.109
1162.	25.8	19	11.812	-5.451	-2.986	-2.417	2.232	0.302	-0.493	-0.242	-0.453
			2.479	0.837	0.999	0.896	0.208	0.176	0.142	0.122	0.093
1174.	17.9	14	10.007	-5.419	-2.416	-1.879	2.146	0.238	-0.671	-0.455	-0.536
			4.947	1.575	1.975	1.762	0.418	0.359	0.304	0.260	0.167
1204.	12.0	13	11.039	-4.741	-2.884	-2.260	2.218	0.502	-0.204	0.024	-0.528
			4.641	1.476	1.828	1.634	0.378	0.320	0.273	0.248	0.154
1235.	19.6	13	12.039	-5.008	-3.381	-2.719	2.279	0.685	-0.192	0.305	-0.593
			4.434	1.440	1.725	1.551	0.341	0.292	0.249	0.220	0.138
1269.	13.1	12	20.529	-7.369	-6.586	-5.624	2.909	1.210	0.373	0.070	-0.339
			4.448	1.432	1.701	1.539	0.332	0.278	0.255	0.215	0.168

K	CHISQ	D	COUPLING CONSTANT	C(I) DC(I) I = 1	2	3	4	5	6	7	8	9
585.	16.1	15	4.745	-11.193	3.202	0.516	-1.544	-2.623	-1.454	-0.924	-0.299	-0.175
			15.909	2.264	7.479	4.993	4.476	3.250	2.215	1.456	0.901	0.489
603.	16.7	15	24.851	-11.629	-6.095	-5.752	4.047	1.362	0.970	1.202	0.895	0.318
			15.112	2.190	7.117	4.835	4.116	3.016	2.075	1.376	0.865	0.481
618.	10.7	15	17.778	-14.901	-2.986	-4.461	0.593	-1.125	-0.424	-0.257	0.038	-0.160
			15.057	2.210	7.106	4.926	3.939	2.912	2.028	1.359	0.854	0.471
635.	16.8	15	3.165	-10.772	4.485	1.370	-2.363	-3.070	-1.524	-0.715	-0.256	-0.232
			14.734	2.177	6.949	4.897	3.728	2.783	1.943	1.316	0.853	0.484
647.	22.7	16	3.031	-10.241	4.847	1.731	-2.242	-2.806	-1.552	-0.677	-0.037	-0.030
			11.225	1.791	5.301	3.795	2.754	2.073	1.451	0.983	0.667	0.421
663.	8.7	16	14.590	-12.334	-0.449	-2.477	-0.029	-1.138	-0.543	-0.037	0.365	0.432
			10.731	1.776	5.063	3.677	2.544	1.930	1.361	0.930	0.643	0.416
680.	20.9	16	15.578	-11.771	-0.431	-2.457	-0.031	-0.803	-0.320	0.144	0.214	0.549
			10.383	1.775	4.890	3.602	2.371	1.814	1.292	0.891	0.625	0.411
698.	6.9	16	-5.119	-8.408	9.569	4.701	-4.280	-3.961	-2.576	-1.199	-0.668	-0.236
			9.981	1.757	4.688	3.496	2.196	1.691	1.223	0.844	0.603	0.414
715.	15.4	16	-6.849	-7.223	10.626	5.473	-4.756	-3.733	-2.586	-1.442	-0.652	0.200
			12.976	2.235	6.078	4.582	2.764	2.160	1.583	1.097	0.752	0.468
733.	13.9	16	-7.568	-8.112	10.263	4.814	-5.362	-3.798	-2.464	-1.289	-1.264	-1.020
			11.959	2.146	5.581	4.258	2.450	1.924	1.416	0.991	0.697	0.440
752.	23.8	15	-3.527	-6.370	7.826	3.699	-3.221	-2.422	-1.920	-1.061	-0.320	0.077
			11.324	2.129	5.258	4.057	2.226	1.748	1.294	0.925	0.681	0.438
772.	11.9	15	12.286	-10.288	-0.347	-2.753	-0.207	-0.152	-0.581	-0.181	0.111	0.256
			10.582	2.116	4.894	3.832	1.976	1.563	1.163	0.835	0.617	0.399
793.	15.8	16	10.916	-9.930	-0.545	-2.689	0.437	0.514	-0.314	-0.727	0.120	-0.145
			8.420	1.855	3.881	3.090	1.472	1.158	0.852	0.601	0.456	0.330
813.	13.8	15	6.024	-9.359	1.152	-1.044	0.148	-0.009	-0.848	-1.120	-0.218	-0.326
			8.024	1.853	3.678	2.963	1.332	1.053	0.783	0.559	0.418	0.304
834.	16.0	15	9.974	-11.494	-1.170	-2.948	0.645	0.102	-0.937	-1.150	-0.271	-0.286
			7.656	1.862	3.489	2.844	1.204	0.958	0.716	0.513	0.386	0.284
857.	9.6	15	10.536	-8.999	-1.410	-2.559	1.955	0.788	-0.774	-0.510	0.105	0.088
			7.364	1.844	3.329	2.739	1.104	0.887	0.670	0.479	0.362	0.273
880.	9.2	11	12.965	-9.193	-2.448	-3.238	2.755	1.151	-0.843	-0.438	0.143	0.301
			8.122	1.852	3.621	2.963	1.243	1.013	0.771	0.563	0.423	0.305
902.	6.9	11	12.532	-9.097	-2.126	-2.898	2.774	0.848	-1.370	-0.890	0.076	0.139
			7.882	1.808	3.483	2.868	1.162	0.955	0.732	0.539	0.409	0.301
926.	8.7	11	9.130	-8.730	-0.520	-1.684	2.067	0.068	-1.890	-1.085	0.046	-0.031
			7.706	1.816	3.375	2.803	1.085	0.895	0.690	0.514	0.397	0.289
951.	16.0	11	7.743	-6.713	0.345	-0.650	2.245	0.054	-2.102	-1.324	-0.026	0.046
			7.506	1.794	3.255	2.722	1.012	0.838	0.652	0.492	0.386	0.282
977.	20.0	19	6.236	-6.641	1.351	0.363	2.070	-0.548	-3.101	-1.534	0.066	-0.423
			4.593	1.224	1.979	1.685	0.565	0.484	0.389	0.282	0.227	0.205
1002.	27.0	18	21.598	-9.819	-5.116	-5.117	3.832	0.768	-2.042	-0.721	0.491	0.045
			4.445	1.177	1.892	1.619	0.526	0.462	0.375	0.267	0.222	0.213
1028.	24.6	18	7.651	-5.651	0.789	0.148	2.380	-0.575	-3.085	-1.244	-0.225	-0.280
			4.247	1.122	1.787	1.535	0.481	0.428	0.349	0.251	0.213	0.202
1056.	18.3	18	17.215	-8.551	-3.662	-3.568	3.041	0.033	-2.216	-0.632	-0.128	-0.163
			4.047	1.090	1.684	1.455	0.436	0.389	0.320	0.230	0.197	0.185
1074.	28.2	18	8.185	-5.423	-0.132	-0.210	2.314	-0.473	-2.437	-1.023	-0.523	-0.071
			3.907	1.081	1.617	1.406	0.408	0.364	0.295	0.214	0.178	0.167
1102.	33.1	18	10.830	-5.194	-1.774	-1.428	2.538	0.001	-1.409	-0.422	-0.302	0.040
			3.597	1.023	1.471	1.289	0.355	0.317	0.257	0.188	0.153	0.147
1131.	38.6	18	5.878	-3.482	-0.218	0.069	1.866	-0.248	-1.096	-0.522	-0.507	0.032
			3.313	0.957	1.338	1.180	0.309	0.280	0.228	0.163	0.136	0.133
1162.	24.2	18	14.269	-5.958	-3.947	-3.257	2.464	0.534	-0.305	-0.137	-0.361	0.154
			3.142	0.927	1.252	1.113	0.277	0.253	0.205	0.148	0.122	0.121
1174.	17.5	13	11.943	-5.805	-3.169	-2.533	2.332	0.410	-0.536	-0.358	-0.483	0.107
			5.884	1.698	2.331	2.065	0.518	0.457	0.376	0.305	0.239	0.180
1204.	12.0	12	10.992	-4.732	-2.867	-2.244	2.214	0.498	-0.207	0.022	-0.531	-0.003
			5.519	1.586	2.154	1.918	0.464	0.424	0.344	0.273	0.227	0.196
1235.	15.6	12	18.043	-6.223	-5.646	-4.726	2.791	1.216	0.207	0.236	-0.270	0.375
			5.351	1.562	2.062	1.846	0.426	0.394	0.319	0.249	0.214	0.189
1263.	12.9	11	13.133	-7.093	-6.064	-5.167	2.702	1.073	0.302	-0.001	-0.392	-0.111
			5.574	1.578	2.114	1.890	0.419	0.431	0.307	0.275	0.211	0.267

enough to be completely neglected causes χ^2 to decrease slowly with increasing M. Because of the statistical errors of the present data, it is not possible to make a clear decision about the order polynomial required by looking for a rapid decrease in χ^2 with increasing M. The importance of the choice of the order of fit is seen in the determination of the coupling constant.

The first coefficient of each fit gives a measurement of the πN coupling constant. The high powers of X, above X^{M-2}, determine C(0); consequently, the value obtained for the coupling constant depends on the order of the fit. This is especially true if M is too small, since an X^{M-1} dependence will attempt to satisfy itself with what it finds in σ_{OPE}. This effect is especially noticeable at the third resonance ($K \approx 1000$) for M = 5. A value of M too large is less serious, but still undesirable since some of the available information about $G^2/4\pi$ is not used in this case. The following rather subjective criterion was used to select the best M at each energy. If a coefficient C(J) varied significantly from zero ($|C(J)| > DC(J)$) in a smooth manner for several adjacent energies, it was considered necessary and M was chosen at least as large as J. On the other hand, the smallest M compatible with the above was used. This resulted in the choices

M = 5	$589 \leq K < 834$
M = 7	$834 \leq K < 977$
M = 8	$977 \leq K \leq 1269$

which give a weighted average of

$$G^2/4\pi = 14.5 \pm 0.6 \ .$$

Unfortunately, this average is sensitive to the choices of M, so the error given, which is due only to statistical errors in the cross section, is too small an estimate. For example, if M = 8 is chosen for all energies, the average is

$$G^2/4\pi = 11.2 \pm 0.8.$$

A reasonable estimate of the error in $G^2/4\pi$ is $\pm$ 3.0.

In order to investigate the resonant states, the Moravcsik-equivalent fits were done with $G^2/4\pi$ fixed to a constant value of 14.7. This eliminates the fluctuations of the C(J) with energy that are due to errors correlated with C(0). The results are given in Table 5 and Figure 10. The fits are shown with the data in Figure 6. The total cross sections, and the 0^o, 90^o, and 180^o cross sections obtained from these fits are given in Table 6 and Figures 11, 12 and 13.

The following conclusions can be drawn from the coefficients, C(J), with the help of Table 3. The energy dependence of C(6) near W = 1672 indicates the presence of at least one resonant state. It must have $j \geq 5/2$ to contribute to C(6). The possibility that it has $j > 5/2$ is eliminated because no bump of the same magnitude is found in C(8) and the 0^o cross section, as we will see, implies the production is almost entirely from an initial helicity $\pm$ 3/2. (A F 7/2 state, for example, gives in general a cross section which is a 6th order polynomial in cos θ. However, only a 4th order polynomial occurs if $|A3+/B3+|^2 = 28/4$.) The resonance can therefore be either in a D (B2+) or F (B3-) wave, or a mixture of both.

TABLE 5

Coefficients From Fits With Fixed Coupling Constant

Results of Moravcsik-equivalent fits with $G^2/4\pi = 14.7$ for M = 8. (The statistical standard deviation of each coefficient is printed directly below its value.) Correlated errors are not indicated. K is the lab photon energy in MeV. D is the number of degrees of freedom. The coefficients are in units of microbarns/steradian.

K	CHISQ	D	C(I) DC(I)	I = 1	2	3	4	5	6	7	8
589.	16.5	17		-11.740	-1.503	-2.654	1.130	-0.704	-0.170	-0.107	0.162
				1.570	0.203	0.497	0.569	0.488	0.420	0.397	0.318
603.	17.3	17		-11.565	-1.358	-2.642	1.205	-0.723	-0.462	0.268	0.318
				1.489	0.190	0.462	0.534	0.462	0.401	0.384	0.313
618.	11.3	17		-13.723	-1.426	-3.165	0.124	-1.428	-0.597	-0.351	0.053
				1.478	0.185	0.447	0.518	0.457	0.406	0.390	0.311
635.	17.5	17		-11.747	-0.972	-2.491	0.451	-0.989	-0.090	0.227	0.303
				1.402	0.173	0.419	0.485	0.432	0.390	0.380	0.311
647.	24.7	18		-12.223	-0.773	-2.478	0.251	-0.989	-0.332	0.112	0.384
				1.080	0.130	0.314	0.377	0.341	0.304	0.303	0.276
663.	10.8	18		-13.868	-0.662	-2.933	-0.473	-1.540	-0.866	-0.261	0.103
				1.040	0.125	0.298	0.358	0.326	0.296	0.298	0.272
680.	24.0	18		-13.427	-0.196	-2.623	-0.757	-1.429	-0.811	-0.186	-0.138
				1.007	0.121	0.284	0.342	0.315	0.290	0.296	0.273
698.	12.0	18		-11.693	0.164	-2.479	-0.305	-0.964	-0.490	0.212	0.177
				0.960	0.116	0.266	0.324	0.303	0.279	0.289	0.271
715.	23.0	18		-12.109	0.308	-2.729	-0.903	-0.760	-0.497	-0.057	-0.053
				1.202	0.134	0.315	0.391	0.387	0.369	0.345	0.297
733.	19.4	18		-9.701	0.008	-2.712	-0.490	0.007	0.330	0.630	0.153
				1.098	0.123	0.285	0.355	0.353	0.338	0.319	0.284
752.	29.4	17		-10.579	-0.809	-3.262	-0.136	0.024	-0.169	0.085	0.201
				1.020	0.115	0.262	0.325	0.333	0.320	0.296	0.277
772.	13.1	17		-11.592	-1.562	-3.877	-0.004	0.023	-0.477	-0.149	0.003
				0.949	0.105	0.239	0.299	0.306	0.293	0.272	0.259
793.	16.0	18		-10.517	-2.278	-4.042	1.118	1.046	0.075	-0.461	0.315
				0.735	0.086	0.190	0.235	0.229	0.211	0.204	0.212
813.	15.2	17		-10.816	-2.799	-4.167	1.633	1.159	0.016	-0.526	0.210
				0.702	0.082	0.182	0.219	0.214	0.197	0.200	0.202
834.	17.0	17		-12.062	-3.284	-4.589	1.487	0.775	-0.427	-0.804	0.004
				0.662	0.076	0.169	0.204	0.199	0.185	0.189	0.190
857.	10.8	17		-10.430	-3.336	-4.223	2.439	1.167	-0.508	-0.325	0.185
				0.628	0.071	0.158	0.187	0.189	0.175	0.178	0.177
880.	11.6	13		-10.379	-3.280	-4.060	2.778	1.169	-0.814	-0.413	0.038
				0.711	0.082	0.178	0.211	0.216	0.208	0.208	0.188
902.	7.7	13		-9.982	-3.114	-3.784	2.963	1.003	-1.242	-0.795	0.070
				0.667	0.078	0.166	0.195	0.205	0.198	0.203	0.183
926.	9.4	13		-10.151	-2.975	-3.758	2.768	0.643	-1.446	-0.767	0.229
				0.638	0.074	0.157	0.184	0.196	0.190	0.195	0.179
951.	17.9	13		-8.693	-2.701	-3.268	3.038	0.714	-1.585	-0.953	0.155
				0.599	0.071	0.147	0.172	0.186	0.183	0.190	0.178
977.	24.7	21		-8.255	-2.261	-2.642	3.172	0.378	-2.356	-1.080	0.451
				0.408	0.046	0.096	0.116	0.135	0.130	0.132	0.133
1002.	30.4	20		-7.837	-2.150	-2.539	3.107	0.160	-2.505	-1.052	0.270
				0.388	0.045	0.093	0.113	0.129	0.125	0.134	0.130
1028.	27.6	20		-7.207	-2.166	-2.364	3.178	0.126	-2.523	-0.878	0.072
				0.358	0.042	0.084	0.104	0.121	0.119	0.127	0.124
1056.	21.5	20		-7.451	-2.576	-2.561	2.863	-0.101	-2.302	-0.718	-0.145
				0.334	0.038	0.077	0.094	0.110	0.110	0.116	0.113
1074.	31.5	20		-7.275	-2.843	-2.584	2.947	0.056	-2.031	-0.723	-0.310
				0.317	0.037	0.074	0.101	0.102	0.105	0.114	0.111
1102.	35.6	20		-6.474	-3.380	-2.857	2.871	0.261	-1.215	-0.259	-0.198
				0.285	0.031	0.065	0.089	0.087	0.091	0.099	0.095
1131.	51.2	20		-6.340	-3.826	-3.148	2.600	0.341	-0.654	-0.165	-0.277
				0.255	0.027	0.058	0.078	0.078	0.080	0.088	0.083
1162.	27.2	20		-6.386	-4.150	-3.459	2.460	0.489	-0.351	-0.133	-0.380
				0.235	0.025	0.052	0.071	0.072	0.072	0.079	0.076
1174.	18.8	15		-6.859	-4.289	-3.548	2.527	0.556	-0.409	-0.253	-0.481
				0.421	0.044	0.095	0.114	0.129	0.128	0.148	0.125
1204.	12.6	14		-5.865	-4.326	-3.547	2.505	0.737	-0.008	0.183	-0.448
				0.383	0.041	0.087	0.105	0.118	0.115	0.144	0.115
1235.	20.0	14		-5.845	-4.416	-3.643	2.475	0.848	-0.057	0.112	-0.544
				0.362	0.037	0.080	0.097	0.110	0.107	0.131	0.105
1269.	14.8	13		-5.549	-4.356	-3.610	2.393	0.874	0.075	-0.145	-0.474
				0.349	0.038	0.076	0.096	0.107	0.115	0.139	0.132

TABLE 6

Cross Sections From Fits

KLAB is in units of MeV. W is the total c. m. energy in MeV. The integral (total) cross section is in units of microbarns. The 0^{o}, 90^{o}, 180^{o} cross section is in units of microbarns/steradian. The errors listed are statistical standard deviations only.

KLAB	W	INTEGRAL	0	90	180
589	1409	84.44 +- 0.84	19.63 +- 0.56	6.21 +- 0.15	3.08 +- 0.29
603	1418	85.59 +- 0.83	19.74 +- 0.55	6.12 +- 0.14	2.80 +- 0.31
618	1428	87.27 +- 0.85	20.66 +- 0.57	6.58 +- 0.14	3.10 +- 0.31
635	1439	89.62 +- 0.89	19.93 +- 0.56	6.92 +- 0.16	2.94 +- 0.30
647	1447	92.33 +- 0.77	20.62 +- 0.44	7.06 +- 0.15	2.89 +- 0.29
663	1457	95.27 +- 0.78	21.10 +- 0.44	7.37 +- 0.15	2.84 +- 0.29
680	1468	99.84 +- 0.79	20.71 +- 0.43	8.01 +- 0.15	2.34 +- 0.29
698	1480	101.42 +- 0.80	19.70 +- 0.42	8.10 +- 0.15	2.78 +- 0.28
715	1491	103.03 +- 0.93	19.53 +- 0.55	8.54 +- 0.16	2.40 +- 0.29
733	1502	95.60 +- 0.89	17.33 +- 0.53	8.21 +- 0.16	2.08 +- 0.28
752	1514	85.62 +- 0.89	17.09 +- 0.51	6.94 +- 0.15	2.24 +- 0.27
772	1526	76.49 +- 0.81	17.14 +- 0.50	5.99 +- 0.13	1.96 +- 0.27
793	1539	65.36 +- 0.64	16.81 +- 0.42	4.74 +- 0.12	2.69 +- 0.25
813	1551	58.31 +- 0.62	17.16 +- 0.41	3.89 +- 0.11	2.59 +- 0.25
834	1564	52.66 +- 0.58	17.29 +- 0.40	3.29 +- 0.10	2.40 +- 0.23
857	1577	49.26 +- 0.54	16.26 +- 0.39	2.59 +- 0.09	2.16 +- 0.23
880	1591	48.94 +- 0.62	16.18 +- 0.43	2.31 +- 0.10	2.03 +- 0.23
902	1604	49.70 +- 0.61	15.07 +- 0.41	2.13 +- 0.10	2.25 +- 0.22
926	1618	50.62 +- 0.61	15.00 +- 0.40	2.15 +- 0.10	2.46 +- 0.21
951	1632	51.62 +- 0.61	12.79 +- 0.38	2.16 +- 0.10	2.41 +- 0.21
977	1647	55.71 +- 0.43	12.17 +- 0.27	2.06 +- 0.05	2.35 +- 0.21
1002	1661	55.74 +- 0.44	10.97 +- 0.26	2.11 +- 0.06	2.15 +- 0.20
1028	1676	53.98 +- 0.42	9.86 +- 0.24	2.02 +- 0.06	1.68 +- 0.20
1056	1692	47.99 +- 0.38	9.36 +- 0.24	1.82 +- 0.05	1.22 +- 0.18
1074	1702	43.82 +- 0.38	9.06 +- 0.22	1.60 +- 0.07	1.01 +- 0.18
1102	1717	35.37 +- 0.32	8.17 +- 0.20	1.27 +- 0.06	0.93 +- 0.15
1131	1733	28.64 +- 0.28	7.55 +- 0.19	1.10 +- 0.05	0.82 +- 0.13
1162	1749	23.54 +- 0.25	7.25 +- 0.18	0.89 +- 0.05	0.68 +- 0.13
1174	1756	21.75 +- 0.43	7.82 +- 0.30	0.69 +- 0.07	0.59 +- 0.13
1204	1772	19.49 +- 0.41	6.83 +- 0.28	0.71 +- 0.06	0.35 +- 0.12
1235	1788	17.32 +- 0.37	6.46 +- 0.27	0.55 +- 0.06	0.15 +- 0.12
1269	1806	16.76 +- 0.39	5.86 +- 0.26	0.58 +- 0.06	0.52 +- 0.27

FIGURE 10

Coefficients From the Data Fitting

The coefficients C(I) are given as a function of total c. m. energy for fit with $G^2/4\pi = 14.7$.

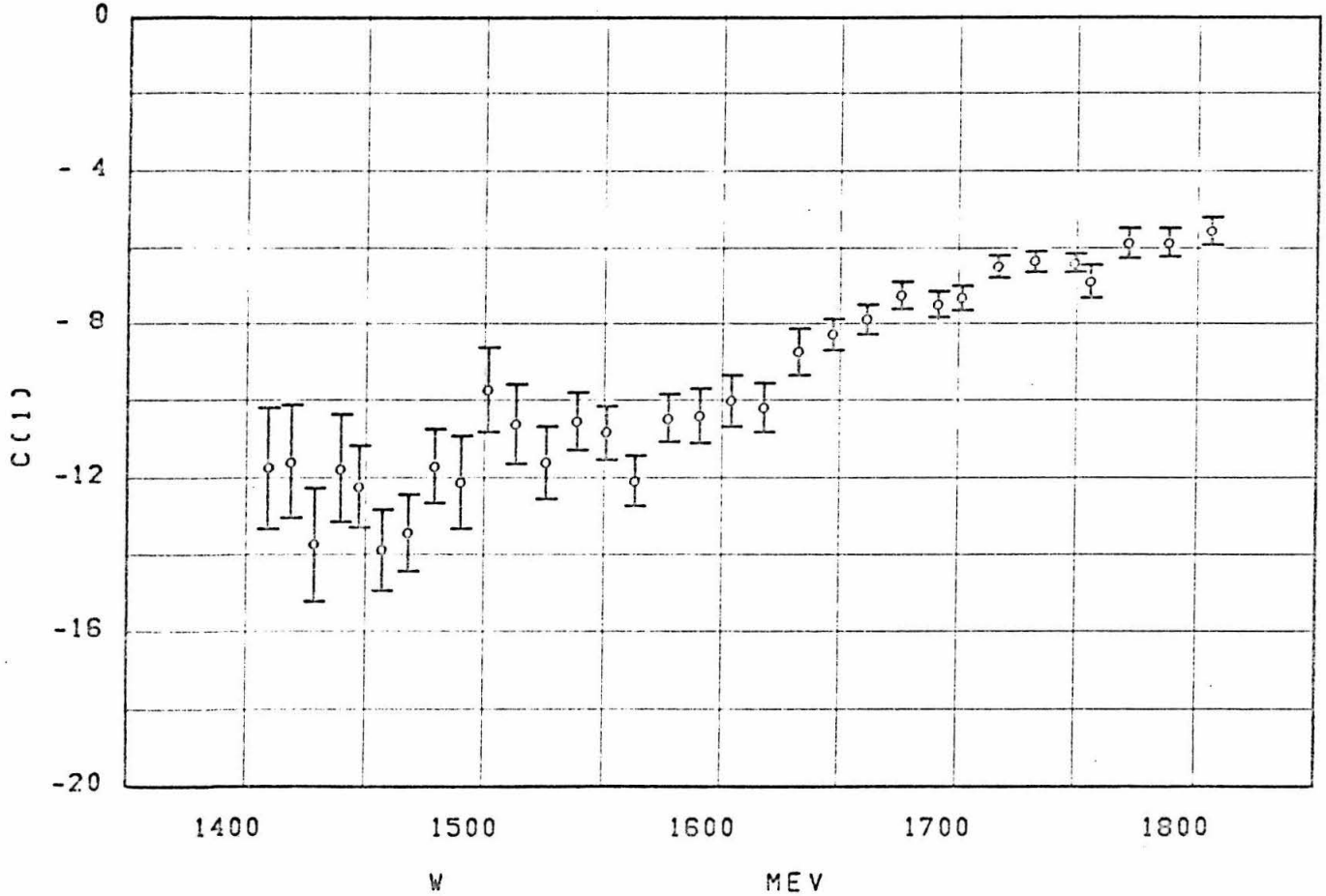

FIGURE 10.1

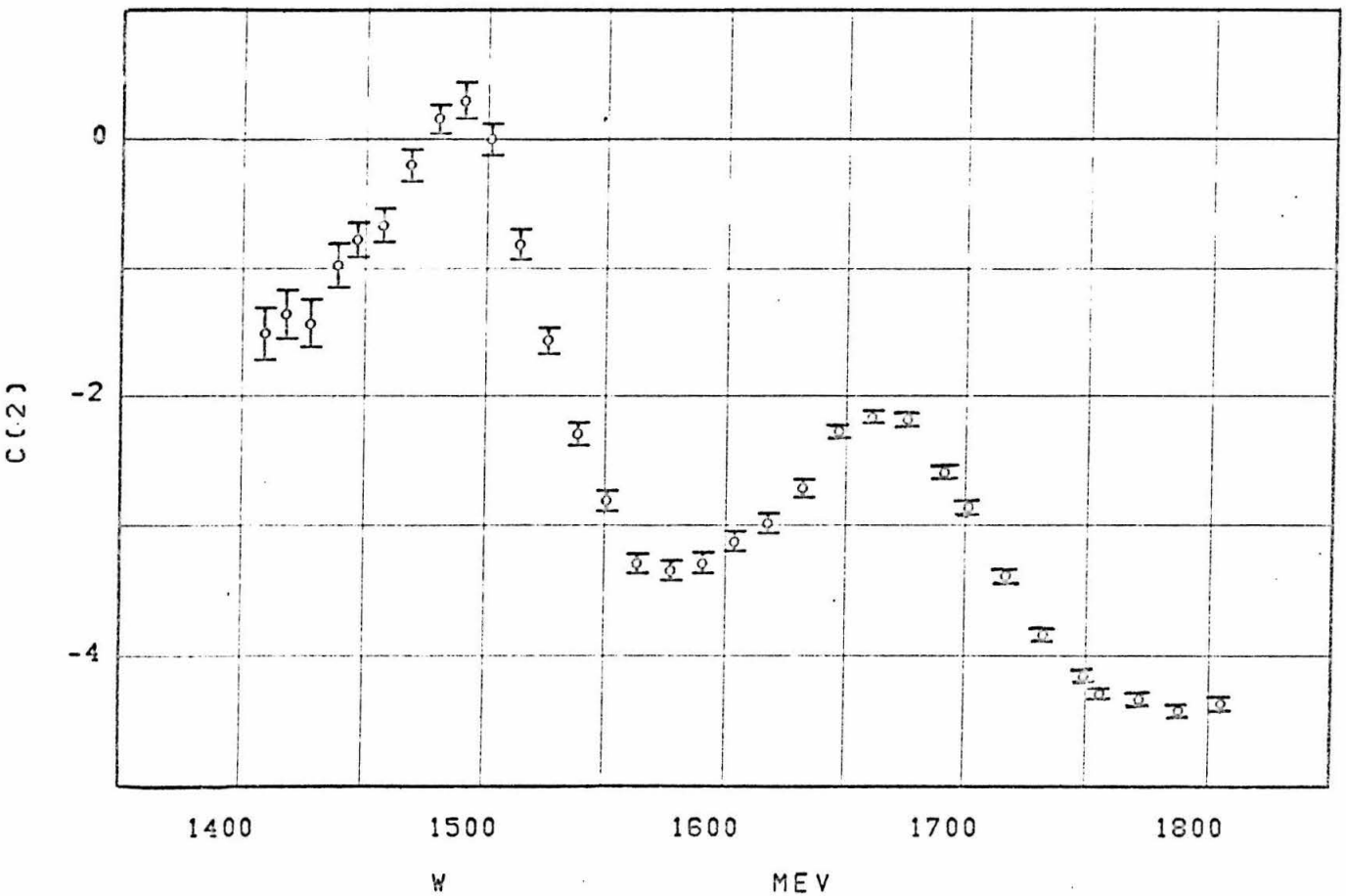

FIGURE 10.2

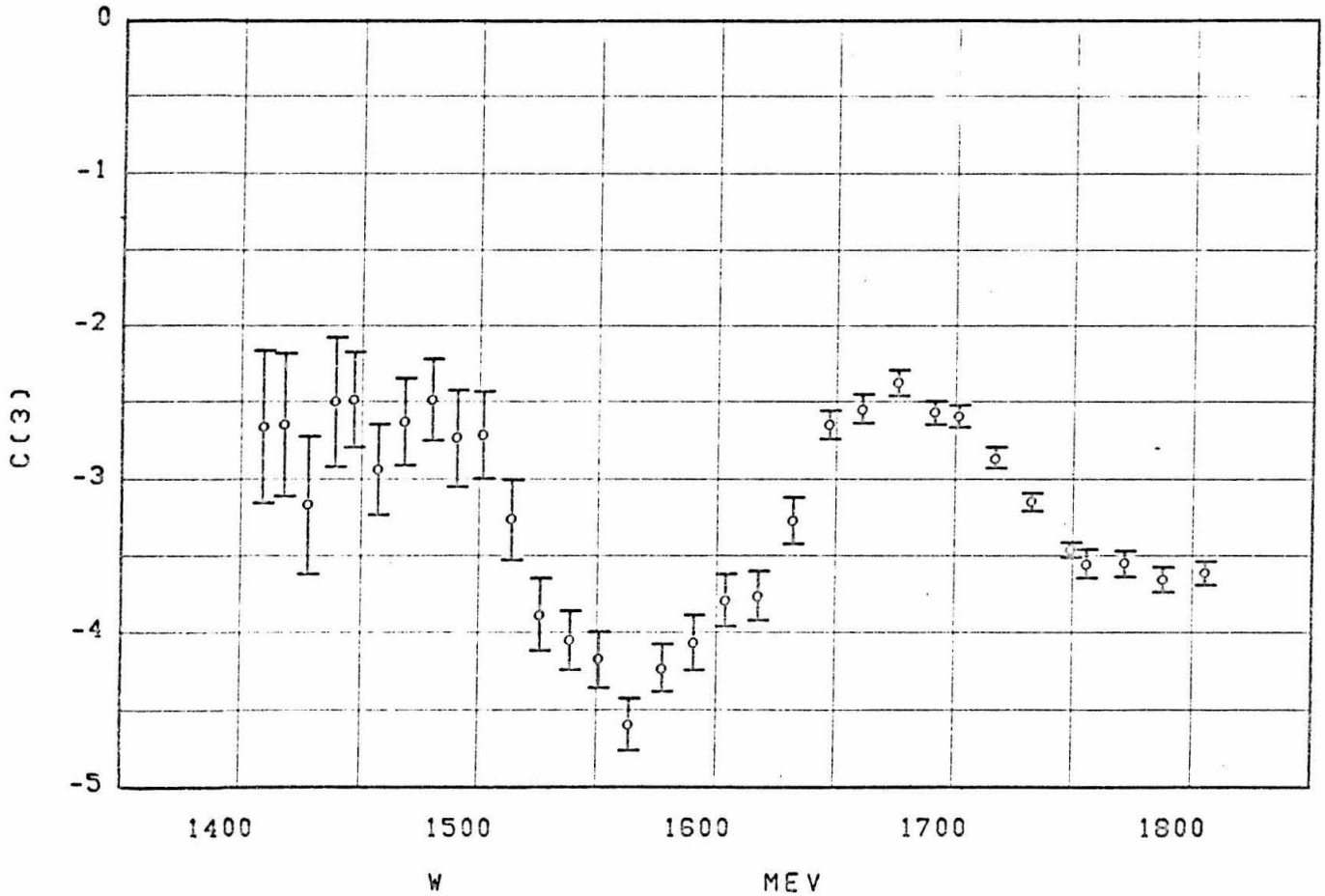

FIGURE 10.3

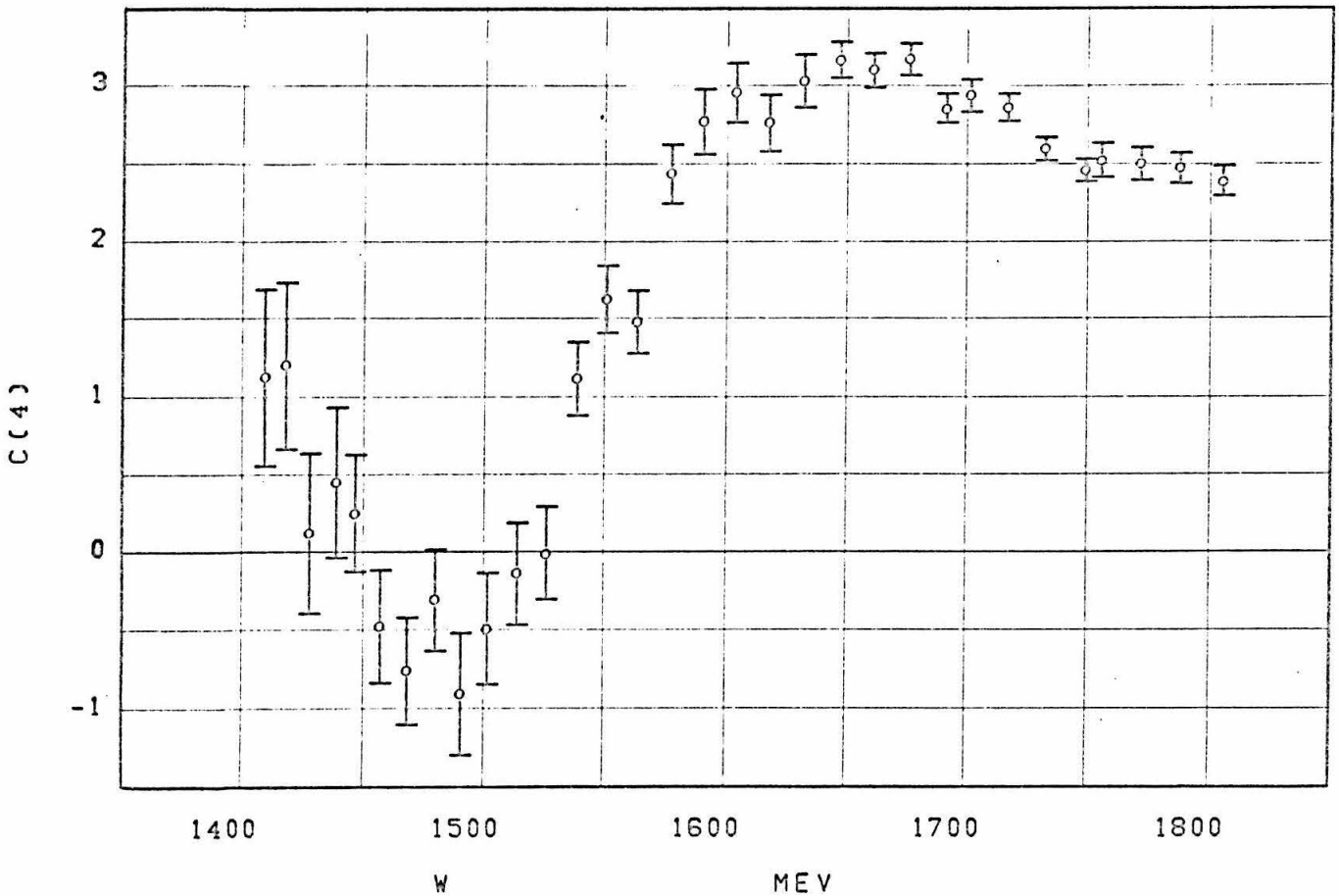

FIGURE 10.4

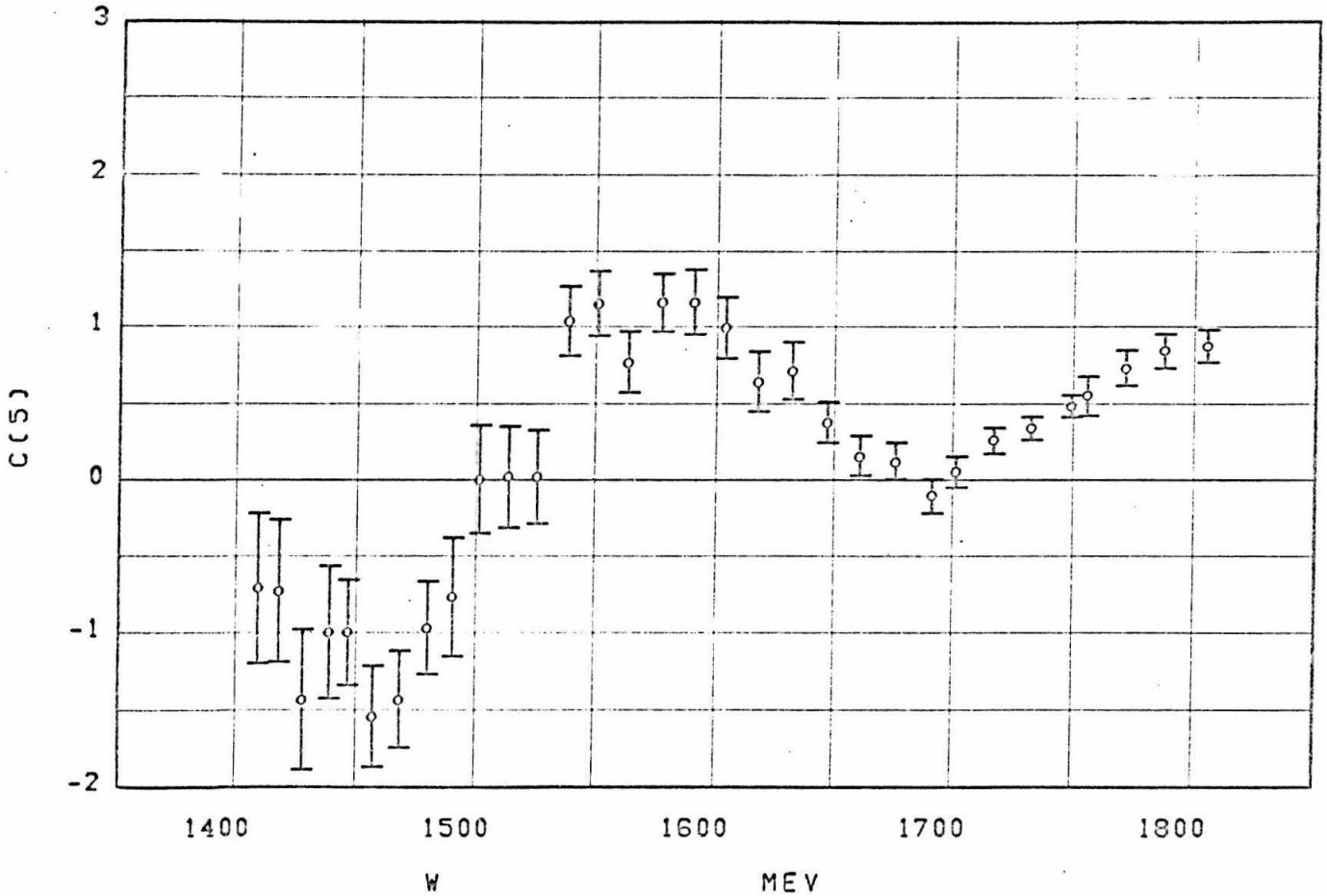

FIGURE 10.5

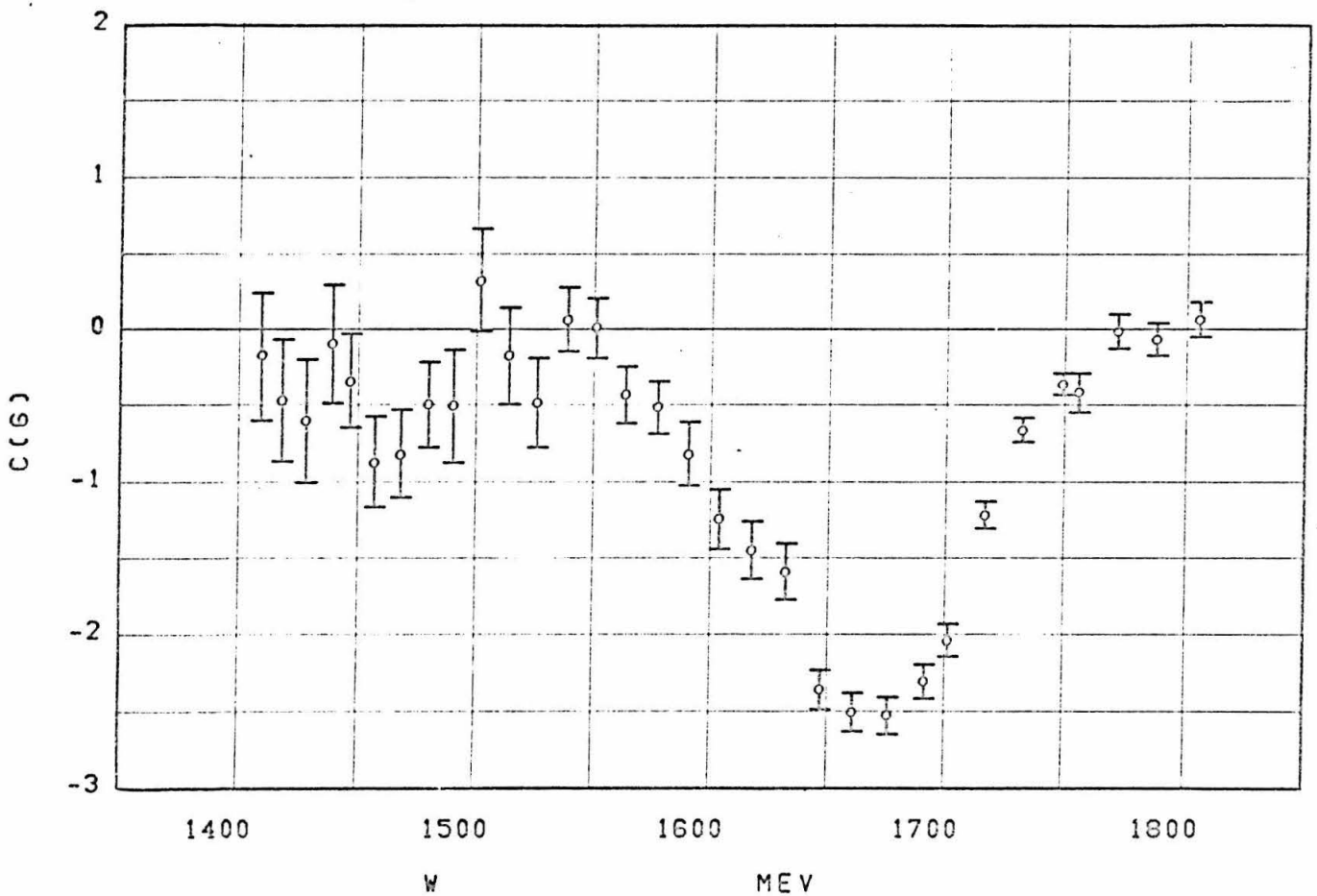

FIGURE 10.6

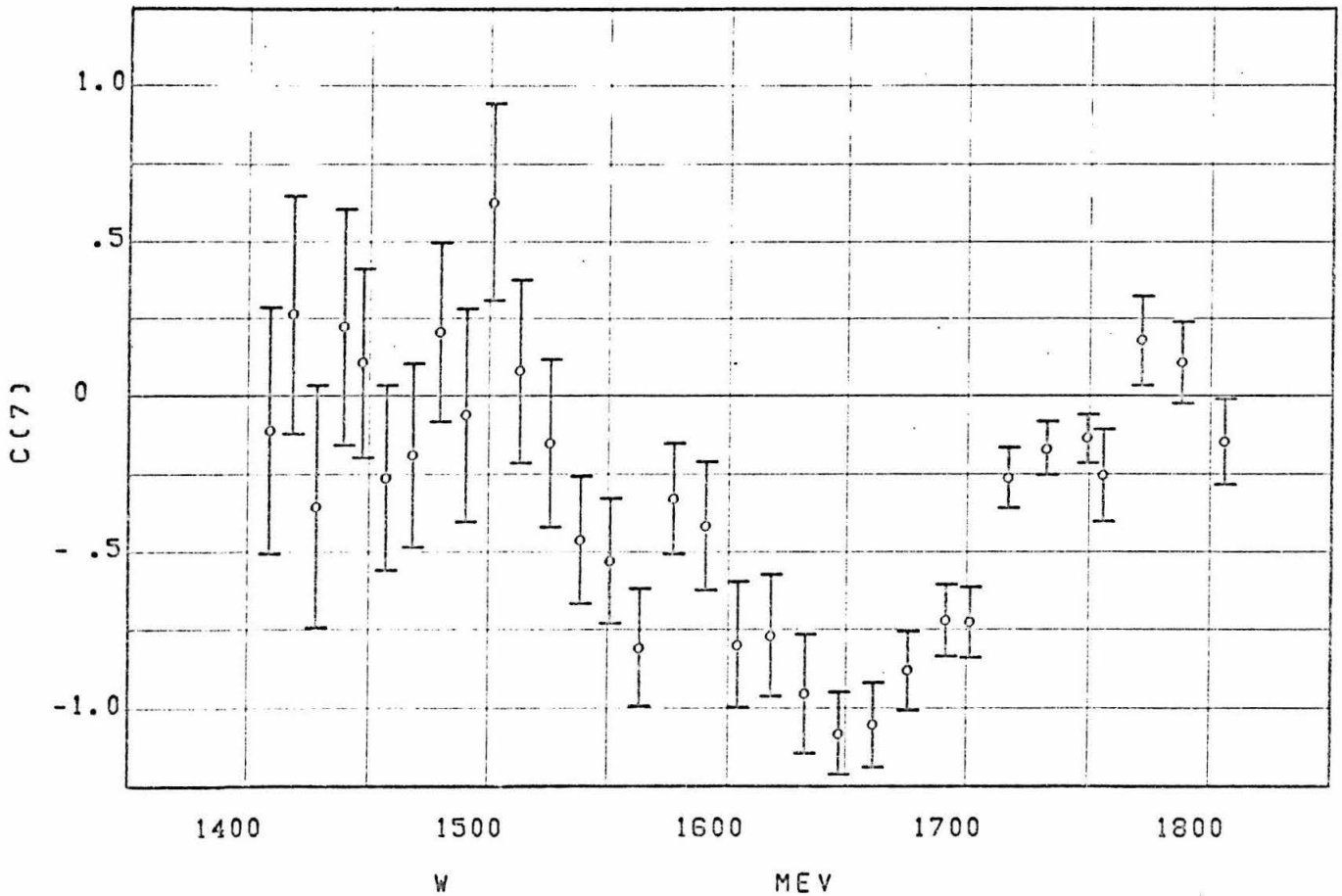

FIGURE 10.7

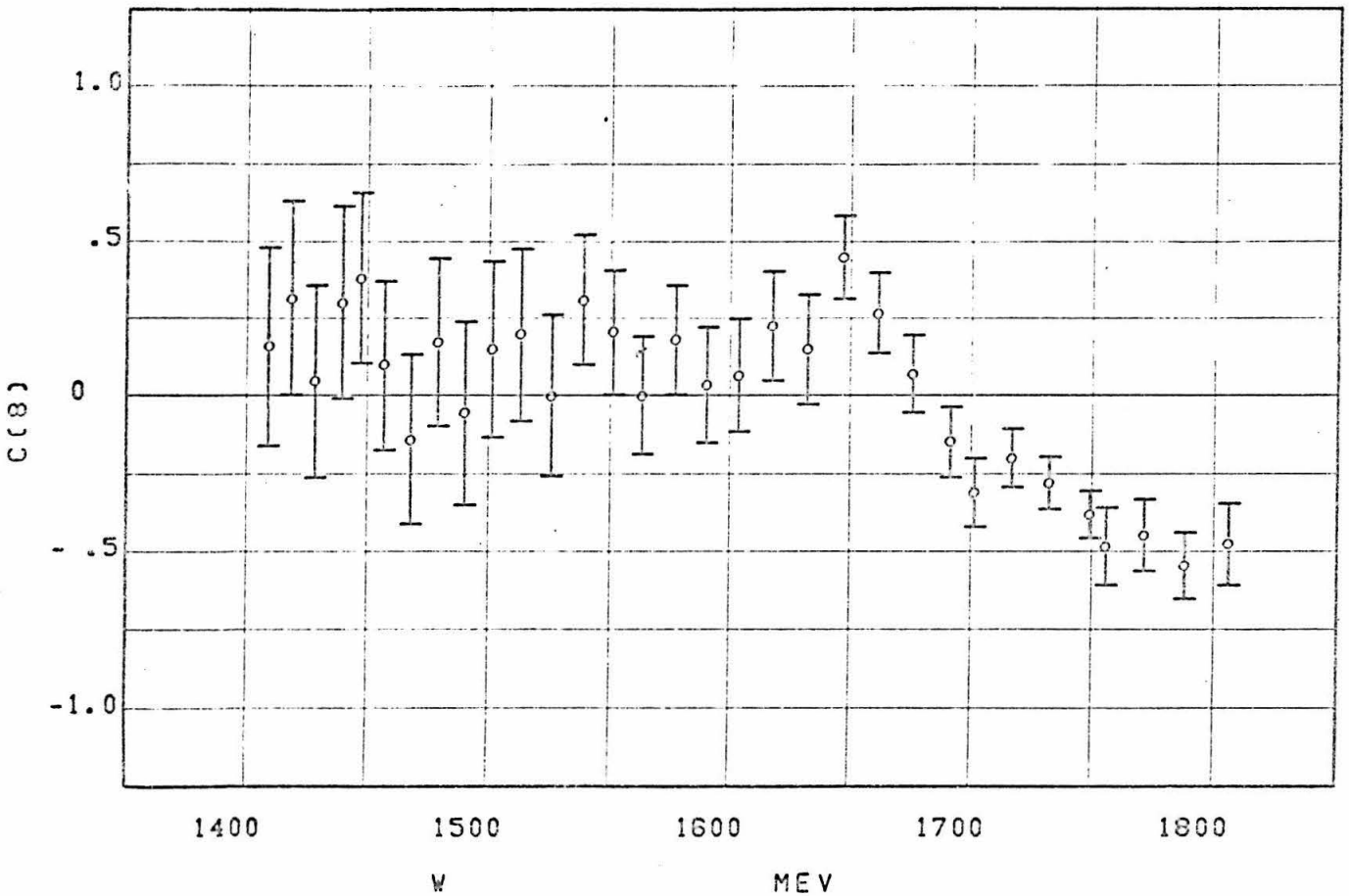

FIGURE 10.8

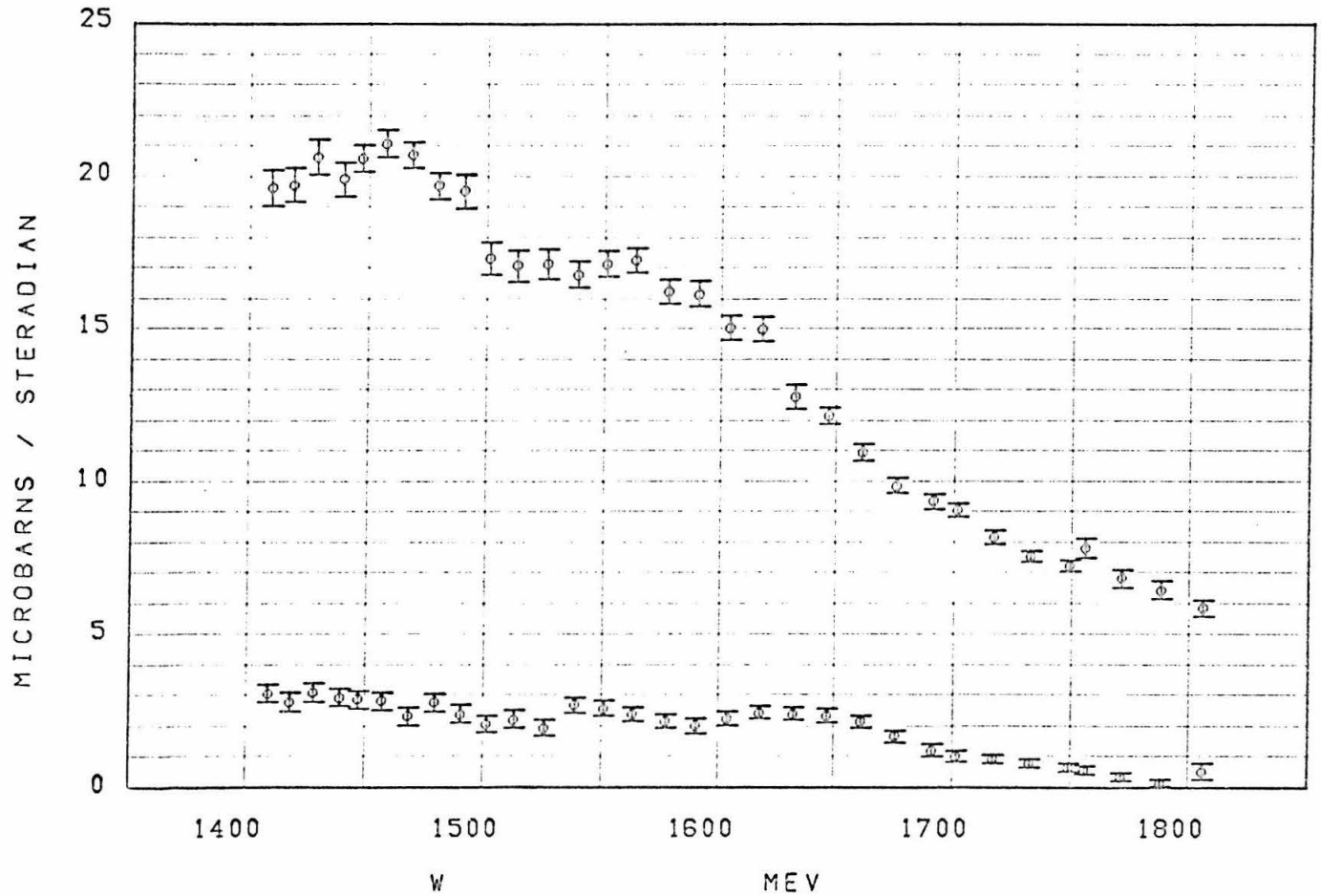
0 AND 180 DEGREE CROSS SECTION
MICROBARNS / STERADIAN
25
20
15
10
5
0
1400
1500
1600
1700
1800
W
MEV

FIGURE 11

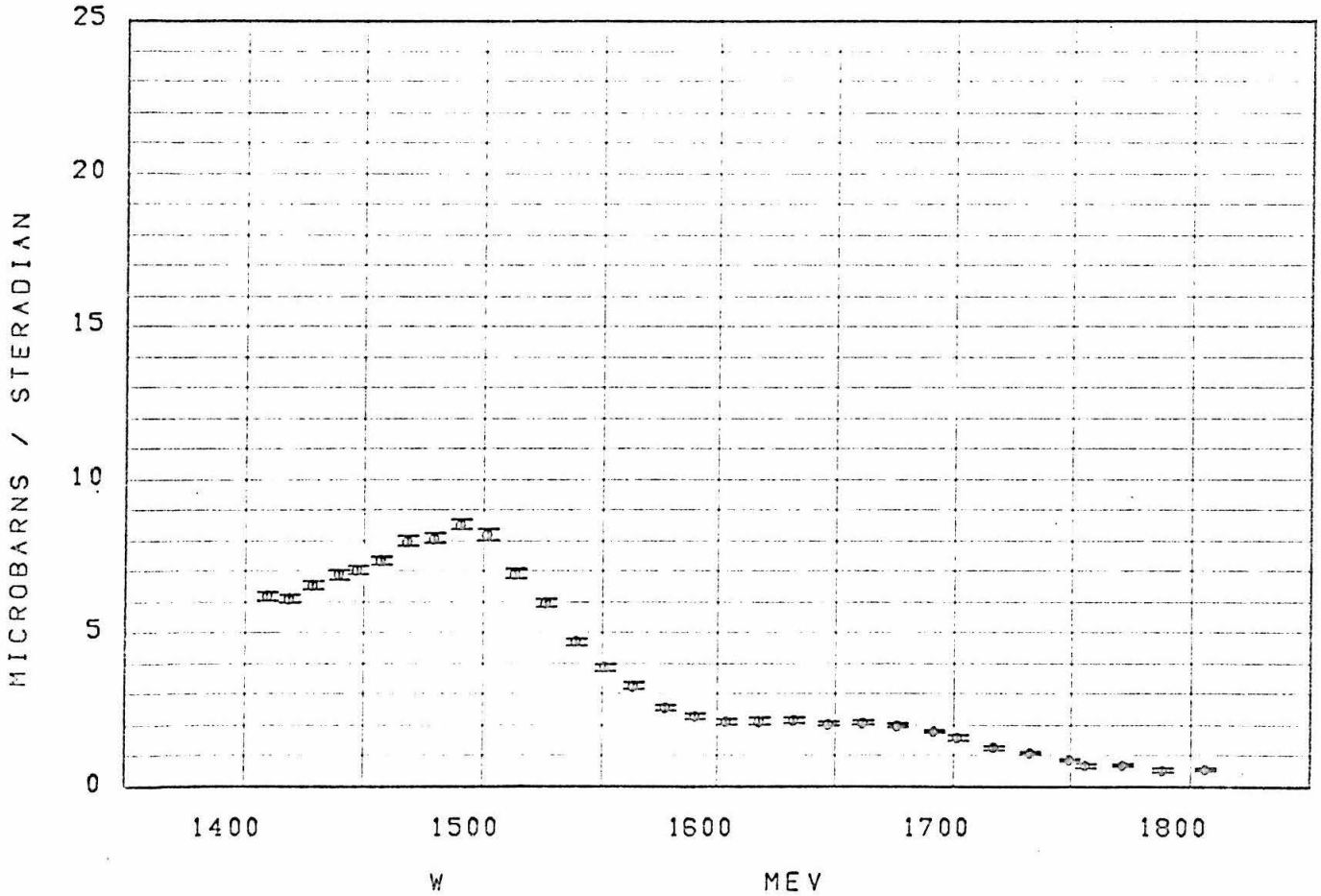
90 DEGREE CROSS SECTION
MICROBARNS / STERADIAN
25
20
15
10
5
0
1400
1500
1600
1700
1800
W
MEV

FIGURE 12

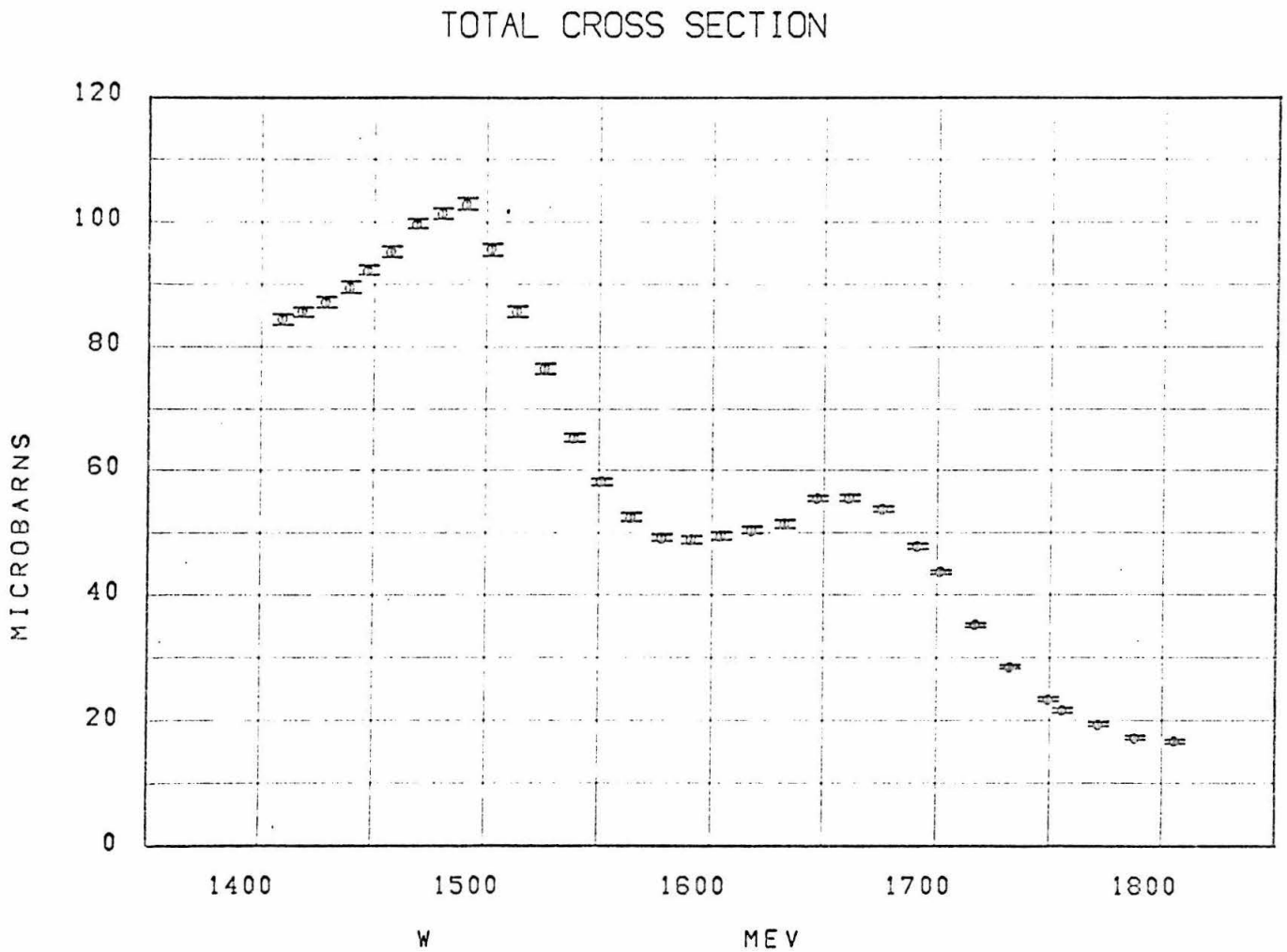
TOTAL CROSS SECTION
120
100
80
60
40
20
0
MICROBARNS
1400
1500
1600
1700
1800
W
MEV

FIGURE 13

The nonzero C(7) near $W \approx 1670$ can come only from the interference of states of opposite parities. The possible pairs of interfering states are: (D 5/2 F 5/2), (D 5/2 F 7/2), (F 5/2 G 7/2), (D 3/2 F 7/2), (P 3/2 G 7/2), (G 7/2 H 7/2) or terms involving $j \geq 9/2$. The most likely choice is the pair (D 5/2 F 5/2) since there is no suggestion of a high $j \geq 7/2$ resonance at $W \approx 1670$ from C(8). The dependence of C(7) upon energy is similar to a Breit-Wigner resonance shape, so it appears that there are both D 5/2 and F 5/2 resonances at nearly identical masses. Another alternative, which gives a similar shape, is for one of the states to be a resonance and the other to be constant or slowly varying, but with a sizeable imaginary part. If we take both states to be resonances, the relative size of C(6) and C(7) give the relative size of the two resonances. In terms of the peak total cross section, the ratio of smallest to largest is 0.07 ± 0.03, where the uncertainty results largely from uncertainties in the resonance masses and the nonresonant background. Which state is larger cannot be decided a priori because of the symmetry of the cross section under parity. However, the interference seen in C(5) with the second resonance, which is a D 3/2 state, suggests that the state with the opposite parity, F 5/2, is the larger.

The photoproduction of a small D 5/2 resonance is interesting in light of an SU(3) quark model proposed by R. G. Moorhouse[20]. Taking sets of quarks in relative L = 0, 1, and 2 angular momentum states, and identifying the various composite quark states with the known particles and resonances, the coupling of a photon to a nucleon and a D 5/2 state is found to be zero. Accordingly, the D 5/2 should not be photoproduced directly as in Figure a. However, it would be possible for it to occur indirectly

as the final state interaction with the meson as shown in Figure b.

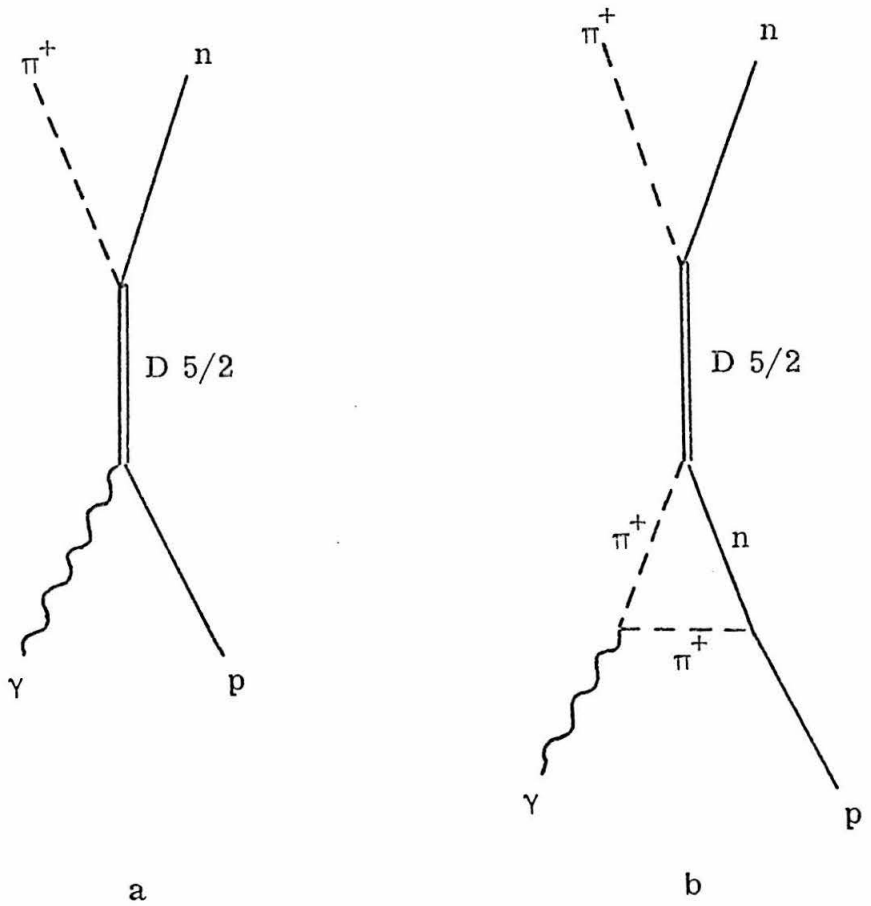

It appears that while it is difficult to test, the suppression of the photoproduced D 5/2 relative to its production by π's, where its amplitude is about 0.6 of the F 5/2, is favorable to the model.

The second resonance shows up strongly in C(2) and C(4) and as interferences in C(3) and C(5), which is consistent with its known spin-parity of D 3/2. The size of the peak in C(2) gives a

peak total cross section of around 44 μb; however, the shape of the peak and attempts to fit C(2) and C(4) to Breit-Wigner forms with nonresonant background suggest that a good part of the bump is due to the nonresonant background. The resonant part alone could be as small as 24 μb at its peak (W ≈ 1519).

The coefficient C(8) shows the effect of the fourth resonance, F 7/2 (1950), both by itself and as an interference with the third F 5/2 resonance. The sign of C(8) suggests the fourth resonance is mainly produced by initial helicity ± 3/2 (B3+). A Breit-Wigner form for B3+ centered at W ≈ 1950 with a full width of 250 MeV and contributing a peak total cross section of 4.3 μb, will explain the C(8) coefficients.

The many states found in the phase shift analyses of πN scattering[7, 8, 9, 10] suggest there is more to look for in photoproduction. There are four states presently known or speculated to be present in πN scattering which are not apparent in the coefficients C(J).

Isotopic Spin	L J	Mass	Width	Seen in πN	Seen in Photoproduction	Predicted in Photoproduction by Moorhouse's Quark Model
1/2	P 1/2	1471	204	yes	possibly	uncertain
1/2	D 3/2	1519	102	yes	yes	yes
1/2	S 1/2	1561	180	maybe	probably	yes
1/2	D 5/2	1652	134	yes	small	no
1/2	F 5/2	1672	104	yes	yes	yes
1/2	S 1/2	1715	240	maybe	no?	no
3/2	S 1/2	1692	230	maybe	no?	yes
3/2	F 7/2	1950	250	yes	yes	

If present in photoproduction, these states (P 1/2 1471, S 1/2 1561, S 1/2 1692, S 1/2 1715) are difficult to discover by the techniques employed here because of their low angular momentum and large widths. We certainly cannot say they are not present, at least in small amounts. In fact the 0^{o} cross section does appear to have bumps at 1471 and 1561 suggestive of the presence of two of the resonances. It is interesting that the S 1/2 at 1715, like the D 5/2, is predicted to be absent in photoproduction.

An interesting result concerning the second and third resonances follows from an examination of the 0^{o} and 180^{o} cross sections in comparison with the total cross section. We see that whereas the bumps in the total cross section amount to around 44 μb and 25 μb for the second and third resonance regions respectively, the 0^{o} and 180^{o} cross sections show little or no structure. From conservation of angular momentum we know that a state with initial helicity $\pm 3/2$ cannot contribute to the 0^{o} or 180^{o} cross section, whereas one with initial helicity $\pm 1/2$ can. Hence we conclude that the second and third resonances are produced mainly from initial helicity $\pm 3/2$. This property was noticed by D. S. Beder in π^{o} photoproduction[21] and given as conditions on the relative strengths of electric and magnetic production of the resonant state. For the second resonance produced by only helicity $\pm 3/2$,

$$A_{2-}^{Res} = 0 \ ,$$

which implies

$$\frac{E_{2-}^{Res}}{M_{2-}^{Res}} = 3 \ .$$

For the third resonance, F 5/2,

$$A_{3-}^{Res} = 0$$

which implies,

$$\frac{E_{3-}^{Res}}{M_{3-}^{Res}} = 2 \ .$$

Electric to magnetic ratios of similar magnitude have been calculated by Bietti[6]. Using an SU(3) sum rule, taking one term in the sum evaluated in a static limit, and assuming identical electric and magnetic form factors, he calculates

$$\frac{E_{2-}^{Res}}{M_{2-}^{Res}} = 2.7 \text{ and } \frac{E_{3-}^{Res}}{M_{3-}^{Res}} = 1.7 \ .$$

In terms of helicity coefficients, these ratios are

$$\frac{A_{2-}^{Res}}{B_{2-}^{Res}} = 0.04 \text{ and } \frac{A_{3-}^{Res}}{B_{3-}^{Res}} = 0.11 \ ,$$

which are small enough to be qualitatively consistent with the data. Since A_{2-}^{Res} and A_{3-}^{Res} are so small, it is their interference with the larger nonresonant background amplitudes that would be most evident. Hence, a more quantitative determination of the above ratios from the data requires knowing the background. Although this background could be calculated from Born terms, the answers would be unsure because of absorption effects and the possible presence of other resonant states. A detailed multipole analysis, including Born terms and the known resonances is needed.

VI. CONCLUSIONS

This experiment has provided a large number of measurements which, when combined with the data of H. A. Thiessen, give a consistent picture of the π^+ photoproduction cross section in the region of the second and third resonances. The angular and energy resolution, and the spacing of data points are fine enough to clearly see the effects of resonances and one π exchange.

An analysis of the data has revealed several interesting properties. The presence of a small photoproduced D 5/2 resonance (or at least an imaginary amplitude) was discovered by its interference with the F 5/2 third resonance. The smallness of the D 5/2 and the apparent absence of an S 1/2 resonance at c. m. energy 1692 is in accord with predictions of a quark model. It was seen that useful information about ratios of electric to magnetic production of the resonances is easily extracted from the data, providing a useful check of a sum rule calculation. It should be noted that the effects of resonances could be extracted from the large nonresonant background only because the detailed energy dependence was measured. Isolated angular distributions would have been considerably less useful.

The measurements of the coupling constant as given by the fits to angular distributions were consistent with the accepted value. Unfortunately, while the statistical error of the value obtained is small, the dependence upon the order of fit and the uncertainty in choosing the order increases the error considerably. It is possible that a fit in which the resonant multipoles are given by Breit-Wigner formulae and the coupling constant varied to fit all the data at once

at all energies could provide a better determination. A successful fit of this type would also give quantitative information about the resonances. Conceivably one could determine the mass, width and size (for production by each helicity) of each resonance. The problem soon grows to include all four single pion photoproduction reactions. Work in this direction is being carried out by Professor Robert L. Walker and Mr. Carl Clinesmith.

APPENDIX I

BEAM AND TARGET

A. Hydrogen Target

The liquid hydrogen target used in this experiment has been described in an earlier thesis[22]. Since no major changes have been made in it, only a brief description will be given here. The liquid hydrogen is contained in a 0.005-inch thick cylindrical mylar cup 3.000 ± 0.005 inches in diameter. The hydrogen is operated at the boiling point and a pressure of 0.5 psi. The hydrogen temperature is 20.3°K and its density is 0.0711 gm/cm^3 [16]. The cross section was calculated from the difference of full minus "empty" target yields, where the empty target actually contains gaseous hydrogen at the same temperature and pressure. The effective density for the difference is 0.0697 gm/cm^3.

During the course of the experiment, the target was checked visually several times a week. The empty target yields were measured within several weeks of the full target measurements so as to discover any contamination which changed with time. None was ever found. As expected, the empty target background is largest at small angles, amounting to about 13% of the full target yield at 3.5 degrees (lab), decreasing to 4% at larger angles.

B. Bremsstrahlung Beam

The bremsstrahlung beam is produced by monoenergetic electrons striking a tantalum target in the synchrotron 10.4 meters

from the hydrogen target used in this experiment. Figure 2 shows the location of the collimators, scrapers and sweep magnets. The beam was 4.45 cm wide and 5.58 cm high at the hydrogen target.

The energy spectrum of the bremsstrahlung is given by

$$n(K)\,dK = \frac{W}{E_o}\,\frac{B(K, E_o)}{K}\,dK$$

where $\int_0^{E_o} B(K, E_o)\,dK = E_o$

$n(K)\,dK$ = number of photons of energy K in dK

E_o = end point energy

W = total energy.

The details of the distribution are contained in $B(K, E_o)$ which was obtained from BPAK 1[23, 24]. The spectrum used for the calculation of cross sections is an average over the beam aperture weighted according to the thickness of the cylindrical hydrogen target, and normalized so as to account for the effective length of the target.

C. Beam Monitoring

Three monitors were used to measure the number of photons in the beam during a data taking run: a thick plate ionization chamber (BC) which stopped the beam, a thin plate ionization chamber (TC) located just after the primary collimator, and a two-counter telescope (M1) directly below the hydrogen

target. The charge collected from the ionization chambers was measured with the standard synchrotron integrators. The south beam quantameter[15] which could be moved in and out of the beam just before the hydrogen target was used to calibrate TC and subsequently BC and M1. Usually a series of short runs was taken with the quantameter alternately in and out of the beam to check that a consistent calibration of monitors had been attained. Typically calibrations were made every day and whenever the synchrotron energy was changed. The quantameter measures the total energy in the beam as given by

$$W = 13.10 \times 10^{18} \frac{T}{P} \frac{\text{MeV}}{\text{Coulomb}}$$

T = Temperature of quantameter gas in ^{o}K

P = Pressure in mm Hg.

The errors in the cross section due to uncertainties in the beam result from uncertainties in $B(K, E_o)$, E_o, and W. $B(K, E_o)$ is discussed in Reference 23 and is attributed an uncertainty of $\pm$ 1.5%. E_o is discussed in Appendix IIC and is in error by less than 0.5%. Determining W for a given run depends on knowledge of T, P and the integrator calibration and on the stability of the three monitors. T and P are accurately known from many measurements during the experiment. A systematic increase in T/P of 0.3%/ month was noted. The integrator calibration is well known and constant to 0.5% except for two periods during the experiment. Unfortunately during the first running period of February and March of 1964, no integrator calibrations were made. Calibrations made in August 1963 and May 1964 by

L. Hatch, which differ by only 0.8% were used. In the second running period during October 1964, numerous calibrations were made, but fluctuations of ± 1.5% occurred, indicating the integrator (No. 249) and/or the calibrator were broken. Various checks and repairs were made to both during the period of difficulty. The problem was finally resolved by switching to another integrator (No. 628).

The three beam monitors BC, TC and M1 give an internal check of their stability, provided only one changes at a time. As might be expected, comparison between pairs of the three monitors indicated that BC was the most reliable and TC the least. However, all three monitors proved to be reliable to about 1.5% over periods of one or two days, with the exception of TC when the synchrotron was at high energy (1320 MeV). Such an instability in TC is not surprising. Being located after the first collimator, it is very sensitive to beam alignment in the collimators, (electrons produced in the primary collimator contribute significantly to the charge collected in this chamber), and at high synchrotron energies, it is known that the electron beam is nearly unstable in vertical position during the beam dump. Because it was most stable, BC was primarily used to calculate W. However, for runs with the spectrometer at an angle less than 12°, the magnet yoke and coils blocked part or all of the beam, making it necessary to use M1 and TC. One or two such runs were always sandwiched between runs with BC unblocked. The following method was used to determine the expected BC BIPS (Beam Integrator Pulse = Full scale deflection on integrator). The ratio Y = BC/TC was considered as a function of the ratio X = M1/TC. Suppose we have three successive runs, the second without a measurement of BC. We then know X_1, X_2,

TABLE 7

Beam Monitoring Summary

Dates	Runs	Integrator No.	Integrator calibration, rms dev. micro-coulomb/Q BIP	No. measurements	T/p	W/Q BIP 10^{12} MeV
6 Feb. 64 - 4 Apr. 64	240 - 454	249	2.270 ± 0.010	2	0.397	11.80
25 Sept. 64 - 26 Sept. 64	511 - 518	249	2.245 ± 0.015	2	0.400	11.76
30 Sept. 64 - 30 Oct. 64	519 - 539	249	2.303 ± 0.002	2	0.400	12.05
9 Oct. 64 - 14 Oct. 64	540 - 561	249	2.265	1	0.400	11.87
14 Oct. 64 - 7 Nov. 64	562 - 665	249	2.238 ± 0.018	15	0.401	11.73
11 Nov. 64 - 29 Jan. 65	666 - 930	628	2.241 ± 0.001	9	0.403	11.83
30 Jan. 65 - 1 May 65	931 - 1091	628	2.241 ± 0.001	2	0.406	11.92
18 Dec. 65 - 18 Dec. 65	1092 - 1093	628	2.256	1	0.412	12.18

X_3, Y_1, Y_3, but not Y_2. As a best estimate of Y_2 we simply use a linear interpolation,

$$Y_2 = Y_1 + (X_2 - X_1) \frac{Y_3 - Y_1}{X_3 - X_1} ,$$

from which the expected BC BIPS are obtained.

$$BC_2 = Y_2 \cdot TC_2$$

The advantage of this method is that, assuming BC is stable, the correct expected BC is calculated if either M1 or TC is stable. In a few cases where the above formula specifies an extrapolation, Y_2 was taken as either Y_1 or Y_3 according to whether X_2 was closest to X_1 or X_3. If it happened that $X_1 = X_3$, the average of Y_1 and Y_3 was used for Y_2. The error in determining BC_2 with this scheme can be estimated from runs with an unblocked beam as the smaller of the variation in Y, and the variation in Y/X = BC/M1. This turned out to be about $\pm$ 0.3%.

As a check of the quantameter itself, it was compared five times with an identical one used in the west beam. The ratios of their sensitivities, corrected to the same T and P and measured on the same integrator, varied from 1.025 to 0.98. In particular, comparisons made three days before and two days after refilling the south beam quantameter indicate a 2.2 $\pm$ 0.2% increase in sensitivity. Its rate relative to BC also increased by 2.3 $\pm$ 0.3%. The cause of this change is not known. In any case, the sensitivity after refilling is believed correct and the data were reduced accordingly.

The south quantameter was calibrated against a Faraday Cup at the Stanford Mark III Linear Accelerator on 2 May 1966[25]. This calibration agreed with both the previous calibrations and the theoretical value with a difference of less than 1.5%.

As a result of the above considerations, the fluctuating error in determining W for any one run was taken as $\pm$ 1.5%. The systematic error in W is estimated as 3%.

APPENDIX II

THE SPECTROMETER

The magnet has been described previously[26, 27] and only minor changes in the counters were made before running this experiment. Thus it will suffice to state the properties of the spectrometer for the apertures used.

A. Acceptance Properties

Measurements of the fringe magnetic field[27] in the central bending plane of the magnet were used to derive the acceptance in momentum and vertical angle. A computer program SPECTROMETER[28] was used to calculate the region of acceptance in relative momentum $Q = (P - P_o)/P_o$ and vertical angle β, for a fixed position in the target. These calculations were done for the 3 x 9 in. A1. Figure 14 shows the four regions corresponding to the four channels of the spectrometer for orbits starting at the center of the H_2 target. When integrated over β and the position in the H_2 target, weighted by the spatial distribution of the beam, the momentum resolution functions shown in Figure 15 are obtained. For this purpose, the spatial distribution of the beam was taken from BPAK1[23, 24], for an endpoint of 1020 MeV and photons of 900 MeV. The horizontal acceptance angle $\Delta\theta$ was calculated according to linear magnet theory using effective edges determined by the fringe field measurements. Table 8 lists the acceptance properties obtained from the fringe field measurement made at a central field of 10 KG. Measurements at 15 KG give ΔQ 0.1% smaller, $\Delta\beta$ 0.3% larger and $\Delta\theta$ 0.2%

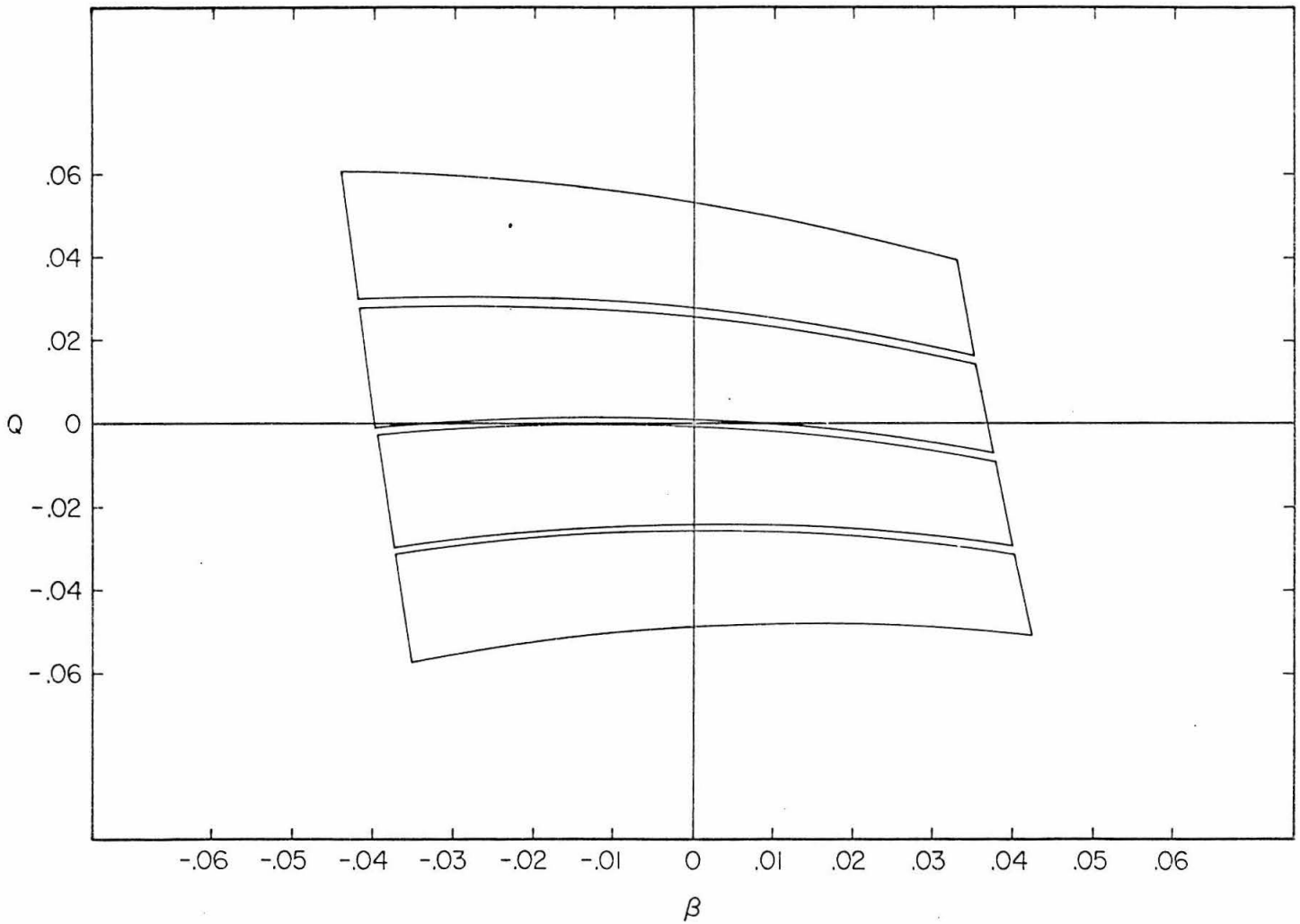

FIGURE 14. Magnet Acceptance

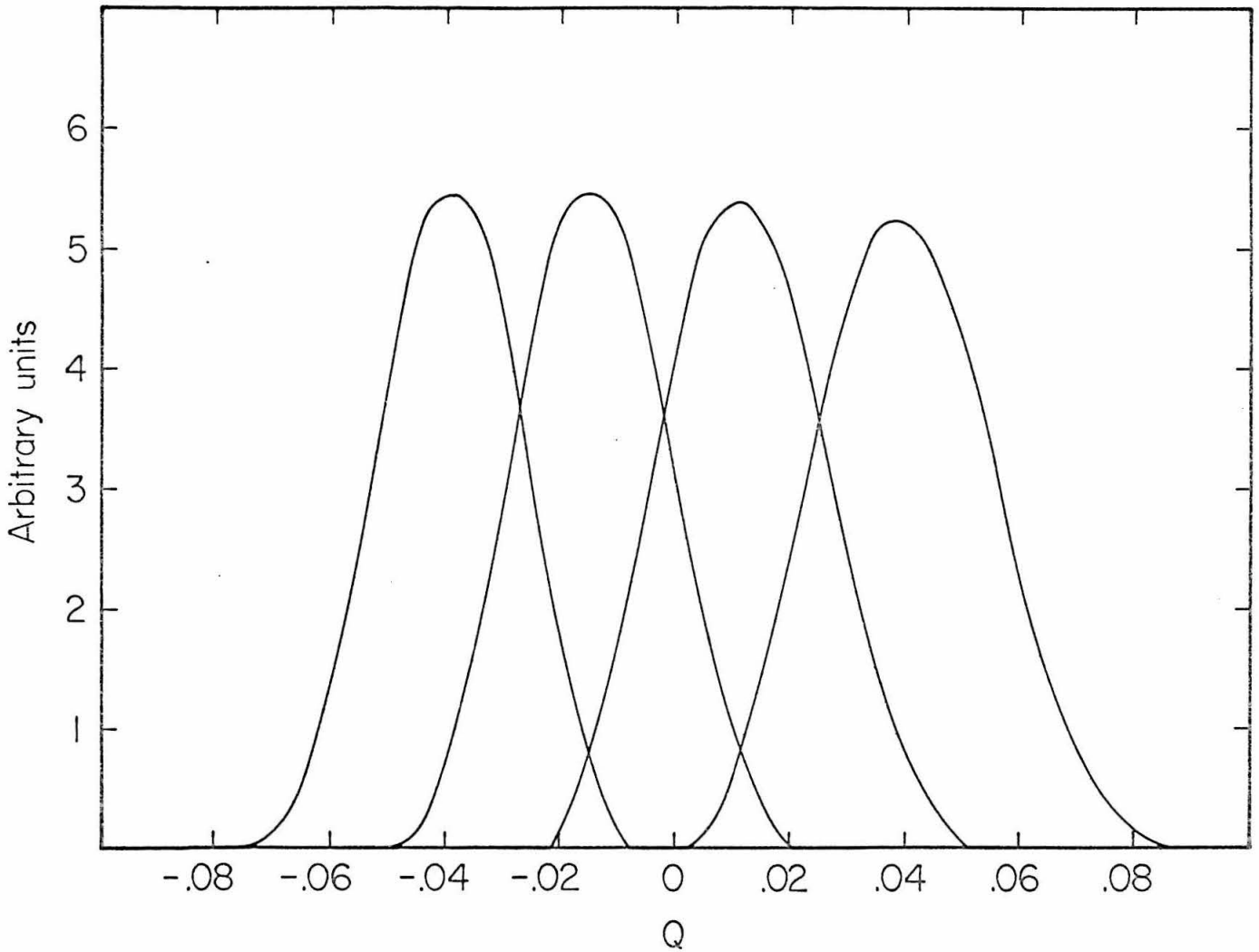

FIGURE 15. Resolution Functions

TABLE 8

Spectrometer Acceptance Properties

A1 size: 3" x 9"
S2 size: 1.18"

Channel	Mean Q	$\Delta\beta$ radians	ΔQ	$\Delta\beta\Delta Q$ radians	$\Delta\theta$ radians	$\Delta\Omega$ steradians	$\Delta Q \Delta\Omega$ steradians
a	0.0403	0.0768	0.0262	0.00202	0.0175	1.344×10^{-3}	3.54×10^{-5}
b	0.0123	0.0769	0.0248	0.00191	0.0175	1.346	3.34
c	-0.0141	0.0770	0.0235	0.00181	0.0175	1.348	3.17
d	-0.0389	0.0771	0.0224	0.00171	0.0175	1.349	2.99

larger than at 10 KG. A linear magnet theory calculation of $\Delta\beta$ and ΔQ agrees with the more exact computer fringe field calculation within 1%. An experimental check of the solid angle using a small counter in front of the magnet to define a known solid angle agrees with the calculated solid angle within the 2% counting statistics.

B. Momentum Calibration

The magnetic field of the magnet was set by a nuclear magnetic resonance (NMR) system. To calibrate the momentum as a function of magnetic field or frequency of the NMR, a floating wire technique was used. The method and apparatus used was identical to that described by H. A. Thiessen[29] except for the correction for the weight of the wire. The wire was made to have the correct slope at the edges of the magnet by suspending it from positions slightly higher than the particle origin and focus points. This accounts for the weight of that part of the wire outside the magnet. The tension in the wire at the origin, where measured, differs from that at the entrance of the magnet by $1/2\ (\frac{\lambda g}{T})^2\ \ell_1^2 T = 2 \times 10^{-6} T$ and is negligible. A correction (α) for the weight of the wire inside the magnet is calculated assuming the orbit is a segment of a circle. The momentum a particle must have to correspond to a floating wire setting is

$$P = 0.00\ 2940\ T/I\ (1 + \alpha)$$

$$\alpha = \frac{\lambda}{T} \frac{R\theta}{\tan\theta}$$

P = Momentum in GeV/c

T = Tension in gm. wt.

I = Current in amperes

λ = Density of wire in gm/inch

R = Radius of orbit in field (104.7 in)

θ = Bending angle of magnet in radians (0.477)

α = Correction for weight of wire in magnet.

Two complete sets of measurements were taken with tensions T = 1173.5 gm and T = 457.5 gm. The corrections for the weight of the wire in the magnet were $\alpha = 0.002$ and $\alpha = 0.005$. The errors assigned to these measurements are $\pm 10^{-3}$ volt on voltage reading across a one ohm shunt resistor, $\pm 5 \times 10^{-4}$ ohm for value of shunt resistor and $\pm$ 0.1 gm for T. The results of a fit of the data to the form

$$P/F = \begin{cases} A & \text{if } F < 30 \text{ MC} \\ A + B\left(\frac{F - 30}{100}\right) + C\left(\frac{F - 30}{100}\right)^2 & \text{if } F \geq 30 \text{ MC} \end{cases}$$

F = NMR frequency

are $A = (18794. \pm 3.) \times 10^{-6} \ \frac{GeV/c}{MC}$

$B = (-9. \pm 60.) \times 10^{-6}$

$C = (-4937. \pm 181.) \times 10^{-6}$

$\chi^2 = 43$ for 35 degrees of freedom.

Notice the errors given by the fit imply an error of about 0.1%. The data and fit are shown in Figure 16.

The fringe field measurements give a check of the momentum calibration at 10 and 15 KG. Table 9.1 lists the results. It should be mentioned, for one who may compare this with previous measurements, that the center of the focus counter is slightly higher than before accounting for a 1.2% increase in momentum for a given field. The origin position (mean height of beam in hydrogen target) was taken to be 0.185 inches above the top edge of the lead marker when lowered into the hydrogen target. In practice the mean beam height will vary depending on radiator settings and collimator lineup. The various systematic errors considered present in the momentum calibration are listed in Table 9.2.

The locations of the hydrogen target and counters A1 and S2 were measured relative to the front vertical surface of the magnet yoke and the top edge of the 8-inch pole-face at a point 2 inches from the corner of the 4-inch gap pole tips. Vertical and horizontal distances were measured with the spectrometer angle set to 0°. The following positions were measured in February and May of 1965 and were used for the momentum calibration given here.

Position	Distance Below 8-inch Gap	Distance in Front of Front Yoke Surface
Center of Beam in Hydrogen Target	10.74 ± 0.1"	107.12 ± 0.1"
Center of Momentum Aperture S2	71.12 ± 0.1"	-139.13 ± 0.10"
Top Edge of 9-inch A1	17.51 ± 0.05"	-45.15 ± 0.08"

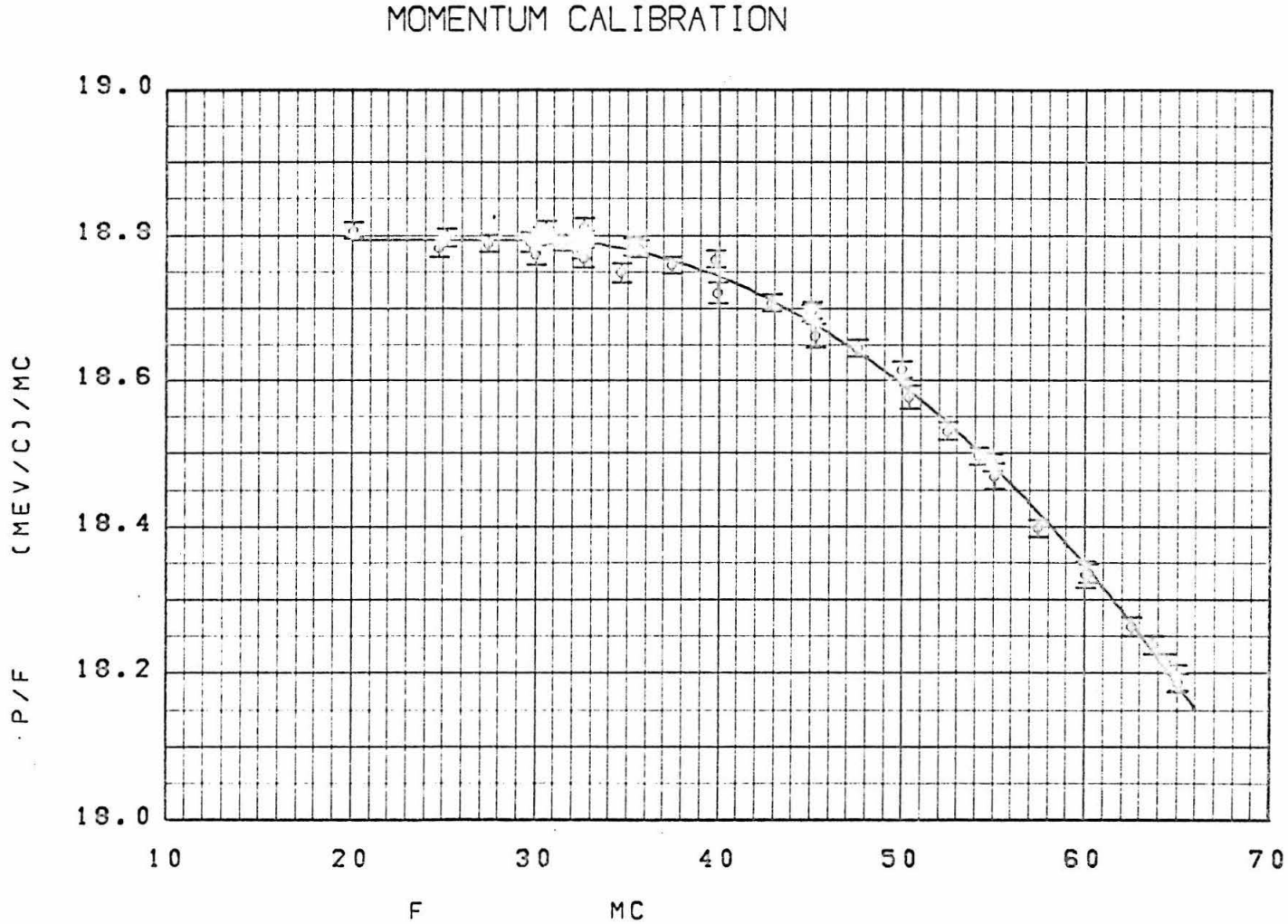
MOMENTUM CALIBRATION
19.0
18.8
18.6
18.4
18.2
18.0
P/F (MEV/C)/MC
10
20
30
40
50
60
70
F MC

FIGURE 16

TABLE 9.1

Momentum Calibration

Field	Floating Wire	Fringe Field
10 KG	796.8 $\pm$ 0.8 MeV/c	796.0 MeV/c
15 KG	1164.2 $\pm$ 1.2	1166.5

TABLE 9.2

Errors in Momentum Determination

Source	Error
Location of Origin	0.2%
Location of Focus	0.2%
Floating Wire Calibration	0.1%

A1 is inclined from the vertical at an angle of 28 ± 1^{o} making it perpendicular to the spectrometer beam.

C. End Point Comparison

It is possible to compare the magnet calibration with the energy meter of the synchrotron by measuring the π^{+} yield as a function of the endpoint energy E_o of the synchrotron. When E_o becomes less than the photon energy needed to produce a pion accepted by the spectrometer, the yield rapidly drops to zero with a slope determined by the bremsstrahlung shape and the magnet resolution. A series of runs with E_o ranging over this step gives a measurement of the ratio E_o mag/E_o meter, where E_o mag is the true E_o if the magnet calibration is correct. In practice, because four momentum channels were used, as few as two settings of E_o, one on the step and one at a normal data setting, would allow a reasonable determination. The middle channels (b, c) gave the best determination of E_o mag/E_o meter since they were chosen to cover the steepest part of the step. The calculation of the ratio was done by running the cross section program (Appendix VI) for several ratios, and finding the ratio for which the χ^2 for the individual runs measuring the same cross section is a minimum. The error due to statistics is the shift needed to increase χ^2 by 1. The result of eight measurements using channels b and c are summarized in Table 10 and Figure 18. Also shown in Figure 18 is the result of an electronic calibration[30] of the energy meter. The set of yields (counts/quantameter BIP) of measurement 7, and the expected yield calculated for E_o mag/E_o meter = 1.021 are shown in Figure 17.

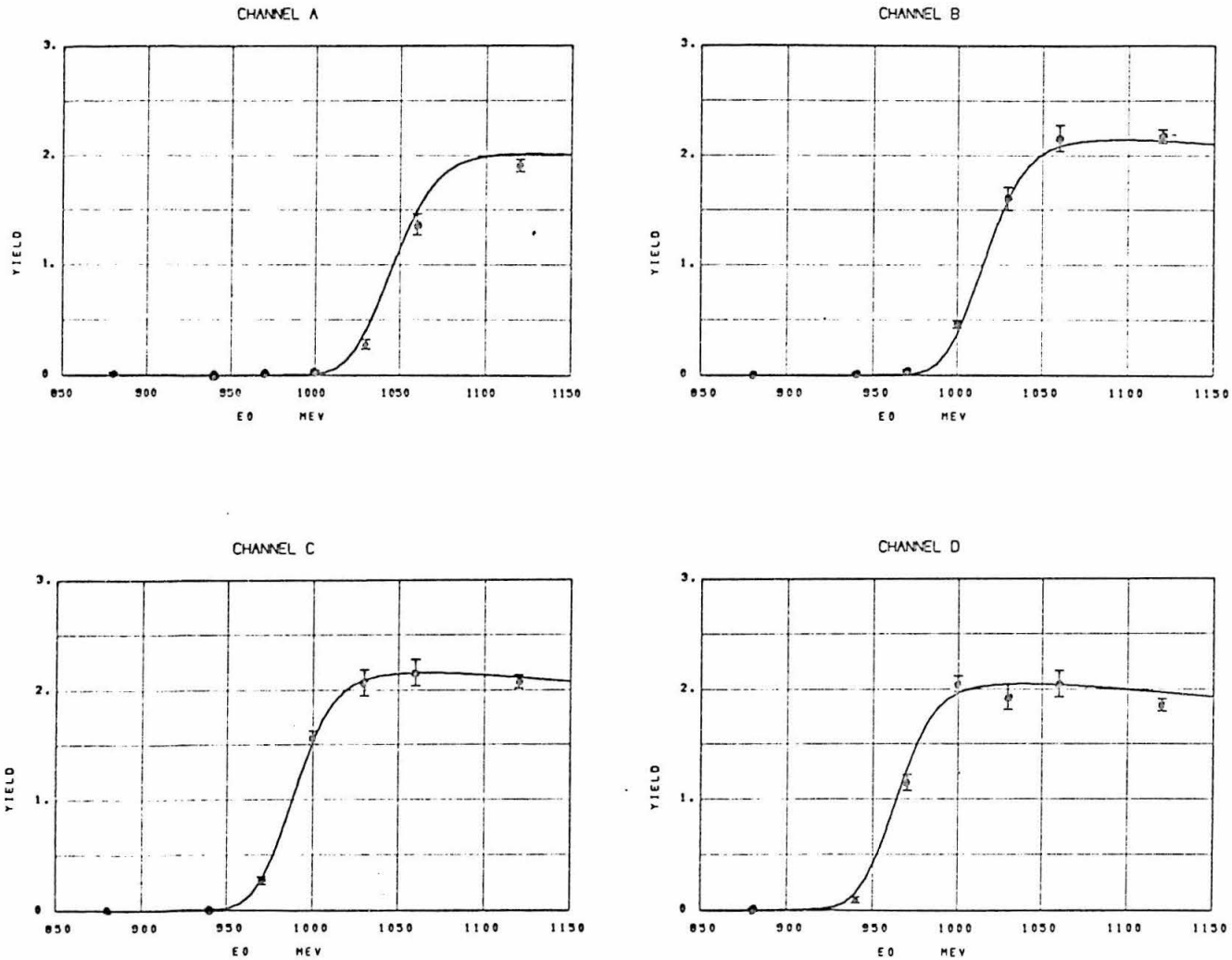

FIGURE 17. Yields for Each Channel vs. E_o

TABLE 10

End Point Calibrations

Measurement	Date	K mag.	$\frac{P}{K}\frac{\partial K}{\partial P}$	E_o meter Settings	$\frac{E_o \text{ mag}}{E_o \text{ meter}}$	χ^2	Degrees of Freedom
1	4 Apr. 64	1118	1.06	1080, 1100, 1220	1.030 ± 0.002	10	3
2	10 Oct. 64	1118	1.06	1100, 1220	1.020 ± 0.002	0.5	1
3	20 Oct. 64	1017	1.06	1000, 1060, 1120	1.020 ± 0.001	16	3
4	26 Nov. 64	917	1.06	900, 1020	1.024 ± 0.002	1.5	1
5	1 Jan. 65	744	1.03	730, 850	1.031 ± 0.002	0.1	1
6	15 Jan. 65	675	1.21	660, 780	1.028 ± 0.005	1.5	1
7	1 May 65	1017	1.06	970, 1000, 1030, 1060, 1120	1.023 ± 0.002	8	7
8	18 Dec. 65	897	1.06	860, 880, 900, 1050	1.025 ± 0.001	15	5

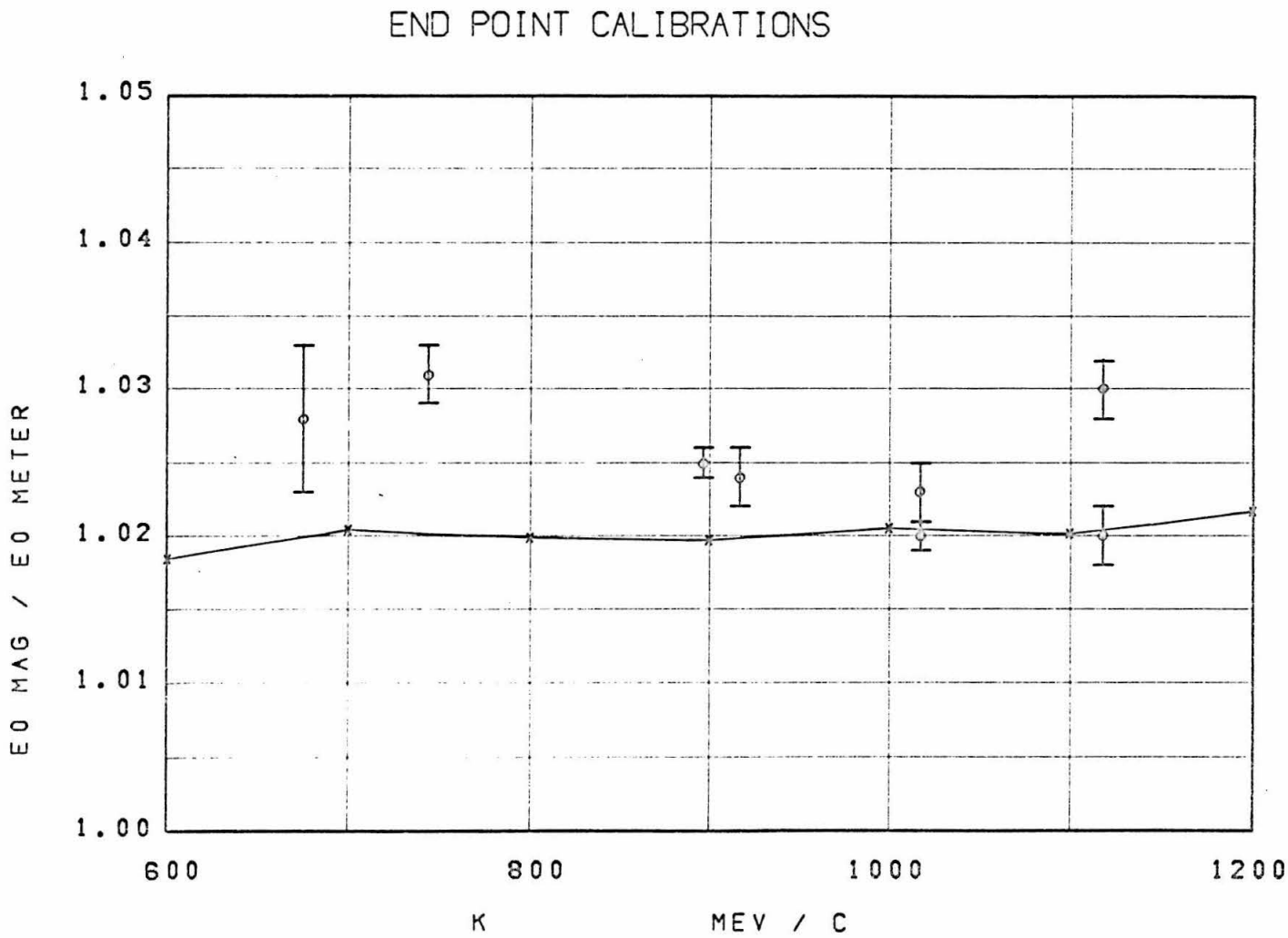
END POINT CALIBRATIONS
1.05
1.04
1.03
1.02
1.01
1.00
EO MAG / EO METER
600
800
1000
1200
K
MEV / C

FIGURE 18

The weighted average of these measurements is E_o mag/E_o meter = 1.025. The rms deviation from the average is 0.004.

To reduce the data, it was assumed that the magnet calibration is correct and the ratio E_o/E_o meter is 1.025 ± 0.005. If the magnet calibration were in error, the error in E_o would be given by

$$\frac{\Delta E_o}{E_o} = \frac{P}{K}\frac{\partial K}{\partial P}\frac{\Delta P}{P} \approx \frac{\Delta P}{P} \ .$$

D. Pion Decay Correction

At 0.5 GeV/c, 21% of the pions decay before traversing the 6.6 meter path from the H_2 target to S3. Since the counters do not distinguish pions and muons, some of the decay muons will count as if they were pions. A Monte Carlo computer program[2, 3, 16, 31] was used to calculate the effective solid angle for detecting a muon from a decayed pion of momentum $(1 + Q)P_o$ for a central magnet momentum of P_o. The resolution functions in Figures19 were obtained in this way. The errors indicated are due to Monte Carlo statistics. Unfortunately, the Monte Carlo program was rather time consuming (25 minutes of 7094 time for each resolution function) so it was necessary to obtain only 6% statistics and not run all possible individual cases. In particular, the program was run for only one momentum channel (c) and that result shifted in Q to obtain the appropriate resolution function for the other channels (In Figures 19, P_o is the mean P for a channel). Two apertures were used during the experiment, one 2.7 times smaller for the 6° and 8° data. Instead of running the

program for both apertures at all five momenta, the results for the large aperture were reduced by a factor of 2.7 for the small aperture data. This is equivalent to assuming the decay correction is the same for both apertures. To check this, the program was run at P_o = 0.5 GeV/c with the small aperture. The ratio (large to small aperture) of the integral of the respective decay pion resolutions is 2.37 ± 0.28 differing from 2.7 by 12 ± 10%. This difference would cause an error in the cross section of less than 0.9 ± 0.8%. The statistical error in the integral of the resolution functions is 6% which results in an error in the cross section of less than 0.5%. In order to provide a convenient form of the resolution functions for calculating cross sections, the values of the resolution functions at a fixed Q were fit with a quadratic in P_o. The lines in Figures 19.1 - 19.5 connect the fitted values for each Q.

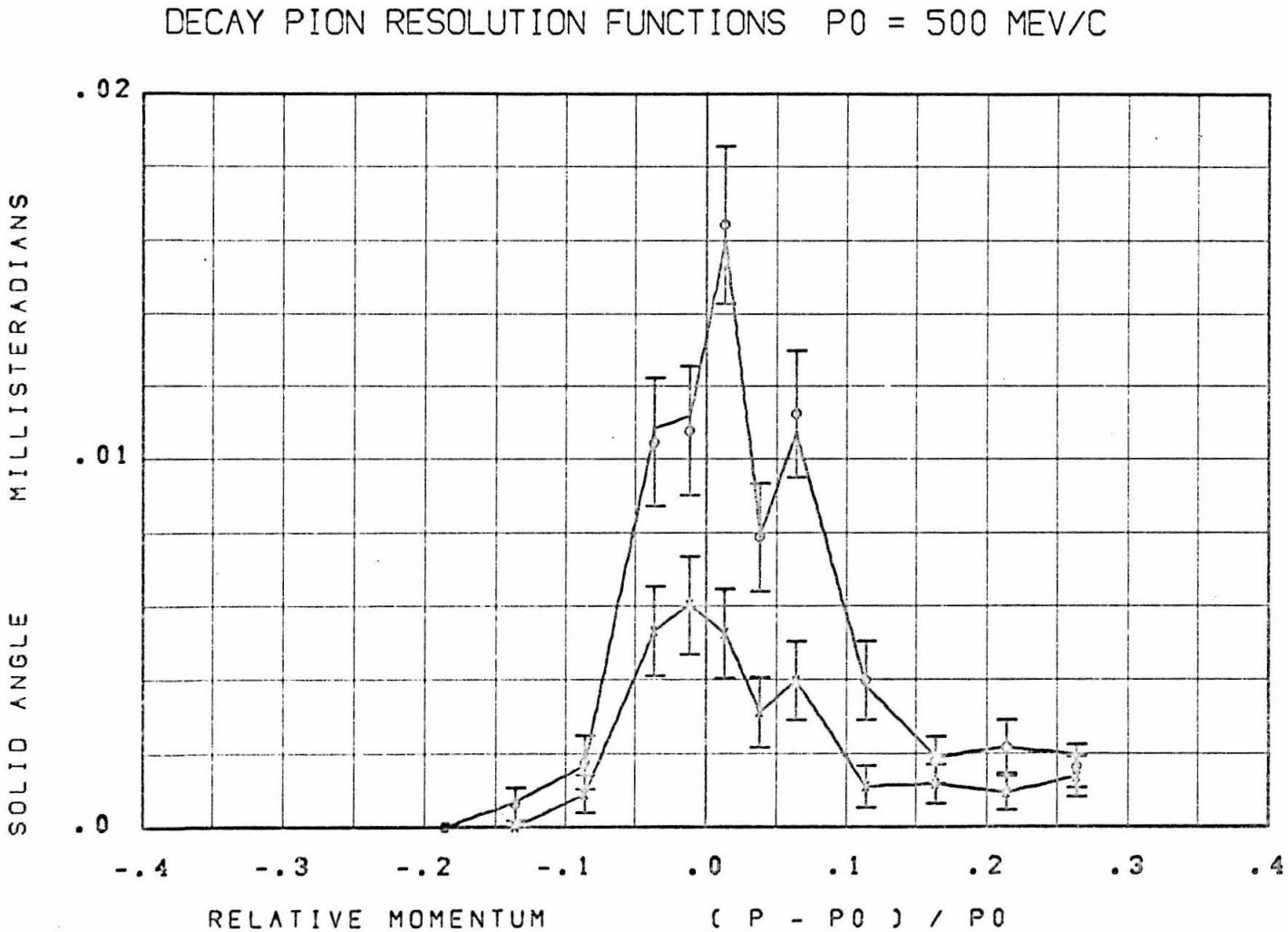
DECAY PION RESOLUTION FUNCTIONS P0 = 500 MEV/C
SOLID ANGLE MILLISTERADIANS
.02
.01
.0
-.4
-.3
-.2
-.1
.0
.1
.2
.3
.4
RELATIVE MOMENTUM (P - P0) / P0

FIGURE 19.1

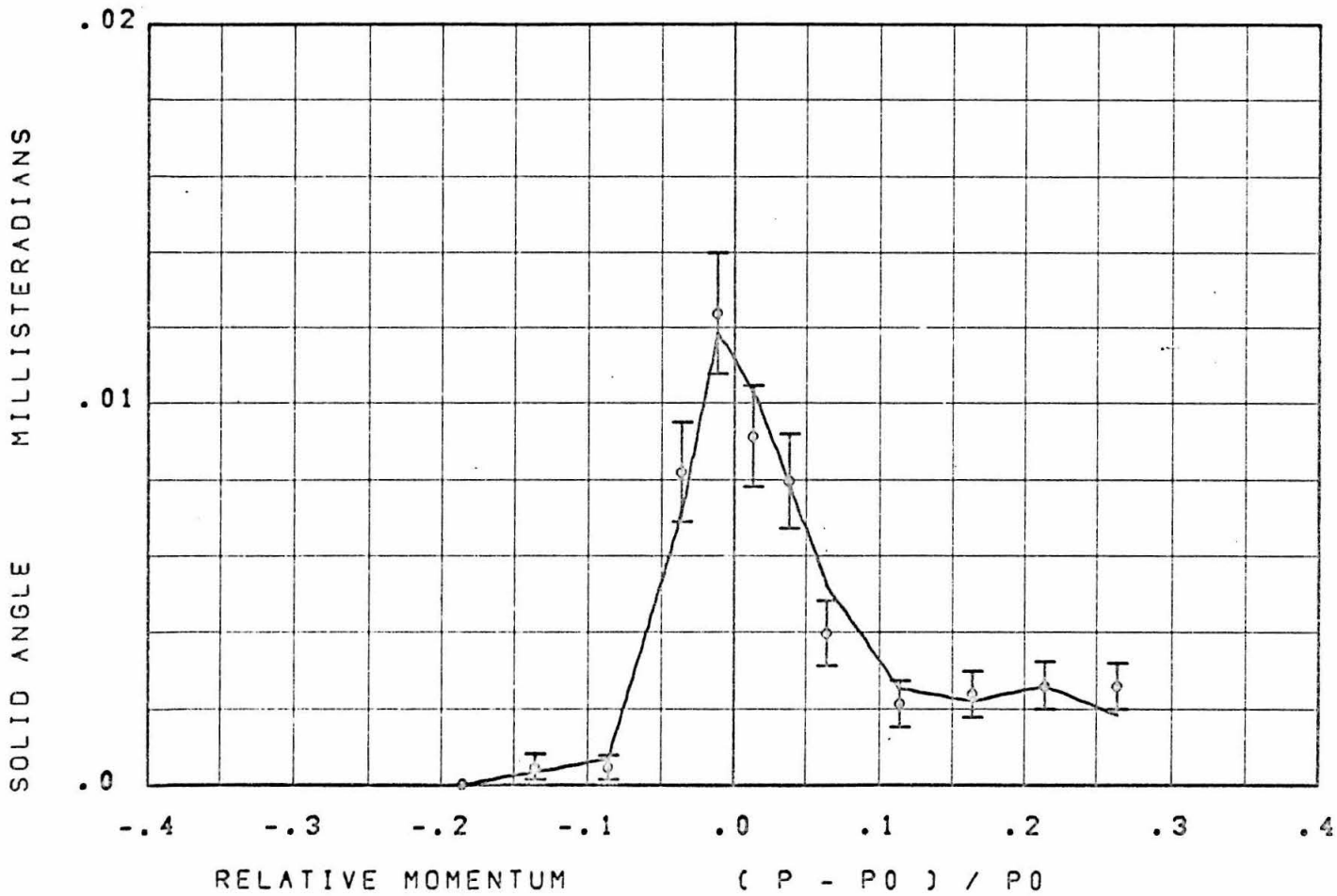
DECAY PION RESOLUTION FUNCTION P0 = 700 MEV/C
SOLID ANGLE MILLISTERADIANS
.02
.01
.0
-.4
-.3
-.2
-.1
.0
.1
.2
.3
.4
RELATIVE MOMENTUM (P - P0) / P0

FIGURE 19.2

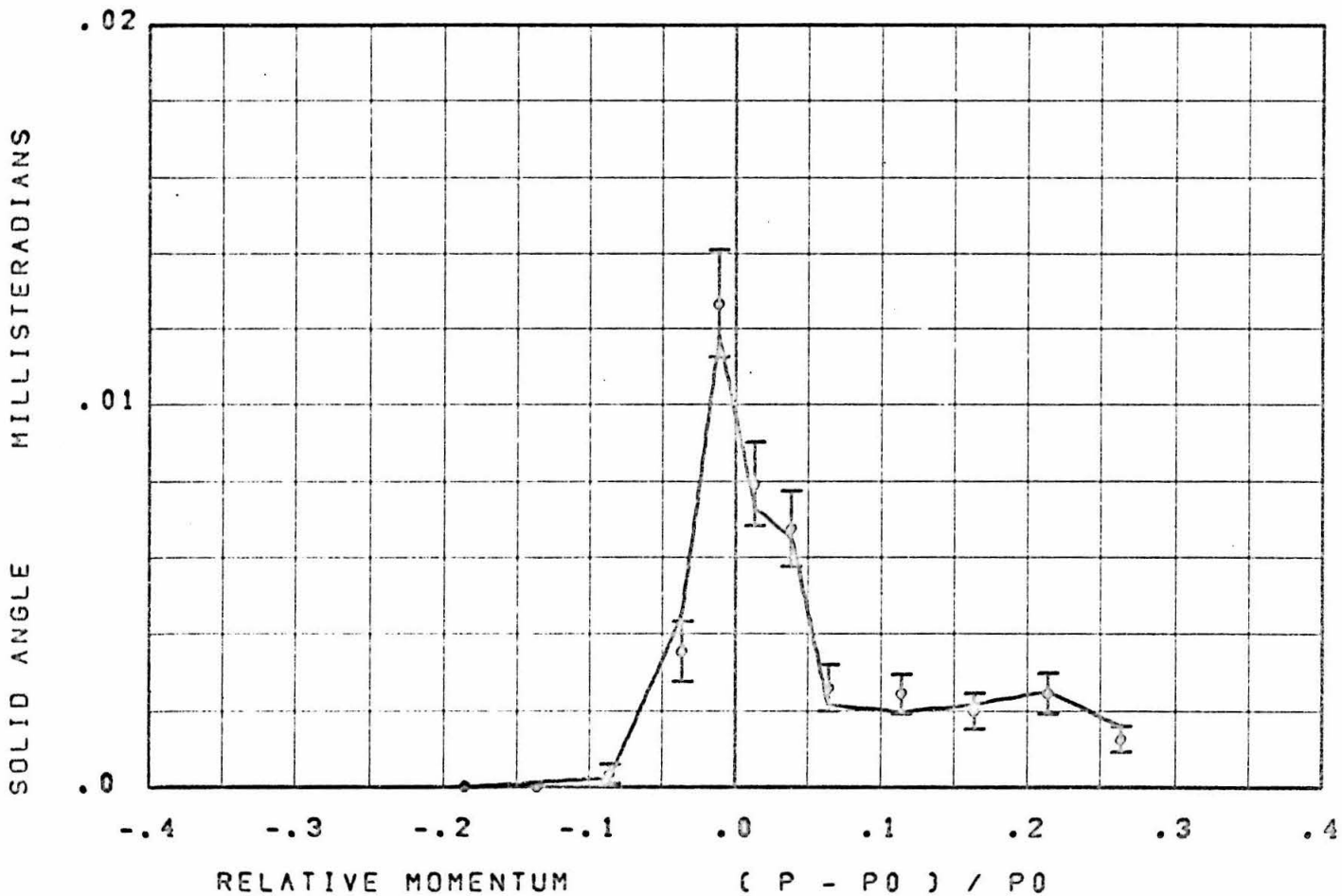
DECAY PION RESOLUTION FUNCTION P0 = 900 MEV/C
SOLID ANGLE MILLISTERADIANS
.02
.01
.0
-.4
-.3
-.2
-.1
.0
.1
.2
.3
.4
RELATIVE MOMENTUM (P - P0) / P0

FIGURE 19.3

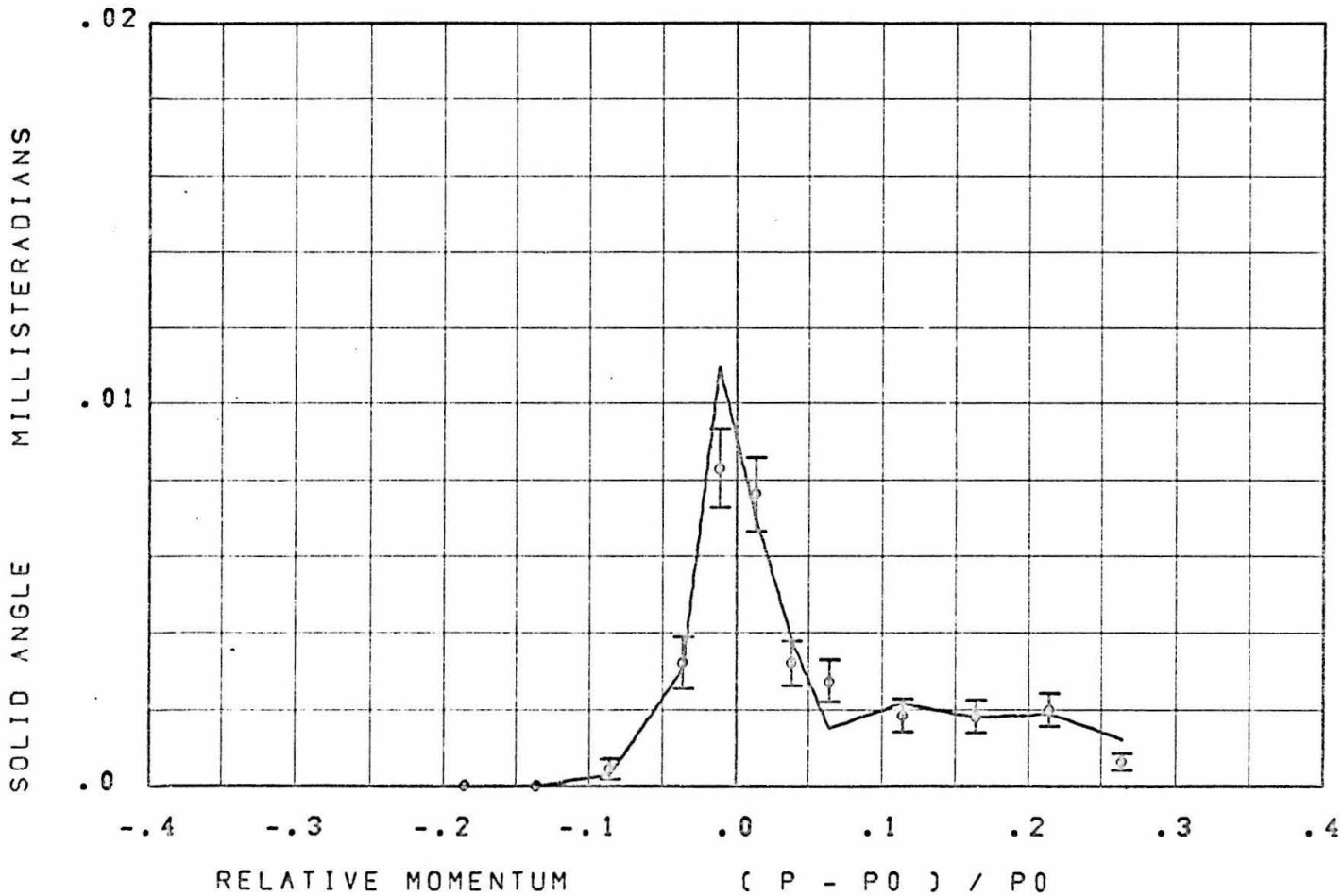
DECAY PION RESOLUTION FUNCTION P0 = 1100 MEV/C
SOLID ANGLE MILLISTERADIANS
.02
.01
.0
-.4
-.3
-.2
-.1
.0
.1
.2
.3
.4
RELATIVE MOMENTUM (P - P0) / P0

FIGURE 19.4

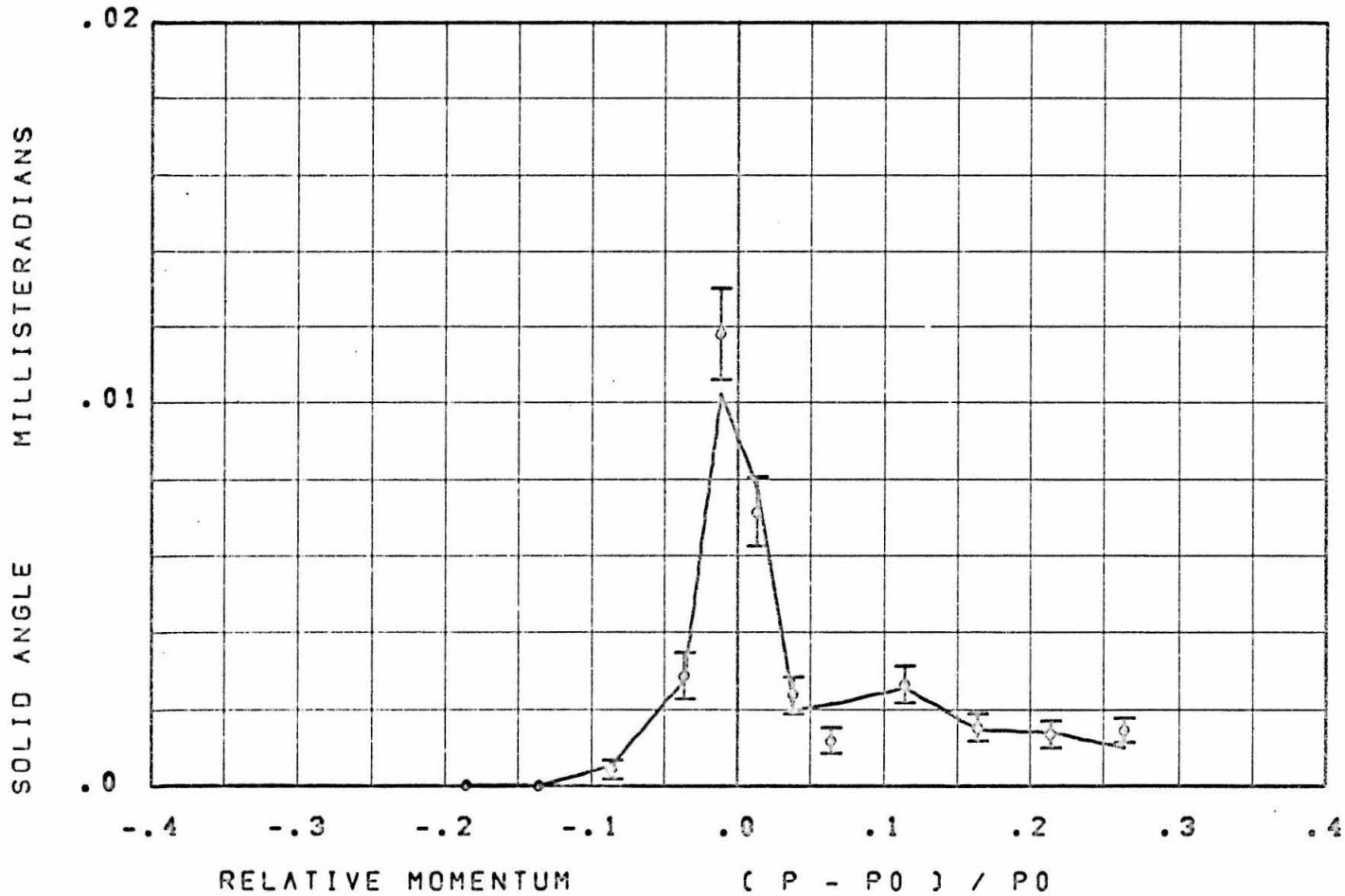
DECAY PION RESOLUTION FUNCTION P0 = 1200 MEV/C
SOLID ANGLE MILLISTERADIANS
.02
.01
.0
-.4
-.3
-.2
-.1
.0
.1
.2
.3
.4
RELATIVE MOMENTUM (P - P0) / P0

FIGURE 19.5

APPENDIX III

COUNTERS AND ELECTRONICS

Some of the counters are described in earlier works[27, 32, 33] so that only a brief description of them is given here. Counters A1, A2, and FC were new at the beginning of this experiment. Table 11 gives a summary of all the counters.

A. Cherenkov Counters

The Plexiglas Cherenkov counter (LC) was used to separate pions from protons. It is 1.5 inches thick and wrapped in black nonreflective paper so only light which internally reflects can reach the photomultiplier tubes. This determines its threshold of $\beta = 0.9$. The lowest momenta pion measured (500 MeV/c) has $\beta = 0.96$ and is well above threshold. At the highest momentum used (1200 MeV/c), protons have $\beta = 0.79$, well below threshold.

The freon Cherenkov counter[32] (FC) was used to detect positrons. It consists of five feet of freon at atmospheric pressure giving a threshold of $\beta = 0.999$ corresponding to momenta of 11 MeV/c for electrons and 2.3 GeV/c for muons. Consequently, for the momentum range used, it counted only electrons. Figure 20 shows a typical spectrum from FC taken at 3.7 degrees to the photon beam at 700 MeV/c with a hydrogen target. The curve is skewed due to saturation of an amplifier.

TABLE 11

The Scintillation Counters

Counter	Purpose	Size (Height)(Width) (Thickness)	Phototube(s)
Large A1	Solid Angle	9" x 3" x 0.25"	6810-A
Small A1	Definition	4" x 2.5" x 0.25"	6810-A
A2	Time of Flight	9" x 5" x 0.25"	7850
S1	Time of Flight	6.5" x 11" x 0.25"	2-7850
S2 a, b, c, d	Momentum definition	1.18" x 11" x 0.25"	1-6810A Each
S3	To require passage through LC and lead	6.5" x 11" x 0.375"	2-7850
Fan	Pole face Scattering Veto	25" - 32" x 0.75" x 0.50"	2-6810A

All scintillation counters except the fans were made of NE-102 plastic.

The Cherenkov Counters

LC	Proton identification	5.75" x 11" x 1.5"	2-6810A
FC	Electron identification	20" x 22" x 60"	7040

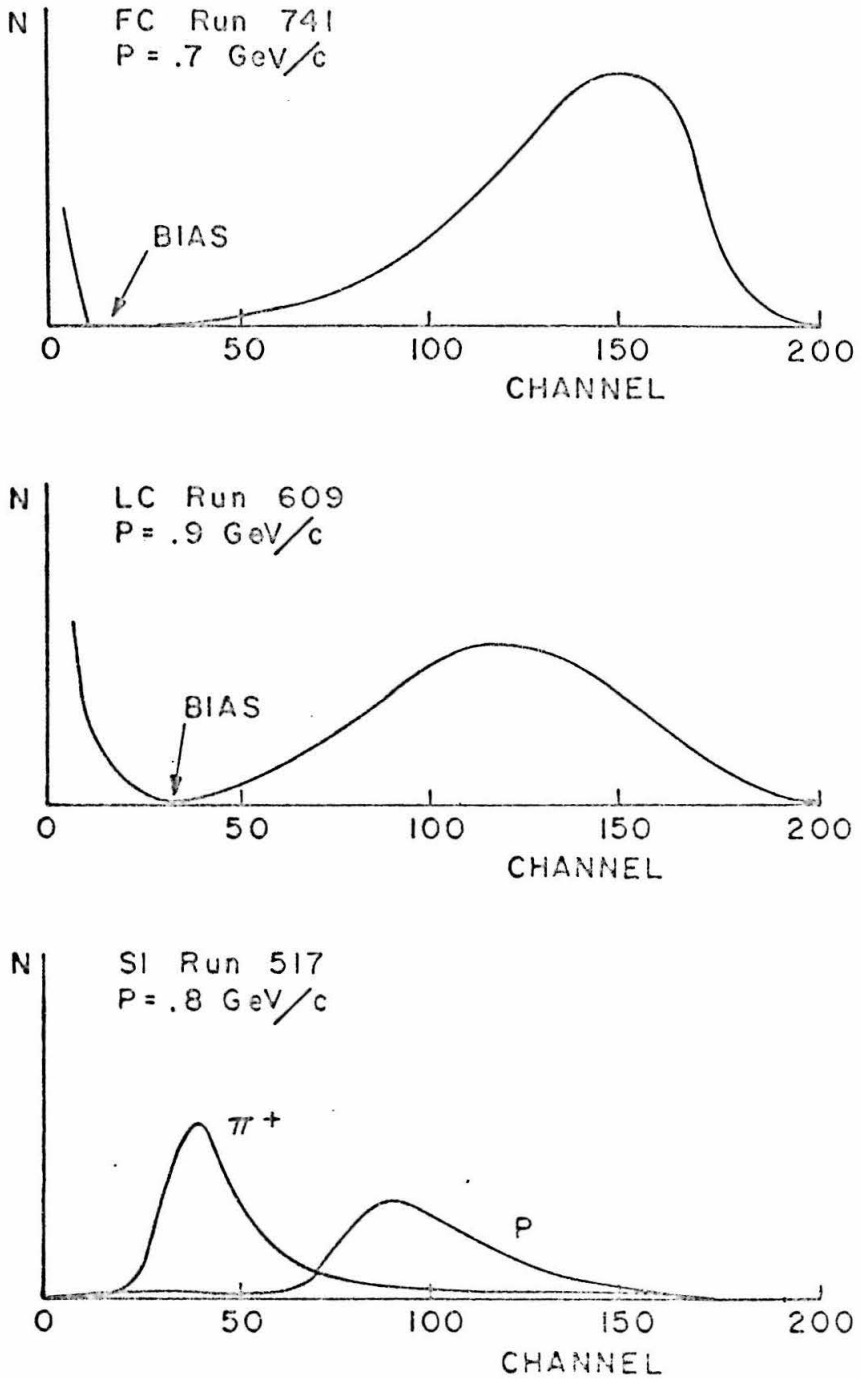

FIGURE 20. Pulse Height Spectra

B. Scintillation Counters

With the exception of A1, all the scintillation counters are similar to those commonly used in this laboratory. A1 is different in that the light is collected with mirrors instead of the usual plastic lightpipe. In this way, the problem of particles passing through the lightpipe and giving sufficient Cherenkov light to trigger the counter is eliminated. The construction of A1 was arranged so that the scintillator could be changed quickly and easily, allowing the solid angle acceptance to be changed. This proved to be very convenient for the small angle measurements. There the aperture was reduced in order to improve the angular resolution of the spectrometer. The smaller aperture also defined a smaller beam through FC thereby increasing its electron efficiency.

C. Monitor Telescope

For purposes of beam monitoring, a counter telescope was placed directly underneath the hydrogen target. The telescope consisted of two 3.75 x 4 inch scintillators, approximately four inches apart and ten inches from the target. In order to reduce the flux of low energy particles triggering the telescope, 1.5 inches of lead was placed above the telescope and 0.5 inches of lead followed by 0.75 inches Plexiglas and 0.5 inches of Bakelite was located between the two scintillators. Four to eight inches of lead were stacked around the telescope to shield it from background. It was firmly mounted on a steel table, independent of the target and the magnet. The signals from RCA 8810 phototubes were connected to a 10 ns coincidence circuit which drove a scalar.

This coincidence rate provided a relative monitor of the beam intensity stable within 1% over short times.

D. Electronics

For the most part, the electronic components are the same as described in Reference 27. The connections to the various components are shown schematically in Figure 21. The setup allowed some flexibility in measuring several rates at once. A particular choice of what rates to measure was made by selecting the inputs to the 50 ns logic by means of switches. Up to four such inputs may be required for an output signal with as many as four signals that could veto it. In addition, there are two outputs, the usual (A) and one (A_c) which ignores the veto signals. The various settings used regularly are given in Table 12. Each setting allows the measurement of four yields. The coincidence signals scaled were A, A_c, A · B, A · C, the latter two for each momentum channel as well as the total counts. These signals are interpreted as follows:

(1) A is the raw particle yield

(2) A_c is A plus events vetoed by Fan counters

(3) A · B is the π^+ yield

(4) As indicated in Table 12, A · C is one of the following:

a) proton yield

b) positron yield

c) S3 absorption

d) π^+ yield measured with larger A2 aperture.

To provide direct checks on the operation of the system, the rates of F · S1, A1 · S1, Tof, FC, S1, S2, and S3 were also scaled. A pulse-height analyzer was used to keep a constant watch over the phototube signals and bias settings. The system was in fact very reliable and seldom required repairs or adjustments.

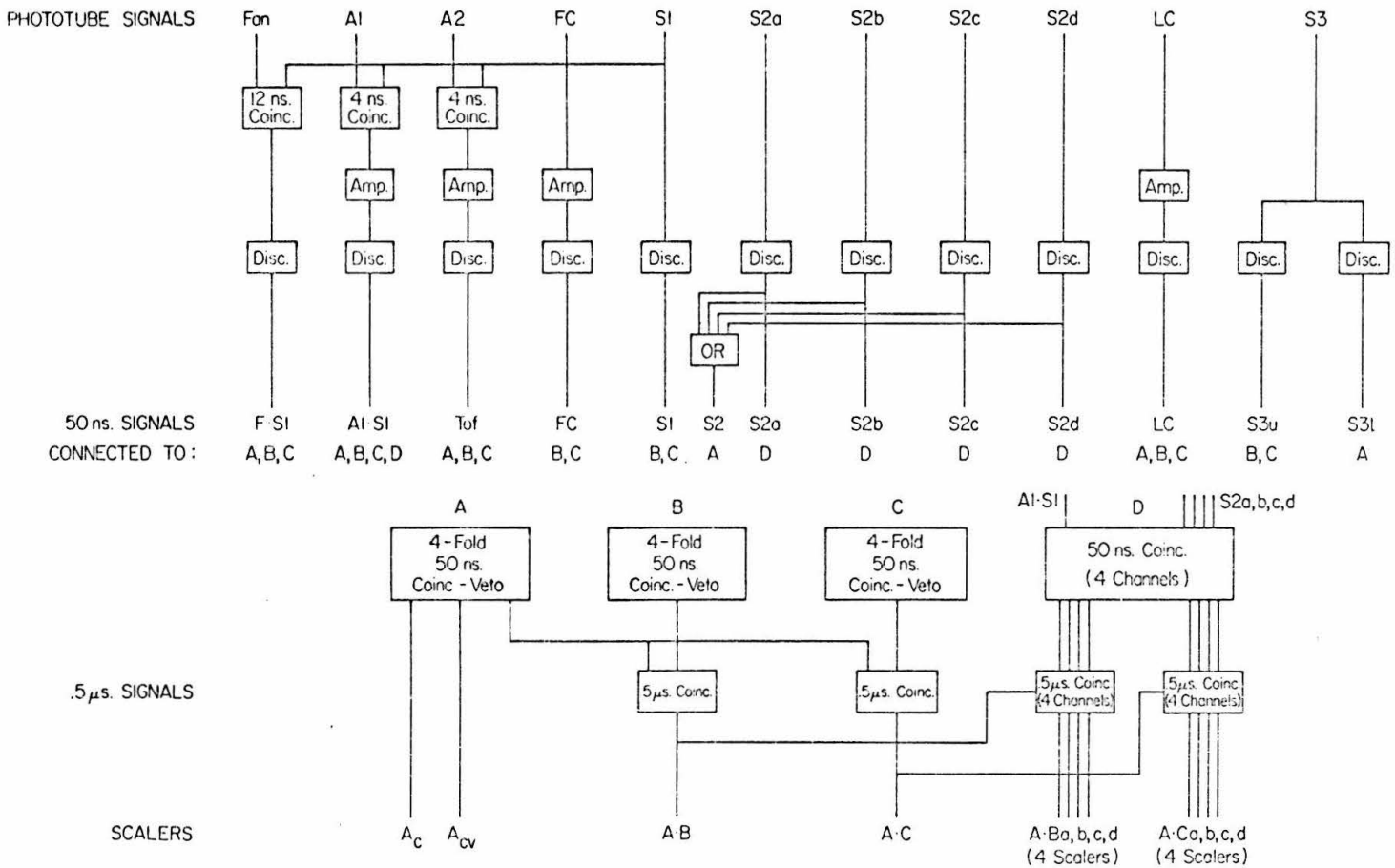

FIGURE 21. ELECTRONICS BLOCK DIAGRAM

TABLE 12

Logic Settings

C means signal in coincidence

V means signal in anticoincidence

Measurement	Proton			Positron			Absorption			Aperture		
Logic unit	A	B	C	A	B	C	A	B	C	A	B	C
50 ns Signal												
F · S1	V	V	V	V	V	V	V	V	V	V	V	V
A1 · S1	C	C	C	C	C	C	C	C	C		C	
Tof	C	C	C	C	C	C	C	C	C	C	C	C
FC		V	V		V	C		V	V		V	V
S1		C	C		C	C		C	C		C	C
S2	C			C			C			C		
LC		C	V		C	C	C			C		
S3u								C	V		C	C
S3ℓ	C			C								

APPENDIX IV

EFFICIENCIES AND RATES

In order to obtain the true pion yield, it is necessary to know the detection efficiency of each required or vetoing counter for various particles and the rates of the various particles encountered. Protons and positrons are the only backgrounds that can be present after the momentum selection and they are nicely taken care of with the two Cherenkov counters. It is also reassuring to monitor a variety of rates to check on the operation of the system. In doing so, one must remember that some of the rates are dependent on parameters to which the pion rate is insensitive. For example, the fast timing circuits are set for pions ($v \approx c$) with a resolution narrow enough to omit some of the slower moving protons. The "proton" rate measured (LC_V), which includes the fast timing requirement, is very dependent on the coincidence circuit output bias and the momentum of the protons. A small change in the bias, whether intentional or not, will thus cause a noticeable change in the LC_V rate but have no consequence on the measured pion rate. In cases such as this, monitoring the auxiliary rate is an oversensitive check of part of the system. There are instances when electronic biases were changed intentionally. In order to reduce the fraction of protons left for LC to identify at higher momenta, it was desirable to set a closer tolerance on the fast timings. Some of the measured rates are given here only to illustrate their order of magnitude.

A. Positron Yield

At small angles to the photon beam, a large number of electrons are produced so it is necessary to detect them with good efficiency to separate the pion yield. The freon gas Cherenkov counter (FC) was more than adequate for the job. Figure 22 shows the relative positron to pion yields obtained while making the cross section measurements. The values plotted are obtained from summing over the four momentum channels. Notice the positron rate is at most three times the pion rate.

The efficiency of FC for counting electrons (or positrons) was measured many times during the experiment and was always found to be better than 99.8%. The measurement was made by generating an electron beam from the photon beam with suitable lead collimators, attenuators and converters. The spectrometer was then set to zero degrees obtaining a nearly pure momentum analyzed electron beam. The same setup was used routinely to test the counters and electronics. No correction of the measured π yields was necessary due to the positron contamination.

B. Proton Yield

Protons were distinguished from pions primarily with the Plexiglas Cherenkov counter (LC). To measure its efficiencies for protons and pions, one must independently define protons and pions. This was done in two ways. In one case, the magnet polarity was switched to select negative particles, eliminating protons. The efficiency of LC for negative pions is thus obtained. The second method is to select pions or protons with time of flight and scintillator pulse heights (dE/dx). Figure 23 shows the results

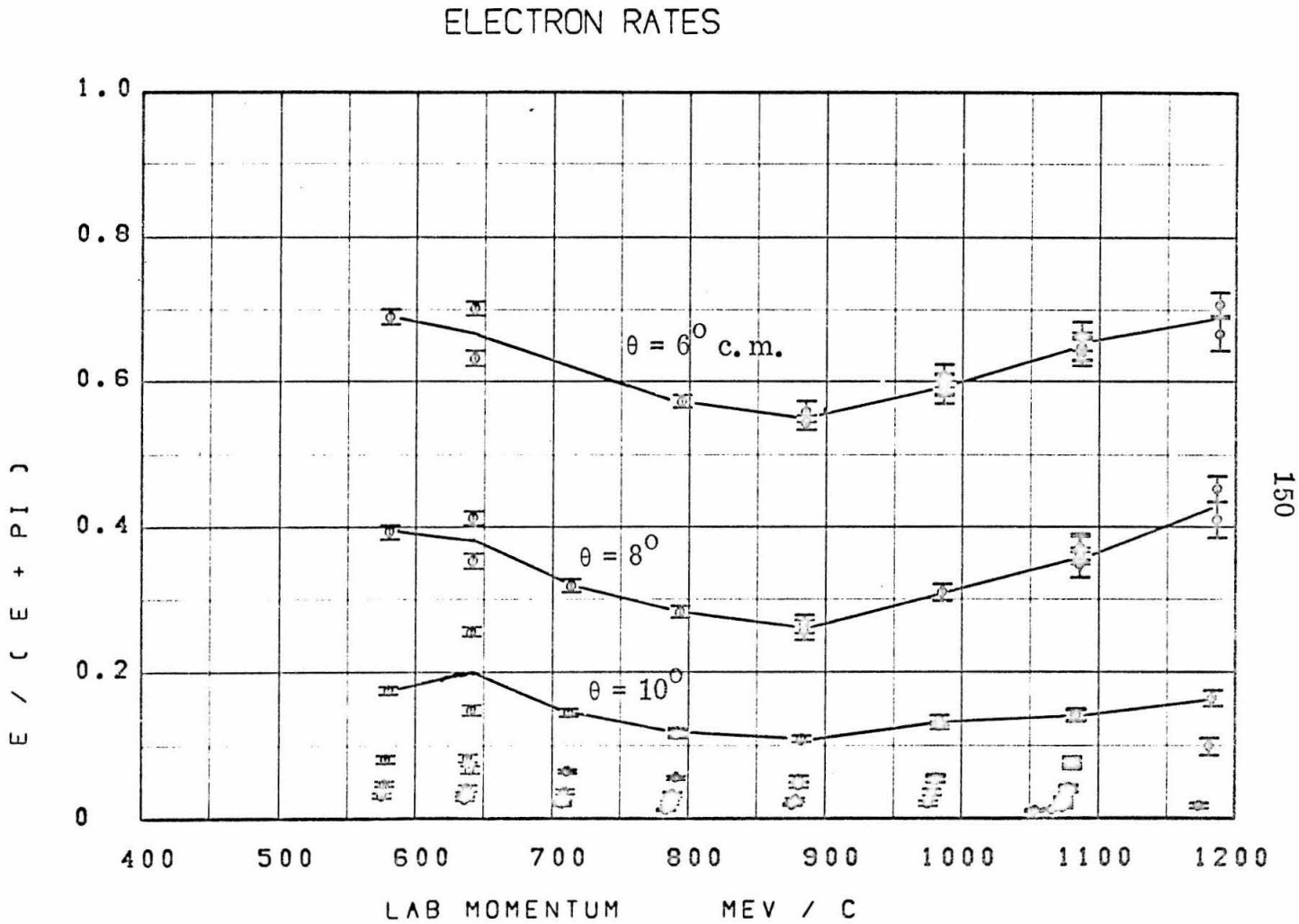
ELECTRON RATES
1.0
0.8
0.6
0.4
0.2
0
E / (E + PI)
θ = 6° c.m.
θ = 8°
θ = 10°
400
500
600
700
800
900
1000
1100
1200
LAB MOMENTUM MEV / C

FIGURE 22

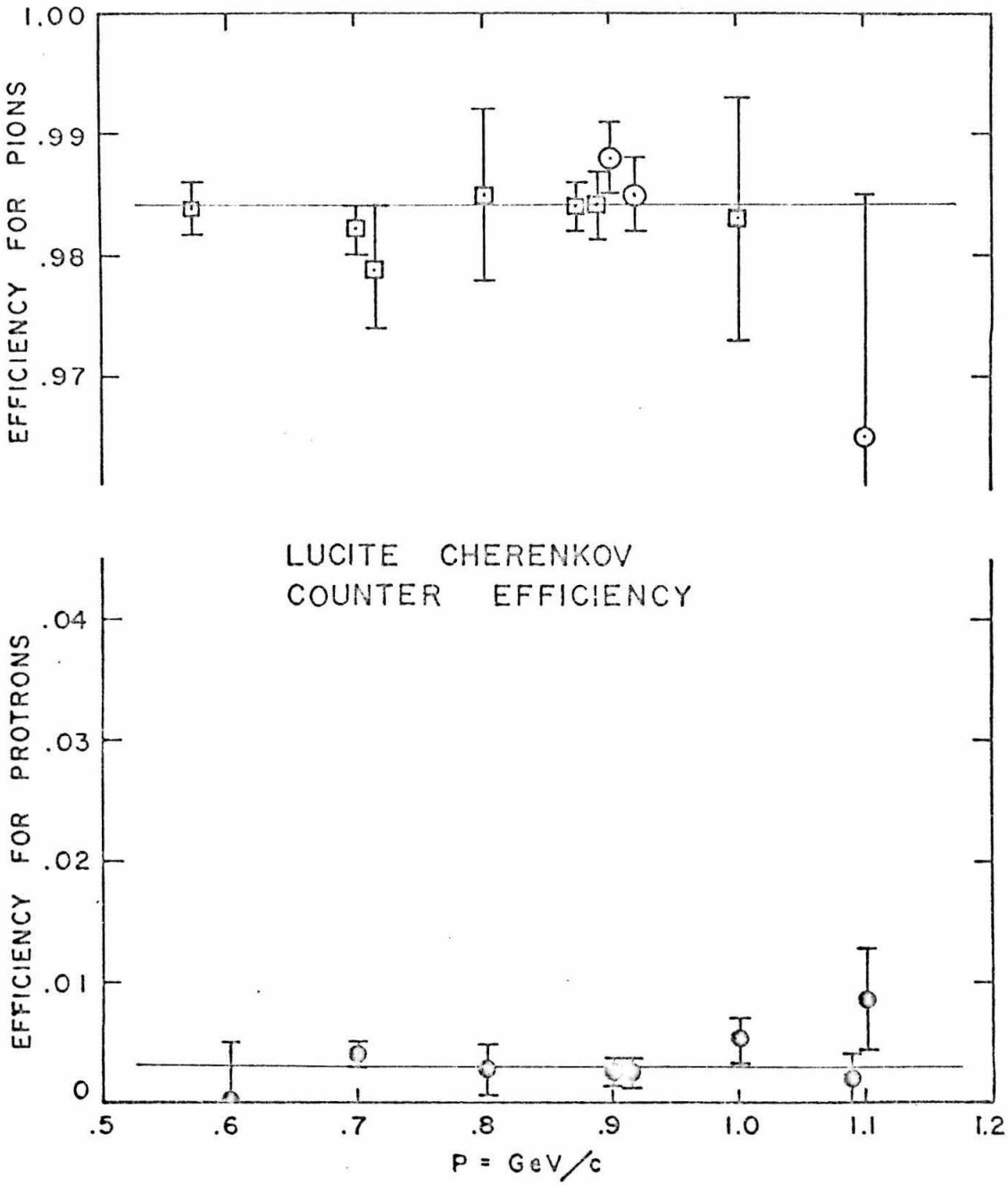
LUCITE CHERENKOV
COUNTER EFFICIENCY
EFFICIENCY FOR PIONS
1.00
.99
.98
.97
EFFICIENCY FOR PROTRONS
.04
.03
.02
.01
0
.5
.6
.7
.8
.9
1.0
1.1
1.2
P = GeV/c

FIGURE 23

of these measurements. The squares are measurements with negative pions. On the basis of these measurements, the pion yields were corrected, taking the efficiency of LC as

$$0.3 \pm 0.3\%$$

for protons and

$$98.4 \pm 0.5\%$$

for pions.

Measurements of the "proton" rate (LC_V) relative to the pion rate LC are shown in Figure 24 plotted vs. momentum. Of course, the proton rate also depends greatly upon angle and the synchrotron endpoint energy which are not indicated. Hence, no functional relationship is to be implied from Figure 24, and it is presented here only to indicate the relative rates encountered. The LC_V rate drops sharply below 750 MeV/c because of the fast timing requirements (Tof, A1 · S1).

In order to make the small correction to the pion yield due to nonzero proton efficiency of LC, an approximation to the proton rate was used as indicated by the line in Figure 24. The correction reduces the pion yield by 0.15% at 800 MeV/c and by 0.6% at 1200 MeV/c.

C. Aperture Checks

The spectrometer is set up so that A1 determines the solid angle acceptance and S2 the momentum acceptance. The other counters are large enough to not further restrict the acceptance.

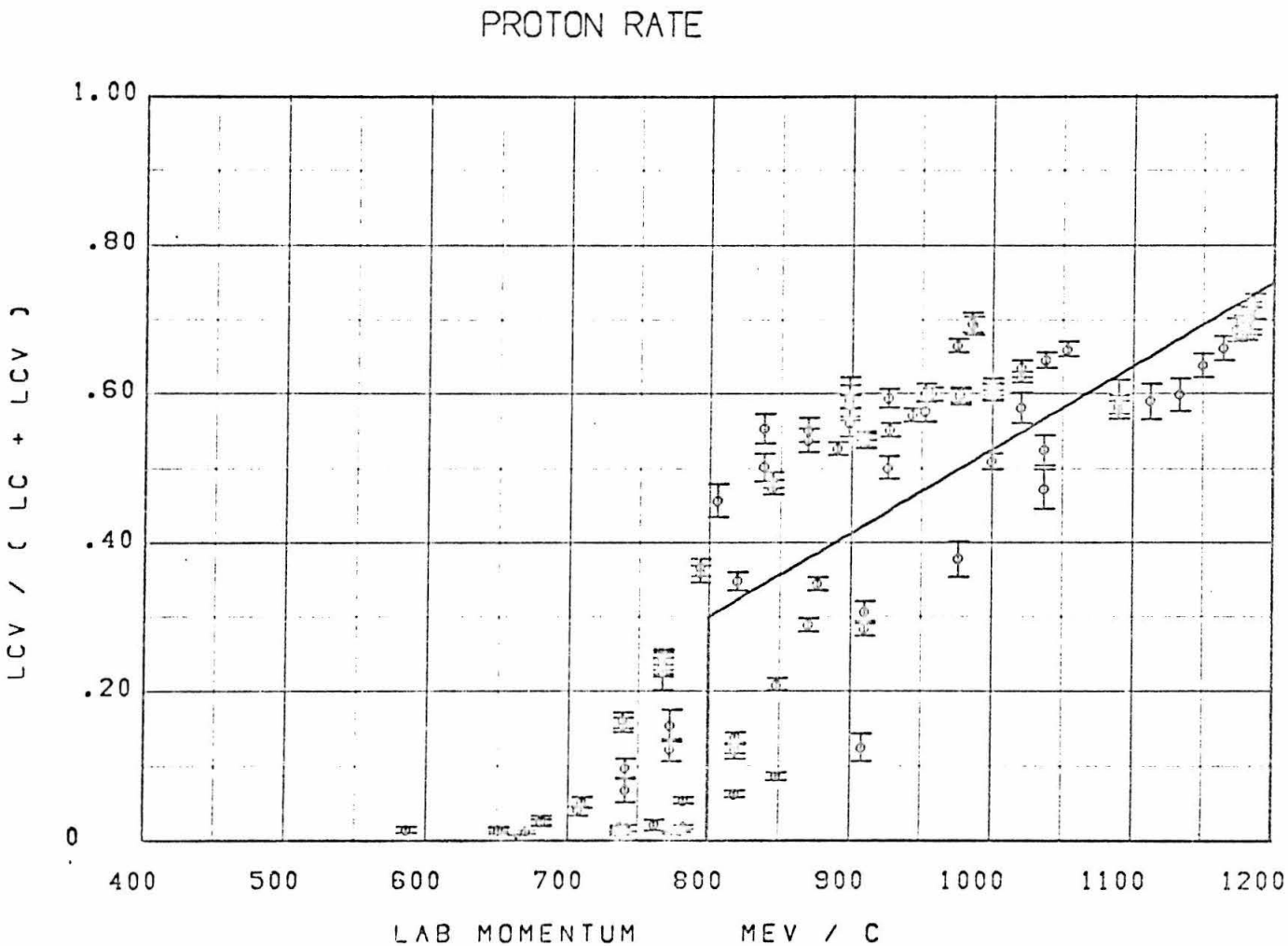
PROTON RATE
1.00
.80
.60
.40
.20
0
LCV / (LC + LCV)
400
500
600
700
800
900
1000
1100
1200
LAB MOMENTUM MEV / C

FIGURE 24

To check that this is so, the A2 efficiency and the S3 efficiency were measured experimentally. The S3 efficiency is complicated by absorption and multiple scattering and is discussed in Appendix V.

The A2 efficiency was measured 15 times during the experiment and averaged 99.2% ± 0.3% (rms). This high efficiency indicates that the air lightpipe aperture (A1) did not suffer from the usual problem of Cherenkov light in a lightpipe. It might be argued that A2 could have been omitted and indeed, for a majority of the time, its presence was unnecessary. It was useful, however, in several ways.

The small fraction of events missing A2 are probably not true pions from the hydrogen target. It was noted that if the magnetic field probe was left in its lowered position inside the magnet field in the path of the spectrometer acceptance, the A2 "efficiency" dropped to 95%. Although data were never taken that way, it does illustrate the effect of scattering inside the magnet and that A2 adds to the selection of proper events.

The solid angle of the spectrometer may also be defined by A2 · $\overline{\text{Fan}}$. A useful check is to measure the ratio of A2 · $\overline{\text{Fan}}$ to A1. I am indebted to Dr. C. Peck for suggesting this measurement to track down the cause of a change in the pion rate, which turned out to be a broken coincidence circuit. The ratio of the two apertures should be 1.35 according to a linear magnet theory calculation, and was measured to be 1.63 when the circuit was broken and 1.37 ± 0.08 when fixed. Routine checks of the system were made from time to time with an electron beam, so that it was easy to determine a date prior to the trouble when the coincidence circuit was known to be working perfectly. Data collected between that date and the date when the circuit was repaired were not used.

D. Multiple Channel Events

A correction to the measured yield was found to be necessary due to events recording simultaneously in more than one momentum channel. When the sum of the counts (S2 SUM) in the four channels was compared with the actual number of events (S2 OR) an excess was found. An investigation of the multiple channel events showed they were not accidentals but were two particles traversing the system at the same time. It was found that most often the double events occurred in adjacent channels. Figure 25 shows the fraction of excess counts as a function of momentum. The points plotted are actually the average of ten measurements. The linear fit was used to correct the yield assuming the multiple events were always in adjacent channels. The exact cause of these events was not known, but it is possible that they were due to nuclear interactions and/or knock-on electron processes in other counters.

E. Fan Veto Rate Correction

The fraction of the events that results from scattering in the pole-face of the magnet and hence are vetoed by the Fan counters was monitored throughout the experiment. At laboratory angles less than 10°, however, the Fan veto was not used because of the high flux of particles, especially electrons, that would cause accidental vetoes. Therefore it was necessary to subtract from the measured pion yield at small angles, the expected fraction that scatter off the pole-face. This was done by taking the average fraction as measured at wider angles at the same photon

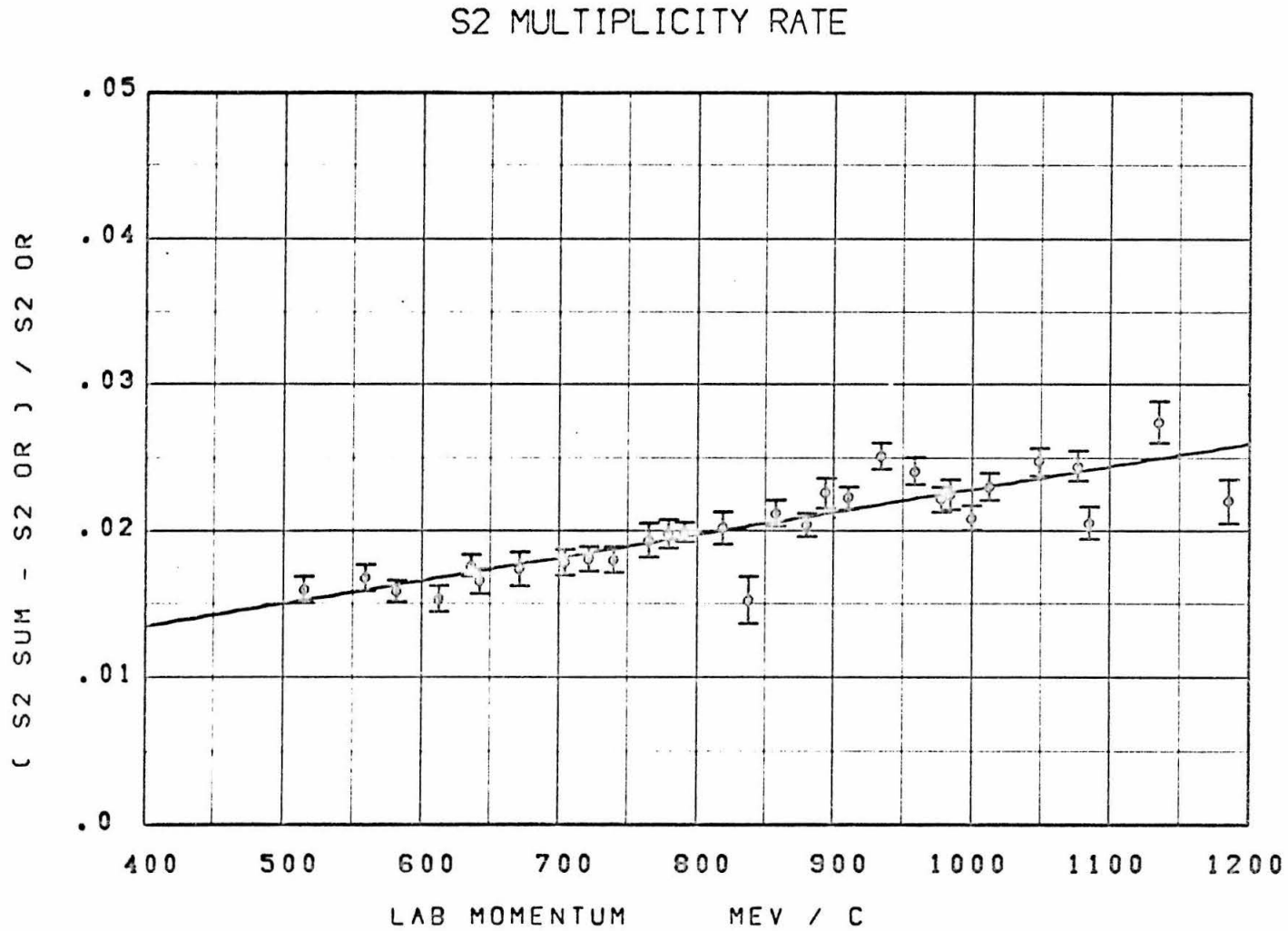
S2 MULTIPLICITY RATE
(S2 SUM - S2 OR) / S2 OR
.05
.04
.03
.02
.01
.0
400
500
600
700
800
900
1000
1100
1200
LAB MOMENTUM MEV / C

FIGURE 25

energy.* The values used are given in Table 13.1. Since the Fan veto rate measurement sometimes includes protons as well as pions (Appendix III-D), the correction implicitly assumes that the relative rate for protons is not too different from that for pions. This assumption was checked by direct measurements and the results are given in Table 13.2. There is a noticeable difference only at low momenta which does not matter in the correction since there the time of flight eliminates protons from the normal measurement.

The dependence of the Fan veto rate upon the synchrotron endpoint energy E_o and upon the size of A1 was also checked directly at 600 MeV/c. Table 13.2 lists the results.

---

* In actuality, the Fan veto rate is a function of momentum. Because the small angle region was emphasized, the average Fan veto rate for angles greater than 10^o is weighted toward the momentum setting of the smaller angles, and is sufficiently accurate for this correction.

TABLE 13.1

Average Fan Veto Rates Used to Correct Small Angle Data

Mean Photon Energy	Fan Veto Rate
611 MeV	0.090
672	0.070
743	0.060
824	0.064
915	0.052
1016	0.045
1117	0.040
1221	0.030

TABLE 13.2

Measurement	Particle	Momentum MeV/c	E_o Mev	Aperture in x in	Fraction of Fan Vetos
Momentum dependence	π^+	600	1300	3 x 9	0.071 ± 0.007
		800	1300	3 x 9	0.059 ± 0.004
		1000	1300	3 x 9	0.031 ± 0.004
		1100	1300	3 x 9	0.030 ± 0.005
Momentum dependence	Proton	600	1300	3 x 9	0.043 ± 0.003
		800	1300	3 x 9	0.036 ± 0.002
		1000	1300	3 x 9	0.043 ± 0.002
		1100	1300	3 x 9	0.025 ± 0.003
E_o dependence	π^+	600	780	3 x 9	0.057 ± 0.005
Aperture dependence	π^+	600	1300	2.5 x 4	0.065 ± 0.006

APPENDIX V

ABSORPTION AND MULTIPLE SCATTERING

The correction for losses due to nuclear absorption and multiple scattering in counters and miscellaneous matter was made in two ways, depending on the location of the absorber. For most of the matter, a geometric cross section was used to describe the losses. The fraction of pions not interacting is $e^{-\sigma N_o t}$, where σ is the cross section per nucleus, t the thickness of the absorber in $(gm/cm^2)/gm$ atomic weight and N_o Avogadro's number. The dependence of σ on atomic number was taken as $\sigma = \sigma_e A^{2/3}$ where σ_e is an "elementary" cross section.

For matter near the last counter S3 this would be too great a correction since an interaction there is likely to produce a charged secondary which will count in S3. Multiple scattering losses are also different for matter near S3. A Monte Carlo calculation[3] shows that generally as many particles are gained as are lost due to multiple scattering, which only results in a broadening of the momentum resolution. However, one might expect scattering near S3 to result in more losses than gains because the beam there is well defined in direction and momentum leaving less of a chance for particles to be gained. In any case the correction made for losses near S3 includes the possibility of losses due to both absorption and multiple scattering.

The net correction is split into two parts.

$$A_N = (1 - V_1)(1 - V_2)$$

(Measured yield) = A_N (Actual yield if no losses)

V_1 is due to counters S1, S2, LC, and the 0.5 inch of lead ahead of S3 (Part B), and V_2 is due to the rest of the matter (Part C).

A. Resolution Broadening

The main effect of multiple scattering is to broaden the momentum resolution. In passing through a thickness dZ of matter with radiation length L(Z), a monoenergetic, collimated beam of singly charged particles will undergo scattering and result in a beam with the same mean direction and a rms spread in angle, (projected onto a plane) given by[34]

$$d(\theta^2_{rms}) = \left(\frac{15\ MeV}{P\ v}\right)^2 \frac{dZ}{L(Z)}$$

where

P = particles momentum

v = particles velocity.

Because of a scatter, a given particle will pass through the focus of the spectrometer at a different transverse position, resulting in wrong determination of its momentum. According to linear magnet theory,

$$Y_f = M(Z)\ Y_Z + K(Z)Y'_Z + D(Z)\ Q$$

Y = position of particle ray perpendicular to central ray direction in vertical plane

Y_f = Y at focus

Y_Z = Y at a distance Z from source (H_2 target)

Y'_Z = slope of ray relative to central ray at position Z

Q = relative momentum $(P - P_o)/P_o$.

The coefficients M, K, D are easily calculated, being just the first row of the transfer matrix for the vector (Y, Y', Q). Since the mean change in angle is zero, there is no mean change in Y_f and the rms spread in Y_f is given by

$$d(Y^2_{f\ rms}) = K(Z)^2\ d(\theta^2_{rms}) .$$

$$Y^2_{f\ rms} = \left(\frac{15\ MeV}{P\ v}\right)^2 \int_o^f \frac{(K(Z))^2\ dZ}{L(Z)}$$

The integral is conveniently done in pieces where L(Z) is constant. K(Z) is linear in front of and after the magnet effective edges with slopes - M(f) (the magnification) and -1 respectively. Inside the magnet K(Z) is a linear combination of the sine and cosine of the remaining bending angle.

The rms spread in Q is given by

$$Q_{rms} = \frac{Y_{f\ rms}}{D(f)} .$$

Table 14 lists the various contributions to Q_{rms} at P = 1.0 GeV. Since $Y_{f\ rms}$ is approximately proportional to 1/P ($v \approx c$), the rms spread in momentum is a constant, 7 MeV/c, independent of momentum.

TABLE 14

Contributions to Multiple Scattering

Material	Radiation Length cm	Thickness cm	Q_{rms} %
Target Wall (Al)	8.86	0.16	0.04
Air, Target to Magnet	3.1×10^4	264	0.15
Air in Magnet	3.1×10^4	127	0.20
Air, Magnet to FC	3.1×10^4	66	0.13
A1	41.3	0.635	0.41
A2	41.3	0.635	0.31
FC Freon	2.8×10^3	157	0.38
FC Mirror	41.3	0.7	0.08
S1	41.3	0.635	0.03
		Net Q_{rms} =	0.70%

B. Losses Near S3

The correction for interaction and scattering in counters S1, S2 and LC and the lead absorber was made on the basis of measured losses obtained mostly from the normal data running and partly from a set of extra measurements made for that purpose. The fraction of particles which miss S3 while satisfying the other pion requirements was recorded for most of the data runs at laboratory angles greater than 14^{o}. Figure 26 shows the S3 miss rate for runs with and without the lead absorber. The measurements with the lead have been combined into groups of four to produce a readable graph. The linear fit to the lead points is given by

$$\text{S3 MISS} = 0.103 - 0.050\ P \quad (P \text{ in GeV/c}).$$

This is interpreted as arising from nuclear absorption and multiple scattering in the lead and LC, with a small contribution from particles which scatter in S1 or S2 and count in LC but not in S3. The desired correction for S1, S2, and LC, and the lead is thus S3 MISS plus that due to scattering in S1 or S2 which does not result in counts in LC.

For this additional correction, measurements were made of the fraction, V, of pions which missed S3 when additional Plexiglas absorbers, of thickness t and the same cross sectional area as the counters, were placed at a distance d in front of S3. Various configurations of counters were used in order to obtain a useful range of d. Each measurement was the difference between absorber and no absorber miss rates with the same counter

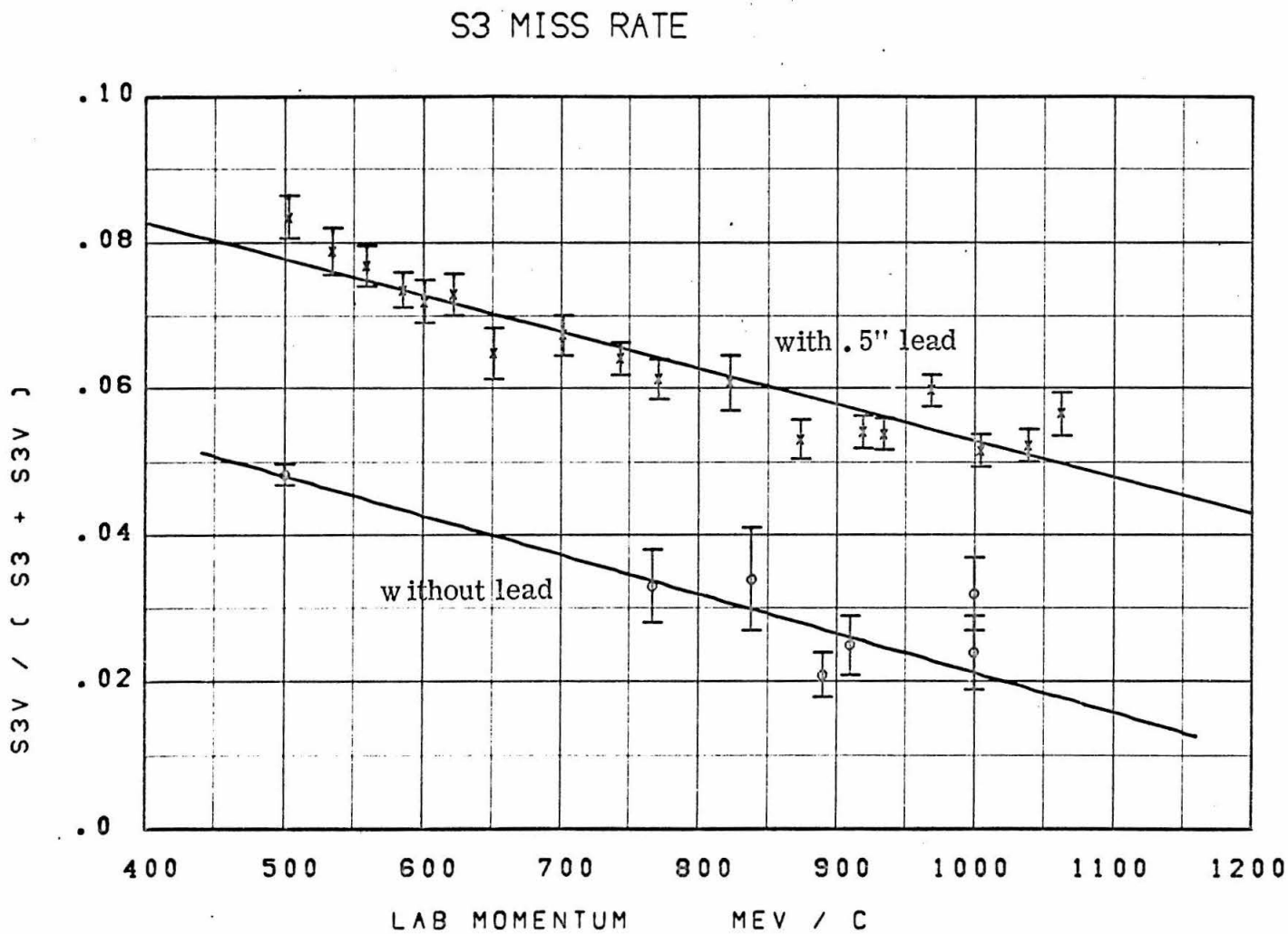
S3 MISS RATE
.10
.08
.06
.04
.02
.0
S3V / (S3 + S3V)
with .5" lead
without lead
400
500
600
700
800
900
1000
1100
1200
LAB MOMENTUM MEV / C

FIGURE 26

configuration and momentum. Figure 27 shows the results of these measurements. The solid lines are a least squares fit to the form

$$V = t(a_1 + a_2\, d + a_3\, P) \quad .$$

The losses due to scattering in S1 that result in no count in LC were obtained by setting t equal to the thickness of S1 and d equal to the distance (for the normal running) from S1 to LC. Evaluating the loss from S2 in a similar way, the amount to be added to S3 MISS is

$$V = 0.014 - 0.006\ P$$

giving a total correction of

$$V_1 = 0.117 - 0.056\ P \quad .$$

This amounts to 0.061 at 1.0 GeV/c and 0.089 at 0.5 GeV/c. The systematic error is estimated to be 0.01.

In order to obtain an estimate of how much of V is due to multiple scattering, a simple calculation was made assuming the beam, counters and absorber are uniform and have the same cross sectional area. The dashed lines in Figure 27 are V minus this calculation. Notice this difference (the nuclear absorption part if the multiple scattering calculation is correct) is nearly independent of energy. This is important in the absorption correction for the rest of the system where the absorption cross section was taken to be independent of energy.

FIGURE 27

Absorption vs. d and p for t = 5 cm

Different symbols refer to different counter configurations

Symbol	S2 Position	LC Position
	Normal	before S1
	Normal	Removed
	before S1	Removed
	before S1	before S1

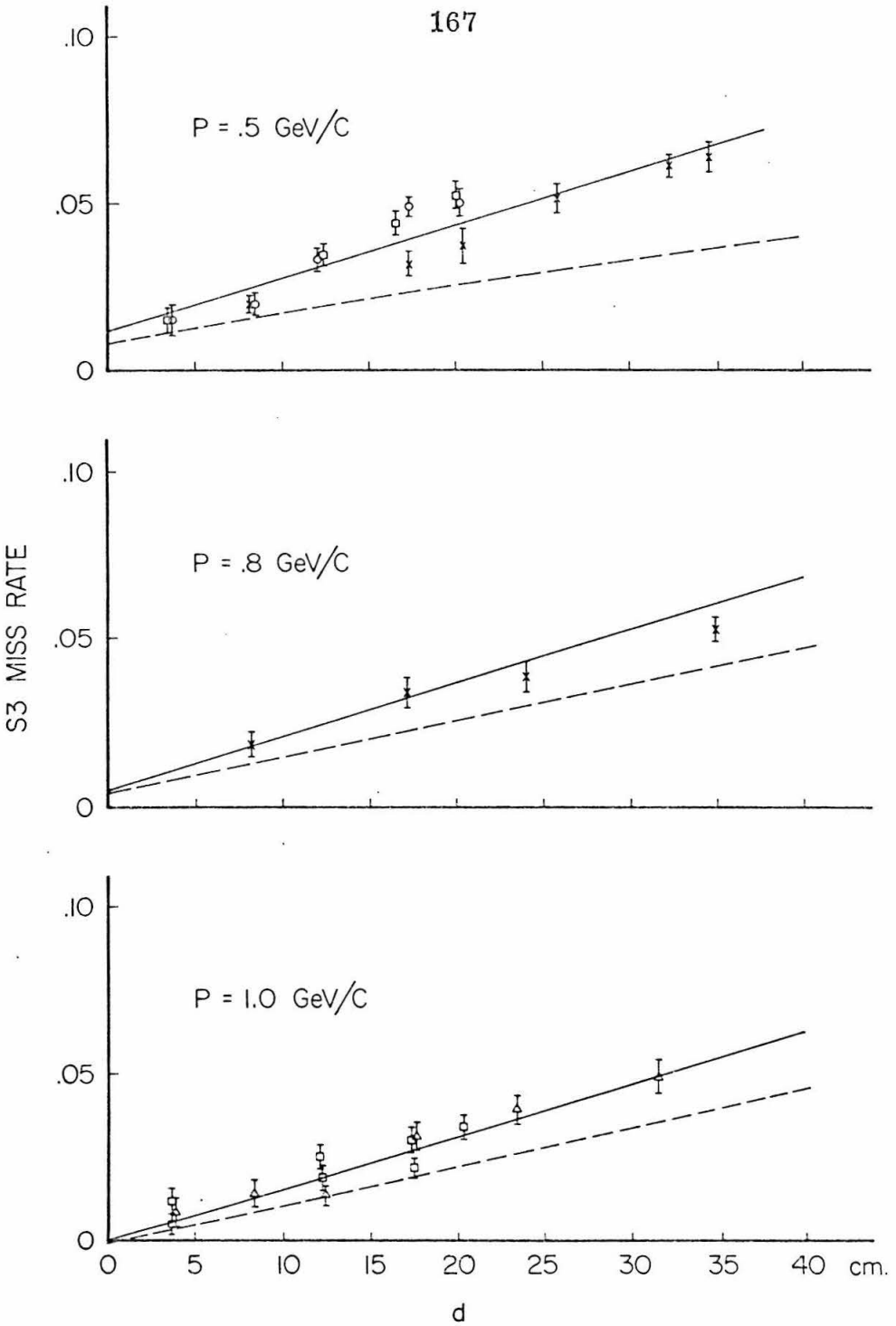
.10
.05
0
P = .5 GeV/C
.10
.05
0
P = .8 GeV/C
S3 MISS RATE
.10
.05
0
P = 1.0 GeV/C
0
5
10
15
20
25
30
35
40
cm.
d

FIGURE 27

C. Geometric Cross Section

In order to determine the "elementary" cross section σ_e, measurements of the fraction of π^+ which miss S3 due to Plexiglas absorbers up to 32 cm thick were made at a momentum of 500 MeV/c. The difference, V, between absorber and no-absorber miss rate was interpreted as the sum of multiple scattering losses and nuclear absorption losses.

$$V = M + (1 - e^{-\sigma_e A^{2/3} N_o t}) F_\pi$$

M = fraction of losses due to multiple scattering

F_π = the fraction of the beam which is π^+ (μ^+ interactions are negligible)

t = thickness of absorber (gm/cm^2/gm atomic weight)

A = atomic number.

The decay correction calculations (Appendix II D) give:

$$F_\pi = 0.916$$

at 500 MeV/c.

To estimate the fraction M lost due to multiple scattering, a simple calculation was made taking a uniform beam the same

size as the last counter.* If ΔY_{rms} is the root mean square transverse displacement at the last counter (S3) due to multiple scattering, the fraction lost for a counter of size 2a x 2b is

$$M_o = \frac{1}{\sqrt{2\pi}} \left(\frac{\Delta Y_{rms}}{a} + \frac{\Delta Y_{rms}}{b} \right)$$

provided $\Delta Y_{rms} \ll a$ and $\Delta Y_{rms} \ll b$. For S3 with dimensions 11 in. x 6.5 in. this is

$$M_o = 0.077\ \Delta Y_{rms}\ cm^{-2}.$$

From section A,

$$(\Delta Y_{rms})^2 = \left(\frac{15\ MeV}{P\ v}\right)^2 \int_{d_o}^{d_o + t} \frac{Z^2}{L}\, dZ$$

d_o = distance from S3 to near surface of absorber

t = thickness of absorber

P = 500 MeV/c

v $\approx c$

L = 41.3 cm

---

* While this assumption would not be good for the normal configuration, it is a reasonable one for the configuration used in these measurements.

$$\Delta Y_{rms} = 0.03 \quad \frac{d_o t^2 + d_o^2 t + 1/3\, t^3}{L}$$

$$M_o = 3.58 \times 10^{-4}\ cm^{-3/2} \quad d_o t^2 + d_o^2 t + 1/3\, t^3 \ .$$

This calculation is admittedly crude, but it is sufficient for the accuracy needed. Since the beam was in fact not uniform and had a cross section smaller than S3, this calculation of M is likely to be too large. Consequently it was taken as an upper limit to the multiple scattering losses and the value used is

$$M = 1/2\ M_o \pm 1/2\ M_o \ .$$

The values thus obtained for σ_e are plotted versus 1/t in Figure 28. Measurements with large t give the best determination of σ_e since reaction products then have a smaller chance of reaching S3. The smooth curve, a quadratic fit in 1/t gives an extrapolated value of

$$\sigma_e = 35.3 \pm 1.3 \text{ millibarn at } 1/t = 0 \ .$$

This value was used to calculate the nuclear absorption cross section $\sigma = \sigma_e A^{2/3}$. The error listed with σ_e and the error bars of Figure 28 are standard deviations resulting only from counting statistics. The systematic error in the estimate of M introduces a greater error of

$$\pm 4.2 \text{ mb} \ .$$

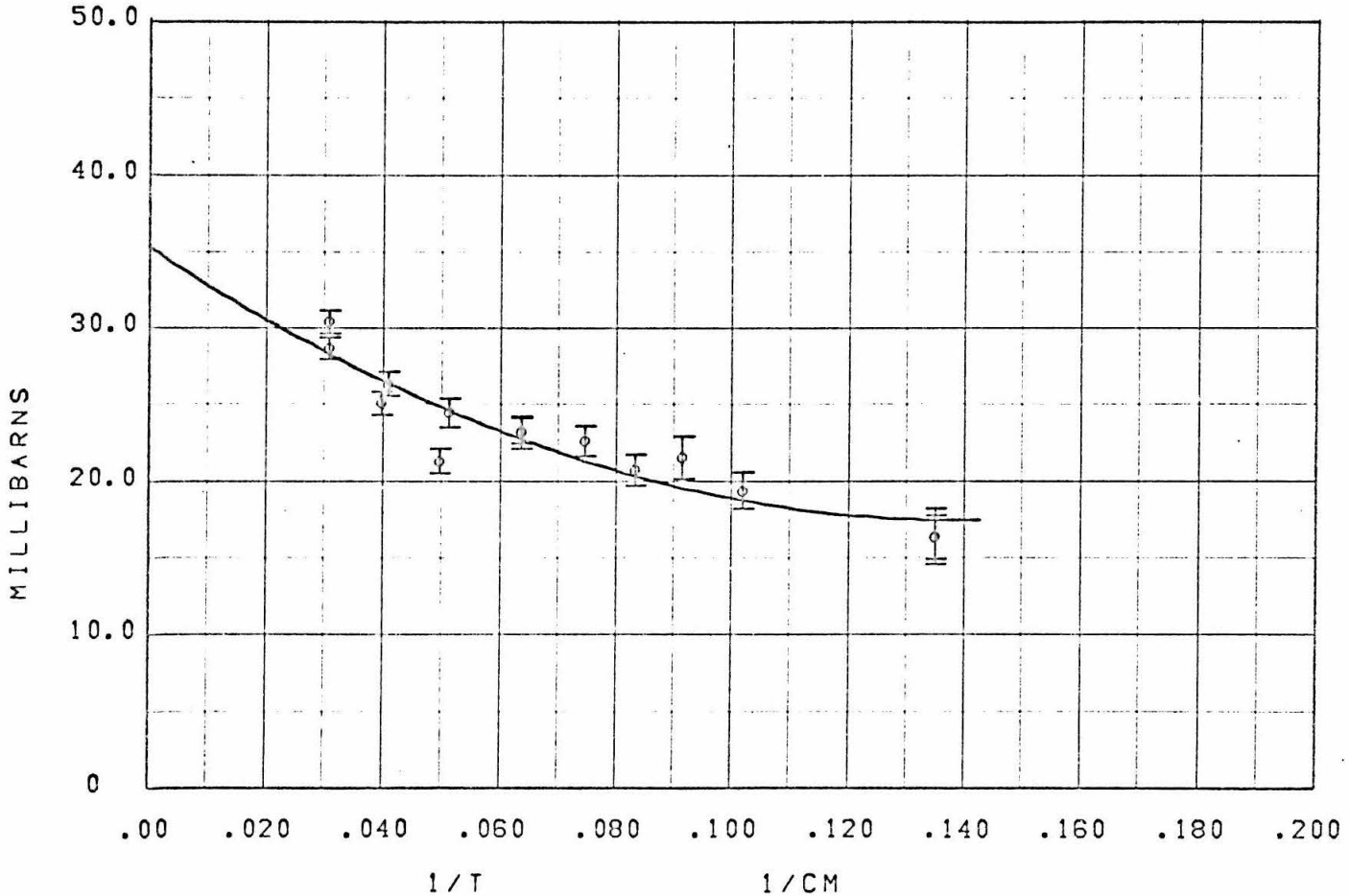
ELEMENTARY ABSORPTION CROSS SECTION VRS 1/T
50.0
40.0
30.0
20.0
10.0
0
MILLIBARNS
.00
.020
.040
.060
.080
.100
.120
.140
.160
.180
.200
1/T
1/CM

FIGURE 28

The absorbing matter in the spectrometer path is listed in Table 15. The collision length L_c, given by

$$L_c^{-1} = \frac{N_o \sigma_e A^{2/3}}{A \text{ (gm - atomic weight)}} ,$$

is also tabulated.

The fraction of the yield lost due to nuclear absorption is given by

$$V_2 = F_\pi \left(1 - e^{-\sigma_e A^{2/3} N_o t}\right) .$$

The fraction F_π varies with momentum from 0.916 at 500 MeV/c to 0.967 at 1200 MeV/c. For convenience a linear relationship was used for this correction giving

$$F_\pi = 0.916 + 0.015 \frac{P - 500}{700} .$$

The other factor in V_2,

$$1 - e^{-\sigma_e A^{2/3} N_o t} ,$$

is 0.045 ± 0.010 for laboratory angles less than 15° and 0.048 ± 0.011 for angles greater than 15°.

TABLE 15.1

Absorbers in Spectrometer Aperture

	Absorber	Density gm/cm^3	Thickness cm	gm/cm^2
H_2	Liquid Hydrogen	0.0707	3.5	0.25
$H_8C_{10}O_4$	Mylar Cup	1.38	0.0127	0.018
C_u	Heat Shield	8.9	0.006	0.05
Al	Outer Shield ($\theta > 15^o$)	2.7	0.16	0.43
$H_8C_{10}O_4$	Mylar Window ($\theta > 15^o$)	1.38	0.025	0.035
N_2, O_2	Air	1.29×10^{-3}	500.	0.646
CF_3Br	Freon	5.18×10^{-3}	157.	0.813
C H	A1	1.05	0.635	0.667
C H	A2	1.05	0.635	0.667
$C_5H_8O_2$	FC Mirror	1.18 ± 0.02	0.7 ± 0.1	0.83
Al	Miscellaneous	2.7	0.3 ± 0.1	0.81
C	Miscellaneous Counter Wrappings	0.5	0.2 ± 0.1	0.10

TABLE 15.2

Absorbers by Element

Element	A	Amount gm/cm^2		σ millibarns	L_c gm/cm^2
		$\theta < 15^o$	$\theta > 15^o$		
H	1.	0.421	0.420	35.3	47
C	12.	1.927	1.905	185	108
N	14.	0.517	0.517	205	113
O	16.	0.411	0.399	224	119
F	19.	0.311	0.311	251	126
Al	27.	0.810	1.240	318	141
Cu	63.5	0.050	0.050	561	188
Br	79.9	0.437	0.437	657	203

(S1, S2, LC counters and 0.5 in. lead not included)

APPENDIX VI

CROSS SECTION CALCULATION

From the measurements of raw yields and efficiencies, the actual π^+ yield is easily calculated. This yield may be expressed as a six-fold integral over the solid angle and momentum apertures and position at the hydrogen target.

$$N_\pi = \int\int\int\int\int\int \frac{d\sigma}{d\Omega} \frac{d\Omega}{d\Omega_\ell} n_p \, n(K, E_o, X, Y) \frac{dK}{dP} A_N$$

$$[e^{-\frac{Lm}{P\tau}} R_o(P, \Omega_\ell, X, Y, Z) + D_o(P, \Omega_\ell, X, Y, Z)]$$

$$dX \, dY \, dZ \, d\Omega_\ell \, dP$$

N_π = number of pions going into spectrometer acceptance

$\frac{d\sigma}{d\Omega}$ = cm cross section

$\frac{d\Omega}{d\Omega_\ell}$ = solid angle transformation to lab

n_p = density of protons in target

$n(K, E_o, X, Y)$ = number of incident photons per unit area and unit energy

K = lab photon energy

E_o = end point of bremsstrahlung spectrum

X = horizontal position at target perpendicular to photon beam

Y = vertical position at target

Z = horizontal position at target along photon beam direction

P = lab π^+ momentum

A_N = absorption correction

L = flight path from target to last counter (6.6 meter)

m = mass of π^+ (139.63 MeV/c^2)

τ = lifetime of π^+ (25.5×10^{-9} sec)

R_o = function (0 or 1) specifying spectrometer acceptance

D_o = probability of π^+ decay with μ^+ detected

Over the region of integration (R_o or D_o nonzero) the factors in the integrand vary slowly so they might be taken outside the integral. This would result in the integral being approximated by the integrand, evaluated at the midpoint of the region of integration, times the volume of the region of integration. The error in this approximation is second order in the "size" of the region of integration and consequently the approximation is sufficiently accurate. In order to analyze the endpoint comparison (Appendix II C), however, it was advantageous to retain the momentum dependence, doing that integral

last, and separately, for each cross section calculation. A momentum resolution function, R(Q), (Appendix II A) was calculated with the following approximations. The acceptance variation with horizontal position at the hydrogen target is ignored and the spatial distribution of the photon beam is taken to be that given by BPAK1[23] for typical values of K = 900 MeV and E_o = 1020 MeV.

$$R(Q) = \frac{\int N(900, 1020, X, Y)\, R_o(P, \Omega_2, O, Y, O)\, dX\, dY\, d\Omega_\ell}{\int N(900, 1020, X, Y)\, dX\, dY}$$

As noted in Appendix II, R is a function only of the relative momentum $Q = (P - P_o)/P_o$. The resolution function used is R, shifted in momentum by 2.7 MeV/c to account for energy loss of pions in the target etc., and broadened by folding in a Gaussian to account for multiple scattering (Appendix V A). These two corrections were done individually for each data point. The decay pion resolution function $D(Q, P_o)$ is defined similarly to R; however, it was calculated by a Monte Carlo program and is a function of P_o as well as Q. The photon spectrum is written as

$$N(K, E_o, X, Y) = \frac{W}{E_o} \frac{B_o(K, E_o, X, Y)}{K}$$

where W is the total energy in the beam and

$$\int B(K, E_o, X, Y)\, dK\, dX\, dY = E_o \ .$$

The average spectrum function is

$$B(K, E_o) = \frac{1}{t} \int B_o(K, E_o, X, Y)\, dX\, dY\, dZ$$

where t is the diameter of the hydrogen target and the integral is over the volume of the target to properly account for its non-uniform thickness. The yield is now given by

$$\frac{N_\pi}{W} = \frac{d\sigma}{d\Omega}\, \varkappa$$

where

$$\varkappa = N_p\, t\, A_N \frac{1}{E_o} \int \frac{d\Omega}{d\Omega_\ell} \frac{dK}{dP} \frac{B(K, E_o)}{K} \left[e^{-\frac{Lm}{P\tau} R(Q) + D(Q, P_o)}\, dP \right]$$

and some of the constant and slowly varying factors have been taken out of the integral. The above integral was performed numerically for each cross section measurement within a computer program. The R(Q) portion was done by Simpson's rule and the $D(Q, P_o)$ part, which is rough due to Monte Carlo statistics, was done by the trapezoid rule.

Various quantities involved in the calculation are given in Tables 16, 17. The results are given in Table 18.

Because of the change of dK/dP with angle, it is evident that each of the four momentum channels does not sweep out an angular distribution at a constant energy. The location of the measured points in K and θ is shown in Figure 29. Solid lines connect points obtained from the four channels for one spectrometer setting. In order to present angular distributions, the data points were interpolated in energy by the following scheme. For each

setting the four cross sections were fitted with a quadratic in K. This is effectively a fit along a line in Figure 29. Each data point was then moved to the desired energy (the dashed lines in Figure 29), chosen so each angular distribution comes from only one channel; by changing the value of the cross section by the same amount the fit changes over the distance moved. The advantage of this method is that the data are not artifically smoothed by the interpolating process. The error assigned to the interpolated cross section is taken to be the same as for the original. The interpolated cross sections are given in Table 1 in the main text.

As a point of summary and to acknowledge the assistance of the computer programs written by others, Table 19 gives the pertinent breakup of the data analysis calculations.

TABLE 16

Kinematic Parameters

POINT	specifies setting for purpose of comparison with Table 17.
LAB K 2PI	is the threshold for counting π^+ at the specified angle and momentum resulting from 2π production.
RMS DELTA K	is the root mean square photon energy ignoring the π decay resolution $D(Q, P_o)$.
A, B, C, D	specify the four momentum channels.

POINT	LAB ANGLE	PO	EO	CM ANGLE A	CM ANGLE B	CM ANGLE C	CM ANGLE D	LAB K A	LAB K B	LAB K C	LAB K D	LAB K 2PI A	LAB K 2PI B	LAB K 2PI C	LAB K 2PI D	RMS DELTA K A	RMS DELTA K B	RMS DELTA K C	RMS DELTA K D
6- 611	4.0	592.5	738.0	6.2	6.1	6.1	6.0	634	618	603	589	782	766	751	736	10.7	10.3	10.0	9.9
8- 611	5.2	591.8	738.0	8.2	8.1	8.1	8.0	634	618	603	589	782	766	751	737	10.7	10.3	10.0	9.9
10- 611	6.6	590.9	738.0	10.3	10.3	10.2	10.1	635	618	603	589	783	766	751	737	10.8	10.3	10.1	10.0
12- 611	7.9	589.8	738.0	12.3	12.3	12.2	12.1	635	618	603	589	783	767	751	737	10.8	10.3	10.1	10.0
14- 611	9.2	588.4	738.0	14.4	14.3	14.2	14.1	635	618	603	589	783	767	752	737	10.8	10.4	10.1	10.0
16- 611	10.5	586.9	738.0	16.4	16.2	16.1	16.0	635	618	603	589	784	767	752	738	10.9	10.4	10.2	10.1
20- 611	13.1	583.3	738.0	20.4	20.3	20.1	20.0	635	619	603	589	785	768	753	739	11.0	10.5	10.3	10.2
25- 611	16.5	577.7	738.0	25.4	25.3	25.1	25.0	635	619	603	588	787	770	754	740	11.2	10.7	10.4	10.3
30- 612	19.8	570.9	738.0	30.5	30.3	30.1	29.9	636	619	603	588	789	772	756	741	11.3	10.9	10.6	10.5
35- 612	23.2	563.0	738.0	35.6	35.3	35.1	34.9	636	619	603	588	792	774	758	743	11.6	11.1	10.8	10.7
40- 612	26.6	554.1	738.0	40.6	40.4	40.1	39.9	637	619	603	588	795	777	761	745	11.9	11.4	11.1	11.0
50- 612	33.7	533.2	738.0	50.8	50.4	50.1	49.8	638	620	603	588	802	784	767	751	12.6	12.1	11.8	11.7
60- 613	41.1	509.0	738.0	60.9	60.5	60.1	59.8	640	621	603	587	812	792	774	757	13.5	13.0	12.7	12.5
6- 672	3.9	655.0	799.5	6.2	6.1	6.1	6.1	698	680	663	647	845	827	811	795	11.5	10.9	10.6	10.4
8- 672	5.1	654.2	799.5	8.2	8.1	8.1	8.0	698	680	663	647	846	828	811	795	11.5	10.9	10.6	10.5
10- 672	6.5	653.1	799.5	10.4	10.3	10.2	10.2	698	680	663	647	846	828	811	795	11.5	11.0	10.6	10.5
12- 672	7.7	651.8	799.5	12.4	12.3	12.2	12.1	698	680	663	647	846	828	811	795	11.5	11.0	10.7	10.5
14- 672	9.0	650.3	799.5	14.4	14.3	14.2	14.1	698	680	663	647	847	829	812	796	11.6	11.0	10.7	10.5
16- 672	10.3	648.6	799.5	16.4	16.3	16.1	16.0	699	680	663	647	847	829	812	796	11.6	11.1	10.7	10.6
20- 672	12.8	644.4	799.5	20.4	20.3	20.1	20.0	699	680	663	647	849	830	813	797	11.7	11.2	10.9	10.7
25- 673	16.0	638.0	799.5	25.5	25.3	25.1	24.9	699	681	663	647	851	832	815	798	11.9	11.4	11.0	10.9
30- 673	19.3	630.2	799.5	30.5	30.3	30.1	29.9	700	681	663	647	853	834	816	800	12.1	11.6	11.2	11.1
40- 673	26.0	610.9	799.5	40.7	40.4	40.1	39.8	701	682	663	647	859	840	821	804	12.7	12.1	11.8	11.6
50- 674	32.9	587.1	799.5	50.8	50.4	50.1	49.8	702	682	664	646	867	847	828	810	13.5	12.9	12.5	12.3
60- 674	40.1	559.3	799.5	60.9	60.5	60.1	59.7	705	683	664	646	878	856	836	817	14.5	13.9	13.5	13.3
70- 675	47.7	528.5	799.5	71.1	70.6	70.1	69.7	707	685	664	645	890	867	845	825	15.9	15.1	14.7	14.4
80- 676	55.8	495.6	799.5	81.2	80.6	80.1	79.6	710	686	664	644	906	880	857	836	17.5	16.7	16.2	15.9
6- 743	3.8	727.4	871.2	6.2	6.1	6.1	6.1	772	752	733	715	919	899	880	863	12.3	11.7	11.3	11.1
8- 743	5.0	726.4	871.2	8.2	8.1	8.1	8.0	772	752	733	715	920	899	881	863	12.4	11.7	11.3	11.1
10- 743	6.3	725.2	871.2	10.4	10.3	10.2	10.2	772	752	733	716	920	900	881	863	12.4	11.7	11.3	11.1
12- 744	7.5	723.8	871.2	12.4	12.3	12.2	12.1	772	752	733	715	920	900	881	864	12.4	11.8	11.4	11.2
14- 744	8.7	722.0	871.2	14.4	14.3	14.2	14.1	773	752	733	715	921	901	882	864	12.5	11.8	11.4	11.2
16- 744	10.0	720.0	871.2	16.4	16.3	16.2	16.0	773	752	733	715	921	901	882	864	12.5	11.9	11.4	11.2
20- 744	12.5	715.3	871.2	20.4	20.3	20.1	20.0	773	753	733	715	923	902	883	865	12.7	12.0	11.6	11.4
25- 744	15.6	707.9	871.2	25.5	25.3	25.1	24.9	774	753	733	715	925	904	885	866	12.9	12.2	11.8	11.6
30- 744	18.8	698.9	871.2	30.6	30.3	30.1	29.9	774	753	734	715	927	906	887	868	13.1	12.4	12.0	11.8
35- 744	22.0	688.5	871.2	35.6	35.4	35.1	34.9	775	754	734	715	931	909	889	870	13.4	12.7	12.3	12.0
40- 745	25.3	676.7	871.2	40.7	40.4	40.1	39.8	776	754	734	715	934	912	892	873	13.7	13.0	12.6	12.4
50- 745	32.0	649.2	871.2	50.9	50.5	50.1	49.8	778	755	734	714	943	920	899	879	14.6	13.9	13.4	13.1
60- 746	39.1	617.3	871.2	61.0	60.5	60.1	59.7	780	756	734	714	954	930	907	886	15.8	15.0	14.4	14.2
70- 747	46.5	581.9	871.2	71.1	70.6	70.1	69.7	783	758	735	713	968	942	918	895	17.2	16.3	15.8	15.5
80- 748	54.5	543.9	871.2	81.2	80.7	80.1	79.6	786	760	735	712	985	957	930	906	19.0	18.1	17.4	17.1

POINT	LAB ANGLE	PO	EO	CM ANGLE A	CM ANGLE B	CM ANGLE C	CM ANGLE D	LAB K A	LAB K B	LAB K C	LAB K D	LAB K 2PI A	LAB K 2PI B	LAB K 2PI C	LAB K 2PI D	RMS DELTA K A	RMS DELTA K B	RMS DELTA K C	RMS DELTA K D
6- 824	3.6	809.5	953.2	6.2	6.1	6.1	6.1	856	834	813	793	1003	981	960	940	13.4	12.6	12.1	11.8
8- 824	4.8	808.4	953.2	8.2	8.1	8.1	8.0	857	834	813	793	1004	981	960	940	13.4	12.6	12.1	11.9
10- 824	6.1	807.0	953.2	10.4	10.3	10.3	10.2	857	834	813	793	1004	982	961	941	13.4	12.6	12.1	11.9
12- 824	7.3	805.3	953.2	12.4	12.3	12.2	12.1	857	834	813	793	1005	982	961	941	13.5	12.7	12.2	11.9
14- 825	8.5	803.3	953.2	14.4	14.3	14.2	14.1	857	834	813	793	1005	983	961	941	13.5	12.7	12.2	12.0
16- 826	9.7	801.0	953.2	16.4	16.3	16.2	16.0	857	834	813	793	1006	983	962	942	13.6	12.8	12.3	12.0
18- 826	10.9	798.4	953.2	18.4	18.3	18.1	18.0	857	835	813	793	1006	984	962	942	13.6	12.9	12.4	12.1
20- 825	12.1	795.5	953.2	20.5	20.3	20.1	20.0	858	835	813	793	1007	984	963	943	13.7	12.9	12.4	12.2
25- 826	15.1	786.9	953.2	25.5	25.3	25.1	24.9	858	835	813	793	1009	986	965	944	13.9	13.1	12.6	12.4
30- 825	18.2	776.6	953.2	30.6	30.3	30.1	29.9	859	835	813	793	1012	989	967	946	14.2	13.4	12.9	12.6
35- 828	21.4	764.6	953.2	35.7	35.4	35.1	34.9	860	836	814	793	1016	992	969	948	14.5	13.7	13.2	12.9
40- 826	24.6	751.0	953.2	40.7	40.4	40.1	39.8	861	836	814	793	1020	995	972	951	14.9	14.1	13.5	13.2
50- 827	31.1	719.4	953.2	50.9	50.5	50.1	49.7	863	838	814	792	1029	1004	979	957	15.9	15.0	14.4	14.1
60- 828	38.0	682.7	953.2	61.1	60.6	60.1	59.7	866	839	815	791	1042	1014	989	965	17.2	16.2	15.6	15.2
70- 829	45.3	641.8	953.2	71.2	70.6	70.1	69.6	870	841	815	791	1057	1027	1000	974	18.8	17.8	17.1	16.6
80- 831	53.1	598.1	953.2	81.3	80.7	80.1	79.6	874	844	815	789	1076	1043	1013	986	20.8	19.7	18.9	18.4
6- 916	3.5	901.3	1045.5	6.2	6.1	6.1	6.1	951	926	902	880	1098	1073	1049	1027	14.5	13.6	13.0	12.7
8- 916	4.7	900.0	1045.5	8.2	8.1	8.1	8.0	951	926	902	880	1098	1073	1049	1027	14.6	13.6	13.1	12.7
10- 915	6.9	898.4	1045.5	10.4	10.3	10.2	10.2	951	926	903	880	1099	1074	1050	1028	14.6	13.7	13.1	12.8
12- 915	7.1	896.4	1045.5	12.4	12.3	12.2	12.1	951	926	903	880	1099	1074	1050	1028	14.6	13.7	13.1	12.8
14- 915	8.2	894.1	1045.5	14.4	14.3	14.2	14.1	952	926	903	880	1100	1074	1051	1028	14.7	13.8	13.2	12.9
16- 916	9.4	891.6	1045.5	16.5	16.3	16.2	16.1	952	927	903	880	1101	1075	1051	1029	14.8	13.9	13.3	12.9
20- 916	11.7	885.1	1045.5	20.5	20.3	20.1	20.0	952	927	903	880	1102	1076	1052	1030	14.9	14.0	13.4	13.1
30- 916	17.7	863.5	1045.5	30.6	30.4	30.1	29.9	954	928	903	880	1107	1081	1056	1033	15.5	14.5	13.9	13.6
40- 917	23.8	834.0	1045.5	40.8	40.4	40.1	39.8	956	929	903	880	1115	1088	1062	1038	16.3	15.3	14.6	14.3
50- 918	30.2	797.5	1045.5	50.9	50.5	50.1	49.7	959	931	904	879	1126	1097	1070	1045	17.4	16.3	15.6	15.2
60- 920	36.9	755.2	1045.5	61.1	60.6	60.1	59.6	963	933	905	878	1140	1108	1080	1053	18.8	17.7	16.9	16.4
70- 921	44.0	708.3	1045.5	71.3	70.7	70.1	69.6	967	935	905	878	1157	1123	1092	1063	20.6	19.4	18.5	18.0
80- 923	51.6	657.9	1045.5	81.4	80.8	80.1	79.5	973	938	906	876	1177	1140	1107	1075	22.7	21.6	20.6	20.0
6-1016	3.4	1002.6	1148.0	6.2	6.2	6.1	6.1	1056	1028	1001	977	1202	1174	1148	1124	15.9	14.8	14.1	13.7
8-1016	4.5	1001.1	1148.0	8.2	8.2	8.1	8.0	1056	1028	1001	977	1203	1175	1148	1124	15.9	14.8	14.1	13.8
10-1016	5.8	999.3	1148.0	10.5	10.4	10.3	10.2	1056	1028	1002	977	1203	1175	1149	1124	15.9	14.9	14.2	13.8
12-1016	6.8	997.0	1148.0	12.4	12.3	12.2	12.1	1056	1028	1002	977	1204	1176	1149	1124	16.0	14.9	14.2	13.8
14-1016	8.0	994.4	1148.0	14.5	14.3	14.2	14.1	1056	1028	1002	977	1204	1176	1150	1125	16.1	15.0	14.3	13.9
16-1016	9.1	991.3	1148.0	16.5	16.3	16.2	16.0	1057	1028	1002	977	1205	1177	1150	1125	16.1	15.1	14.4	14.0
20-1016	11.3	984.0	1148.0	20.5	20.3	20.1	20.0	1057	1029	1002	977	1207	1178	1151	1126	16.3	15.2	14.5	14.1
25-1017	14.2	972.7	1148.0	25.6	25.3	25.1	24.9	1058	1029	1002	977	1209	1180	1153	1128	16.6	15.5	14.8	14.4
30-1017	17.1	959.1	1148.0	30.6	30.4	30.1	29.9	1059	1030	1002	976	1213	1183	1156	1130	16.9	15.8	15.1	14.7
35-1017	20.0	943.2	1148.0	35.7	35.4	35.1	34.8	1060	1030	1002	976	1217	1187	1158	1132	17.3	16.2	15.4	15.0
40-1018	23.0	925.3	1148.0	40.8	40.4	40.1	39.8	1062	1031	1003	976	1221	1190	1162	1135	17.8	16.7	15.9	15.4
45-1019	26.1	905.4	1158.2	45.9	45.5	45.1	44.7	1063	1032	1003	976	1227	1195	1166	1138	18.4	17.2	16.4	15.9
50-1019	29.2	883.6	1148.0	51.0	50.5	50.1	49.7	1065	1033	1003	976	1233	1200	1170	1142	19.0	17.8	17.0	16.5
55-1020	32.4	860.0	1148.0	56.1	55.6	55.1	54.7	1067	1034	1004	975	1240	1206	1175	1146	19.8	18.5	17.6	17.1
60-1021	35.7	835.0	1158.2	61.2	60.6	60.1	59.6	1070	1036	1004	975	1248	1213	1180	1150	20.7	19.3	18.4	17.9

POINT	LAB ANGLE	PO	EO	CM ANGLE				LAB K				LAB K 2PI				RMS DELTA K			
				A	B	C	D	A	B	C	D	A	B	C	D	A	B	C	D
65-1022	39.1	808.6	1148.0	66.3	65.7	65.1	64.6	1072	1037	1005	974	1257	1220	1187	1155	21.5	20.2	19.3	18.7
70-1023	42.7	781.0	1158.2	71.3	70.7	70.1	69.6	1075	1039	1005	974	1266	1229	1193	1161	22.7	21.3	20.3	19.6
75-1024	46.3	752.5	1158.2	76.4	75.8	75.1	74.5	1079	1041	1006	973	1277	1238	1201	1167	23.8	22.5	21.3	20.6
80-1026	50.1	723.3	1148.0	81.5	80.8	80.1	79.5	1082	1043	1006	973	1289	1248	1209	1174	24.4	23.7	22.6	21.8
86-1027	54.0	693.5	1158.2	86.6	85.8	85.1	84.5	1086	1045	1007	972	1303	1259	1219	1182	26.1	25.2	23.9	23.1
91-1028	58.2	663.4	1158.2	91.7	90.9	90.2	89.5	1090	1047	1007	971	1317	1271	1228	1190	27.3	26.8	25.5	24.5
6-1117	3.3	1104.9	1250.5	6.2	6.2	6.1	6.1	1162	1131	1102	1074	1308	1277	1248	1221	17.2	16.0	15.2	14.8
8-1117	4.4	1103.5	1250.5	8.2	8.2	8.1	8.0	1162	1131	1102	1075	1309	1278	1249	1221	17.2	16.1	15.3	14.8
10-1118	5.6	1101.1	1250.5	10.5	10.4	10.3	10.2	1162	1131	1102	1075	1309	1278	1249	1222	17.3	16.1	15.3	14.8
12-1118	6.6	1098.5	1250.5	12.5	12.3	12.2	12.1	1162	1131	1102	1074	1310	1279	1249	1222	17.4	16.2	15.3	14.9
14-1118	7.7	1095.4	1250.5	14.5	14.3	14.2	14.1	1162	1131	1102	1074	1310	1279	1250	1222	17.4	16.2	15.4	15.0
16-1117	8.8	1091.8	1250.5	16.5	16.3	16.2	16.0	1162	1131	1102	1074	1311	1279	1250	1222	17.5	16.3	15.5	15.1
20-1118	11.0	1083.6	1250.5	20.5	20.3	20.2	20.0	1163	1131	1102	1074	1313	1281	1251	1224	17.7	16.5	15.7	15.2
25-1118	13.8	1070.6	1250.5	25.6	25.4	25.1	24.9	1164	1132	1102	1074	1315	1283	1253	1225	18.0	16.8	15.9	15.5
30-1118	16.6	1054.9	1250.5	30.6	30.4	30.1	29.8	1165	1132	1102	1073	1318	1286	1255	1227	18.4	17.1	16.3	15.8
35-1118	19.4	1036.7	1250.5	35.7	35.4	35.1	34.8	1166	1133	1102	1073	1322	1289	1258	1229	18.8	17.6	16.7	16.2
40-1119	22.3	1016.2	1255.6	40.8	40.4	40.1	39.7	1167	1133	1102	1072	1327	1293	1261	1231	19.4	18.1	17.2	16.6
45-1119	25.3	993.5	1250.5	45.9	45.5	45.1	44.7	1169	1134	1102	1072	1333	1298	1265	1235	20.0	18.7	17.7	17.2
50-1120	28.3	968.7	1250.5	51.0	50.5	50.1	49.7	1171	1136	1102	1072	1339	1303	1270	1238	20.7	19.4	18.4	17.8
55-1121	31.5	942.1	1250.5	56.1	55.6	55.1	54.6	1173	1137	1103	1071	1347	1310	1275	1242	21.5	20.1	19.1	18.5
60-1122	34.7	913.9	1250.5	61.2	60.6	60.1	59.6	1176	1139	1104	1071	1355	1317	1281	1247	22.4	21.0	20.0	19.3
65-1124	38.0	884.1	1250.5	66.3	65.7	65.1	64.6	1179	1140	1104	1071	1365	1325	1287	1253	23.2	22.0	20.9	20.2
70-1125	41.4	853.0	1250.5	71.4	70.7	70.1	69.5	1183	1142	1105	1070	1376	1334	1295	1258	24.2	23.2	22.0	21.2
75-1126	45.0	820.7	1250.5	76.5	75.8	75.1	74.5	1187	1144	1105	1069	1388	1343	1303	1265	25.1	24.5	23.2	22.4
80-1128	48.7	787.7	1250.5	81.6	80.8	80.1	79.5	1191	1147	1106	1069	1401	1354	1312	1272	26.0	25.9	24.5	23.6
86-1130	52.6	754.1	1250.5	86.7	85.9	85.1	84.5	1196	1149	1107	1068	1416	1367	1322	1280	26.9	27.5	26.1	25.1
91-1131	56.6	720.1	1250.5	91.7	90.9	90.1	89.4	1201	1152	1108	1067	1432	1380	1332	1289	27.9	29.2	27.8	26.7
6-1221	3.2	1208.9	1353.0	6.3	6.2	6.1	6.1	1269	1235	1204	1174	1416	1382	1350	1320	18.6	17.3	16.4	15.9
8-1221	4.3	1206.9	1353.0	8.3	8.2	8.1	8.0	1269	1235	1204	1174	1416	1382	1350	1320	18.6	17.3	16.4	15.9
10-1221	5.4	1204.4	1353.0	10.5	10.4	10.3	10.2	1270	1236	1204	1174	1417	1383	1351	1321	18.7	17.4	16.5	15.9
12-1221	6.5	1201.4	1353.0	12.5	12.4	12.3	12.2	1270	1236	1204	1174	1417	1383	1351	1321	18.7	17.4	16.5	16.0
14-1221	7.5	1197.8	1353.0	14.5	14.4	14.2	14.1	1270	1236	1203	1173	1417	1383	1351	1321	18.8	17.5	16.6	16.1
16-1221	8.5	1193.7	1353.0	16.5	16.4	16.2	16.1	1270	1235	1203	1173	1418	1384	1352	1321	18.9	17.6	16.7	16.2
20-1220	10.7	1184.0	1353.0	20.6	20.4	20.2	20.0	1270	1235	1203	1173	1419	1385	1352	1322	19.1	17.8	16.9	16.3
25-1220	13.4	1169.1	1353.0	25.6	25.4	25.1	24.9	1270	1235	1203	1172	1422	1387	1354	1323	19.5	18.1	17.2	16.6
30-1220	16.1	1151.4	1353.0	30.7	30.4	30.1	29.8	1271	1236	1202	1171	1425	1389	1356	1325	19.9	18.5	17.5	17.0
35-1220	18.8	1130.9	1353.0	35.8	35.4	35.1	34.8	1272	1236	1202	1171	1429	1393	1359	1327	20.4	19.0	18.0	17.4
40-1221	21.7	1107.8	1353.0	40.9	40.5	40.1	39.7	1274	1237	1202	1170	1434	1397	1362	1329	20.9	19.5	18.5	17.9
50-1222	27.5	1054.1	1353.0	51.0	50.5	50.1	49.6	1277	1238	1202	1168	1446	1407	1370	1335	22.3	20.9	19.8	19.1
60-1224	33.7	992.2	1353.0	61.2	60.6	60.1	59.5	1283	1241	1203	1167	1463	1420	1381	1344	24.0	22.8	21.5	20.8
70-1226	40.3	924.1	1353.0	71.4	70.7	70.1	69.5	1290	1245	1204	1166	1484	1438	1395	1355	25.7	25.1	23.8	22.9
80-1230	47.4	851.3	1353.0	81.6	80.8	80.1	79.4	1300	1251	1206	1164	1512	1460	1413	1370	27.4	28.1	26.6	25.5
91-1234	56.2	775.8	1353.0	91.8	91.0	90.1	89.4	1311	1257	1208	1162	1546	1488	1435	1387	30.1	31.5	30.2	28.9

TABLE 17

Sample Yields

For each point the results of a typical run are given and a corresponding empty target run (denoted by B after the run number). Points lacking an empty target run were corrected by averaging two runs adjacent in angle at the same energy. W is in units of 10^{15} MeV.

POINT	W	EO	RUN	COUNTS A	B	C	D	KAPPA A	B	C	D
6- 611	5.446	738.0	917	912	961	833	858	8.90	8.64	8.30	7.88
	3.262	738.0	903B	42	44	47	54				
8- 611	5.449	738.0	918	840	864	868	761	8.89	8.63	8.28	7.87
	2.174	738.0	904B	19	17	18	24				
10- 611	4.384	738.0	912	1717	1655	1572	1550	23.49	22.81	21.89	20.80
	1.088	738.0	905B	25	29	16	31				
12- 611	2.215	738.0	927	789	762	735	727	23.44	22.75	21.84	20.75
	1.088	738.0	906B	18	20	20	21				
14- 611	4.384	738.0	913	1480	1379	1368	1294	23.37	22.68	21.77	20.69
16- 611	2.753	738.0	928	837	880	790	798	23.29	22.61	21.70	20.62
	1.088	738.0	907B	14	16	15	19				
20- 611	3.296	738.0	914	796	823	795	772	21.19	20.57	19.75	18.77
	1.088	738.0	908B	13	18	17	11				
25- 611	2.188	738.0	929	552	521	494	486	20.87	20.26	19.45	18.48
30- 612	3.266	738.0	916	772	713	709	696	20.54	19.95	19.15	18.20
	1.089	738.0	901B	10	11	6	8				
35- 612	2.193	738.0	925	502	489	505	418	20.17	19.59	18.80	17.87
40- 612	3.289	738.0	923	762	731	703	644	19.75	19.18	18.41	17.51
	1.076	738.0	900B	13	12	16	11				
50- 612	2.187	738.0	930	461	464	387	389	18.76	18.23	17.51	16.65
	3.279	738.0	909B	34	24	35	22				
60- 613	4.353	738.0	911	843	808	757	703	17.62	17.13	16.45	15.65
	2.202	738.0	910B	15	20	15	11				
6- 672	4.679	799.5	835	725	802	729	748	8.67	8.43	8.10	7.70
	2.324	799.5	890B	35	27	32	38				
8- 672	4.684	799.5	836	645	660	730	627	8.65	8.42	8.09	7.69
	2.324	799.5	891B	21	34	24	22				
10- 672	2.349	799.5	831	842	912	820	785	22.87	22.24	21.37	20.31
	1.163	799.5	892B	27	25	30	26				
12- 672	2.339	799.5	838	814	752	732	748	22.81	22.19	21.32	20.26
	1.163	799.5	893B	16	19	26	24				
14- 672	2.349	799.5	832	760	735	710	719	22.74	22.12	21.25	20.20
16- 672	2.334	799.5	839	691	659	675	668	22.66	22.04	21.18	20.13
	1.163	799.5	894B	23	21	15	13				
20- 672	2.338	799.5	840	557	624	559	537	21.01	20.43	19.64	18.66
	1.161	799.5	895B	15	9	20	11				
25- 673	2.335	799.5	834	589	540	515	424	20.68	20.12	19.33	18.38
30- 673	3.503	799.5	829	824	815	746	723	20.35	19.80	19.03	18.10
	1.163	799.5	889B	12	13	7	10				
40- 673	2.257	799.5	790	529	536	482	436	19.55	19.03	18.29	17.40
	1.152	799.5	888B	11	15	10	10				
50- 674	2.349	799.5	833	496	517	462	476	18.55	18.07	17.38	16.54
	1.151	799.5	887B	9	10	10	9				
60- 674	2.349	799.5	830	446	451	444	422	17.39	16.96	16.32	15.54
	1.161	799.5	896B	9	9	8	12				
70- 675	2.342	799.5	837	394	418	350	343	16.10	15.73	15.15	14.43
80- 676	4.660	799.5	841	620	623	566	521	14.72	14.41	13.90	13.24
	2.351	799.5	897B	9	10	14	11				

POINT	W	EO	RUN	COUNTS A	B	C	D	KAPPA A	B	C	D
6- 743	7.208	871.2	779	934	921	955	1039	8.49	8.28	7.96	7.56
	4.910	871.2	8228	38	77	68	69				
8- 743	7.183	871.2	780	884	926	891	867	8.48	8.26	7.95	7.55
	4.910	871.2	8238	45	43	57	52				
10- 743	4.797	871.2	772	1355	1408	1479	1519	22.40	21.84	21.00	19.96
	1.207	871.2	8128	20	23	32	27				
12- 744	4.841	871.2	775	1320	1336	1344	1420	22.34	21.78	20.95	19.91
	2.422	871.2	8198	38	52	58	40				
14- 744	4.800	871.2	773	1131	1262	1270	1275	22.27	21.72	20.88	19.85
16- 744	4.770	871.2	777	1096	1112	1157	1228	22.19	21.64	20.81	19.78
	2.458	871.2	8208	33	33	32	25				
20- 744	4.760	871.2	784	933	973	1009	1039	20.76	20.25	19.47	18.51
	4.825	871.2	8168	44	49	53	55				
25- 744	2.380	871.2	783	434	481	458	466	20.43	19.92	19.17	18.22
30- 744	2.388	871.2	769	408	432	494	497	20.10	19.61	18.87	17.94
	2.453	871.2	8258	18	17	17	17				
35- 744	2.373	871.2	782	429	424	442	463	19.71	19.24	18.52	17.61
40- 745	4.785	871.2	768	837	936	956	1012	19.28	18.82	18.12	17.24
	2.422	871.2	8188	18	25	23	32				
50- 745	2.379	871.2	778	373	439	453	485	18.27	17.86	17.20	16.37
60- 746	2.403	871.2	771	318	393	401	453	17.09	16.74	16.13	15.37
	2.458	871.2	8218	10	24	17	21				
70- 747	2.424	871.2	781	268	346	401	390	15.78	15.50	14.95	14.26
80- 748	7.139	871.2	785	623	793	940	952	14.38	14.17	13.69	13.07
	4.907	871.2	8248	25	19	24	28				
6- 824	10.031	953.2	705	1219	1288	1247	1230	8.43	8.24	7.91	7.52
	7.490	953.2	7168	69	83	75	98				
8- 824	10.014	953.2	706	1110	1197	1137	1054	8.42	8.23	7.90	7.51
	7.490	953.2	7178	58	73	77	75				
10- 824	4.925	953.2	701	1358	1329	1403	1316	22.24	21.73	20.87	19.83
	5.010	953.2	7198	81	92	111	115				
12- 824	4.983	953.2	710	1203	1247	1261	1185	22.18	21.67	20.82	19.78
14- 825	5.010	953.2	702	1114	1151	1152	1114	22.11	21.61	20.76	19.72
	5.010	953.2	7208	53	69	55	91				
16- 825	5.065	953.2	713	1024	1029	1047	1040	22.02	21.53	20.68	19.66
18- 825	4.980	953.2	711	962	928	1021	999	21.93	21.44	20.60	19.58
	5.005	953.2	7228	52	54	58	63				
20- 825	3.714	953.2	708	682	649	641	671	21.83	21.34	20.51	19.49
	2.415	953.2	6648	21	31	25	21				
25- 825	3.340	953.2	714	565	538	577	556	20.17	19.70	18.97	18.03
30- 825	4.715	953.2	693	695	739	749	748	19.83	19.38	18.67	17.75
	4.226	953.2	7238	23	37	28	41				
35- 826	4.984	953.2	712	768	733	756	706	19.41	19.01	18.31	17.42
40- 826	4.721	953.2	692	617	654	635	689	18.97	18.59	17.91	17.04
	2.504	953.2	7158	18	12	14	17				
50- 827	3.527	953.2	694	385	370	411	427	17.94	17.61	16.99	16.17
60- 828	5.014	953.2	707	434	428	452	512	16.74	16.48	15.91	15.16
	3.699	953.2	6658	14	14	8	21				
70- 829	4.981	953.2	704	271	300	347	450	15.41	15.22	14.72	14.05
80- 831	4.978	953.2	709	201	268	303	384	13.96	13.88	13.45	12.85
	2.520	953.2	7218	6	7	9	6				

PCINT	W	EO	RUN	COUNTS A	B	C	D	KAPPA A	B	C	D
6- 915	9.785	1045.5	682	962	1062	1066	1118	8.24	8.08	7.78	7.38
	6.612	1045.5	6598	65	54	61	75				
8- 915	4.263	1045.5	673	323	391	403	401	8.23	8.07	7.77	7.37
	7.636	1045.5	7308	49	60	50	72				
10- 915	5.017	1045.5	668	967	1108	1154	1126	21.73	21.32	20.52	19.47
	5.214	1045.5	7268	91	77	88	95				
12- 915	4.911	1045.5	677	966	1074	1036	1073	21.67	21.26	20.46	19.42
14- 915	4.911	1045.5	678	865	926	1014	970	21.60	21.19	20.40	19.35
	5.214	1045.5	7278	50	47	84	66				
16- 916	4.911	1045.5	679	898	890	900	916	21.51	21.11	20.32	19.29
	2.548	1045.5	7328	27	20	34	27				
20- 916	4.904	1045.5	670	829	854	807	774	20.26	19.89	19.15	18.17
	2.548	1045.5	7338	14	35	22	13				
30- 916	4.970	1045.5	667	815	820	800	717	19.56	19.22	18.51	17.58
	7.264	1045.5	6568	55	43	47	72				
40- 917	4.983	1045.5	666	759	760	683	632	18.69	18.39	17.73	16.85
	6.609	1045.5	6558	54	40	40	31				
50- 918	4.909	1045.5	671	703	629	595	512	17.61	17.37	16.76	15.95
60- 920	4.898	1045.5	669	448	440	390	385	16.35	16.20	15.67	14.94
	2.551	1045.5	7348	12	14	10	10				
70- 921	4.921	1045.5	675	305	285	264	241	14.98	14.92	14.47	13.81
80- 923	4.916	1045.5	676	159	193	199	178	13.47	13.56	13.19	12.61
	2.545	1045.5	7318	8	3	12	7				
6-1016	5.059	1148.0	457	326	340	427	446	8.16	8.04	7.75	7.34
	4.926	1148.0	4128	37	41	50	60				
8-1016	7.249	1148.0	580	434	492	497	558	8.08	7.96	7.67	7.27
	6.992	1148.0	6218	45	43	55	53				
10-1016	4.969	1148.0	272	735	780	830	889	21.51	21.20	20.43	19.37
	4.916	1148.0	4098	65	65	78	101				
12-1016	7.314	1148.0	570	979	1130	1164	1269	21.27	20.95	20.19	19.15
	7.150	1148.0	6258	86	80	103	88				
14-1016	7.213	1148.0	588	1032	1161	1147	1200	21.19	20.88	20.13	19.09
	6.986	1148.0	6178	67	71	78	96				
16-1016	7.314	1148.0	571	1041	1123	1156	1191	20.20	19.91	19.19	18.20
	7.150	1148.0	6268	64	64	73	89				
20-1016	4.977	1148.0	271	726	715	756	704	20.00	19.72	19.01	18.03
	4.906	1148.0	4148	40	40	50	48				
25-1017	7.314	1148.0	572	1156	1305	1226	1182	19.70	19.43	18.74	17.78
	7.251	1148.0	6328	43	53	49	61				
30-1017	7.242	1148.0	563	1131	1312	1258	1184	19.28	19.03	18.36	17.43
	6.979	1148.0	6198	48	67	57	65				
35-1017	7.216	1148.0	587	1184	1385	1294	1189	18.86	18.64	17.99	17.08
	7.148	1148.0	6288	29	58	47	49				
40-1018	7.225	1148.0	602	1175	1240	1241	1250	18.38	18.19	17.56	16.69
	6.996	1148.0	6188	43	45	37	53				
45-1019	7.251	1148.0	581	1085	1267	1244	1145	17.85	17.69	17.09	16.25
	7.155	1148.0	6278	36	39	52	48				
50-1019	4.987	1148.0	281	636	671	727	699	17.27	17.15	16.59	15.78
55-1020	7.320	1148.0	569	755	911	1024	878	16.64	16.56	16.04	15.27
	7.262	1148.0	6338	25	18	32	38				

POINT	W	EO	RUN	COUNTS A	COUNTS B	COUNTS C	COUNTS D	KAPPA A	KAPPA B	KAPPA C	KAPPA D
60-1021	5.047	1158.2	277	480	503	503	497	16.03	15.89	15.37	14.62
	4.929	1148.0	4108	14	29	22	15				
65-1022	7.309	1148.0	573	488	632	633	593	15.26	15.30	14.83	14.15
70-1023	7.304	1148.0	575	396	508	512	493	14.51	14.61	14.22	13.57
	6.952	1148.0	6148	16	21	22	17				
75-1024	7.256	1158.2	583	302	365	399	351	13.84	13.90	13.50	12.89
80-1026	7.508	1158.2	567	228	279	306	273	13.05	13.20	12.85	12.28
	6.975	1148.0	6158	9	8	12	13				
86-1027	7.256	1158.2	584	180	196	226	237	12.22	12.50	12.19	11.67
91-1028	14.488	1158.2	598	252	342	341	351	11.34	11.79	11.53	11.04
	8.400	1148.0	6238	10	11	11	13				
6-1117	7.397	1250.5	530	344	385	427	423	7.97	7.89	7.62	7.22
	14.442	1250.5	6398	71	84	113	126				
8-1117	14.296	1250.5	517	601	654	650	752	7.95	7.88	7.60	7.20
	14.442	1250.5	6408	58	75	100	98				
10-1118	7.370	1250.5	525	677	824	905	930	21.00	20.80	20.08	19.03
	7.134	1250.5	6368	66	90	89	106				
12-1118	5.228	1250.5	397	466	536	596	648	21.03	20.84	20.12	19.06
	5.190	1250.5	4478	37	52	64	61				
14-1118	5.065	1250.5	437	516	602	609	642	20.95	20.76	20.05	19.00
	5.479	1250.5	11148	32	44	56	54				
16-1117	7.370	1250.5	535	699	817	931	905	20.77	20.58	19.87	18.83
	7.082	1250.5	6508	45	49	66	67				
20-1118	7.286	1250.5	557	736	798	883	931	19.76	19.60	18.93	17.94
	7.082	1250.5	6518	40	52	54	56				
25-1118	7.286	1250.5	558	757	813	960	1006	19.45	19.30	18.65	17.68
	7.082	1250.5	6528	37	55	45	57				
30-1118	5.716	1250.5	518	553	662	701	827	19.02	18.89	18.26	17.32
	7.191	1250.5	6388	35	37	48	46				
35-1118	7.141	1250.5	519	629	715	856	1033	18.58	18.48	17.87	16.96
	10.181	1250.5	6458	43	55	46	56				
40-1119	7.037	1250.5	511	681	753	888	1057	18.09	18.01	17.43	16.55
	8.127	1250.5	6378	32	37	45	44				
45-1119	8.890	1250.5	551	722	804	993	1234	17.54	17.50	16.95	16.10
	9.636	1250.5	6498	29	36	59	47				
50-1120	7.430	1250.5	536	464	622	778	879	16.94	16.95	16.43	15.62
	7.085	1250.5	6448	18	26	26	27				
55-1121	7.421	1250.5	524	377	517	630	804	16.29	16.35	15.87	15.10
	7.101	1250.5	6488	12	19	27	31				
60-1122	1.907	1250.5	513	77	103	138	160	15.58	15.72	15.28	14.55
	7.110	1250.5	6348	15	15	17	23				
65-1124	7.336	1250.5	553	203	312	426	507	14.82	15.06	14.66	13.98
	7.108	1250.5	6168	10	12	16	20				
70-1125	7.150	1250.5	515	158	228	317	406	14.00	14.38	14.02	13.38
	7.107	1250.5	6358	6	9	15	18				
75-1126	7.326	1250.5	554	116	146	223	286	13.10	13.67	13.36	12.76
	7.179	1250.5	6178	6	10	11	16				
80-1128	5.289	1250.5	430	81	103	147	193	12.14	12.93	12.68	12.14
	5.213	1250.5	4528	5	5	12	12				
86-1130	7.316	1250.5	555	76	109	148	181	11.07	12.20	12.01	11.52
91-1131	14.618	1250.5	556	99	180	222	290	9.98	11.46	11.33	10.89
	7.260	1250.5	6428	4	3	6	5				

PCINT	W	EO	RUN	COUNTS A	COUNTS B	COUNTS C	COUNTS D	KAPPA A	KAPPA B	KAPPA C	KAPPA D
6-1221	8.752	1353.0	869	338	366	363	425	7.80	7.79	7.54	7.14
	7.932	1353.0	879B	32	44	40	60				
8-1221	8.763	1353.0	871	235	303	330	372	7.79	7.77	7.52	7.12
	7.932	1353.0	880B	26	34	38	40				
10-1221	4.423	1353.0	872	309	370	425	437	20.55	20.52	19.86	18.82
	3.966	1353.0	881B	32	26	36	41				
12-1221	2.032	1353.0	860	146	175	187	195	20.49	20.46	19.80	18.76
	3.966	1353.0	882B	24	43	32	41				
14-1221	4.447	1353.0	846	340	387	392	370	20.41	20.38	19.73	18.69
16-1221	4.351	1353.0	873	313	375	344	404	20.38	20.35	19.70	18.67
	4.309	1353.0	883B	26	30	28	44				
20-1220	4.499	1353.0	847	382	374	378	362	19.52	19.50	18.88	17.90
	5.386	1353.0	884B	20	28	32	30				
25-1220	4.041	1353.0	862	377	376	364	405	19.20	19.20	18.59	17.63
30-1220	2.244	1353.0	851	173	180	225	215	18.76	18.77	18.19	17.25
	1.983	1353.0	878B	9	10	10	13				
35-1220	2.167	1353.0	858	185	168	192	169	18.31	18.35	17.79	16.88
40-1221	8.866	1353.0	843	607	621	619	733	17.80	17.87	17.34	16.46
	6.011	1353.0	877B	19	23	19	17				
50-1222	4.320	1353.0	868	187	197	240	283	16.60	16.78	16.30	15.50
	1.959	1353.0	876B	10	7	12	7				
60-1223	4.551	1353.0	848	114	144	149	189	15.17	15.52	15.13	14.41
70-1226	4.549	1353.0	849	65	70	108	99	13.42	14.15	13.84	13.22
	5.386	1353.0	885B	5	5	7	8				
80-1230	4.440	1353.0	850	34	37	56	67	11.32	12.68	12.49	11.96
91-1234	16.392	1353.0	863	83	107	139	140	8.93	11.13	11.10	10.68
	7.447	1353.0	886B	3	5	5	8				

TABLE 18

Average Cross Sections

The cross sections listed are averages over D + 1 runs. Units are microbarns/steradian for cross sections, and MeV for K.

CM ANGLE	LAB K	CROSS SECTION	CHI SQ	D	CM ANGLE	LAB K	CROSS SECTION	CHI SQ	D	CM ANGLE	LAB K	CROSS SECTION	CHI SQ	D	CM ANGLE	LAB K	CROSS SECTION	CHI SQ	D
6.2	634	17.35+-0.70	0.	0	6.1	618	18.84+-0.74	0.	0	6.1	603	16.69+-0.71	0.	0	6.0	589	17.88+-0.76	0.	0
8.2	634	16.35+-0.66	0.	0	8.1	618	17.46+-0.69	0.	0	8.1	603	18.22+-0.72	0.	0	8.0	589	16.33+-0.71	0.	0
10.3	635	15.69+-0.48	0.	0	10.3	618	15.38+-0.48	0.	0	10.2	603	15.71+-0.48	0.	0	10.1	589	15.63+-0.51	0.	0
12.3	635	14.49+-0.59	0.	0	12.3	618	14.31+-0.60	0.	0	12.2	603	14.35+-0.61	0.	0	12.1	589	14.89+-0.64	0.	0
14.3	635	13.82+-0.44	0.	0	14.2	618	13.14+-0.43	0.	0	14.2	603	13.59+-0.45	0.	0	14.1	589	13.38+-0.45	0.	0
16.4	635	12.50+-0.50	0.	0	16.2	618	13.48+-0.53	0.	0	16.1	603	12.58+-0.52	0.	0	16.0	589	13.21+-0.55	0.	0
20.4	635	10.83+-0.44	0.	0	20.3	619	11.33+-0.47	0.	0	20.1	603	11.42+-0.48	0.	0	20.0	589	11.94+-0.49	0.	0
25.4	635	11.51+-0.55	0.	0	25.3	619	11.09+-0.55	0.	0	25.1	603	11.11+-0.56	0.	0	24.9	588	11.39+-0.58	0.	0
30.5	636	10.98+-0.45	0.	0	30.3	619	10.43+-0.45	0.	0	30.1	603	11.09+-0.46	0.	0	29.9	588	11.15+-0.48	0.	0
35.6	636	10.75+-0.54	0.	0	35.3	619	10.84+-0.55	0.	0	35.1	603	11.75+-0.58	0.	0	34.9	588	10.01+-0.56	0.	0
40.6	637	10.75+-0.30	1.4	2	40.3	619	10.97+-0.30	0.	2	40.1	603	10.58+-0.31	0.7	2	39.8	588	10.59+-0.31	0.5	2
50.8	638	10.68+-0.56	0.	0	50.4	620	11.24+-0.57	0.	0	50.1	603	9.50+-0.55	0.	0	49.8	588	10.28+-0.57	0.	0
60.9	640	10.60+-0.42	0.	0	60.5	621	10.30+-0.42	0.	0	60.1	603	10.15+-0.42	0.	0	59.7	587	9.99+-0.42	0.	0
6.2	698	16.54+-0.49	0.6	1	6.1	680	18.43+-0.53	0.7	1	6.1	663	18.18+-0.54	1.3	1	6.1	647	18.88+-0.57	0.2	1
8.2	698	16.28+-0.48	8.5	1	8.1	680	15.82+-0.49	2.4	1	8.1	663	17.87+-0.52	0.	1	8.0	647	16.17+-0.51	0.	1
10.4	698	15.04+-0.38	0.7	1	10.3	680	16.45+-0.40	0.	1	10.2	663	15.55+-0.40	0.7	1	10.2	647	15.86+-0.41	1.0	1
12.4	698	14.08+-0.36	1.5	1	12.3	680	13.97+-0.36	0.2	1	12.2	663	14.51+-0.38	3.6	1	12.1	647	14.81+-0.39	0.	1
14.4	698	13.29+-0.37	0.2	1	14.3	680	13.59+-0.38	0.3	1	14.2	663	13.71+-0.39	0.5	1	14.1	647	14.39+-0.40	0.	1
16.4	699	12.70+-0.38	1.7	1	16.3	680	12.31+-0.38	0.7	1	16.1	663	12.95+-0.39	0.1	1	16.0	647	13.49+-0.41	0.1	1
20.4	699	11.28+-0.32	1.8	1	20.3	680	12.29+-0.34	0.8	1	20.1	663	11.69+-0.34	0.8	1	20.0	647	11.96+-0.35	0.1	1
25.5	699	11.04+-0.31	2.1	2	25.3	681	11.26+-0.32	0.6	2	25.1	663	11.03+-0.33	0.7	2	24.9	647	10.76+-0.33	13.5	2
30.5	700	11.23+-0.32	0.4	1	30.3	681	11.23+-0.33	0.	1	30.1	663	10.92+-0.32	0.	1	29.9	647	11.17+-0.33	0.6	1
40.7	701	11.67+-0.23	2.3	4	40.4	682	11.77+-0.23	3.6	4	40.1	663	11.49+-0.23	2.2	4	39.8	647	11.18+-0.23	2.3	4
50.8	702	11.83+-0.34	4.2	1	50.4	682	12.18+-0.35	1.2	1	50.1	664	11.60+-0.35	3.2	1	49.8	646	11.71+-0.36	0.	1
60.9	705	11.41+-0.35	4.8	1	60.5	683	10.97+-0.34	0.1	1	60.1	664	11.33+-0.35	0.1	1	59.7	646	10.96+-0.36	0.	1
71.1	707	10.25+-0.31	0.1	2	70.6	685	10.71+-0.32	1.4	2	70.1	664	10.12+-0.31	3.7	2	69.7	645	9.90+-0.32	0.5	2
81.2	710	9.08+-0.27	1.1	1	80.6	686	8.98+-0.27	0.	1	80.1	664	8.46+-0.27	0.3	1	79.6	644	8.47+-0.27	1.8	1
6.2	772	14.34+-0.56	0.	0	6.1	752	13.53+-0.58	0.	0	6.1	733	14.90+-0.61	0.	0	6.0	715	17.19+-0.67	0.	0
8.2	772	13.43+-0.54	0.	0	8.1	752	14.53+-0.57	0.	0	8.1	733	14.14+-0.59	0.	0	8.0	715	14.57+-0.61	0.	0
10.4	772	11.67+-0.40	0.	0	10.3	752	12.49+-0.41	0.	0	10.2	733	13.44+-0.45	0.	0	10.2	716	14.60+-0.47	0.	0
12.4	772	11.50+-0.39	0.	0	12.3	752	11.68+-0.40	0.	0	12.2	733	12.11+-0.42	0.	0	12.1	715	13.90+-0.45	0.	0
14.4	773	9.92+-0.36	0.	0	14.3	752	11.30+-0.39	0.	0	14.2	733	11.78+-0.41	0.	0	14.1	715	12.71+-0.43	0.	0
16.4	773	9.59+-0.31	0.8	1	16.3	752	10.07+-0.32	0.2	1	16.2	733	11.14+-0.34	0.4	1	16.0	715	12.80+-0.37	2.4	1
20.4	773	9.00+-0.34	0.	0	20.3	753	9.59+-0.36	0.	0	20.1	733	10.32+-0.38	0.	0	20.0	715	11.17+-0.41	0.	0
25.5	774	8.51+-0.46	0.	0	25.3	753	9.69+-0.49	0.	0	25.1	733	9.54+-0.50	0.	0	24.9	715	10.20+-0.53	0.	0
30.6	774	8.38+-0.39	1.3	1	30.3	753	9.06+-0.41	0.7	1	30.1	734	10.13+-0.45	2.9	1	29.9	715	11.25+-0.48	0.	1
35.6	775	8.79+-0.47	0.	0	35.4	754	8.83+-0.48	0.	0	35.1	734	9.61+-0.51	0.	0	34.9	715	10.50+-0.55	0.	0
40.7	776	8.58+-0.27	0.6	2	40.4	754	9.45+-0.29	2.6	2	40.1	734	10.48+-0.31	0.2	2	39.8	715	11.71+-0.34	1.5	2
50.8	778	8.26+-0.47	0.	0	50.5	755	9.91+-0.52	0.	0	50.1	734	10.58+-0.55	0.	0	49.8	714	11.81+-0.61	0.	0
61.0	780	7.50+-0.45	0.	0	60.5	756	9.34+-0.52	0.	0	60.1	734	9.91+-0.55	0.	0	59.7	714	11.74+-0.61	0.	0
71.1	783	6.70+-0.45	0.	0	70.6	758	8.94+-0.52	0.	0	70.1	735	10.68+-0.58	0.	0	69.7	713	10.84+-0.60	0.	0
81.2	786	5.77+-0.23	0.1	1	80.7	760	7.53+-0.26	0.	1	80.1	735	9.11+-0.29	0.6	1	79.6	712	9.75+-0.31	0.	1

CM ANGLE	LAB K	CROSS SECTION	CHI SQ	D	CM ANGLE	LAB K	CROSS SECTION	CHI SQ	D	CM ANGLE	LAB K	CROSS SECTION	CHI SQ	D	CM ANGLE	LAB K	CROSS SECTION	CHI SQ	D
6.2	856	13.30+-0.47	0.	0	6.1	834	14.14+-0.50	0.	0	6.1	813	14.41+-0.51	0.	0	6.1	793	14.51+-0.54	0.	0
8.2	857	12.24+-0.45	0.	0	8.1	834	13.34+-0.48	0.	0	8.1	813	13.06+-0.49	0.	0	8.0	793	12.68+-0.49	0.	0
10.4	857	11.16+-0.26	3.2	1	10.3	834	11.23+-0.27	1.3	1	10.2	813	12.01+-0.29	3.8	1	10.2	793	12.24+-0.30	0.1	1
12.4	857	10.28+-0.36	0.	0	12.3	834	10.80+-0.37	0.	0	12.2	813	11.36+-0.39	0.	0	12.1	793	10.98+-0.40	0.	0
14.4	857	9.64+-0.24	0.1	1	14.3	834	9.87+-0.25	0.2	1	14.2	813	10.67+-0.26	0.2	1	14.1	793	10.17+-0.27	0.4	1
16.4	857	8.70+-0.32	0.	0	16.3	834	8.86+-0.33	0.	0	16.2	813	9.45+-0.35	0.	0	16.0	793	9.66+-0.37	0.	0
18.4	857	8.33+-0.32	0.	0	18.3	835	8.19+-0.32	0.	0	18.1	813	9.39+-0.35	0.	0	18.0	793	9.60+-0.36	0.	0
20.5	858	8.39+-0.24	2.5	1	20.3	835	7.88+-0.24	1.6	1	20.1	813	8.36+-0.25	3.4	1	20.0	793	8.85+-0.26	0.	1
25.5	858	8.06+-0.38	0.	0	25.3	835	7.65+-0.38	0.	0	25.1	813	8.68+-0.41	0.	0	24.9	793	8.71+-0.42	0.	0
30.6	859	7.39+-0.22	1.3	1	30.3	835	7.71+-0.22	0.	1	30.1	813	8.15+-0.24	0.	1	29.9	793	8.28+-0.25	0.2	1
35.7	860	7.62+-0.31	0.	0	35.4	836	7.35+-0.31	0.	0	35.1	814	7.94+-0.33	0.	0	34.9	793	7.64+-0.33	0.	0
40.7	861	6.86+-0.11	4.3	6	40.4	836	7.02+-0.12	7.2	6	40.1	814	7.43+-0.12	13.1	6	39.8	793	7.89+-0.13	4.1	6
50.9	863	5.85+-0.18	5.5	2	50.5	838	5.86+-0.18	1.1	2	50.1	814	6.32+-0.19	0.8	2	49.7	792	7.14+-0.21	0.1	2
61.0	866	4.99+-0.26	0.	0	60.6	839	4.91+-0.27	0.	0	60.1	815	5.45+-0.28	0.	0	59.7	791	6.38+-0.32	0.	0
71.2	870	3.46+-0.16	0.1	1	70.6	841	3.85+-0.17	0.9	1	70.1	815	4.72+-0.20	2.3	1	69.6	791	5.85+-0.22	1.9	1
81.3	874	2.72+-0.21	0.	0	80.7	844	3.68+-0.25	0.	0	80.1	815	4.26+-0.27	0.	0	79.6	789	5.81+-0.32	0.	0
6.2	951	10.76+-0.35	0.3	1	6.1	926	12.37+-0.37	0.	1	6.1	902	12.28+-0.38	2.9	1	6.0	880	13.87+-0.42	0.4	1
8.2	951	8.83+-0.38	1.0	1	8.1	926	10.79+-0.43	0.8	1	8.1	902	11.52+-0.45	0.2	1	8.0	880	11.71+-0.48	0.2	1
10.4	951	8.19+-0.32	0.	0	10.3	926	9.67+-0.35	0.	0	10.2	903	10.37+-0.38	0.	0	10.2	880	10.64+-0.39	0.	0
12.4	951	8.67+-0.23	1.0	1	12.3	926	9.61+-0.25	0.2	1	12.2	903	9.58+-0.26	0.1	1	12.1	880	10.54+-0.28	0.1	1
14.4	952	7.71+-0.31	0.	0	14.3	926	8.47+-0.32	0.	0	14.2	903	9.33+-0.36	0.	0	14.1	880	9.55+-0.37	0.	0
16.4	952	7.90+-0.22	0.2	1	16.3	927	8.30+-0.23	0.1	1	16.2	903	8.45+-0.24	0.1	1	16.1	880	9.30+-0.25	0.5	1
20.5	952	8.08+-0.32	0.	0	20.3	927	8.10+-0.33	0.	0	20.1	903	8.16+-0.33	0.	0	20.0	880	8.42+-0.34	0.	0
30.6	954	8.07+-0.23	0.3	1	30.3	928	7.92+-0.23	2.0	1	30.1	903	8.43+-0.24	0.2	1	29.9	880	7.92+-0.24	0.8	1
40.8	956	8.47+-0.15	10.8	4	40.4	929	7.96+-0.14	0.3	4	40.1	903	7.83+-0.14	4.5	4	39.8	880	7.25+-0.14	0.4	4
50.9	959	7.77+-0.24	0.	1	50.5	931	7.02+-0.23	0.1	1	50.1	904	6.83+-0.22	0.3	1	49.7	879	6.51+-0.22	1.3	1
61.1	963	5.33+-0.23	0.	1	60.6	933	5.31+-0.23	0.	1	60.1	905	5.15+-0.23	3.5	1	59.6	878	4.87+-0.23	0.8	1
71.3	967	3.88+-0.25	0.	0	70.7	935	3.66+-0.24	0.	0	70.1	905	3.41+-0.24	0.	0	69.6	878	3.30+-0.24	0.	0
81.4	973	2.17+-0.20	0.	0	80.8	938	2.81+-0.22	0.	0	80.1	906	2.71+-0.23	0.	0	79.5	876	2.65+-0.23	0.	0
6.2	1056	7.46+-0.20	1.7	4	6.2	1028	7.77+-0.21	3.3	4	6.1	1001	9.39+-0.24	4.1	4	6.1	977	9.95+-0.26	4.4	4
8.2	1056	6.81+-0.27	0.2	1	8.2	1028	7.52+-0.29	1.6	1	8.1	1001	8.01+-0.31	0.	1	8.0	977	9.23+-0.34	0.6	1
10.4	1056	6.00+-0.19	1.7	1	10.4	1028	6.91+-0.21	0.4	1	10.3	1002	7.17+-0.22	1.0	1	10.2	977	8.23+-0.25	0.1	1
12.4	1056	5.69+-0.15	0.	2	12.3	1028	6.59+-0.16	1.7	2	12.2	1002	6.99+-0.17	1.0	2	12.1	977	8.21+-0.19	4.3	2
14.5	1056	5.91+-0.17	6.0	1	14.3	1028	6.95+-0.19	2.5	1	14.2	1002	7.33+-0.20	0.	1	14.1	977	7.95+-0.22	0.	1
16.4	1057	6.13+-0.18	8.6	1	16.3	1028	6.89+-0.19	4.8	1	16.2	1002	7.40+-0.20	3.0	1	16.0	977	8.00+-0.22	2.1	1
20.5	1057	6.70+-0.21	0.7	1	20.3	1029	6.97+-0.21	0.2	1	20.1	1002	7.56+-0.23	0.2	1	20.0	977	7.55+-0.23	1.2	1
25.6	1058	7.73+-0.12	3.7	5	25.3	1029	8.42+-0.13	4.1	5	25.1	1002	8.62+-0.13	8.3	5	24.9	977	8.64+-0.14	4.0	5
30.6	1059	7.91+-0.18	0.9	2	30.4	1030	8.78+-0.19	1.3	2	30.1	1002	8.80+-0.20	1.3	2	29.9	976	8.94+-0.20	1.0	2
35.7	1060	8.02+-0.16	5.6	3	35.4	1030	9.43+-0.17	8.9	3	35.1	1002	9.47+-0.18	1.1	3	34.8	976	9.40+-0.18	1.0	3
40.8	1062	8.51+-0.11	8.4	8	40.4	1031	9.32+-0.12	8.1	8	40.1	1003	9.44+-0.12	3.6	8	39.8	976	9.51+-0.12	4.9	8
45.9	1063	8.16+-0.18	0.1	2	45.5	1032	9.41+-0.20	1.0	2	45.1	1003	9.51+-0.20	0.2	2	44.7	976	9.36+-0.20	0.3	2
51.0	1065	7.34+-0.23	0.7	1	50.5	1033	8.07+-0.24	7.1	1	50.1	1003	8.25+-0.25	1.0	1	49.7	976	8.39+-0.26	0.3	1
56.1	1067	6.01+-0.17	0.	1	55.6	1034	7.53+-0.20	0.8	1	55.1	1004	8.10+-0.21	2.5	1	54.7	975	7.32+-0.20	0.8	1
61.2	1070	5.48+-0.20	1.8	1	60.6	1036	6.01+-0.21	0.2	1	60.1	1004	6.39+-0.22	0.8	1	59.6	975	6.84+-0.23	2.1	1
66.2	1072	4.36+-0.15	1.4	1	65.7	1037	5.52+-0.17	0.3	1	65.1	1005	5.75+-0.18	0.5	1	64.6	974	5.59+-0.18	0.2	1
71.3	1075	3.58+-0.08	4.0	7	70.7	1039	4.38+-0.09	4.7	7	70.1	1005	4.60+-0.09	10.6	7	69.6	974	4.74+-0.10	5.2	7
76.4	1079	2.84+-0.13	0.1	1	75.8	1041	3.50+-0.14	0.	1	75.1	1006	4.02+-0.15	0.7	1	74.5	973	3.53+-0.15	0.1	1
81.5	1082	2.10+-0.12	1.4	1	80.8	1043	2.64+-0.13	0.6	1	80.1	1006	3.03+-0.15	0.	1	79.5	973	2.87+-0.15	0.2	1
86.6	1086	1.77+-0.11	1.8	1	85.8	1045	2.13+-0.12	0.4	1	85.1	1007	2.41+-0.13	0.	1	84.5	972	2.38+-0.13	3.4	1
91.7	1090	1.34+-0.06	2.0	3	90.9	1047	1.88+-0.07	0.4	3	90.1	1007	2.02+-0.07	1.4	3	89.5	971	2.14+-0.08	1.5	3

CM ANGLE	LAB K	CROSS SECTION	CHI SQ	D	CM ANGLE	LAB K	CROSS SECTION	CHI SQ	D	CM ANGLE	LAB K	CROSS SECTION	CHI SQ	D	CM ANGLE	LAB K	CROSS SECTION	CHI SQ	D
6.2	1162	5.35+-0.17	1.2	4	6.2	1131	5.52+-0.17	10.3	4	6.1	1102	6.49+-0.20	5.2	4	6.1	1074	7.01+-0.21	2.1	4
8.2	1162	4.49+-0.15	3.6	3	8.2	1131	4.95+-0.16	2.3	3	8.1	1102	5.34+-0.17	3.1	3	8.0	1075	6.36+-0.20	0.2	3
10.5	1162	4.03+-0.12	1.0	2	10.4	1131	4.48+-0.13	3.5	2	10.3	1102	5.31+-0.14	1.7	2	10.2	1075	5.81+-0.16	0.2	2
12.5	1162	4.13+-0.12	1.7	2	12.3	1131	4.64+-0.13	1.4	2	12.2	1102	5.16+-0.14	0.4	2	12.1	1074	5.74+-0.15	2.8	2
14.5	1162	4.44+-0.16	0.7	1	14.3	1131	5.12+-0.18	1.3	1	14.2	1102	5.28+-0.18	1.1	1	14.1	1074	5.92+-0.20	1.3	1
16.5	1162	4.16+-0.12	2.3	2	16.3	1131	4.77+-0.13	4.3	2	16.2	1102	5.49+-0.14	4.7	2	16.0	1074	5.99+-0.15	3.4	2
20.5	1163	4.51+-0.13	4.1	2	20.3	1131	4.91+-0.13	4.6	2	20.2	1102	5.85+-0.15	0.8	2	20.0	1074	6.58+-0.16	0.6	2
25.6	1164	5.04+-0.13	0.	2	25.3	1132	5.35+-0.14	1.2	2	25.1	1102	6.42+-0.16	3.1	2	24.9	1074	7.55+-0.18	2.8	2
30.6	1165	4.97+-0.10	3.3	4	30.4	1132	5.64+-0.11	3.7	4	30.1	1102	6.53+-0.12	3.9	4	29.8	1073	7.40+-0.13	4.9	4
35.7	1166	4.68+-0.10	2.7	3	35.4	1133	5.47+-0.11	7.4	3	35.1	1102	6.43+-0.13	0.6	3	34.8	1073	8.26+-0.15	0.2	3
40.8	1167	4.62+-0.06	18.9	13	40.4	1133	5.54+-0.06	9.5	13	40.1	1102	6.81+-0.07	3.9	13	39.7	1072	8.37+-0.08	17.0	13
45.9	1169	4.33+-0.12	1.4	2	45.5	1134	5.09+-0.13	0.9	2	45.1	1102	6.38+-0.15	0.8	2	44.7	1072	8.21+-0.17	1.4	2
51.0	1171	3.58+-0.12	0.3	2	50.5	1136	4.59+-0.13	1.0	2	50.1	1102	6.01+-0.16	0.7	2	49.7	1072	7.41+-0.18	9.0	2
56.1	1173	3.04+-0.10	0.1	2	55.6	1137	4.22+-0.12	0.6	2	55.1	1103	5.24+-0.14	0.6	2	54.6	1071	6.90+-0.17	5.1	2
61.2	1176	2.34+-0.06	0.7	5	60.6	1139	3.18+-0.07	0.8	5	60.1	1104	4.19+-0.09	2.2	5	59.6	1071	5.57+-0.10	4.5	5
66.3	1179	1.79+-0.08	0.7	2	65.7	1140	2.65+-0.10	2.0	2	65.1	1104	3.89+-0.12	0.3	2	64.5	1071	4.74+-0.14	0.9	2
71.4	1183	1.49+-0.05	5.8	10	70.7	1142	2.20+-0.06	18.5	10	70.1	1105	2.97+-0.07	10.5	10	69.5	1070	3.94+-0.08	16.5	10
76.5	1187	1.14+-0.09	0.	1	75.8	1144	1.48+-0.10	2.7	1	75.1	1105	2.40+-0.13	6.6	1	74.5	1069	2.91+-0.15	0.	1
81.6	1191	0.86+-0.08	6.9	2	80.8	1147	1.47+-0.09	0.2	2	80.1	1106	1.85+-0.11	2.7	2	79.5	1069	2.60+-0.13	2.0	2
86.7	1196	0.85+-0.09	0.1	1	85.9	1149	1.11+-0.10	0.2	1	85.1	1107	1.49+-0.11	1.5	1	84.4	1068	1.93+-0.13	1.0	1
91.7	1201	0.62+-0.07	0.	0	90.9	1152	1.04+-0.08	0.	0	90.1	1108	1.27+-0.09	0.	0	89.4	1067	1.76+-0.11	0.	0
6.2	1269	4.38+-0.24	0.1	1	6.2	1235	4.75+-0.25	0.3	1	6.1	1204	5.01+-0.26	1.1	1	6.1	1174	5.80+-0.30	0.1	1
8.2	1269	3.29+-0.16	5.5	2	8.2	1235	3.75+-0.17	0.5	2	8.1	1204	4.15+-0.19	1.6	2	8.0	1174	4.70+-0.20	5.1	2
10.5	1270	3.29+-0.14	4.0	2	10.4	1236	3.72+-0.14	3.1	2	10.3	1204	4.16+-0.16	2.2	2	10.2	1174	4.65+-0.17	0.1	2
12.5	1270	3.31+-0.22	0.2	1	12.4	1236	3.47+-0.24	0.7	1	12.3	1204	4.09+-0.25	0.3	1	12.1	1174	4.39+-0.27	0.4	1
14.5	1270	3.45+-0.22	0.	0	14.4	1236	3.84+-0.23	0.	0	14.2	1203	4.10+-0.24	0.	0	14.1	1173	3.90+-0.25	0.	0
16.5	1270	3.36+-0.16	0.8	1	16.4	1235	3.80+-0.17	0.3	1	16.2	1203	3.93+-0.17	2.5	1	16.1	1173	4.45+-0.19	0.	1
20.6	1270	4.16+-0.24	0.	0	20.4	1235	3.99+-0.23	0.	0	20.2	1203	4.13+-0.24	0.	0	20.0	1173	4.18+-0.25	0.	0
25.6	1270	4.65+-0.26	0.	0	25.4	1235	4.58+-0.27	0.	0	25.1	1203	4.54+-0.27	0.	0	24.9	1172	5.35+-0.30	0.	0
30.7	1271	3.87+-0.33	0.	0	30.4	1236	4.00+-0.33	0.	0	30.1	1202	5.23+-0.38	0.	0	29.8	1171	5.17+-0.40	0.	0
35.8	1272	4.47+-0.36	0.	0	35.4	1236	4.00+-0.34	0.	0	35.1	1202	4.78+-0.37	0.	0	34.8	1171	4.40+-0.37	0.	0
40.9	1274	3.70+-0.11	2.9	2	40.5	1237	3.77+-0.12	1.4	2	40.1	1202	3.99+-0.12	1.4	2	39.7	1170	4.79+-0.14	3.4	2
51.0	1277	2.49+-0.17	3.1	1	50.5	1238	2.70+-0.17	3.3	1	50.1	1202	3.28+-0.20	3.7	1	49.6	1168	3.99+-0.21	0.	1
61.2	1283	1.52+-0.16	0.	0	60.6	1241	1.93+-0.18	0.	0	60.1	1203	1.99+-0.19	0.	0	59.5	1167	2.74+-0.22	0.	0
71.4	1290	0.99+-0.14	0.	0	70.7	1245	1.02+-0.13	0.	0	70.1	1204	1.62+-0.17	0.	0	69.5	1166	1.53+-0.17	0.	0
81.6	1300	0.62+-0.12	0.	0	80.8	1251	0.60+-0.11	0.	0	80.1	1206	0.93+-0.14	0.	0	79.4	1164	1.16+-0.16	0.	0
91.8	1311	0.52+-0.06	0.	0	91.0	1257	0.53+-0.06	0.	0	90.1	1208	0.70+-0.07	0.	0	89.4	1162	0.70+-0.07	0.	0

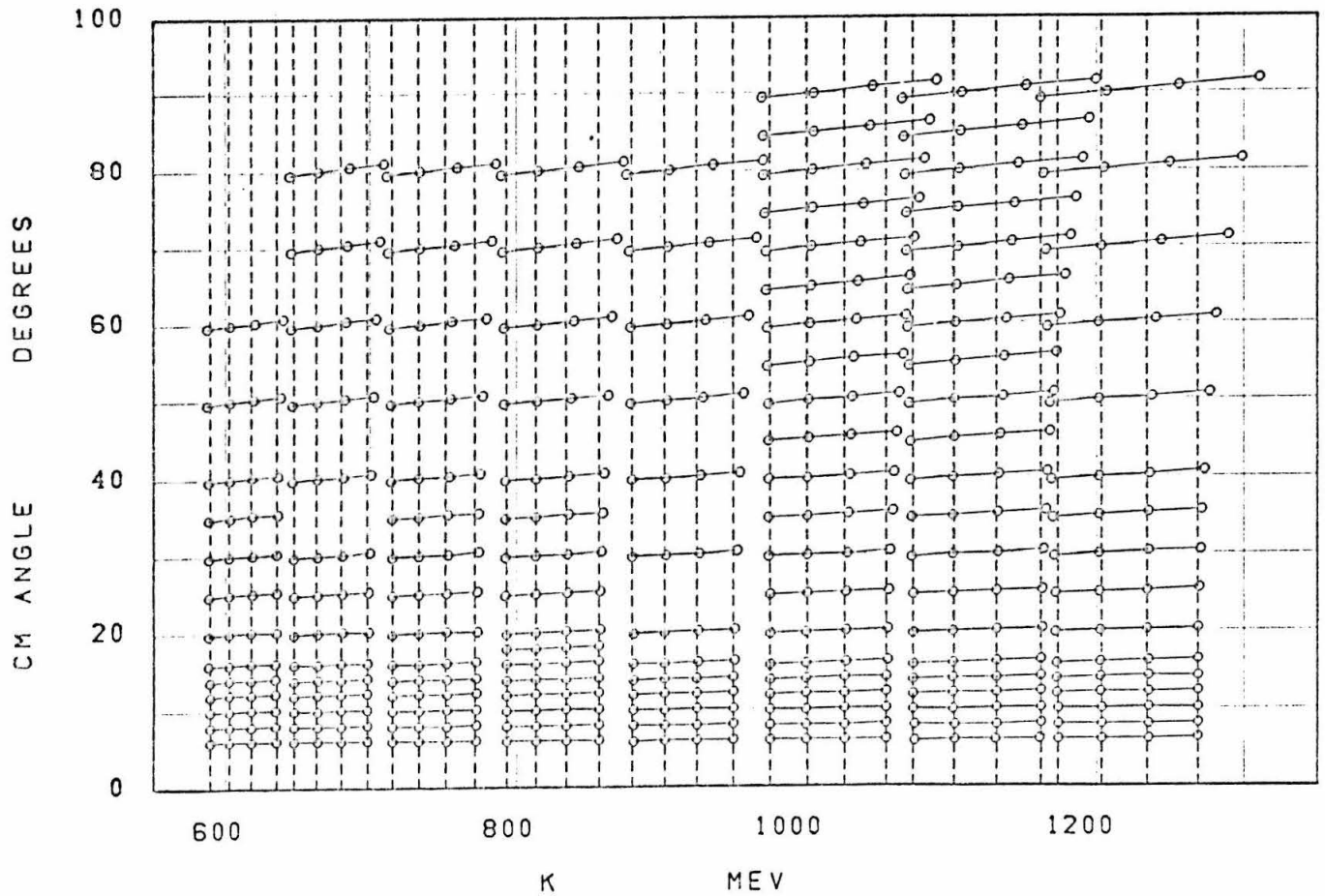
KINEMATIC SETTINGS
100
80
60
40
20
0
CM ANGLE DEGREES
600
800
1000
1200
K
MEV

FIGURE 29

TABLE 19

Computer Programs

Program	Author(s)	Purpose
SPECTRØMETER	Dr. C. W. Peck	Calculate spectrometer acceptance and orbits from fringe field measurements.
009, DATA	Dr. H. A. Thiessen	Integrate acceptance to obtain R(Q).
PIMU	Dr. J. Boyden Dr. J. Kilner Dr. H. A. Thiessen	Calculate decay pion resolution $D(Q, P_o)$.
MUF	Dr. H. A. Thiessen	Parameterize $D(Q, P_o)$ for use in CRØS.
BPAK1	F. B. Wolverton	Provide bremsstrahlung spectrum.
BR	M. G. Hauser	Average bremsstrahlung spectrum and provide a table interpolation function for use in CRØS.
CRØS	Dr. H. A. Thiessen S. D. Ecklund	Calculate cross sections.
MØN	S. D. Ecklund	Sort data and calculate rates for use in CRØS.
015	S. D. Ecklund	Interpolate data in K.
MØRF, MØRG	S. D. Ecklund	Fits to angular distributions.
PTA	S. D. Ecklund	Generate plots.
PHØT	C. R. Clinesmith S. D. Ecklund	Born term and multipole fitting of data.

REFERENCES

1. F. P. Dixon, R. L. Walker, Phys. Rev. Lett. 1, 142 (1958); Phys. Rev. Lett. 1, 458 (1958).

   F. P. Dixon, Ph. D. Thesis, California Institute of Technology (1960).

2. J. H. Boyden, Ph. D. Thesis, California Institute of Technology (1962).

   R. L. Walker, Proc. of the 1960 Int. Conf. on High Energy Physics at Rochester, 16, (1960).

3. J. R. Kilner, Ph. D. Thesis, California Institute of Technology (1963).

4. M. J. Moravcsik, Phys. Rev. 104, 1451 (1956); J. G. Taylor, M. J. Moravcsik, J. L. Uretsky, Phys. Rev. 113 No. 2, 689 (1959).

5. R. L. Walker, "Photoproduction of Elementary Particles", preliminary draft (1962).

6. A. Bietti, Phys. Rev. 142 No. 4, 1258 (1966); Phys. Rev. 144 No. 4, 1289 (1966).

7. P. Bareyre, C. Brickman, A. V. Stirling, G. Villet, Physics Letters 18 No. 3, 342 (1965).

8. L. D. Roper, R. M. Wright, B. T. Feld, Phys. Rev. 138, B190 (1965).

9. B. H. Bransden, P. J. O'Donnel, R. G. Moorhouse, Physics Letters 11, 339 (1964).

10. P. Auvil, C. Lovelace, A. Donnachie, A. T. Lea, Physics Letters 12, 76 (1964).

11. J. Cence, Physics Letters 20, 306 (1966).

12 B. M. Chasan et. al., Phys. Rev. 119 No. 2, 811 (1960).

13. J. V. Allaby, H. L. Lynch, D. M. Ritson, Phys. Rev. 142 No. 4, 887 (1966).

14. M. G. Hauser, private communication.

15. R. R. Wilson, Nuclear Instruments 1, 101 (1957).

16. H. A. Thiessen, Ph. D. Thesis, California Institute of Technology, (1966).

17. M. Beneventano, Nuovo Cimento 28, 1464 (1963).

18. M. Jacob, G. C. Wick, Annals of Physics 7, 404 (1959);

Jean Hebb, private communication.

19. G. F. Chew, M. L. Goldberger, F. E. Low, Y. Nambu, Phys. Rev. 106, 1345 (1957).

20. R. G. Moorhouse, Phys. Rev. Lett. 16 No. 17, 771 (1966).

21. D. S. Beder, Nuovo Cimento 33, 94 (1964).

22. R. E. Diebold, Ph. D. Thesis, California Institute of Technology, (1963).

23. F. B. Wolverton, "Thick Radiator Bremsstrahlung. Angular Dependence of the Spectrum for Electron Energies Greater Than 300 MeV", 1966 (to be published). An instruction manual for program BPAK1 has been placed in the Synchrotron Library.

24. M. G. Hauser, "BR/Function to Obtain Synchrotron Beam Spectrum by Table Interpolation", unpublished (1966). This program write-up has been placed in the Synchrotron Library.

25. H. A. Thiessen, "Calibration of the South Quantameter", CTSL Internal Report No. 22, unpublished.

26. P. L. Donoho, "A Magnetic Spectrometer for Analysis of Particles of Momentum up to 1200 MeV/c", unpublished (1957).

27. C. W. Peck, Ph. D. Thesis, California Institute of Technology, (1964).

28. C. W. Peck, private communication.

29. H. A. Thiessen, "Calibration of the 600 MeV/c Magnet", CTSL Internal Report No. 26, unpublished (1966).

30. H. A. Thiessen, "A Recalibration of the Beam Energy Meter", CTSL Internal Report No. 21, unpublished (1966).

31. H. A. Thiessen, "π-M Decay Analysis Program, unpublished (1964). A copy of this program writeup has been placed in the Synchrotron Library.

32. F. B. Wolverton, private communication; A similar counter is described in: J. Sayag, "A Gas Cherenkov Counter for Electrons", J. Phys. Radium (French), 23, 12, 163A, (1962).

33. H. Brody, Ph. D. Thesis, California Institute of Technology, (1959).

34. Rosenfeld et. al., Rev. Mod. Phys. 36, 4, 977, (1964).